Comprehensive Multibody AeroServoElastic Analysis of Integrated Rotorcraft Active Controls

Dipartimento di Ingegneria Aerospaziale
Politecnico di Milano

Dottorato di Ricerca in Ingegneria Aerospaziale, XII Ciclo

Pierangelo Masarati

Tutor: Professor Paolo Mantegazza

Contents

List of Figures

List of Tables

Motivation

This work originates from the need to model the dynamics of a rotorcraft. The problem of the simulation of rotorcraft dynamics has been discussed for years, as shown by the large amount of literature on the subject and, moreover, by the large number of formulations and computer codes available nowadays. But it is not a well established topic yet, as proven by the discussions on the suitability of the various approaches, as well as on the very first principles the formulations should rely on. A very important question is: do we need a dedicated analysis formulation, or should we use a general purpose mechanical analysis tool? This point is not trivial since it encompasses efficiency as well as versatility and code reusability considerations. Another question is: should we use an approach that is aware of the nature of the problem, or should we give up any assumption? In the first case, by assuming for instance that we are dealing with a mechanical system, we might take advantage of the conservation properties, say, of the momenta rather than of the total energy, by using dedicated algorithms, while in the second case more general algorithms would give more freedom in formulating, say, multidisciplinary problems with a reduced overhead both from the implementation and the computation standpoint. Surely there is no right recipe for this problem, and many of the solutions that have been presented substantially meet their goal, as we hope the one we are presenting will. Maybe we should better clarify the point: this work is not intended to present "the" solution to the problem of the analysis of the dynamics of a rotorcraft; it rather proposes "a" means that represents a good trade-off between all the possible choices for the modelling of general, multidisciplinary mechanisms with a high level of refinement in the details of the kinematics, with a good compromise between efficiency, flexibility and accuracy in the modelling of structural components, and with sufficient flexibility to allow to consider multidisciplinary, in this case control-related, models. The formulation presented herein results from years of investigation at the Dipartimento di Ingegneria Aerospaziale *of the* Politecnico di Milano*, under the coordination of Professor* Paolo Mantegazza*. As a consequence, some of the work shown in the following chapters represents someone else's contribution to the project, and is included only to ease the readability and to provide a basis for the results. In the*

middle-ages, philosophers, talking about their role in science compared to that of the geniuses of the ancient times, used to say that "we are dwarfs, but because we are standing on giants' shoulders, we can see farther".
I want to acknowledge the cooperation, to different extents, of many people, starting from Paolo Mantegazza*, my tutor, who gave me the most invaluable help: he rarely interfered with my work. The advice of* Gian Luca Ghiringhelli *was also invaluable, expecially for all the structural and piezoelectric analysis part.* Massimiliano Lanz *and* Marco Borri *were sources of fine suggestions and of important bibliographic references.* Marco Borri *represented a very special counterpart because his views on the subject have a remarkable theoretical and algorithmic orientation, so his critics to the foundations of this work were very important in highlighting flaws and inconsistencies.* Massimiliano Lanz *and* Gabriele Gilardi *had a substantial role in the formulation of the integration scheme, based on an idea of* Paolo Mantegazza*, while* Stefano Marazzani *cooperated in the development of the finite volume beam formulation.* Marco Morandini *deserves a special place due to his invaluable suggestions both from the theoretical and the computational standpoint. Finally,* Mark W. Nixon*, from NASA Langley, not only made all the correlations with the V-22 wind-tunnel model possible, but he also honored me with his friendship, that lasts after the end of my experience at LaRC.*

Introduction

The dissertation is basically divided in three parts, reflecting to some extent the chronological, not only the logical sequence in which the research work has been carried on.

The approach to the modelling of the dynamics of a rotorcraft that has been used in this work is presented first. The framework of the first principles equations of motion of a system of constrained bodies is described; details on the formulation for the handling of finite rotations are given. Algorithmic implications of the selected approach and implementation notes are discussed; the original approach to the modelling of flexible bodies, significantly the characterisation of beam sections and an original discrete beam model, is presented. A plate model, developed in analogy with the beam model, is also formulated and discussed, with a *caveat*: it has not been implemented nor used in the work.

The second part refers to the active control of the rotorcraft system. The Generalised Predictive Control formulation that has been adopted is presented first, in a discrete time form that has been preferred since it is respectful of the way digital real-time control is practically performed. The suggestion of the predictive control came from a short course I attended to, held by Professors *Bolzern*, *Bittanti* and *Colaneri* at the *Dipartimento di Elettronica* of the *Politecnico di Milano*. At that time, I was collecting information on anything that could be helpful for my work; I found the predictive control really suitable for the problem at hand, so I made some tests and put it aside, because I was deeply involved with the mechanical modelling at that time. The following year, at NASA Langley, I found out that there were people working exactly on predictive control for the tiltrotor wind tunnel model, following the suggestions of *Jer-Nan Juang*. Thanks to very enlightening talks with Professor *Juang*, to whom my acknowledge goes, I got a little more confident in such topic, and I decided to catch up with it.

The last part is dedicated to the application of the structural modelling and of the control to the simulation of rotorcrafts. The most important example is represented by the analysis and the active control of the wind-tunnel model of the V-22 tiltrotor that is currently under investigation at Langley's *Transonic Dynamics Tunnel* (TDT). This work became possible thanks to the cooperation of the Army Research Laboratory at the Langley Research Center, and remarkably to the invauable help of Dr. *Mark W. Nixon*. Other applications involve the modelling of a "smart" rotor, with induced twist actuation of the rotor blades. A model of this kind is under investigation at the *Active Material and Structures Laboratory* of MIT by Professor *Hagood*, and a cooperative effort is underway with NASA Langley, under the coordination of Dr. *Wilkie*, but no wind tunnel testing has been performed until recently. In this case only open-loop control has been investigated, the major task still being the construction of the smart blades and of the testing apparatus.

The nomenclature used throughout the work sometimes might appear non-homogeneous, at a first glance. This is because an attempt has been made to preserve the original nomenclature used in formulating each part. Where non "official" nomenclature was established, or where required by the need to link different formulations in a tight manner, an effort to using a uniform nomenclature has been made. To avoid any ambiguity, every chapter defines its own set of symbols with a brief description. The context and brief notes where the symbols are used should clarify whether a symbol is "local", and thus defined in the nomenclature of the chapter, or it is "global", and thus should be sought for in a preceeding chapter's nomenclature. The bibliography is unique; brief bibliographic notes are reported throughout the text where required by the subject.

Part I

Rotorcraft modelling

Chapter 1

Dynamics of a free rigid body

The equations of motion of a rigid body result from *Newton*'s first principles; they basically state that the rate of change of the linear and angular momenta is proportional to the applied forces and couples, respectively.

x	position of a reference point
v	velocity of a reference point
R	rotation matrix
ω	angular velocity
β	linear momentum
γ_P	angular momentum referred to pole P
m	mass associated to a body
S	first order inertia moment
J	second order inertia moment

1.1 Momenta definition

The linear and angular momenta, β and γ, of a body of mass m and inertia J, attached to a moving point x at some relative distance resulting in a first-order inertia moment S with respect to x, are:

$$\left\{ \begin{array}{rcl} \beta & = & m\dot{x} + \omega \times S, \\ \gamma & = & S \times \dot{x} + J\omega, \end{array} \right. \tag{1.1}$$

where $\dot{x}$ and $\omega = \mathrm{ax}\left(\dot{R}R^T\right)$ respectively are the velocity and the angular velocity[1] of x. The determination of the inertia properties of a rigid body is detailed in Appedix A.

[1] The operator $\mathrm{ax}(\cdot)$ extracts the "axial" of the operand, a matrix; $v = \mathrm{ax}(m)$ is the vector that contains the skew-symmetric part of matrix m. Its partial inverse is represented by operator $(\cdot)\times$, yielding $\mathrm{ax}(m)\times = v\times = \mathrm{skw}(m)$. The nature of the angular velocity is discussed in Chapter 3.

1.2 Equilibrium equations

The total angular momentum, referred to a fixed pole O, is $\gamma_O = \gamma + x \times \beta$, and its time derivative results in $\dot{\gamma}_O = \dot{\gamma} + \dot{x} \times \beta + x \times \dot{\beta}$. By subtracting the moment due to the derivative of the linear momentum, $x \times \dot{\beta}$, the time derivative of the angular momentum is referred again to the moving pole, yielding $\dot{\gamma}_O - x \times \dot{\beta} = \dot{\gamma} + \dot{x} \times \beta$. The usual moving pole angular equilibrium results from equating the moving pole angular momentum rate to the applied couples. Together with the force equilibrium, obtained by equating the derivative of the momentum to the applied forces, it represents the inertial contribution to the equilibrium of a rigid body:

$$\left\{ \begin{array}{rcl} \dot{\beta} & = & F, \\ \dot{\gamma} + \dot{x} \times \beta & = & M; \end{array} \right. \tag{1.2}$$

F, M are external forces and couples that may depend on the configuration, as discussed in Chapter 5.

1.3 Rigid-body dynamics as ODEs

The dynamics problem is stated in terms of a system of first-order differential equations. It is important to notice that the left-hand side of the equilibrium equations, Eq. 1.2 is linear in the derivatives of the momenta regardless of the parametrisation that is used for the kinematic unknowns, i.e. the displacements and significantly the rotations[2]. The dynamics of the model are described by the collection of Equations 1.1 and 1.2, written for each body that is used in the discretisation. The equations are written in the general, implicit form

$$f(y, \dot{y}, t) = 0, \tag{1.3}$$

being y the array of the unknowns and t the time. Equation 1.3 represents an implicit Ordinary Differential Equation (ODE); together with a set of initial conditions it yields an Initial Value (IV) problem, whose integration, to some extent, is a well-established topic and can be carried out by means of consolidated numerical techniques. The addition of kinematic constraint equations makes the problem a little more difficult, as will be shown in the next section.

[2]The rotations, here represented by the rotation matrix R, are the real unknowns of the problem. After a parametrisation is chosen, the rotation parameters become the practical unknowns.

Chapter 2

Algebraic constraints

The system of differential equations given by Equation 1.3 describes the dynamics of the bodies that are used to discretise the problem. The external forces and couples F and M, shown in Eq. 1.2, may contain configuration dependent interaction forces that are used to represent the elasticity and generally the dynamic interaction between bodies. But there is an important class of interactions that are purely kinematic and that require special treatment.

2.1 Reduced vs. redundant coordinate set

In fact, when a multibody model is considered, great advantages both in the implementation and in the numerical treatment of the problem can be achieved by using a *Redundant Coordinate Set* formulation. It consists in writing the complete dynamics of each body and by explicitly constraining their kinematic degrees of freedom to obtain the desired kinematic behaviour of the system. Consider for instance a revolute joint, namely the assembly of two bodies whose relative motion is represented by an axial rotation. The system has 6 rigid body degrees of freedom plus one relative rotation degree of freedom. If such reduced system is directly considered, only 7 differential equations need be written to describe the dynamics of the system, in the spirit of the *Reduced Coordinate Set* approach. This approach, with different formulations, has been historically used for constrained dynamics analysis since it allows large problems to be described by means of comparatively small systems of purely differential equations. Moreover, efficient explicit integration schemes can be used, with step size control to ensure the numerical stability of the integration. On the other hand, the writing of the motion in terms of relative degrees of freedom may represent a problem, and generally leads to complicated, cumbersome formulations and implementations, and requires sophisticated automatic reduction techniques. The *Redundant*

Coordinate Set approach, on the contrary, allows to write the free-body dynamics equations for each body in the global reference frame, with the addition of algebraic constraint equations. They contribute to the equilibrium of the bodies by means of algebraic unknowns that represent the reaction forces and couples. The system may become very large if compared to the reduced set case; consider for instance a rigid model of an articulated helicopter rotor: a single blade has two independent degrees of freedom, e.g. the flap and the lag angles, the feathering being constrained by the pitch link. A reduced set approach would result in a system of first-order differential equations of order 4. A redundant set approach might result in dozens of degrees of freedom: one body is required to model the hub, one is required after the flap hinge, one after the lag hinge, and finally one, representing the rigid blade, after the feathering hinge. These four bodies require 24 degrees of freedom. Six degrees of freedom are required by the revolute joint that grounds the hub and enforces the rotation, 5 by each of the revolute joints that model the three hinges, and one by the distance joint that models the pitch link, resulting in 22 reaction unknowns. Because the dynamics of the bodies, Eqs. 1.1 and 1.2, are written as a system of first-order equations, the bodies actually require 12 degrees of freedom each, so the problem at hand would have order 70, compared to order 4 of the reduced set case. Of course the redundant set approach allows a very simple, general formulation, resulting in ease and flexibility of implementation, and in very sparse system matrices; by efficiently handling the sparsity with specialised linear algebra solvers, very good performances have been obtained.

2.2 Constrained rigid-body dynamics as DAEs

A system of *Differential-Algebraic Equations* (DAE) results by adding the algebraic constraints to Eqs 1.1 and 1.2. Differential-algrebraic equations require special treatment to be solved; the problem has captured the attention of the investigators during the last decades [17]. From a heuristic point of view, differential algebraic equations may be considered very stiff differential equations, with vanishing inertia terms; they will be discussed with more detail in Chapter 4. The direct, simultaneous integration of such equations requires implicit, unconditionally stable integration formulas, as the one that is proposed in this work in Section 4.2. Equation 1.3 is modified by the addition of the dependence on the algebraic unknowns v, while the algebraic constraint equations g are added, yielding

$$\left\{ \begin{array}{rcl} f(y, \dot{y}, v, t) & = & 0, \\ g(y, \dot{y}, t) & = & 0. \end{array} \right. \tag{2.1}$$

When a constrained mechanics problem is considered, Eq. 2.1 assumes the form[1]

$$\left\{ \begin{array}{rcl} A(y,t)\,\dot{y} - z & = & 0, \\ \dot{z} + G^T v - Q(y,\dot{y},t) & = & 0, \\ \Phi(y) & = & 0, \end{array} \right. \tag{2.2}$$

which is the Euler equation of a problem known as Lagrangian of the first kind; it represents a Differential-Algebraic Equation of index three[2]. In Eq. 2.2, A is the inertia matrix, Q are arbitrary external forces and couples, and $G = \partial\Phi/\partial y$ is the derivative of the holonomic constraints[3] with respect to the kinematic unknowns. The constraint matrices resulting from the linearisation of Eq. 2.2 are symmetric when the problem is formulated by applying a variational principle; in this work the symmetry is lost, at least for the angular equilibrium equations, that are conjugated to the perturbation of the rotation angles, rather than to the perturbation of the rotation parameters; this is discussed in Section 3.2. The same consideration may hold for the general equations that will be introduced in Chapter 8.

[1]The momentum differential unknowns in Eq. 2.2 are represented by z, the symbol y referring to the kinematic unknowns only.

[2]Quoting from [17], Definition 2.2.2, p. 17: "The minimum number of times that all or part of the DAE $F(y,\dot{y},t) = 0$ must be differentiated with respect to t in order to determine $\dot{y}$ as a continuous function of y, t is the index of the DAE".

[3]Non-holonomic constraints require special treatment, that is not illustrated since it is not relevant to the discussion presented here.

Chapter 3

Kinematics of finite rotations

Three-dimensional, finite rotations are not additive; in fact the configuration resulting from two successive finite rotations is given by the multiplication of the two relative rotation matrices, namely $R_{0\rightarrow 2} = R_{1\rightarrow 2}R_{0\rightarrow 1}$ and in general, regardless of the parametrisation, the total rotation cannot be expressed as the addition of the two partial rotations. The handling of finite rotations is key to the effectiveness of a multibody formulation. In fact, the fundamental idea of the multibody approach to the structural dynamics is to express the kinematics in a global frame, in order to simplify the writing of the contribution of the inertia to the equilibrium, at the cost of a more complicated description of interactional forces, either related to flexibility or to kinematic constraints, which have little need, if any, for the time derivatives of the kinematic unknowns.

3.1 Finite rotation properties

A rotation between two reference frames is described by means of an orthonormal rotation matrix R. The orthonormality property descends from the consideration that the scalar, or inner, or dot product between two vectors is independent of the reference frame the vectors are referred to, namely $a \cdot b = \tilde{a} \cdot \tilde{b}$. Thus, being $a = R\tilde{a}$ and $b = R\tilde{b}$, as a result

$$R \cdot R \;=\; R^T R \;=\; RR^T \;=\; I \tag{3.1}$$

holds, implying that $R^T = R^{-1}$. This important property has deep implications on the mathematical nature of the rotations. The relationship between the configuration matrix R and its perturbation θ_{d} can be determined by differentiating a vector $v = R\tilde{v}$ that is constant in a local reference frame, namely $\mathrm{d}\tilde{v} = 0$, resulting in $\mathrm{d}v = \mathrm{d}R\tilde{v}$; by considering Eq. 3.1, the differentiation of v results in $\mathrm{d}v = \mathrm{d}RR^T v$.

Matrix $\mathrm{d}RR^T$ is skew-symmetric, and thus can be written as a cross product matrix, namely

$$\theta_\mathrm{d}\times \ = \ \mathrm{d}RR^T; \tag{3.2}$$

operator $(\cdot)\times$, applied to a vector a, gives the matrix that, multiplied by another vector b, yields the vector product $a \times b$, as described in footnote 1, page 5. When in Eq. 3.2 a differentiation with respect to time is considered, the angular velocity is obtained, namely

$$\omega\times \ = \ \dot{R}R^T \tag{3.3}$$

By rearranging Eq. 3.3 as follows,

$$\dot{R} \ = \ \omega \times R, \tag{3.4}$$

the exponential nature of finite rotations is emphasized. The solution of Eq. 3.4 is

$$R \ = \ \mathrm{e}^{\int \omega dt \times}. \tag{3.5}$$

The exponent is represented by a skew-symmetric matrix, whose eigenvalues are zero and $\pm j \left|\int \omega dt\right|$, so matrix R has constant, unit spectral radius, the imaginary eigenvalues giving a pure rotation. Because matrix R depends on the rotation parameters p only, the differentiation of a vector v that is constant in the local frame can be expressed as $\mathrm{d}v = \mathrm{d}RR^T v = W(\mathrm{p}, \mathrm{dp})\, v$, resulting in

$$\theta_\mathrm{d}(\mathrm{p}, \mathrm{dp}) \ = \ \mathrm{ax}\left(W(\mathrm{p}, \mathrm{dp})\right) \ = \ G(\mathrm{p})\, \mathrm{dp}. \tag{3.6}$$

Matrix G is required to differentiate the rotations, in order to yield rotation velocities, curvatures, and to linearise the equations, so its efficient computation can be very important, as will be shown in Section 3.4

3.2 Rotation parametrisation

Many different parametrisations have been proposed in the literature; a comprehensive review is not the aim of this work. The fundamental distinction is between invertible and singular parametrisations, the latter usually being three-parameter, while the former require four parameters, like the well-known *quaternion* formulation, and the *Euler parameters*. The four-parameter formulas are required when a total rotation approach is used, and the singularities must be intrinsically avoided. But there are many reasons related to the efficiency of the implementation to prefer an updated rotation approach. When an updated approach is used, the three-parameter formulations are more appealing because they require reduced computational effort. The risk of incurring in singularities is null when considering that comparatively small rotations between two successive time steps are required anyway to obtain reasonable accuracy.

3.2.1 Rotation vector

Among the three-parameter formulations, the *rotation vector* parametrisation is very important, because it directly represents the geometric rotation. It consists in a vector $\Phi = \varphi n$ whose direction n is the rotation axis and whose magnitude φ is the total rotation angle. The parametrised rotation matrix is

$$R = I + \sin(\varphi)\, n\times + (1 - \cos(\varphi))\, n\times n\times .$$

The corresponding differentiation matrix G, given by Eq. 3.6, is

$$G = I + \frac{1-\cos(\varphi)}{\varphi} n\times + \left(1 - \frac{\sin(\varphi)}{\varphi}\right) n\times n\times .$$

The determinant of the matrix is

$$\det(G) = 2\frac{1-\cos(\varphi)}{\varphi^2};$$

it is singular[1], of course, the singularity lying in the uncertainty on the direction of the rotation when a 2π angle is considered. One major drawback, from a numerical standpoint, is that computationally inefficient trigonometric functions are required to compute the two matrices. It is interesting to notice that in case of plane problems, the rotation degenerates into a scalar rotation about the axis normal to the plane, and thus it becomes additive, while $\dot{\varphi}$ coincides with the angular velocity ω, thus making such parametrisation very attractive.

3.2.2 Gibbs-Rodriguez parameters

The *Gibbs-Rodriguez* parameters are related to the rotation vector by

$$g = 2\tan\left(\frac{\varphi}{2}\right) n.$$

The form with the parameters multiplied by 2 is preferred to the more traditional one because it yields linearised expressions identical to those obtained with the rotation vector. It is apparent that the parameters are singular when the argument of the tangent is $\pm\pi/2$ due to the tangent function. The rotation matrix R is:

$$R = I + \frac{4}{4+g^T g}\left(g\times + \frac{1}{2} g\times g\times\right),$$

and matrix G is:

$$G = \frac{4}{4+g^T g}\left(I + \frac{1}{2} g\times\right).$$

Notice that now no trigonometric function evaluation is required, resulting in higher computational efficiency.

[1] The singularity occurs only at $\varphi = 2\pi + 2k\pi$, with k positive integer, while for $\varphi = 0$ the determinant has unit value.

3.3 Updated approach

The updated approach that is required to allow the use of three-parameter formulas relies on the consideration that a change in configuration from R_0 to R_1 is represented by

$$R_1 = R_{0\to1}R_0. \tag{3.7}$$

When solving an initial value problem, R_0 represents the solution at time t_0 and remains constant for the rest of the integration, the unknown configuration being R_1. So, by parametrising only the *relative* rotation matrix, $R_{0\to1}$, one can make the rotation parameters small, at least confined to the desired range, by changing the time step. In fact, the rotation parameters that describe a relative rotation are of the order of magnitude of $|\omega\Delta t|$; by the way, this rough estimate can be used to control the time step to avoid the singularities related to the three-parameter formulation. When the solution at a given time step is obtained, the reference matrix R_0 is updated by means of the rule expressed by Eq. 3.7 and the rotation parameters are reset. The unknown rotation matrix at time t_i becomes

$$R_i = R_\Delta R_{i-1},$$

and the angular velocity becomes

$$\omega_i\times = \dot{R}_\Delta R_\Delta^T,$$

because the reference rotation matrix R_{i-1} is constant, and thus

$$\omega_i = G_\Delta \dot{g}.$$

The linearisation of the rotation-related quantities with respect to the unknown rotation parameters yields

$$\begin{aligned}\Delta R_i &= (G_\Delta \Delta g)\times R_i,\\ \Delta\omega_i &= G_\Delta \Delta\dot{g} + H_\Delta(g,\dot{g})\Delta g,\end{aligned}$$

with

$$H_\Delta = -\frac{2}{4+g^Tg}\left(\dot{g}\times + G_\Delta \dot{g} g^T\right).$$

3.4 Updated-updated approach

The updated approach fixes the problem of the possible singularity of the rotation parameters, but does not improve the handling of the rotations. In fact the rotation matrix, R, and the rotation derivative matrix, G, depend in a nonlinear manner on the rotation parameters, thus making the linearisation of the rotation-related quantities very complicate, time consuming and error prone from the implementor's standpoint. As will be shown in Section 4.2, the integration of the solution is obtained by collocating the nonlinear system of equations at the end of the time step and solving iteratively. The tentative solution at such time is predicted, and the final solution is determined by correcting the predicted value in a *Newton-Raphson* way, or corresponding modified algorithm. The key idea of the *updated-updated* approach consists in referring the rotation unknowns to the *predicted* configuration at the end of the current time step rather than to the *corrected* configuration at the beginning of the time step, resulting from the solution at the previous time step. In this manner, the rotation unknowns represent the rotation parameters related to the correction phase only, resulting in really "small" and thus quasi-linear variables. In fact, since the accuracy of the prediction formulas is quadratic for a linear problem, as shown in Section 4.2, the unknown rotation parameters are expected to have order of magnitude $o\left(\Delta t^2\right)$, regardless of the amplitude of the angular velocity. The unknown rotation matrix R_i now becomes

$$R_i = R_\delta R_i^{(0)},$$

where $R_i^{(0)}$ is the predicted configuration at time t_i, and the lower case δ refers to a perturbation of rotation. The angular velocity becomes

$$\omega_i \times = \dot{R}_\delta R_\delta^T + R_\delta \dot{R}_i^{(0)} R_i^{(0)^T} R_\delta^T,$$

or

$$\omega_i = \omega_\delta + \omega_i^{[0]},$$

where the perturbation of angular velocity $\omega_\delta = G_\delta \dot{g}$ is added to the reference, predicted angular velocity, $\omega_i^{[0]} = R_\delta \omega_i^{(0)}$, rotated into the corrected reference frame by matrix R_δ. The linearisation of matrix R and of the angular velocity ω yields

$$\Delta R_i = (G_\delta \Delta g) \times R_i, \tag{3.8}$$

$$\Delta \omega_i = \Delta (G_\delta \dot{g}) + (G_\delta \Delta g) \times \omega_i^{[0]}, \tag{3.9}$$

A first important result is that when the rotation parameters are reset, after the prediction, matrices R and G both degenerate into the identity matrix, so that

Eqs. 3.8, 3.9 become

$$\Delta R_i = \Delta g \times R_i^{(0)}, \tag{3.10}$$

$$\Delta \omega_i = \Delta \dot{g} + \Delta g \times \omega_i^{(0)}. \tag{3.11}$$

Successive iterations require to consider Eqs. 3.8, 3.9 instead of Eqs. 3.10, 3.11; however, since the correction parameters g, $\dot{g}$ are expected to be small, Eqs. 3.10, 3.11 represent a valid approximation when computing the Jacobian matrix. Such approximation can be viewed as a sort of intrinsically modified Newton-Raphson correction algorithm, whose accuracy remains quasi-quadratic with appreciable savings in computational time. The same idea, of course, can be applied to any rotation parametrisation.

Chapter 4

Algorithmic implications

The solution of an initial value problem described by a system of differential-algebraic equations requires special attention, due to the singularity of the algebraic equations if treated in the same manner of the differential ones. Consider a differential equation of the form of Eq. 1.3, here rewritten for clarity:

$$f(y, \dot{y}, t) = 0,$$

If the equation is differentiable in a neighborhood of the solution, and provided the derivative with respect to $\dot{y}$ is non-singular, it can be written in explicit form:

$$\Delta\dot{y} = -\frac{\partial f}{\partial \dot{y}}^{-1} \left(f + \frac{\partial f}{\partial y} \Delta y \right). \tag{4.1}$$

The system becomes algebraic-differential when this operation is no longer possible, because $f_{/\dot{y}}$ is structurally singular[1], as in the case we are interested in. Of course it would be possible, after separating the system in its differential and algebraic parts,

$$\left\{ \begin{array}{rcl} f(y, \dot{y}, z) & = & 0, \\ g(y) & = & 0, \end{array} \right. \tag{4.2}$$

where now f refers only to the differential part of the problem, to rewrite it in ordinary differential form, by first differentiating both equations,

$$\left\{ \begin{array}{l} f_{/y}\Delta y + f_{/\dot{y}}\Delta\dot{y} + f_{/z}\Delta z + f = 0, \\ g_{/y}\Delta y + g = 0; \end{array} \right. \tag{4.3}$$

[1]There are problems in which f is not invertible only in a limited number of singular points, that represent bifurcations or locking points of mechanisms. This is not the case of the problem we are considering; we are dealing with a problem that has a structural singularity of some rank r that remains constant irrespective of time, the possible extra singular points still representing bifurcation conditions for the differential-algebraic problem.

the second, algebraic equation is then differentiated with respect to time,

$$g_{/y}\Delta\dot{y} + \left(g_{/yt} + g_{/yy}\dot{y}\right)\Delta y + g_{/t} + g_{/y}\dot{y} \;=\; 0, \tag{4.4}$$

while $\dot{y}$ is explicitated from the first of Eqs. 4.3 and projected orthogonally to the constraint by substituting it into Eq. 4.4. This allows to statically determine the algebraic unknown Δz as function of Δy,

$$g_{/y}f_{/\dot{y}}^{-1}f_{/z}\Delta z \;=\; g_{/t} + g_{/y}\dot{y} - g_{/y}f_{/\dot{y}}^{-1}f + \left(g_{/yt} + g_{/yy}\dot{y} - g_{/y}f_{/\dot{y}}^{-1}f_{/y}\right)\Delta y,$$

which, substituted in the first of Eqs. 4.3, transforms it in an ordinary differential equation that implicitly satisfies the algebraic constraint of g.
The differential-algebraic problem can be written in a simpler, more redundant way by considering a new unknow w, whose time derivative is the algebraic unknown z, namely $\dot{w} = z$, and by maintaining the redundant form of two blocks of equations, that become ordinary differential, namely

$$\left[\begin{array}{cc} f_{/\dot{y}} & f_{/z} \\ g_{/y} & 0 \end{array}\right]\left\{\begin{array}{c} \Delta\dot{y} \\ \Delta\dot{w} \end{array}\right\} \;=\; -\left[\begin{array}{c} f_{/y} \\ g_{/yt} + g_{/yy}\dot{y} \end{array}\right]\Delta y - \left\{\begin{array}{c} f \\ g_{/t} + g_{/y}\dot{y} \end{array}\right\}$$

The differential and the algebraic unknowns are determined simultaneously, the system being non-singular due to the time differentiation of equation g. It is important to notice that the system that is actually integrated is no longer $f = 0, g = 0$, but rather $f = 0, \dot{g} = 0$. This has important implications in the problems at hand because, due to numerical errors in the integration, the solution may drift, and the original algebraic costraint $g = 0$ may be violated; notice that the possible occurrence of such violation is related to numerical reasons only. Different techniques have been proposed in the literature to solve this problem[2]; the point is still debated. The differential-algebraic formulation of the problem can cure the problem, because the constraint equation is directly satisfied; this approach is followed in the present work.

4.1 Unconditional stability

The above presented procedures somehow collide with the key idea of the redundant coordinate set approach, because they add unnecessary complexity, namely

[2]The interested reader should consult [17], pp. 150–157 for a brief presentation of the stabilization schemes, the references reported there for further details, or [20] for a presentation focused on structural dynamics problems; any good textbook on the solution of constrained dynamics problems should suffice.

the need to differentiate equation g with respect to time[3], to a problem that can be easily and efficiently solved in a direct manner, with a dedicated but still general solution scheme.

The first requirement for such scheme is to be unconditionally stable, to be able to integrate the infinitely stiff algebraic equations. Quoting from [17], p. 77, an integration algorithm

> "is A-stable if $\lim_{n \to \infty} y_n = 0$ for all $\mathrm{Re}\,(\lambda) < 0$ and a fixed positive h [the time step] when applied to the problem $\dot{y} = \lambda y$."

To solve a differential-algebraic problem, an A-stable algorithm is required, but this is not enough. In fact, since an unconditionally stable algorithm can integrate systems whose characteristic period is quite shorter than the time step h, and this is surely the case of the problem at hand, the dynamics related to such high frequency motions are likely to be captured with poor accuracy, if any. As a consequence, spurious oscillations and misleading aliased high frequency behaviour may appear in the results.

The second requirement for the integration scheme is to be able to filter the high frequency, algorithmic oscillations while preserving good accuracy in integrating the low frequencies we are mainly interested in. Again from [17], p. 77, an integration algorithm

> "is L-stable if it is A-stable and, in addition, $\lim_{\mathrm{Re}(\lambda) h \to -\infty} |y_{n+1}/y_n| = 0$".

This means that, being the time step h always positive, if the system is stable, and thus $\mathrm{Re}\,(\lambda) < 0$, when the time step gets larger and larger, and thus $\mathrm{Re}\,(\lambda)\,h \to -\infty$, the free oscillations of the system, i.e. the ratio $|y_{n+1}/y_n|$, must vanish. Such requirement, expecially in low order integration schemes, may be too strong, resulting in a considerable loss in accuracy for comparatively small values of $\mathrm{Im}\,(\lambda)\,h$, so it will be relaxed by imposing that $\lim_{\mathrm{Re}(\lambda) h \to -\infty} |y_{n+1}/y_n| = \rho_\infty$, where ρ_∞, such that $0 \leq \rho_\infty \leq 1$, is called the asymptotic spectral radius of the integration scheme.

[3] Strictly speaking, the time differentiation of the constraint equations is required to bring to index two an arbitrarily high index differential-algebraic system of equations. The satisfaction of the derivatives of the constraints should be implicit when the constraint equation is directly considered, but practically it is obtained only within the accuracy of the solution method. As a consequence, the presented approach may suffer from stability problems in critical conditions, when long time steps are used to integrate stiff problems. However these considerations do not appreciably affect results in practical cases, when the step size is driven by accuracy.

4.2 Integration formula

A family of integration schemes, based on a polynomial interpolation of the unknowns and on the numerical solution of the fundamental theorem of integral calculus, is presented. The algorithm is introduced and discussed for the solution of ordinary differential equations; it is subsequently generalised to implicit differential equations and to algebraic-differential equations as well.

4.2.1 Interpolation

Consider a multistep interpolation based on the unknowns and their derivatives at $r+1$ time steps,

$$y(\xi) \;=\; \sum_{i=0}^{r} \left(m_i(\xi)\, y_{n-i} + h n_i(\xi)\, \dot{y}_{n-i}\right), \tag{4.5}$$

where $\xi = (t - t_n)/h$ is the non-dimensional time, m, n are shape functions and r is the number of step intervals of the scheme. The unknowns are y_n, $\dot{y}_n$, at the end of the time step.

4.2.2 Solution

The solution is obtained from the fundamental theorem of integral calculus, namely

$$y_n \;=\; y_{n-r} + \int_{t_{n-r}}^{t_n} \dot{y}\, dt,$$

which, after discretisation, becomes

$$y_n \;\cong\; y_{n-r} + h \sum_i w_i \dot{y}(\xi_i)\,. \tag{4.6}$$

Internal points ξ_i and weights w_i depend on the numerical integration scheme. A comprehensive description of some possible schemes is reported in Appendix B.

4.2.3 Linearisation

Consider an explicit ODE first, in the form

$$\dot{y} \;=\; f(y,t);$$

the numerical solution becomes

$$y_n \;=\; y_{n-r} + h \sum_i w_i f\left(y(\xi_i), t(\xi_i)\right),$$

the linearisation of which yields

$$\Delta y_n - h \sum_i w_i f_{/y}\big|_{\xi_i} \Delta y(\xi_i) \;=\; -(y_n - y_{n-r}) + h \sum_i w_i f|_{\xi_i}.$$

The perturbation of y at ξ_i can be expressed as function of the unknown, Δy_n, by means of the interpolation formula, Eq. 4.5, yielding

$$\Delta y(\xi_i) \;=\; \left(m_0(\xi_i) I + h n_0(\xi_i) f_{/y}\big|_{\xi=0}\right) \Delta y_n. \tag{4.7}$$

So the solution is

$$\begin{aligned}\left(I - h \sum_i w_i f_{/y}\big|_{\xi_i} \left(m_0(\xi_i) I + h n_0(\xi_i) f_{/y}\big|_{\xi=0}\right)\right) \Delta y_n & \\ = \; -(y_n - y_{n-r}) + h \sum_i w_i f|_{\xi_i}. &\end{aligned} \tag{4.8}$$

It is important to notice that Eq. 4.8 requires the computation of multiple Jacobian matrices, as well as some Jacobian multiplications, which are costly operations and lead to loss of matrix sparsity.

4.2.4 Stability

The stability properties of the algorithm, at least in a linear case, that corresponds to a local stability, can be investigated by considering a problem in the form $\dot{y} = \lambda y$, where λ is an arbitrary complex parameter. By considering that in a homogeneous difference equation the solution at time i can be seen as $y(t_i) = \rho y(t_{i-1})$, and by substituting the assumed value of $\dot{y}$ in Equation 4.6, one obtains

$$\rho^r \;=\; 1 + h \sum_i w_i \lambda \sum_{j=0}^{r} \left(m_j(\xi_i)\, \rho^{r-j} + h n_j(\xi_i)\, \lambda \rho^{r-j}\right),$$

which, by exchanging the order of summations over i and j, yields

$$\rho^r \;=\; 1 + \lambda h \sum_{j=0}^{r} \rho^{r-j} \left(\sum_i w_i m_j(\xi_i) + \lambda h \sum_i w_i n_j(\xi_i)\right), \tag{4.9}$$

namely a polynomial in ρ of order r, which may be linear or quadratic in λh, depending on the value of the shape functions n_j. The formula is A-stable if all the r roots satisfy the inequality $|\rho| \leq 1$, with $\mathrm{Re}(\lambda) < 0$, for any λh. The formula is L-stable if in addition the numerator of all the roots is one order less than the denominator in λh. If they are of the same order, then the ratio of the highest order terms of the numerator and the denominator represents the asymptotic value of the spectral radius; its norm is comprised between 1 and 0, and the formula has a behaviour between A- and L-stable, because it adds some algorithmic dissipation. Consider for instance the single-step case: the root is

$$\rho = \frac{1+\lambda h\left(\sum_i w_i m_1(\xi_i) + \lambda h \sum_i w_i n_1(\xi_i)\right)}{1-\lambda h\left(\sum_i w_i m_0(\xi_i) + \lambda h \sum_i w_i n_0(\xi_i)\right)}$$

Thus the formula is L-stable provided $\sum_i w_i n_0(\xi_i) > 0$ and $\sum_i w_i n_1(\xi_i) = 0$, or, in case $\sum_i w_i n_0(\xi_i) = 0$, for $\sum_i w_i m_0(\xi_i) > 0$ and both $\sum_i w_i n_1(\xi_i) = 0$, $\sum_i w_i m_1(\xi_i) = 0$. Similar conditions can be analytically formulated in case of a two-step method; higher step numbers are of little practical use. Figure 4.1 shows the spectral radius of some integrators of the family.

4.2.5 Implicit ODEs

The case of an implicit ODE, in the form

$$F(y, \dot{y}, t) = 0, \tag{4.10}$$

is straightforward, since the linearisation of the problem yields

$$F_{/\dot{y}} \Delta\dot{y} + F_{/y} \Delta y + F = 0, \tag{4.11}$$

and the perturbation of $\dot{y}$ can be explicitated as shown in Eq. 4.1; then the solution procedure is analogous to that of the explicit ODEs, only the inversion of $F_{/\dot{y}}$ is required.

4.2.6 Algebraic-differential equations

When $F_{/\dot{y}}$ in Eq. 4.11 is not invertible, the system is differential-algebraic, and a different approach must be used. Consider a problem of the form of Eq. 4.10, whose linearisation is presented in Eq. 4.11. Consider now the approximated form of the fundamental theorem of integral calculus, Eq. 4.6, whose perturbation yields

$$\Delta y_n = h \sum_j w_j \Delta\dot{y}(\xi_j). \tag{4.12}$$

The perturbation of $\dot{y}$ is required at each collocation point ξ_i, so the problem must be solved in all those points. The perturbation of y at time ξ can be obtained from the linearisation of the interpolation formula, Eq. 4.7, using Eq. 4.12 to express the perturbation of y at the end of the time step in terms of the perturbations of $\dot{y}$. So the system now consists of as many equations as the collocation points are, plus the problem collocated at the end of the time step, if this is not one of the collocation points yet. The unknowns are the $\Delta\dot{y}$ at the points in which the system is solved, resulting in

$$\begin{aligned} F_{/y}\big|_{\xi_i} \left(m_0(\xi_i)\, h \sum_j w_j \Delta\dot{y}\left(\xi_j\right) + h n_0(\xi_i)\, \Delta\dot{y}\,(0) \right) & \\ + F_{/\dot{y}}\big|_{\xi_i} \Delta\dot{y}(\xi_i) \quad = \quad & - F\big|_{\xi_i} \end{aligned} \tag{4.13}$$

for each collocation point.

4.2.7 Note on the classification of the method

The formulation that has been presented for the solution of differential-algebraic equations clearly shows that the proposed method closely resembles the general Implicit *Runge-Kutta* (IRK) method for the integration of differential equations. The basic formulas of IRK schemes are here recalled; the solution of $F\left(y, \dot{y}, t\right)$ is obtained by solving the system

$$F\left(Y_i, \dot{Y}_i, t_{n-1} + c_i h\right) \;=\; 0,$$

at some intermediate points i, while the final solution is

$$y_n \;=\; y_{n-1} + h \sum_j b_j \dot{Y}_j;$$

estimates of the intermediate values of $y\left(t_{n-1} + c_i h\right)$ may be obtained as

$$Y_i \;=\; y_{n-1} + h \sum_j a_{ij} \dot{Y}_j.$$

The scheme can be summarised in the so called *Butcher* diagram

$$\begin{array}{c|c} c & \mathcal{A} \\ \hline & b^T \end{array} \;=\; \begin{array}{c|ccc} c_1 & a_{11} & \cdots & a_{1M} \\ \vdots & \vdots & \ddots & \vdots \\ c_M & a_{M1} & \cdots & a_{MM} \\ \hline & b_1 & \cdots & b_M \end{array}.$$

By considering a single-step scheme, the c_i become $1 - \xi_i$, the b_j become the weights w_j; there is no immediate correspondence for the a_{ij}, because the internal values of y are interpolated from the boundary values of y and of its derivative rather than from the internal values of $\dot{y}$. Only for specific cases a direct equivalence may be found: being $j = 1$ the beginning of the time step and $j = M$ the end of the time step, the general expression is $a_{i1} = m_0(\xi_i)\, w_1 + n_1(\xi_i)$, $a_{iM} = m_0(\xi_i)\, w_M + n_0(\xi_i)$, the other cases being $a_{ij} = m_0(\xi_i)\, w_j$. The property $\sum m_i = 1$ has been exploited to collect y_{n-1}.

The single-step, cubic interpolation, 4^{th} order accurate with no algorithmic dissipation method, detailed in Appendix B, coincides with the *Lobatto IIIA* of order 4, while the *Crank-Nicholson* formula, as is well known, is the *Lobatto IIIA* of order 2; the single-step, parabolic interpolation, 3^{rd} order accurate, L-stable method coincides with the *Radau IIA* method of order 3 (see [50], pp. 72–77).
The additional requirements for *stiffly accurate* methods, namely $c_M = 1$, $a_{Mj} = b_j$ for $j = 1, \ldots, M$ and $\mathcal{A}$ being nonsingular, in many cases are satisfied: the first by definition, since the proposed method naturally requires the last evaluation point to be the end of the time step to allow the explicitation of the problem; the second results from the satisfaction of the first, since the same formula, Eq. 4.6, is used to evaluate both the final and the intermediate tentative values of y, and $m_0(0) = 1$ and $n_0(0) = n_1(0) = 0$ hold. The last requirement depends on the nature of the interpolation function m_0 and on the order and the nature of the numerical integration scheme. The proposed schemes usually satisfy the criterion provided they do not use the beginning of the time-step as an internal point[4]; this holds true for the formulas that introduce algorithmic dissipation. No correspondence with IRK exists in case $r > 1$; in such case this formula can be interpreted as a multistep extension of the IRK methods; only very high-order methods can be formulated, which seem to be of little practical use in mutibody analysis due to excessive computational overhead, but may represent an interesting choice for specific, accuracy demanding problems.
This formulation may help in putting the RK methods in a new light, since it shows how those popular integration formulas may be cast in a finite element-like numerical integration scheme. Moreover, the family of integration formulas is even broader since it operates a sort of unification of RK and multistep integration schemes.

4.2.8 Higher-order formulas

Higher-order formulas have been developed, all of them requiring multiple Jacobian matrix computations and Jacobian multiplications[5]. When a single-step, third-order Hermitian polynomial interpolation is used, a fourth-order accurate formula with no algorithmic dissipation, or a third-order accurate formula with tunable algorithmic dissipation are obtained. This approach has been considered unfeasible for a multibody implementation because of the overhead due to the multiple Jacobian manipulation and to the loss of matrix sparsity that reduces the efficiency; only the two-step, second-order formula has been actually implemented in a multibody code. In Appendix B some higher-order formulas are de-

[4] In which case $a_{1j} = 0$ by definition.
[5] Or an increase of problem size, resulting from the addition of intermediate states as unknowns.

tailed, and their accuracy and stability properties are discussed along with the second-order formulas introduced in the following section. Figures 4.1, 4.2, 4.3 show a comparison of the spectral radii and of the damping and phase properties of some of the formulas that result from the proposed scheme.

4.2.9 Second-order formula

The second-order formula results from a two-step, parabolic interpolation for the m_i, with $n_i = 0$. The trapezoid rule, with three points corresponding to the start-, the mid- and the end-point of the considered time interval, is used. Since y is assumed to be parabolic, the integration of its derivative with the trapezoid rule strictly requires two points only, thus the three-point integration leaves an indetermination on the value of the weights, yielding

$$y_n = y_{n-2} + h\left(\left(\frac{1}{2}+\delta\right)\dot{y}_n + (1-2\delta)\,\dot{y}_{n-1} + \left(\frac{1}{2}+\delta\right)\dot{y}_{n-2}\right). \qquad (4.14)$$

A parabolic prediction for the $\dot{y}_n$, based on the derivatives of the cubic Hermitian polynomials with y_{n-i} and $\dot{y}_{n-i}$, $i = 1,2$, is used, namely

$$\dot{y}_n = -\frac{12}{h}y_{n-1} + \frac{12}{h}y_{n-2} + 8\dot{y}_{n-1} + 5\dot{y}_{n-2}; \qquad (4.15)$$

the formula has been implemented also with variable time-step, not presented here for sake of conciseness. A second-order accurate *Crank-Nicholson* formula, applied to the interval $[t_{n-2}, t_{n-1}]$,

$$y_{n-1} - y_{n-2} - \frac{h}{2}\left(\dot{y}_{n-1} + \dot{y}_{n-2}\right) = 0,$$

and multiplied by a weight $1-\alpha$, is added to the right-hand side of Eq. 4.14, yielding

$$\begin{aligned} y_n &= (1-\alpha)\,y_{n-1} + \alpha y_{n-2} \\ &+ h\left(\left(\frac{1}{2}+\delta\right)\dot{y}_n + \left(\frac{1}{2}(1+\alpha) - 2\delta\right)\dot{y}_{n-1} + \left(\frac{\alpha}{2}+\delta\right)\dot{y}_{n-2}\right). \end{aligned} \qquad (4.16)$$

The formula is intrinsically second-order accurate, as results from Figure 4.3; the parameters α, δ are used to tune the stability properties. They can be written in terms of the desired asymptotic spectral radius as

$$\begin{aligned} \alpha &= \frac{4\rho_\infty^2 - (1-\rho_\infty)^2}{4-(1-\rho_\infty)^2}, \\ \delta &= \frac{1}{2}\frac{(1-\rho_\infty)^2}{4-(1-\rho_\infty)^2}, \end{aligned}$$

where Equation 4.9 has been solved for coincident, real-valued asymptotic roots. Notice that, for $\rho = 1$, resulting in $\alpha = 1$, $\delta = 0$, a Crank-Nicholson like formula,

$$y_n = y_{n-2} + h\left(\frac{1}{2}\dot{y}_n + \dot{y}_{n-1} + \frac{1}{2}\dot{y}_{n-2}\right),$$

is obtained, with a three-point weighting of $\dot{y}$ in a formally single-step formula with $2h$ step size. In case of $\rho = 0$, with $\alpha = -1/3$, $\delta = 1/6$, the L-stable, two-step *Backwards Differentiation Formula* (BDF)[6],

$$y_n = \frac{4}{3}y_{n-1} - \frac{1}{3}y_{n-2} + \frac{2}{3}h\dot{y}_n,$$

is obtained. It should be noticed that the BDF are second-order accurate, but inefficient in most practical problems due to excessive algorithmic dissipation starting at very small $\mathrm{Im}(\lambda h)$, virtually at zero. This was the main reason the presented formula has been investigated, since it ensures better performances with little, if any, extra computational effort with respect to BDF. Figure 4.1 shows a comparison of the spectral radii that characterise some of the formulas of the family. Consider now the series expansion of the residual of the proposed formula,

$$E = -\left(\frac{1}{2}(1+\alpha) + 6\delta\right)h^3 + O\left(h^4\right);$$

the coefficient of the term in h^3, when $\rho_\infty = 1$, is -1, while, for $\rho_\infty = 0$, it is $-4/3$. There is an extremum point, for an intermediate ρ_∞, which happens to be at $\rho_\infty = -4 + \sqrt{21} \approx 0.58$ and yields an error $E = \left(3 - \sqrt{21}\right)/2 \approx -0.79$, whose absolute value is minimum.

When applied to the differential-algebraic problem, the formula simply results in the solution of the problem collocated at the end of the time step since, being $n_0 = 0$, there is no need for Jacobian multiplications, and the intermediate values of y, $\dot{y}$ are known because the formula is collocated exactly at the time step boundaries. The problem is

$$F_{/\dot{y}}\Delta\dot{y}_n + F_{/y}\Delta y_n = -F,$$

and Δy is expressed in terms of $\Delta\dot{y}$ by perturbing Eq. 4.16, yielding

$$\Delta y_n = h\left(\frac{1}{2} + \delta\right)\Delta\dot{y}_n, \tag{4.17}$$

so the problem becomes algebraic in $\Delta\dot{y}_n$:

$$\left(F_{/\dot{y}} + h\left(\frac{1}{2} + \delta\right)F_{/y}\right)\Delta\dot{y}_n = -F, \tag{4.18}$$

[6]See Ref. [17], pp. 41–42.

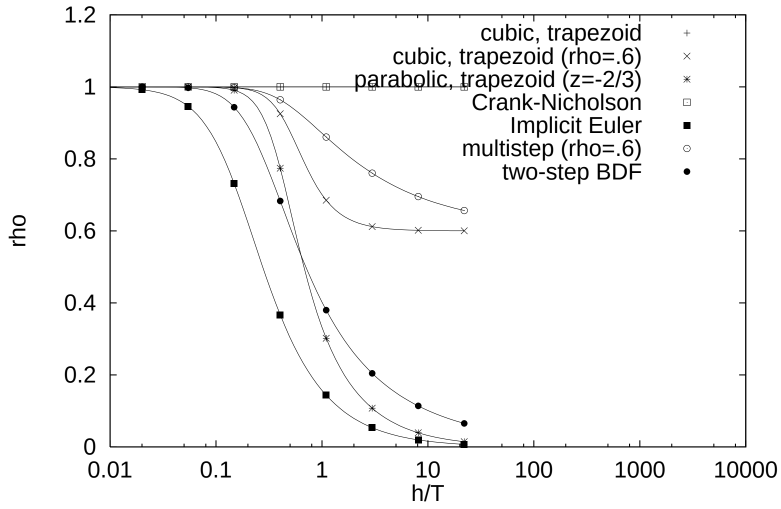

Figure 4.1: Integration formulas — spectral radii, ρ.

with Eq. 4.17 as update rule, while Eqs. 4.15 and 4.16 are used to predict $\dot{y}$ and y respectively. Notice that this is a special case of Eq. 4.13, written at $\xi = 0$ only, with $m_0 = 1$, $n_0 = 0$ and $w = 1/2 + \delta$.

4.2.10 Further remarks on stability

The proposed method is shown to be tunable between *A*- and *L*-stability, ranging from none to total algorithmic dissipation. These considerations involve the linear stability, that is local. The global stability of the integration is a completely different matter, and it cannot be ensured by the formula alone. On the contrary, the problem and the integration formulas must be designed to intrinsically ensure global stability in some sense. For purely mechanical problems the formulation can be rewritten to intrinsically preserve[7] the total energy and the angular momentum balance. This approach is surely more respectful of the nature of the problem, but might lack in generality when multidisciplinary, multifield integrated problems are addressed, as in this case. Surely some preservation law can be drawn out of every discipline, e.g. chemical reactions, electric networks and so on, but such an effort is considered too expensive when the major limitation of the general, "off-the-shelf" approach here considered, is simply the need to reduce the

[7]Such formulation is somewhat useless, in fact most of the authors refer to energy dissipating rather than energy preserving algorithms. This is because except for very simple cases, "stiff" and practical problems usually require the dissipation of high frequency perturbations that originate from the numerical approximation. See for instance [6].

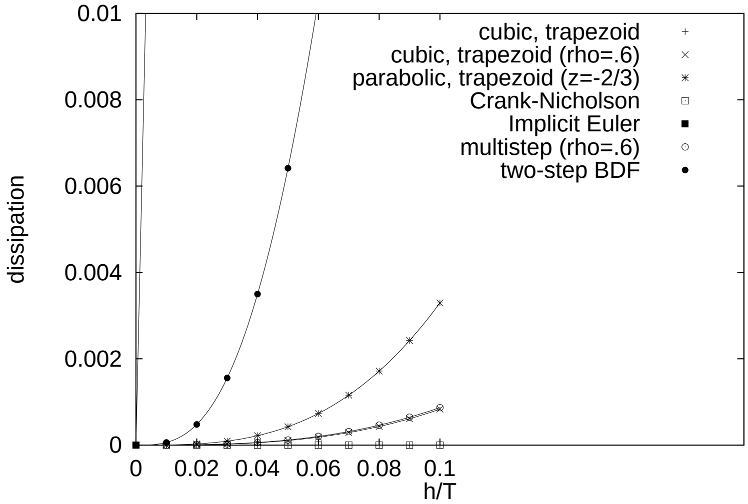

Figure 4.2: Integration formulas — damping error, ε_ξ (undamped system).

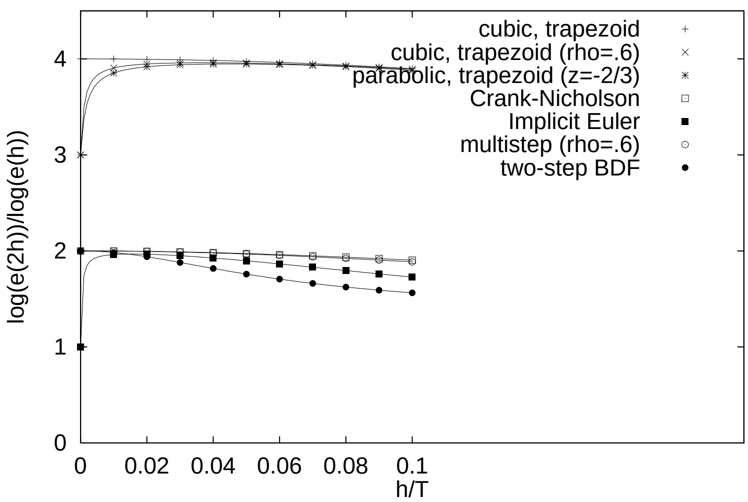

Figure 4.3: Integration formulas — phase error order, $\log_2\left(\varepsilon_\varphi(2h)/\varepsilon_\varphi(h)\right)$ (slightly damped system).

integration time step to achieve satisfactory stability properties. In fact accuracy requirements already demand for a time step size that in the vast majority of the applications provides for global stability of the integration. One idea that has been proposed to try to catch up with energy preserving schemes, and thus to provide some global stabilisation, is that of adding a scalar constraint on the total energy of the system[8]. This seems to be unpractical because, as emerged from a talk with Professor *Borri*, it might inhibit the use of energy dissipating formulas; in fact, the energy at high frequency, that is dissipated by the algorithm, could be pumped back into the system at low frequencies by the constraint. The problem might be fixed by imposing the constraint on the time derivative of the total energy, so the energy itself would be free to drift, and its growth would be a clear sign of loss of stability; however these aspects have not been investigated.
The above reported value for $\rho_\infty \approx 0.60$ proved to give adequate damping in most applications with very good accuracy, without any stability loss. Higher values, of the order of $0.85 \div 0.90$, led to instabilities when integrating stiff mechanical systems rotating at high speed ($|\omega h| \approx 0.1$); in non-rotational problems even $\rho_\infty = 1$ can be used, at the cost of undesirable lack of algorithmic dissipation. Smaller values have been used, sometimes with appreciable loss of accuracy.

4.3 Start-up of the simulation

This section deals with practical problems that arise when integrating a differential-algebraic problem. A differential-algebraic initial-value problem consists in a differential-algebraic equation with appropriate initial conditions. These initial conditions are represented by the state of the system, namely the position and the velocity of the bodies when a mechanical problem is considered. The initial state of the system must satisfy the algebraic constraints[9] to be consistent. Moreover, the velocities must satisfy the time derivative of the constraint to allow a consistent initial motion of the system; the other unknowns require some additional specifications. The linear and angular momenta can be computed from their definitions as functions of the state and thus are determined. The derivatives of the momenta and the constraint reactions, on the other hand, must satify the equilibrium at the initial time, as they result from the problem. The point is that the algebraic part of the problem allows multiple solutions, what is called, for linear, constant coefficient DAEs, a *pencil*[10]. This can be clarified by considering that in a constrained problem the acceleration of a constrained body, for a given state, can assume any value, provided the corresponding inertia force is balanced by an appropriate con-

[8]Such constraint needs not be a pure preservation, unless the system is closed.
[9]The same applies to the velocities, that must satisfy the non-holonomic constraints.
[10]See Ref. [17], p. 18.

straint reaction. The choice of the initial values for linear and angular momentum derivatives, and for constraint reactions, requires to decide which problem we want to solve. The "right" problem is the one that complies not only with the algebraic constraint, but also with its time derivatives up to one order less than the index of the DAE problem; up to second order for mechanical systems, to yield continuous values for the derivatives of the linear and angular momentum. In such case, the initial motion of the system will account for the presence of the constraint and yield a regular solution. If such condition on the satisfaction of the highest derivative of the constraint is not fulfilled, the problem is still legal, but it is ill-posed, because as the integration starts, the constraint is violated and the constraint reactions must restore the compatibility, yielding a solution that is discontinuous in the derivatives of the momenta and in the constraint reactions. However the above described solution is regular only in a local sense. In fact, a solution respective of the equilibrium and of the derivatives of the constraints can still lead to a rough solution in some global sense. Consider the practical example of a flexible rotor blade whose integration starts with the blade rotating at constant angular velocity but with no centrifugal loads. The state is correct in terms of positions and velocities; the constraint at the root is satisfied as well as its derivatives up to second order are; nonetheless, an axial load wave propagates from root to tip as soon as the inertia along the blade "feels" the centripetal effect of the constraint. Moreover, since the axial stiffness of the blade is usually high, the celerity of the wave is high, so it cannot be integrated accurately at typical integration time steps, leading to the numerical problems discussed earlier in this chapter. This problem is well-posed, the initial conditions comply with balance and constraint equations to the desired order, the solution is "regular", but "stiff". In this case the stiffness of the problem is emphasized by the initial conditions, as usually happens. A globally regular solution starts from steady initial values of the state; in the previously mentioned example, the rotor blade must be appropriately strained to apply the right centripetal effect to its inertia. A steady set of initial values results from the solution of an initial trim problem; it is not sufficient for the state to be respectful of equilibrium and compatibility, it must satisfy also the trim condition. Steady in some cases means "static"; in dynamic systems, like helicopter rotors, it rather means "periodic". In this work, the steady initial values are not directly determined. On the contrary, usually the integration does not even start at locally regular initial values. A locally regular solution is obtained by integrating the system, during the very first steps, by a procedure detailed later, while a globally regular, steady solution, i.e. a trimmed condition, is obtained by artificially cancelling, by means of the algorithmic dissipation, the transient due to the initial values, in absence of external perturbations. The different phases of the start-up are detailed in the following.

4.3.1 Initial assembly

In usual problems, the initial conditions are available only to some extent, and under some conditions. The canonical initial conditions of an initial value problem are the values of the unknowns at the initial time; the initial value of the derivatives is computed from the problem itself, e.g. $\dot{y} = f(y,t)$ in case of an ordinary differential problem. The initial values must be available and must satisfy the algebraic part of the problem, i.e. $\Phi(y_0,t_0) = 0$. Moreover, they should also satisfy higher-order time derivatives of the algebraic constraint, which are implied by the algebraic constraint itself, but not not automatically satisfied by the numerical solution, otherwise the constraint would be violated as the integration starts.
In case of a simplified mechanical problem, written in Lagrangian form of the first kind, i.e. Eq. 2.2, the initial conditions are the position and the velocity of each body at the initial time, while the initial value of the linear and angular momentum, as well as their time derivative, must be obtained from the problem. Both the position and the velocity of each body are not independent, so the satisfaction of the algebraic equations must be ensured. An assembly procedure has been developed, based on the idea that the differential part of the system should be left free to change its initial conditions under the algebraic constraints, since the highest-order derivatives of the differential unknowns, as well as the algebraic unknowns, can accomplish for the satisfaction of the differential equations. An algebraic system is written, with the algebraic part of the original problem, and with fictitious springs that keep the differential unknowns close to their tentative initial position, namely

$$\left\{\begin{array}{rcl} K\Delta y + \Phi^T_{/y}\Delta\zeta & = & -K(y-y_0) - \Phi^T_{/y}\zeta, \\ \Phi_{/y}\Delta y & = & -\Phi(y,t_0). \end{array}\right.$$

Here K is a fictitious stiffness matrix that may have the very simple form of a scaled identity matrix, $K = kI$, or it may be more articulated, with independent diagonal coefficients and even element stiffness matrices for flexible elements in a finite element fashion, to allow the tuning of the compatibility, i.e. to force some specific degrees of freedom to change their initial value instead of others. The latter choice has been made in the implementation, so that the flexible elements contribute with their stiffness matrices, and each node has independent diagonal stiffness coefficients. The fictitious algebraic unknowns ζ have been used instead of z because their value is discarded after the assembly, since they do not represent the actual algebraic reactions, but simply a measure, in a *Lagrangian multiplier* sense, of the activation of the algebraic constraints. The same procedure is applied to the time derivatives of the y; in this case the time derivative of the constraint equation is added, together with extra fictitious reactions that enforce the satisfaction of the extra constraints. The result is an initial solution that is compatible to the first order. It is important to understand that the solution strongly depends on the initial values, which include the initial velocities. The compatibility of the velocities is not explicitly stated by the differential-algebraic problem; nonetheless, it is strongly required because of the index of the problem. If a non-compatible tentative initial solution is used, the compatible initial solution that results from the assembly procedure depends on the values of the fictitious springs, and thus it might be quite different from the initial solution actually desired by the user, so this procedure should be considered a sort of compatibility check rather than a really "universal" startup technique. Imagine for instance the purely kinematic one-dimensional problem of two rigidly linked points, that are given a compatible initial relative position equal to the length of the joint but different, non-compatible initial velocities; the assembly procedure will make the two initial velocities equal, but their value will be the mean of their incompatible velocities, weighted by the stiffness of the respective fictitious springs. The point is there is no "right" solution to such problem; on the other hand, it is not easy to supply a thoroughly compatible set of initial values. Thanks to this procedure, the user can "suggest" the desired behaviour by means of the stiffness of the springs. In the previous example, where the user might be trying to simplify the input by supplying the velocity of one point only, expecting the rest of the system to follow it, the desired behaviour can be obtained by giving unit weight to the node whose velocity is given, and null weight to the remaining nodes; as a result, the mechanism is pulled by the first node and a compatible set of initial velocities is obtained.

4.3.2 Derivatives computation

After ensuring the satisfaction of the algebraic equations, the differential equations must be satisfied as well, to start from a balanced as well as compatible initial solution. In an explicit differential problem, this operation is very simple, consisting in computing the initial derivatives as

$$\dot{y}_0 = f(y_0, t_0);$$

in an implicit, differential-algebraic problem the same operation requires some care. Consider again the example of a mechanical system, after the compatibility has been assessed and restored if required. Suppose the initial position and velocity of the bodies are known, and the algebraic equations are satisfied. The linear and angular momenta can be computed from their definition since the velocities are known. The only uncertainty is on the derivatives of the momenta and on the value of the algebraic reactions. They should be computed by solving the differential system made of the equilibrium equations plus the second-order time derivative of the constraints, requiring a dedicated solution procedure. In the present work, a rather different strategy has been investigated, consisting in solving the entire system in the usual form, thus resorting to the normal routines for the computation of the Jacobian and of the residual, and in iterating the solution at the initial time with a modified updating procedure. In fact, when solving at the initial time for the derivatives only, the idea is to integrate the system with a null time step, so that the update rule of Eq. 4.17 does not affect the value of the momenta, that are exactly computed by means of the initial velocities. This is not possible because the system becomes singular: consider the application of the second-order formula of Eq. 4.18 to a simplified, linear system in Lagrangian form of the first kind,

$$\begin{bmatrix} M & -cI & 0 \\ cK & I & \Phi^T_{/y} \\ \Phi_{/y} & 0 & 0 \end{bmatrix} \begin{Bmatrix} \Delta\dot{y} \\ \Delta\dot{z} \\ \Delta v \end{Bmatrix} = \begin{Bmatrix} -M\dot{y}+z \\ F-Ky-\dot{z}-\Phi^T_{/y}v \\ -\Phi/c \end{Bmatrix}$$

where c is the coefficient of the update formula of Eq. 4.17; the last block-row, containing the algebraic equations, has been divided by c for numerical purposes[11]. If a null time step is considered, the matrix is singular, because the coupling terms between the differential unknowns vanish, being $c \approx h$. So an arbitrary time step is used, but the computation of the solution is modified by updating the derivatives of the differential unknowns and the algebraic unknowns only, except for the derivatives of the displacements, namely the $\dot{y}$. They are left untouched, as are the differential unknowns: the y, computed by means of the initial assembly procedure, and the momenta z, directly computed from their definition by means of the compatible initial velocities. Due to their peculiar structure, the mechanical problems are usually linear in the derivatives of the momenta and in the algebraic unknowns, so the solution requires very little iterations, usually one only, to obtain initial derivatives that satisfy the equilibrium. The very important drawback is that such solution is not respectful of the second-order derivative of the constraint equation, resulting in "non-compatible" derivatives of the momenta, so special attention, in Section 4.3.4, will be dedicated to the problem. The main advantage is that no dedicated procedures for the determination of the initial conditions are required.

4.3.3 Self-starting algorithm

The integration formula presented in Section 4.2 is two-step, so it is not able to start automatically when the initial conditions at one point only are provided. The problem has been overcome by using, for the first step, a second-order accurate,

[11] As suggested in [17], pp. 144–148, to obtain a better scaling of the matrix and thus to reduce roundoff errors.

single-step Crank-Nicholson formula. This formula is self-starting because it is single-step, and it has the desired second-order accuracy, so the numerical solution is guaranteed to remain confined in a neighborhood of the exact solution[12]. The Crank-Nicholson rule is A-stable, with no algorithmic dissipation, so numerical oscillations may arise; they can be damped by introducing some algorithmic dissipation in the subsequent time steps performed with the formula proposed in Section 4.2. The algorithmic dissipation may be required also for the reasons addressed in the following section.

4.3.4 Second derivative of the constraints

Earlier in this chapter, the problem of satisfying the second-order time derivative of the constraints has been introduced. This problem is very important, as a very simple example will show. Consider, for instance, a rigid pendulum performing a plane motion under the effect of gravity acceleration. In the spirit of the multibody approach, it is modelled by a rigid body, constrained by a distance joint, namely $x^2 + y^2 = l^2$, being x and y the coordinates of the mass and l the length of the pendulum. If we assume that the initial position and velocity respectively satisfy the constraint equation and its derivative, i.e. the velocity os tangent to the circular path of the pendulum, and we compute the momentum, its derivative and the reaction force as shown in Section 4.3.2, we obtain an initial solution that satisfies the constraint and the equilibrium, but with constraint reaction and momentum derivatives that account for the gravitational effect only. So, as the integration starts, the solution violates the constraint, because the derivative of the momentum does not account for the centripetal effect of the constraint, which descends from its second-order derivative. The integration does not fail, but oscillations in the reaction force arise, and the solution is perturbed. Notice that this effect resembles the behaviour of a flexible pendulum, the rigid one being a sort of limit case of a true pendulum, and the algebraic constraint being a sort of limit case of a stiff spring [49]
A procedure to overcome this effect has been developed, consisting in performing a sort of *numerical* differentiation of the constraint by integrating the system with a very short time step, to minimize the amplitude of the oscillations, and with high algorithmic dissipation, to completely dampen the numerical oscillations as quickly as possible. After achieving a good estimate of the momentum derivatives and of the reaction forces, the system is restarted with the desired time step. Such procedure showed a good behaviour in many problems of different complexity,

[12]As shown in [17], Section 3.2, the BDF convergence properties for a semi-explicit index three DAE require the starting conditions to satisfy some accuracy properties. See Appendix C for further details.

including rotorcraft simulations. The main reason for its choice is to avoid to implement the second-order derivatives of the constraints, that can be very cumbersome. Of course, if very special problems must be considered, whose solution requires a very accurate start-up, it may be necessary, and even convenient, to make such an effort.

Chapter 5

Configuration-dependent interactions

The bodies that build up a system may exchange relative, or internal forces of different nature, e.g. elastic, gravitational, electromagnetic, contact, or friction forces, and many other kinds of interactions. In many cases those forces depend on the configuration of the system, i.e. on the absolute or relative position, velocity and acceleration of the bodies. In this section we basically deal with elastic interaction, but other sources of relative forces may be treated in a similar way. It is important to notice that, regardless of the mathematical model those forces are based on, their application to a multibody context will result in discrete forces that act on discrete bodies, and the configuration field they are computed from will result from some interpolation of the configurations of the discrete bodies that represent the multibody model. In fact, in the present work, the definition "multibody" has the currently accepted meaning of "nonlinear finite elements, with exact nodal kinematics". As a consequence, a multibody model may range from a very simple collection of rigid bodies joined by kinematic constraints, to a rather sophisticated model of a structural elastic component, such as a rotor blade, or a complete helicopter, with flexible components modelled with a finite element-like discretisation of a three-dimensional continuum.

V^3		space of vectors in $\Re^3$
p	V^3	position of a point
v	V^3	velocity of a point ($= \dot{p}$)
R	$\mathrm{LIN}\left(V^3\right)$	rotation matrix (from local to global frame)
$\omega\times$	$\mathrm{lin}\left(V^3\right)$	angular velocity
x	V^3	position of a reference point (node)
f	V^3	offset (relative position, $= R\tilde{f}$)

5.1 Lumped flexible elements

A lumped flexible element is represented by a discrete force or moment that acts between a pool of bodies, usually two, depending on their relative configuration, i.e. the distance, or the relative rotation, or both[1]. This allows to introduce the expressions for the relative entities that can be used to compute the actions related to flexible elements. The configuration of a body is expressed by means of its *position* in the global frame, x, whose time derivative is the global *velocity* of the body, $\dot{x}$, that has already been used in the definition of the momenta, Eq. 1.1. The orientation of the body is expressed by means of its *rotation matrix*, R, that transforms a vector in the local reference frame, usually denoted with a tilde $\tilde{(\cdot)}$, into its representation in the global frame. The time derivative of the rotation matrix is related to the angular velocity, ω; they have been both introduced in the discussion on the finite rotations in Chapter 3. A point whose position is used to compute the force may be offset from the node by a vector $\tilde{f}$, that is usually constant in the local frame. As a result, the position of an arbitrary point rigidly attached to a node is

$$p = x + f, \tag{5.1}$$

where $f = R\tilde{f}$ is the offset in the global frame. The orientation at the point, if required, is that of the body, possibly corrected by a constant orientation matrix R_h, namely

$$R_p = RR_h.$$

Consider for instance a simple spring, represented by a force acting along the line between two points that depends on their distance. The distance is a vector $d = (x_2 + f_2) - (x_1 + f_1)$, whose norm is the length of the spring, $l = |d|$. The force is $F = (d/l)\,s(\varepsilon)$, the scalar force expressed by the constitutive law s arbitrarily depending on the normalised elongation of the spring, $\varepsilon = l/l_0 - 1$, based on some initial measure of the length, l_0. This force is applied to both nodes 1 and 2, with opposite sign, $F_1 = -F$, $F_2 = F$, in the points with offsets f_1 and f_2 from the respective nodes, so the nodes themselves are also subject to the moments $M_1 = -f_1 \times F$, $M_2 = f_2 \times F$. The introduction of a dependence of s on the relative velocity of the points leads to a visco-elastic element. The relative velocity is related to the time derivative of the distance d, namely $\dot{l} = d \cdot \dot{d}/l$, where $\dot{d} = (\dot{x}_2 + \omega_2 \times f_2) - (\dot{x}_1 + \omega_1 \times f_1)$; in other words, it represents the projection of $\dot{d}$ in direction d/l. More sophisticated models, based on three-dimensional

[1] A finite element beam, for instance, falls into this category, but, as commonly accepted, it is treated differently since it is intended to describe a structured one-dimensional continuum.

springs, with anisotropic constitutive laws, or rotational springs, may be formulated, and have been actually implemented in the code; their definition and implementation is beyond the scope of this section, and will be treated in Appendix D.2. It is important to remark that in such complex lumped elastic components, the geometry of the actual component must be reproduced with care, to ensure the finite strains are correctly described and the model is representative of the component. An example of such a complex lumped viscoelastic component is an elastomeric bearing, currently used in many commercial rotorcrafts.

5.2 Beam model

A beam element is a good example of a rather simple flexible component that can be introduced in a multibody model in a finite element style. It can be used to model very important structural components with an acceptable degree of accuracy and refinement expecially in rotorcraft modelling, when the flexibility of the blade is to be considered without excessive detail.

B	$\Re$	domain of the beam
S	$\Re^2$	domain of the section
s	$B \times S \mapsto V^3$	position of a point
p	$B \mapsto V^3$	position of the reference line
R	$B \mapsto \mathrm{LIN}\left(V^3\right)$	rotation matrix (from local to global frame)
t	$S \mapsto V^3$	offset of a point from the reference line
e_i	$B \mapsto V^3$	directions of R
l	$B \mapsto V^3$	slope of the reference line ($= p_{/\xi}$)
$\rho\times$	$B \mapsto \mathrm{lin}\left(V^3\right)$	curvature of the beam ($= R_{/\xi}R^T$)
ν	$B \mapsto V^3$	generalised strains of the reference line
$\kappa\times$	$B \mapsto \mathrm{lin}\left(V^3\right)$	generalised elastic curvature of the section
v	$B \mapsto V^3$	velocity of the reference line
$\omega\times$	$B \mapsto \mathrm{lin}\left(V^3\right)$	angular velocity of the section
ψ	$B \mapsto V^6$	generalised deformations
F	$B \mapsto V^3$	internal forces
M	$B \mapsto V^3$	internal moments
ϑ	$B \mapsto V^6$	generalised internal forces
τ	$B \mapsto V^6$	generalised external forces per unit length
x	V^3	position of a node
f	V^3	offset of the reference line from a node

5.2.1 Definitions

A beam is a structural component whose geometric, structural and inertial properties change very smoothly along one direction, that is predominant over the other two. More detailed and specialised definitions of the beam model may be misleading, because they imply underlying assumptions that restrict somehow the model to special cases. The restricting assumptions that are made in this work will be presented as soon as they are required, to clearly indicate the properties of the model we call "beam". The predominant direction of the structural component naturally identifies a line, or better the slope of a line, that will be used as reference. A plane, nearly normal to the predominant direction of the beam, will identify a section of the component, and some reference on this section will allow us tho choose two orthogonal axes to define a local reference system. The beam is generated by a rigid rototranslation of the section along a predominant direction. A continuous, regular and limited variation of the section may be accepted, at some cost that will be highlighted later[2]; a sharp change of section properties, on the contrary, can be handled by partitioning the domain of definition of the beam in multiple, piecewise uniform beams, with some interface represented by continuity boundary conditions. This suggests that, for practical purposes, a finite element-like string of piecewise uniform beams can be used to describe a tapered beam. Notice that we are not defining a system based on some geometric, structural or inertial property of the structural component, but we are simply trying to put some references onto a geometric entity to give a quantitative description of its properties, under the assumption that a different choice of references, with an appropriate reduction to a common reference configuration, will be able to give the same description. The reference line is called p. The direction e_1 of the section frame is close to that of the slope l of the line p, being $l = p_{/\xi}$, where ξ is a local abscissa. In fact, the section reference frame needs not be exactly normal to the slope of the reference line; the only assumption we make is that $e_1 \cdot l$ be positive regardless of the deformation level.

5.2.2 Kinematics of the beam

An arbitrary point on the section is identified by a vector $\tilde{t}$ in the frame of the section. In reference conditions, we assume its component in direction $\tilde{e_1}$ be null, so that the reference section is plane[3]. It may be non-null in a deformed condition,

[2]Basically, a non-uniform beam section requires to solve a variable coefficient linear differential system of equations, where a uniform beam section results in the solution of a constant coefficient system.

[3]This assumption is not strictly required and may be relaxed, allowing warped reference sections to be considered, but, since the properties of the section are required to be independent of the

to describe an out-of-plane warping of the section. So the position of an arbitrary point of the structural component, in an arbitrary configuration, is $s = p + t$, where $t = R\tilde{t}$ is the relative position of the point in the section, rotated into the global frame. The rate of change of the position of point s along the reference line gives a deeper insight into the beam model. Consider first a beam whose section is rigid, namely vector $\tilde{t}$ is constant. The reference line and the orientation of the section both depend on the local abscissa ξ, so the axial derivative of s yields

$$s_{/\xi} = p_{/\xi} + R_{/\xi}\tilde{t}.$$

By substituting the previously defined slope of p, and recalling the properties of the derivative of a rotation matrix (Eq. 3.2), it becomes

$$s_{/\xi} = l + \rho \times t, \tag{5.2}$$

where $\rho = \mathrm{ax}\left(R_{/\xi}R^T\right)$ is the curvature of the beam. So the change of configuration along the reference line of the beam can be described by means of two intrinsic vectorial quantities, the slope of the line and the curvature of the reference orientation of the section.

5.2.3 Strains and curvatures

The elastic deformation of the beam is defined as the change in the axial rate of the position, Eq. 5.2, due to a change in the configuration of the system. In order to be comparable, the two position rates must be rotated back to a common reference frame, called the material frame, which may be represented by the section frame with no loss in generality. By denoting with the subscript $(\cdot)_0$ the reference entities and with no subscripts the deformed entities, the difference between the axial rates results in[4]

$$R^T s_{/\xi} - R_0^T s_{0/\xi} = \left(R^T l - R_0^T l_0\right) + \left(R^T \rho \times R - R_0^T \rho_0 \times R_0\right) t,$$

or

$$R^T s_{/\xi} - R_0^T s_{0/\xi} = \left(\tilde{l} - \tilde{l}_0\right) + \left(\tilde{\rho} \times - \tilde{\rho}_0 \times\right) \tilde{t}.$$

The elastic strains and curvatures, in the material frame, are

$$\tilde{\nu} = \tilde{l} - \tilde{l}_0, \tag{5.3}$$

$$\tilde{\kappa} = \tilde{\rho} - \tilde{\rho}_0, \tag{5.4}$$

yielding

$$R^T s_{/\xi} - R_0^T s_{0/\xi} = \tilde{\nu} + \tilde{\kappa} \times \tilde{t}.$$

axial position, a reference section can always be redefined in order to be plane.

[4]Remember that $\tilde{t} = \tilde{t}_0$ because null warping is assumed.

5.2.4 Note on the linearisation of the curvature

The strains ν do not require any special attention; on the contrary, the curvature κ, when considered in view of the updated-updated approach introduced in Section 3.4, can be written as

$$\begin{aligned}\kappa &= \theta'_\delta + R_\delta \theta'^{(0)} \\ &= \kappa_\delta + \kappa^{[0]},\end{aligned}$$

where $\theta' = G(\mathrm{p})\,\mathrm{p}'$ regardless of the rotation parameters p that are considered. The strains are linearised in the material frame, because the constitutive law is naturally expressed in such frame. The linearisation of the curvature yields

$$\Delta\tilde{\kappa} = R^T \left(\theta_\Delta \times^T \kappa + \Delta\kappa\right). \tag{5.5}$$

Notice that the linearisation of the curvature in the global frame yields

$$\Delta\kappa = \Delta\kappa_\delta + \theta_\Delta \times \kappa^{[0]},$$

and its substitution in Eq. 5.5 simply yields

$$\Delta\tilde{\kappa} = R^T \left(\Delta\kappa_\delta + \kappa_\delta \times \theta_\Delta\right).$$

By considering the simplifications allowed by the updated-updated approach, such formulas can be effectively approximated with

$$\Delta\theta' \cong \Delta\mathrm{p}' + \Delta\mathrm{p} \times \theta'^{(0)},$$

and

$$\Delta\tilde{\theta}' \cong R^{(0)T} \left(\Delta\mathrm{p}' + \theta'_\delta \times \Delta\mathrm{p}\right).$$

The latter expression can be simplified even further by recalling that, according to the updated-updated approach, the perturbation of the curvature can be discarded when linearising, namely $\theta'_\delta \cong 0$, thus yielding

$$\Delta\tilde{\theta}' \cong R^{(0)T} \Delta\mathrm{p}'.$$

5.2.5 Strain and curvature time rates

The time rates of strain and curvature may be required to introduce some dependency of the internal forces on the dynamics of the beam, i.e. to introduce some viscoelatic effects in the internal forces and couples of the beam. The velocity of the arbitrary point s is defined as

$$\dot{s} = v + \omega \times t,$$

where $v = \dot{p}$ is the velocity of the reference line and ω is the angular velocity of the section. The axial derivative of the velocity yields

$$\frac{\mathrm{d}}{\mathrm{d}\xi}\dot{s} \; = \; v_{/\xi} + \omega_{/\xi} \times t + \omega \times \rho \times t,$$

while the time derivative of the axial rate of s results in

$$\frac{\mathrm{d}}{\mathrm{d}t} s_{/\xi} \; = \; \dot{l} + \dot{\rho} \times t + \rho \times \omega \times t;$$

it is apparent from *Schwartz*' theorem that $\dot{p}_{/\xi} = \dot{l}$; by the same theorem, the relation $\dot{\rho} = \omega_{/\xi} + \omega \times \rho$ can be inferred. The time rates of the strain and of the curvature, in the material frame, are

$$\begin{aligned} \dot{\nu} &= R^T \left(\dot{l} - \omega \times l\right), \\ \dot{\kappa} &= R^T \left(\dot{\rho} - \omega \times \rho\right). \end{aligned}$$

Their linearisation is straightforward.

5.2.6 Equilibrium

The differential equilibrium equations for a rigid section beam can be easily obtained by considering that the axial derivative of the work made by the internal forces of the beam subject to a rigid rototranslation must be null. The virtual displacement of the reference point of the beam at abscissa *xi*, due to a rigid rototranslation, is $\delta p(\xi) = \delta p(0) + \delta\varphi(0) \times (p(\xi) - p(0))$, while the virtual rotation is $\delta\varphi(\xi) = \delta\varphi(0)$. Being $F(\xi)$, $M(\xi)$ the internal forces and moments of the beam at point ξ, such condition results in

$$\frac{\partial}{\partial \xi}\left(\left(\delta p(0) + \delta\varphi(0) \times (p(\xi) - p(0))\right) \cdot F(\xi) + \delta\varphi(0) \cdot M(\xi)\right) \; = \; 0,$$

which, after simple algebra manipulation, yields

$$F_{/\xi} \; = \; 0, \tag{5.6}$$

$$M_{/\xi} + l \times F \; = \; 0, \tag{5.7}$$

where $l = p_{/\xi}$ has been used, and the moments equation has been evaluated in $p = 0$ without any loss in generality. These equations will be used to write a discrete form of the equilibrium of a portion of beam in Section 5.4.

5.3 Beam section characterisation

The internal forces of the beam must be written as functions of the generalised deformations, namely the strains and the curvatures, by means of an adequate constitutive law. The constitutive law is required to close the system of the equilibrium equations, in which the internal forces and moments are unknown, by writing them in terms of the generalised strains, and thus of the configuration of the beam. This result can be obtained by finding a compatible solution for the problem of a sample section of the beam loaded by indicial internal forces. The constitutive law of the beam is not determined from the first principles of micromechanics of materials; the constitutive problem is simply scaled down to the continuum mechanics, by eliminating the dependence on the geometry of the section through the determination of a set of solutions that are respectful of the kinematic and natural boundary conditions of the beam section. Many authors have been working on the characterisation of beam sections, a complete review being out of the scope of this dissertation; the interested reader should consult the good one given by *Hodges* in 1990 [56], and refreshed in 1999 [86]. Only a brief review of the previous works done at the *Dipartimento di Ingegneria Aerospaziale* of the *Politecnico di Milano* is presented. The very first note on the characterisation of semi-monocoque sections appeared in 1977 by *Mantegazza* [67], followed by a comprehensive formulation of the problem for the linear analysis of arbitrary sections, presented in 1983 by *Giavotto et al.* [44], specialised to the analysis of rotor blades by *Borri* and *Mantegazza* in 1985 [13] and subsequently extended and generalised in a geometrically nonlinear framework by *Borri* and *Merlini* in 1986 [14]. In 1992 *Borri et al.* solved the problem of the characterisation of a twisted/curved beam [12], and in 1994 *Ghiringhelli* and *Mantegazza* showed the possibility to use a commecial finite element code to characterise a straight, untwisted beam [31]. In 1997 *Ghiringhelli* and *Ghiringhelli et al.* extended the formulation to the analysis of thermal loads [28] and to the electroelastic characterisation of a composite beam embedding piezoelectric materials [34]. The extension to the analysis of piezoelectric materials represents a fundamental part of the graduation thesis of the author [68]; it is reported and generalised in Section 9.1. The notation introduced in [31] is basically preserved in this work, with some differences, the most important being the change in the denomination of the reference axes; in the original work, the beam axis was z, with x and y lying in the section, while here the beam axis is ξ, and η and ζ define a Cartesian frame on the section.

$\mathcal{M}$, $\mathcal{C}$, $\mathcal{L}$, $\mathcal{E}$, $\mathcal{R}$, $\mathcal{A}$		stiffness matrices of the section
U_0, U_1	$B \mapsto V^{3\times N}$	indicial section discrete warping
P_0, P_1	$B \mapsto V^{3\times N}$	indicial section nodal work
Ψ_0, Ψ_1	$B \mapsto V^6$	indicial generalised deformations
Θ_0, Θ_1	$B \mapsto V^6$	indicial generalised internal forces

5.3.1 Kinematics of the section

Consider the position s of a point on an arbitrary section, discarding the previous assumption of constant warping $\tilde{t}$. The differentiation of s now requires the three-dimensional gradient, defined as

$$\nabla(\cdot) \;=\; \left\{(\cdot)_{/\xi}, (\cdot)_{/\eta}, (\cdot)_{/\zeta}\right\}. \tag{5.8}$$

The gradient operator, Eq. 5.8, applied to position s yields

$$\nabla s \;=\; \{l, 0, 0\} + \{\rho\times, 0, 0\}\, t + R\nabla\tilde{t},$$

and the linear[5] strains at such point are represented by the symmetric part of ∇s, in which the differentiation with respect to the local transverse coordinates on the section, $\{\eta, \zeta\}$, is also considered, namely

$$d \;=\; \frac{1}{2}\left(\nabla s + \nabla s^T\right).$$

The elastic strains are obtained as the difference between the deformed and the reference symmetric part of the gradient of the position, rotated back into the material frame, namely $\varepsilon = R^T d - R_0^T d_0$; the elastic gradient is

$$\begin{aligned} R^T\nabla s - R_0^T\nabla s_0 \;&=\; \left\{\tilde{l} - \tilde{l}_0, 0, 0\right\} + \{\tilde{\rho}\times, 0, 0\}\,\tilde{t} \\ &\quad - \{\tilde{\rho}_0\times, 0, 0\}\,\tilde{t}_0 + \nabla\left(\tilde{t} - \tilde{t}_0\right); \end{aligned}$$

the gradient of the reference warping, $\nabla\tilde{t}_0$, represents a measure of the axes η and ζ, since the reference warping $\tilde{t}$ is assumed to be independent of ξ and to have null component in direction $\tilde{e}_1$. By arranging the strains as $\varepsilon = \{\gamma_{23}, \varepsilon_{22}, \varepsilon_{33}, \varepsilon_{11}, \gamma_{12}, \gamma_{13}\}$, the following compact matrix notation can be used:

$$\tilde{\varepsilon} \;=\; \left\{\begin{array}{c} 0 \\ \tilde{\nu} + \tilde{\rho}\times\tilde{t} - \tilde{\rho}_0\times\tilde{t}_0 + \tilde{t}_{/\xi} \end{array}\right\} + \mathcal{D}\left(\tilde{t} - \tilde{t}_0\right)$$

or, by recalling that $\tilde{\rho} = \tilde{\rho}_0 + \tilde{\kappa}$, Eq. 5.4,

$$\tilde{\varepsilon} \;=\; \left\{\begin{array}{c} 0 \\ \tilde{\nu} + \tilde{\kappa}\times\tilde{t} + \tilde{\rho}_0\times\left(\tilde{t} - \tilde{t}_0\right) + \tilde{t}_{/\xi} \end{array}\right\} + \mathcal{D}\left(\tilde{t} - \tilde{t}_0\right)$$

[5] A more general, nonlinear formulation can be obtained by considering *Green*'s strain tensor, in matrix notation: $d = 1/2\left(\nabla s + \nabla s^T\right) + \nabla s^T\cdot\nabla s$.

where $\tilde{\nu}$, $\tilde{\kappa}$ are the generalised deformations of the rigid section as defined in Section 5.2, and operator $\mathcal{D}(\cdot)$ performs the strain-related differentiation in the plane of the section, i.e.

$$\mathcal{D}(\cdot) = \left[\begin{array}{ccc} 0 & (\cdot)_{/\zeta} & (\cdot)_{/\eta} \\ 0 & (\cdot)_{/\eta} & 0 \\ 0 & 0 & (\cdot)_{/\zeta} \\ 0 & 0 & 0 \\ (\cdot)_{/\eta} & 0 & 0 \\ (\cdot)_{/\zeta} & 0 & 0 \end{array}\right]$$

The general case of a constant curvature/pretwist beam is presented. It has been first studied by Borri *et al.* in [12]; it is here formulated by considering a linearisation about a reference, warped and deformed condition.

Assume that the geometric and structural properties of the section remain constant along the axis. This assumption is required by the scheme here considered; it may lead to a model with poor convergence if a smoothly axially varying properties beam is analysed [55]. An acceptable model in most cases may be obtained by "sampling" the actual beam in a finite number of sections, that are analysed each under the assumption of constant axial properties[6]. The strains become

$$\tilde{\varepsilon} = \left\{ \begin{array}{c} 0 \\ \tilde{\nu} + \tilde{\kappa} \times \tilde{t} + \tilde{\rho}_0 \times (\tilde{t} - \tilde{t}_0) + \tilde{t}_{/\xi} \end{array} \right\} + \mathcal{D}(\tilde{t} - \tilde{t}_0)$$

and their perturbation, with respect to the reference configuration, yields

$$\begin{aligned} \Delta\tilde{\varepsilon} = {} & \left[\begin{array}{c} 0 \\ I \end{array}\right] \Delta\tilde{\nu} + \left[\begin{array}{c} 0 \\ -\tilde{t}\times \end{array}\right] \Delta\tilde{\kappa} + \left[\begin{array}{c} 0 \\ I \end{array}\right] \Delta\tilde{t}_{/\xi} \\ & + \left(\left[\begin{array}{c} 0 \\ \tilde{\rho}\times \end{array}\right] + \mathcal{D}(\cdot) \right) \Delta\tilde{t} \end{aligned}$$

[6]There are different ways of relaxing this assumption; none of them has been investigated yet, since the stepwise constant approximation gave acceptable results in practical applications. The simplest possibility is to consider an "affine" change of properties; in this case, the geometry of the section is defined by means of vector t, defined as $t = Qt^*$, being t^* a reference position at some abscissa ξ^* and $Q = Q(\xi)$ a symmetric projection matrix that "scales" the position. This approach is very simple and requires very little changes to the formulation, but it is of little use in practical cases, because practical tapered beams do no taper in such a smooth way; think, for instance, of a semi-monocoque tapered wing, with piecewise constant thickness panels and piecewise constant section flange stringers.

5.3.2 Internal work

The strain work per unit length made by a virtual variation of strains against the stresses in the section is

$$\frac{\partial}{\partial \xi}\delta L_i = \int_S \delta\tilde{\varepsilon}^T \tilde{\sigma}\, J \mathrm{d}S$$

where $J = \det(\nabla s_0)$ is the measure of the integration volume. The virtual variation of the strains is

$$\begin{aligned}\delta\tilde{\varepsilon} &= \begin{bmatrix} 0 \\ I \end{bmatrix} \delta\tilde{\nu} + \begin{bmatrix} 0 \\ -\tilde{t}\times \end{bmatrix} \delta\tilde{\kappa} + \begin{bmatrix} 0 \\ I \end{bmatrix} \delta\tilde{t}_{/\xi} \\ &\quad + \left(\begin{bmatrix} 0 \\ \tilde{\rho}\times \end{bmatrix} + \mathcal{D}(\cdot) \right) \delta\tilde{t},\end{aligned}$$

so the internal work per unit volume is

$$\delta\tilde{\varepsilon}^T \tilde{\sigma} = \left\{ \begin{array}{c} \delta\tilde{t}_{/\xi} \\ \delta\tilde{t} \\ \delta\tilde{\psi} \end{array} \right\}^T \left\{ \begin{array}{c} \Sigma^*_{t_\xi} \\ \Sigma^*_t \\ \Sigma^*_\psi \end{array} \right\}.$$

The Σ^* represent reference generalised stresses that work against the different terms of the strains; the asterisk $(\cdot)^*$ means they are entities per unit volume, so their integration over the domain S must be performed yet. They are defined in Appendix E. The perturbation of the internal work yields

$$\frac{\partial}{\partial \xi}\Delta\delta L_i = \int_S \Delta\left(\delta\tilde{\varepsilon}^T \tilde{\sigma}\right) \mathrm{d}S = \int_S \left(\delta\tilde{\varepsilon}^T \frac{\partial\tilde{\sigma}}{\partial\tilde{\varepsilon}} \Delta\tilde{\varepsilon} + (\Delta\delta\tilde{\varepsilon})^T \tilde{\sigma} \right) \mathrm{d}S,$$

being

$$(\Delta\delta\tilde{\varepsilon})^T \tilde{\sigma} = \delta\tilde{t}^T \tilde{\sigma}_S \times \Delta\tilde{\kappa} + \delta\tilde{\kappa}^T \tilde{\sigma}_S \times \Delta\tilde{t},$$

where $\tilde{\sigma}_S = [0\ I]\,\tilde{\sigma}$ are the stresses on the section of the beam. The last defined contribution to the strain work accounts for the nonlinear (quadratic) effect that couples the warping $\tilde{t}$ to the curvature $\tilde{\kappa}$. When a linear elastic constitutive law is considered, the stiffness of the material $\partial\tilde{\sigma}/\partial\tilde{\varepsilon} = D$ can be used. By considering, at the right-hand side, some imposed strains ε_p and stresses σ_p, a general solution can be found, e.g. accounting for thermal [28] rather than piezoelectric effects [34]. The piezoelectric case has been implemented to characterise the active twist rotor blade; it is described in Section 9.1 and detailed in Appendix G. The internal work per unit volume results in

$$\Delta\left(\delta\tilde{\varepsilon}^T \tilde{\sigma}\right) = \left\{ \begin{array}{c} \delta\tilde{t}_{/\xi} \\ \delta\tilde{t} \\ \delta\tilde{\psi} \end{array} \right\}^T \begin{bmatrix} \mathcal{M}^* & \mathcal{C}^* & \mathcal{L}^* \\ & \mathcal{E}^* & \mathcal{R}^* \\ \text{sym.} & & \mathcal{A}^* \end{bmatrix} \left\{ \begin{array}{c} \Delta\tilde{t}_{/\xi} \\ \Delta\tilde{t} \\ \Delta\tilde{\psi} \end{array} \right\},$$

where the asterisk again remarks that the stiffness matrices are per unit volume. They are defined in Appendix E.

5.3.3 External work

The work made by a virtual variation of displacement against all the stresses that act on the section on both sides, the stresses on the boundary and the forces per unit volume can be divided in two main parts. The first is related to external stresses w_c that act on the boundary of the section and forces per unit volume w_V inside the section; it is a true external work because it is made by external dead loads. The work made by the stresses that act on the two sides of the section, on the contrary, is related to the transmission of loads along the beam, in form of internal forces. The whole external work is thus

$$\frac{\partial}{\partial \xi}\delta L_e = \frac{\partial}{\partial \xi}\int_S \delta s^T \sigma_S \,\mathrm{d}S + \int_S \delta s^T w_V \,\mathrm{d}S + \int_c \delta s^T w_c \,\mathrm{d}c,$$

Notice that the external work has been written in the global frame since the loads and the displacements are naturally known in such frame.

Transmission work

The term $\left(\delta s^T \sigma_S\right)_{/\xi}$ requires the axial derivative of the virtual variation of the displacement[7],

$$\delta s = \delta p + \delta\varphi \times t + R\delta\tilde{t}, \tag{5.9}$$

that is

$$\delta s_{/\xi} = \delta p_{/\xi} + \delta\varphi_{/\xi} \times t + \delta\varphi \times \rho \times t + \delta\varphi \times R\tilde{t}_{/\xi} + \rho \times R\delta\tilde{t} + R\delta\tilde{t}_{/\xi}$$

which, by considering that in analogy with the time derivative of the curvature $\delta\varphi_{/\xi} = \delta\rho + \rho \times \delta\varphi$, and recalling that $p_{/\xi} = l$, results in

$$\delta s_{/\xi} = \delta l + \delta\rho \times t + \rho \times \delta\varphi \times t + \rho \times R\delta\tilde{t} + \delta\varphi \times R\tilde{t}_{/\xi} + R\delta\tilde{t}_{/\xi}.$$

As a consequence, and considering that $\sigma_{S/\xi} = \rho \times \sigma_S + R\tilde{\sigma}_{S/\xi}$,

$$\begin{aligned}\left(\delta s^T \sigma_S\right)_{/\xi} = {} & \delta\tilde{p}^T \left(\tilde{\rho} \times \tilde{\sigma}_S + \tilde{\sigma}_{S/\xi}\right) + \delta\tilde{l}^T \tilde{\sigma}_S \\ & + \delta\tilde{\varphi}^T \left(\tilde{t}_{/\xi} \times \tilde{\sigma}_S + \tilde{t} \times \tilde{\sigma}_{S/\xi}\right) + \delta\tilde{\rho}^T \tilde{t} \times \tilde{\sigma}_S \\ & + \delta\tilde{t}^T \tilde{\sigma}_{S/\xi} + \delta\tilde{t}^T_{/\xi}\tilde{\sigma}_S;\end{aligned} \tag{5.10}$$

[7]Notice that, in Eq. 5.9, the warping in the material frame, $\delta\tilde{t}$, has been assumed as independent warping variable.

notice that the work per unit volume made by the transmission of the internal forces has been written in the material frame. Recalling the definitions of the generalised strains and curvatures of the beam, Eqs. 5.3 and 5.4, the virtual variation of the generalised deformations is

$$\begin{aligned}
\delta\tilde{\nu} &= R^T \left(\delta\varphi \times^T l + \delta l\right), \\
\delta\tilde{\kappa} &= R^T \left(\delta\varphi \times^T \rho + \delta\rho\right),
\end{aligned}$$

thus yielding

$$\begin{aligned}
\delta\tilde{l} &= \delta\tilde{\nu} - \delta\tilde{\varphi} \times^T \tilde{l}, \\
\delta\tilde{\rho} &= \delta\tilde{\kappa} - \delta\tilde{\varphi} \times^T \tilde{\rho}.
\end{aligned}$$

By substituting the above written expressions in Eq. 5.10, the transmission work per unit volume finally becomes

$$\begin{aligned}
\left(\delta s^T \sigma_S\right)_{/\xi} = \; & \delta\tilde{p}^T \left(\tilde{\rho} \times \tilde{\sigma}_S + \tilde{\sigma}_{S/\xi}\right) + \delta\tilde{\nu}^T \tilde{\sigma}_S \\
& + \delta\tilde{\varphi}^T \left(\tilde{l} \times \tilde{\sigma}_S + \tilde{t}_{/\xi} \times \tilde{\sigma}_S + \tilde{t} \times \tilde{\sigma}_{S/\xi} + \tilde{\rho} \times \tilde{t} \times \tilde{\sigma}_S\right) \\
& + \delta\tilde{\kappa}^T \tilde{t} \times \tilde{\sigma}_S \\
& + \delta\tilde{t}^T \tilde{\sigma}_{S/\xi} + \delta\tilde{t}^T_{/\xi} \tilde{\sigma}_S;
\end{aligned}$$

By noting that $\tilde{p}$, $\tilde{\nu}$, $\tilde{\varphi}$ and $\tilde{\kappa}$ do not depend on the position in the section, the internal forces result from the integrals

$$\begin{aligned}
F &= \int_S \sigma_S \,\mathrm{d}S, \\
M &= \int_S t \times \sigma_S \,\mathrm{d}S.
\end{aligned}$$

The integral of the transmission work thus results in

$$\begin{aligned}
\int_S \left(\delta s^T \sigma_S\right)_{/\xi} \mathrm{d}S = \; & \delta p^T F_{/\xi} + \delta\nu^T F \\
& + \delta\varphi^T \left(l \times F + M_{/\xi}\right) + \delta\kappa^T M \\
& + \int_S \left(\delta\tilde{t}^T \tilde{\sigma}_{S/\xi} + \delta\tilde{t}^T_{/\xi} \tilde{\sigma}_S\right) \mathrm{d}S;
\end{aligned} \tag{5.11}$$

Notice that, by independently perturbing δp, the differential force equilibrium equation $F_{/\xi} = 0$ is obtained; at the same time, by independently perturbing $\delta\varphi$, the moment equilibrium equation $l \times F + M_{/\xi} = 0$ is obtained.

Dead loads work

The work made by the dead loads is a novel contribution to the formulation and it appears here for the first time. Assume the external loads w_V, w_c have the form $w = R\tilde{W}(\eta,\zeta)\, g(\xi)$, so that they are known in the form of a load mode $\tilde{W}$, depending on the position in the section, that multiplies a scalar function of the axial position, g. The external work becomes

$$\begin{aligned}
&\int_S \delta s^T w_V \; \mathrm{d}S + \int_c \delta s^T w_c \; \mathrm{d}c \\
&\quad = \left(\delta p^T F_e + \delta\varphi^T M_e + \int_S \delta\tilde{t}^T \tilde{W}_V \; \mathrm{d}S + \int_c \delta\tilde{t}^T \tilde{W}_c \; \mathrm{d}c \right) g\left(\xi\right),
\end{aligned}$$

where

$$\begin{aligned}
F_e &= R\left(\int_S \tilde{W}_V \; \mathrm{d}S + \int_c \tilde{W}_c \; \mathrm{d}c \right) \\
M_e &= R\left(\int_S \tilde{t} \times \tilde{W}_V \; \mathrm{d}S + \int_c \tilde{t} \times \tilde{W}_c \; \mathrm{d}c \right)
\end{aligned}$$

The external work contribution has been written for straight beams only, and will be discussed in Appendix E. It is intended mainly for the accurate stress recovery in case of important distributed load effects on the stress distribution of the beam. Notice that the external loads may contribute also to the differential equilibrium of the beam, since they work against the virtual variations of configuration of the reference line.

5.3.4 Discretisation

The problem of characterising the section results from equating the internal and the external work, and by independently perturbing the reference configuration, the generalised deformations and the warping. In general cases, a discretisation needs be applied to the warping to resolve the integrals in the stiffness matrix and in the external and the transmission work. The warping t can be described by an arbitrary set of nodal unknowns u through an appropriate set of shape functions, i.e. $\tilde{t} = N(\eta,\zeta)\, \tilde{u}(\xi)$. The differentiation of the warping thus yields $\nabla\tilde{t} = N\tilde{u}_{/\xi} + \mathcal{D}(N)\, \tilde{u}$. The details of the discretisation of the internal work are reported in Appendix E. It is important to notice that after discretisation the integral form of the internal and external work can be easily written in terms of a constant coefficient linear differential equation. In case of non-uniform, regularly varying beam section, a variable coefficient equation would result.
An isoparametric interpolation of the nodal displacements has been used to implement brick finite elements.

5.3.5 Solution

A simplified configuration of the beam is considered, to allow an easy understanding of the formulation of the curved/twisted characterisation. Let's assume that in reference condition the angle between the slope of the reference line and the section remains constant; this means that in the material frame the slope of the line must be constant, namely $\left(R^T l\right)_{/\xi} = 0$, yielding $l_{/\xi} = \rho \times l$. Consider now the curvature. It is tranformed from the local to the global frame by matrix R, namely $\rho = R\tilde{\rho}$. The axial differentiation of the curvature yields $\rho_{\xi} = \rho \times R\tilde{\rho} + R\tilde{\rho}_{\xi}$, which on turn results in $\rho_{\xi} = R\tilde{\rho}_{\xi}$, because, being a an arbitrary vector, $a \times a = 0$ by definition. Let's assume that the curvature is constant in the local frame, i.e. $\tilde{\rho}_{\xi} = 0$; as a result, it must be constant also in the global frame. These assumptions lead to the so called *helicoidal* beam model, discussed by *Borri et al.* in [10, 11] and in [12]. It owes the name to the property that its geometry, namely the reference line and the section orientation, is completely described by a helicoidal rototranslation of a section, with constant curvature. This work is not directly considering a helicoidal beam; it is rather assuming that an arbitrarily curved and twisted beam can be locally approximated by a helicoidal model.
The balance of the discretised internal and transmission work[8] results in

$$\begin{bmatrix} \mathcal{M} & \mathcal{C} & \mathcal{L} \\ & \mathcal{E} & \mathcal{R} \\ \text{sym.} & & \mathcal{A} \end{bmatrix} \begin{Bmatrix} \Delta\tilde{u}_{/\xi} \\ \Delta\tilde{u} \\ \Delta\tilde{\psi} \end{Bmatrix} = \begin{Bmatrix} \Delta\tilde{P} \\ \Delta\tilde{P}_{/\xi} \\ \Delta\tilde{\vartheta} \end{Bmatrix}$$

where $\tilde{P}$ are the nodal forces that work for the warping shape functions,

$$\tilde{P} = \int_S N^T \tilde{\sigma}_S \, \mathrm{d}S$$

By considering a set of concentrated loads, the perturbations of the internal forces, in the material frame, are

$$\Delta\tilde{\vartheta} = \begin{bmatrix} I & 0 \\ \tilde{p}\times & I \end{bmatrix} \begin{Bmatrix} R^T F_0 \\ R^T M_0 \end{Bmatrix}.$$

Here $p = p(\xi)$ is assumed as the position of the point where the section is being analysed, in the reference configuration; without any loss in generality, the position where the forces are applied is assumed as the origin for p, i.e. $p(0) = 0$. Assume the unknowns as well can be expressed as a combination of constant terms, denoted by subscript $(\cdot)_0$, and of terms linearly depending on $\tilde{p}$, denoted by subscript $(\cdot)_1$, both multiplied by the unknown concentrated forces and moments $\tilde{\vartheta}_0$,

[8] The external, dead loads are not considered herein because they do not intervene in the characterisation of the beam section. They are described in Appendix E.

namely

$$\begin{aligned}
\Delta\tilde{u} &= \left(\tilde{U}_0 + \tilde{p} \times \tilde{U}_1\right)\tilde{\vartheta}_0, \\
\Delta\tilde{P} &= \left(\tilde{P}_0 + \tilde{p} \times \tilde{P}_1\right)\tilde{\vartheta}_0, \\
\Delta\tilde{\psi} &= \left(\tilde{\Psi}_0 + \tilde{p} \times \tilde{\Psi}_1\right)\tilde{\vartheta}_0,
\end{aligned}$$

where the operation $\tilde{p} \times \tilde{U}$ must be intended as the cross product of $\tilde{p}$ by the $\tilde{U}$ of each node of the discretisation; again, $\tilde{p} \times \tilde{\psi}$ must be intended as the cross product of $\tilde{p}$ by both the strains and the curvature in $\tilde{\psi} = \{\tilde{\nu}, \tilde{\kappa}\}$. The derivatives of the unknowns take the form

$$\begin{aligned}
\Delta\tilde{u}_{/\xi} &= \left(\tilde{l} \times \tilde{U}_1\right)\tilde{\vartheta}_0, \\
\Delta\tilde{P}_{/\xi} &= \left(\tilde{l} \times \tilde{P}_1\right)\tilde{\vartheta}_0.
\end{aligned}$$

By assuming a local linearisation of $\tilde{p}$ in the unknowns, and considering that the p resulting from the initial assumptions is a sine in ξ plus higher-order terms, they result in

$$\begin{aligned}
\Delta\tilde{u} &\cong \left(\tilde{U}_0 + \left(\tilde{l}\xi\right) \times \tilde{U}_1\right)\tilde{\vartheta}_0, \\
\Delta\tilde{P} &\cong \left(\tilde{P}_0 + \left(\tilde{l}\xi\right) \times \tilde{P}_1\right)\tilde{\vartheta}_0, \\
\Delta\tilde{\psi} &\cong \left(\tilde{\Psi}_0 + \left(\tilde{l}\xi\right) \times \tilde{\Psi}_1\right)\tilde{\vartheta}_0,
\end{aligned}$$

so the problem becomes

$$\left[\begin{array}{ccc} \mathcal{M} & \mathcal{C} & \mathcal{L} \\ & \mathcal{E} & \mathcal{R} \\ \text{sym.} & & \mathcal{A} \end{array}\right]\left\{\begin{array}{c} \tilde{l} \times \tilde{U}_1 \\ \tilde{U}_0 + \xi\tilde{l} \times \tilde{U}_1 \\ \tilde{\Psi}_0 + \xi\tilde{l} \times \tilde{\Psi}_1 \end{array}\right\} = \left\{\begin{array}{c} \tilde{P}_0 + \xi\tilde{l} \times \tilde{P}_1 \\ \tilde{l} \times \tilde{P}_1 \\ \tilde{\Theta}_0 + \xi\tilde{\Theta}_1 \end{array}\right\}.$$

The problem can be solved by separately considering the linear and the constant part of the solution; the linear part, after some manipulation, becomes

$$\left[\begin{array}{cc} \mathcal{E} & \mathcal{R} \\ \text{sym.} & \mathcal{A} \end{array}\right]\left\{\begin{array}{c} \tilde{l} \times \tilde{U}_1 \\ \tilde{l} \times \tilde{\Psi}_1 \end{array}\right\} = \left\{\begin{array}{c} 0 \\ \tilde{\Theta}_1 \end{array}\right\},$$

whose solution is substituted in the constant part, yielding

$$\left[\begin{array}{cc} \mathcal{E} & \mathcal{R} \\ \text{sym.} & \mathcal{A} \end{array}\right]\left\{\begin{array}{c} \tilde{U}_0 \\ \tilde{\Psi}_0 \end{array}\right\} = \left\{\begin{array}{c} 0 \\ \tilde{\Theta}_0 \end{array}\right\} + \left[\begin{array}{cc} \mathcal{C} - \mathcal{C}^T & \mathcal{L} \\ \text{skw.} & 0 \end{array}\right]\left\{\begin{array}{c} \tilde{l} \times \tilde{U}_1 \\ \tilde{l} \times \tilde{\Psi}_1 \end{array}\right\}.$$

The section properties can be computed by condensing the warping degrees of freedom, i.e. by left- and right-multiplying the internal work matrix by the solution arrays, to obtain the strain energy in terms of compliance properties of the section, namely

$$\frac{\partial}{\partial\xi}\Delta\delta L_i = \delta\tilde{\vartheta}_0^T C(\xi)\,\Delta\tilde{\vartheta}_0.$$

The dependence of matrix C on the position where the solution is evaluated has been highlighted; however, as expected, it can be easily shown that such dependence is only formal: in fact the section properties do not depend on the axial abscissa, and matrix C can be evaluated at $\xi = 0$ without any loss in generality. The stiffness properties[9] D are finally obtained by inverting the compliance matrix C.

5.3.6 Note on the determination of the warping

The way the warping is defined does not ensure it is decoupled from any rigid displacement of the section, because the warping shape functions usually contain rigid displacement modes. So, while the stiffness properties are correct, being based on an appropriate evaluation of the strain energy due to both the warping and the generalised displacements, the generalised deformations and the warpings are underdetermined. A strain-energy based criterion for the decoupling has been proposed by *Borri* and *Merlini* [14]; it is based on the consideration that by setting the work of the warping against the section stresses, the last addendum in Equation 5.11, equal to zero[10],

$$\int_S \delta\tilde{t}^T \tilde{\sigma}_S \, \mathrm{d}S \;=\; 0,$$

the strain energy can be written as function of the generalised deformations and of the internal forces only. Such constraint resolves for the six underdetermined displacement unknowns. The reasons to prefer an *a posteriori* decoupling of the results are essentially related to the loss in sparsity if such constraint is explicitated, or to the increase in complexity if it is added in a *Lagrangian Multiplier* sense. The *a posteriori* decoupling requires to constrain the matrix prior to solution due to its singularity. By using an arbitrary statically determinate constraint, the warping in general is not decoupled; at this point, by considering a decoupled warping made of the original warping plus a rigid displacement, the decoupling rigid displacement can be determined, and the initially computed coupled solution can be corrected.

5.4 Finite volume beam formulation

The fundamental idea of the finite volume beam model consists in directly writing the equilibrium equation of a finite portion of beam, considering the external

[9]Notice that the same symbol, D, has been used for both the material constitutive law and the beam section stiffness matrix; despite it might be misleading, it is intended to underline they both are constitutive matrices. The correct meaning should be clarified by the context.

[10]Or simply equal to a constant value [12]

as well as the internal forces and couples. The internal forces and couples are expressed as functions of the configuration by means of a constitutive law.

5.4.1 Finite equilibrium

The forces that participate in the equilibrium are the internal forces $\vartheta = \{F, M\}$ at the two extremities of the portion, ϑ_a and ϑ_b, being $B_a^b := [a, b]$ the domain of the portion and a, b the so-called *evaluation points* for the internal forces, and the external loads applied in the domain B_a^b. It results in

$$\mathcal{U}(p_b - x_0)^T \vartheta_b - \mathcal{U}(p_a - x_0)^T \vartheta_a = \mathcal{F}_a^b. \tag{5.12}$$

Matrix $\mathcal{U}$ is defined as

$$\mathcal{U}(p) = \begin{bmatrix} I & p\times^T \\ 0 & I \end{bmatrix},$$

where p is a relative position (a distance); the matrix simply transports the internal shear to the pole where the equilibrium of the moments is computed[11]; x_0 is the position of the pole used to compute the moments. The external loads are defined as

$$\mathcal{F}_a^b = \int_a^b \mathcal{U}(p(\xi) - x_0)^T \tau \, \mathrm{d}\xi,$$

being τ the distributed forces and couples, that were not considered in Eqs. 5.6, 5.7. Notice that the same result can be obtained by writing the weak form of the equilibrium of the beam in a weighted residuals manner, namely by integrating the differential equilibrium equations, Eqs. 5.6, 5.7, weighted by a constant piecewise, or Heavyside, weight function, as shown in [69, 37].

5.4.2 Constitutive law

The internal forces at the boundaries of the portion of beam can be written in terms of the generalised deformations by means of an arbitrary constitutive law. In case of linear elasticity, or in general when a linearised elastic constitutive law is required, the constitutive matrix computed in Section 5.3 can be used. The constitutive equation of a finite portion of beam, Eq. 5.12, becomes

$$\mathcal{U}(p_b - x_0)^T \mathcal{R}_b D_b \mathcal{R}_b^T \psi_b - \mathcal{U}(p_a - x_0)^T \mathcal{R}_a D_a \mathcal{R}_a^T \psi_a = \mathcal{F}_a^b, \tag{5.13}$$

[11] The transpose of matrix $\mathcal{U}$ performs what has been termed *South-West cross product* by *Borri* and his co-workers, a generalised cross product between the configuration of a point, $\{p, R\}$, and forces and moments, $\vartheta = \{F, M\}$, at such point, resulting in a change of pole for the moments; a recent description of such work can be found in [15].

where $\mathcal{R}$ is a block-diagonal matrix made of two conventional rotation matrices, namely

$$\mathcal{R} = \begin{bmatrix} R & 0 \\ 0 & R \end{bmatrix}.$$

5.4.3 Linearisation

The linearisation of Eq. 5.13 involves the linearisation of matrices $\mathcal{U}_i$, $\mathcal{R}_i$, and of the generalised deformations ψ_i, $i = a, b$. It results in

$$\begin{aligned} \Delta\left(\mathcal{U}\left(p_i - x_j\right)^T \mathcal{R}_i D_i \tilde{\psi}_i\right) &= \Delta\mathcal{U}\left(p_i - x_j\right)^T \vartheta_i \\ &\quad + \mathcal{U}\left(p_i - x_j\right)^T \Delta\mathcal{R}_i \tilde{\vartheta}_i \\ &\quad + \mathcal{U}\left(p_i - x_j\right)^T \mathcal{R}_i D_i \Delta\tilde{\psi}_i, \end{aligned} \tag{5.14}$$

where i is an evaluation point, and j is a reference point, usually a multibody node, with

$$\Delta\mathcal{U}\left(p_i - x_j\right) = \begin{bmatrix} 0 & \left(\Delta p_i - \Delta x_j\right) \times^T \\ 0 & 0 \end{bmatrix}, \tag{5.15}$$

$$\Delta\mathcal{R}_i = \begin{bmatrix} \theta_\Delta \times R_i & 0 \\ 0 & \theta_\Delta \times R_i \end{bmatrix},$$

$$\Delta\tilde{\psi}_i = \begin{Bmatrix} R_i^T \left(\Delta l_i + l_i \times \theta_\Delta\right) \\ R_i^T \left(\Delta\kappa_i + \kappa_i \times \theta_\Delta\right) \end{Bmatrix}.$$

The expression with the local strains $\tilde{\psi}$ has been preferred to that with the global ones because its linearisation points out that the initial axial slope and curvature do not depend on the configuration unknowns and thus do not affect the linearisation of the deformations.
The external loads may require some linearisation, at least for the role of matrix $\mathcal{U}$ in computing the distributed moment due to distributed transverse forces. Their linearisation is not presented since it is straightforward, and it is not required when only concentrated loads applied at the pole x_0 are considered.

5.4.4 Discretisation

The interpolation of position and rotation parameters allows one to directly write Equation 5.14 in terms of perturbations of the nodal unknowns. A three-node beam element, shown in Figure 5.1, has been implemented; as pointed out in

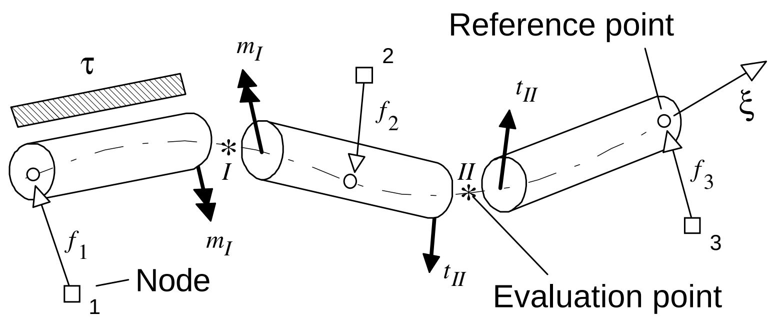

Figure 5.1: Finite volume three-node beam element.

[69, 37], this is the lowest order element that gives the exact solution for end-applied loads; the optimal evaluation points correspond to the two *Gauss* integration points that exactly integrate polynomials up to third degree [69, 37]. Eq. 5.14 must be written for three portions of beam, centered on each of the three nodes, with the boundary portions ending on the boundary nodes, so the equilibrium equation of the element results in

$$\left[\begin{array}{cc} \mathcal{U}(p_I - x_1)^T & 0 \\ -\mathcal{U}(p_I - x_2)^T & \mathcal{U}(p_{II} - x_2)^T \\ 0 & -\mathcal{U}(p_{II} - x_3)^T \end{array}\right] \left\{\begin{array}{c} \vartheta_I \\ \vartheta_{II} \end{array}\right\} = \left\{\begin{array}{c} \mathcal{F}_1^I \\ \mathcal{F}_I^{II} \\ \mathcal{F}_{II}^3 \end{array}\right\}$$

being $1,2,3$ the nodes of the beam, and I,II the evaluation points. An arbitrary point on the reference line is $p = N_j p_j$, being N_j the j-th node parabolic shape function; an arbitrary rotation parameter set is $g = N_j g_j$; the summation over the index of the shape functions is assumed. The position p relative to a node is obtained from Eq. 5.1 as $p_j = x_j + f_j$. The kinematic entities involved in the equilibrium equation of the beam are

$$\begin{aligned} p &= N_j\left(x_j + f_j\right), \\ g &= N_j g_j, \\ l &= N_j'\left(x_j + f_j\right), \\ \kappa &= G_\delta(g) N_j' g_j + R_\delta(g)\,\kappa^{(0)}; \end{aligned}$$

their linearisation yields

$$\begin{aligned} \Delta p &\cong N_j\left(\Delta x_j + \Delta g_j \times f_j\right), \\ \Delta g &= N_j \Delta g_j, \\ \Delta l &\cong N_j'\left(\Delta x_j + \Delta g_j \times f_j\right), \\ \Delta\kappa &\cong N_j' \Delta g_j + \Delta g \times \kappa^{(0)}, \end{aligned}$$

where the simplifications allowed by the updated-updated formulation have been exploited[12].

5.4.5 Implementation notes

The finite volume beam has been successfully used in the analysis of various structural components. Its application to the modelling of rotor blades represents a challenge, and requires the awareness of its behaviour in such peculiar application. This formulation is naturally oriented towards a C^0 description of the generalised strains, and thus requires the ability to determine the six stiffness terms as shown in Section 5.3. The use of a nonlinear formulation intrinsically accounts for the prestress effects that result from the centrifugal forces on a rotorcraft blade. On the other hand, this requires some care in distributing the inertia along the blade. A consistent formulation of the inertia forces has been developed, but it has not been implemented yet because it resulted in an unacceptable overhead due to the need of numerically integrating the inertia forces over each portion of the beam; in fact, since the inertia forces directly depend on the displacements instead of their spatial derivatives, their contribution cannot be brought to a boundary evaluation by integrating by parts. The use of a finite element-like approach to the modelling of rotor blades might sound unusual to rotorcraft people, who are used to a modal description of the flexibility of the blades. Such an approach is due to historical reasons and possibly resulted from the need to have very small, efficient models for highly time-consuming analyses on computers very limited both in memory and CPU speed. Moreover, a modal model allows the analyst to consider only the desired contributions in terms of frequency spectrum and spatial components, e.g. the desired mix of flapwise bending and torsion. It is not our intention to criticize such approach, which still represents a legitimate choice for certain analyses, but a finite element-like approach surely allows the analyst a higher flexibility and accuracy in modelling structural components, and, in case of a fully nonlinear model, as the one here presented, allows to overcome the fundamental limitation of the modal approach, the intrinsically limited flexible displacements.

[12] Any rotation parametrisation can be used by substituting g with p and by using the appropriate definitions of matrices R and G.

5.5 Plate model

The plate model is defined in a way much similar to the beam; in this case, the reference domain is a surface, and the section is represented by a line that, at least in reference configuration, is chosen to be nearly normal to the surface. In some sense the plate model here considered is dual to the beam model presented in the previous sections of this chapter, in that the domain in which it is defined is a surface, p, while the section, which will be called the “fibre”, is a segment, i.e. a bounded one-dimensional domain. Most of the definitions introduced for the beam are here extended to account for the change in dimensionality of the domains of definition for the various entities. The nomenclature used throughout the sections dedicated to the plate analysis closely resembles the one introduced for the beam, to highlight the analogies. The reader should notice how most of the expressions used for the beam maintain their meaning, provided the appropriate domain of definition of the involved entities is considered.

B	$\Re^2$	domain of the plate
S	$\Re$	domain of the plate fibre
s	$B \times S \mapsto V^3$	position of a point
p	$B \mapsto V^3$	position of the reference surface
t	$S \mapsto V^3$	offset of a point from the reference surface
R	$B \mapsto \mathrm{LIN}\left(V^3\right)$	rotation matrix (from local to global frame)
e_i	$B \mapsto V^3$	directions of R
l	$B \mapsto V^3 \times V^3$	plane tangent to the reference surface ($= \nabla p$)
$\rho\times$	$B \mapsto \mathrm{lin}\left(V^3\right) \times V^3$	curvature of the plate ($= \nabla R R^T$)
ν	$B \mapsto V^3 \times V^3$	generalised strains of the reference surface
$\kappa\times$	$B \mapsto \mathrm{lin}\left(V^3\right) \times V^3$	generalised elastic curvature of the plate
ψ	$B \mapsto V^6 \times V^3$	generalised deformations
F	$B \mapsto V^3 \times V^3$	internal force fluxes
M	$B \mapsto V^3 \times V^3$	internal moment fluxes
ϕ	$B \mapsto V^3$	external forces per unit surface
μ	$B \mapsto V^3$	external moments per unit surface
ϑ	$B \mapsto V^6 \times V^3$	generalised internal force fluxes
τ	$B \mapsto V^6$	generalised external forces per unit surface

5.5.1 Definitions

A plate model is defined by a reference surface p, whose position with respect to the plate is arbitrarily chosen. The surface is defined on a local bidimensional domain, with local abscissæ ξ, η. A reference frame of the plate at an arbitrary point is defined by a rotation matrix R. Direction e_3 is chosen to be nearly normal to the reference surface p, while the other two directions are arbitrarily selected such that in reference condition, $e_1^T l_\xi > 0$ and $e_2^T l_\eta > 0$, being l_i the derivatives of p with respect to the abscissæ on the reference surface. An abscissa ζ is taken in direction e_3.

5.5.2 Kinematics of the plate

By mutuating the symbols from the beam model, the position of an arbitrary point can be described as $s = p + t$, where t is a vector in the global frame that describes a relative position with respect to the reference surface p, obtained by transforming a vector in the local frame by means of R, namely $t = R\tilde{t}$. The gradient of the displacements allows to characterise the plate in terms of intrinsic strain measures. By considering that both p and R depend on the local coordinates of the reference plane only, and by assuming that $\tilde{t}$ does not depend on the position on the plate, or in other words that there is no warping and the plate has constant thickness and properties, the gradient of the displacement is

$$\nabla s = \nabla p + \nabla R\tilde{t},$$

or

$$\nabla s = l + \rho \times t$$

where $l = \left\{l_\xi, l_\eta, 0\right\}$ is the slope of the surface p (the gradient operator has been defined in Eq. 5.8), and ρ is the curvature of the plate, obtained from the gradient of the reference frame as

$$\begin{aligned} \rho &= \operatorname{ax}\left(\nabla R R^T\right) \\ &= \left\{\operatorname{ax}\left(R_{/\xi} R^T\right), \operatorname{ax}\left(R_{/\eta} R^T\right), 0\right\}. \end{aligned}$$

The expression of ∇s can be explicitated as $\nabla s = \left\{l_\xi + \rho_\xi \times t, l_\eta + \rho_\eta \times t, 0\right\}$. The difference between the gradient of the position in deformed and in reference configuration, both transformed back to the material frame, determines the measure of the strains of the plate

$$\begin{aligned} R^T \nabla s - R_0^T \nabla s_0 &= \left(R^T l - R_0^T l_0\right) + \left(R^T \rho \times t - R_0^T \rho_0 \times t_0\right) \\ &= \left(\tilde{l} - \tilde{l}_0\right) + \left(\tilde{\rho} \times \tilde{t} - \tilde{\rho}_0 \times \tilde{t}_0\right) \end{aligned}$$

or, considering that $\tilde{t} = \tilde{t}_0$, due to the null warping assumption,

$$R^T \nabla s - R_0^T \nabla s_0 = \tilde{\nu} + \tilde{\kappa} \times \tilde{t},$$

where the generalised deformations of the plate,

$$\begin{aligned} \tilde{\nu} &= \tilde{l} - \tilde{l}_0, \\ \tilde{\kappa} &= \tilde{\rho} - \tilde{\rho}_0, \end{aligned}$$

have been introduced.

5.5.3 Plate equilibrium

The differential equilibrium of the plate results from considering that the work made by the internal forces for a rigid displacement is null. The virtual rigid displacement and rotation at point $p(\xi,\eta)$ are $\delta p(\xi,\eta) = \delta p(0,0) + \delta\varphi(0,0) \times (p(\xi,\eta) - p(0,0))$ and $\delta\varphi(\xi,\eta) = \delta\varphi(0,0)$, as previously shown for the beam. The null internal work condition results in

$$\nabla(\delta p(\xi,\eta)\cdot F(\xi,\eta) + \delta\varphi(\xi,\eta)\cdot M(\xi,\eta)) = 0, \tag{5.16}$$

where $F = \{F_\xi, F_\eta, 0\}$, $M = \{M_\xi, M_\eta, 0\}$ are the fluxes of internal forces on the fibre of the plate. The condition in Eq. 5.16 results in

$$\begin{aligned} \nabla^T F &= 0 &\quad (5.17)\\ \nabla^T M + (l\times)^T F &= 0 &\quad (5.18) \end{aligned}$$

where $l = \nabla p$ has been used. Notice that, by properly defining the differential operators, and by exchanging the dimensions of the reference and of the section domains, the plate intrinsic model is perfectly dual to that of the beam.

5.5.4 Singularity and compatibility

The equilibrium equations, Eqs. 5.17, 5.18 contain the equilibrium about the drill degree of freedom. By considering that usually a plate constitutive law is not able to capture the stiffness related to such degree of freedom, the drill component of the equilibrium equation simply states the symmetry of the in-plane shear fluxes, resulting in a singular constitutive matrix for a finite plate. At the same time, the definition of the generalised deformations of the plate that have been introduced in Section 5.5.2 do not imply the symmetry of the strains. By following the scheme proposed in [58], a general way to enforce the symmetry of the strains and of the stresses in the weak formulation of the equilibrium of the plate will be introduced in Section 5.7, dedicated to the finite volume formulation for the plates.
The deformations must satisfy a compatibility relation that is implicit in case they are expressed as the gradients of the configuration, but it must be enforced when a strain-based formulation is considered, as in Section 5.6. The condition results from the consideration that the strains must be non-rotational, namely $\nabla\times(\nabla s) = 0$, where operator $\nabla\times(\cdot)$ performs the rotor operation, yielding

$$\begin{aligned} \nabla\times\nu &= 0, &\quad (5.19)\\ \nabla\times\kappa &= 0. &\quad (5.20) \end{aligned}$$

This relationship will also be used to obtain the elastic properties of the plate in terms of compatible as well as balanced load conditions.

5.6 Plate fibre characterisation

The plate fibre characterisation follows the same approach used for the beam section. The domain of the fibre is much simpler than that of the plate, consisting in a segment of line[13] in the reference configuration. The plate fibre analysis has been implemented only in case of linear, flat initial reference surface. The extension to the general case of nonlinear (coupling between generalised deformations and warping strains) is straightforward, following the scheme developed for the beam; it is presented and discussed. This part of the work is original and is presented here for the first time.

$\mathcal{M}$, $\mathcal{C}$, $\mathcal{L}$, $\mathcal{E}$, $\mathcal{R}$, $\mathcal{A}$		stiffness matrices of the fibre
$\Xi = \{\mathcal{X}, \mathcal{Y}, \mathcal{Z}\}$	$V^{6\times 3} \times V^3$	strain collocation matrix
U_0, U_1	$B \mapsto V^{3\times N} \times V^3$	indicial fibre discrete warping
P_0, P_1	$B \mapsto V^{3\times N} \times V^3$	indicial fibre nodal work
Ψ_0, Ψ_1	$B \mapsto V^6 \times V^3$	indicial generalised deformations
Θ_0, Θ_1	$B \mapsto V^6 \times V^3$	indicial generalised internal forces

5.6.1 Kinematics of the fibre

The strains at an arbitrary point on the fibre result from the gradient of the position, ∇s, where the gradient of the warping is considered as well, resulting in

$$\nabla s = l + \rho \times t + R\nabla \tilde{t}.$$

The difference between the gradient at some configuration and that in the reference configuration, both rotated back to the material frame, yields a measure of the strains in the fibre:

$$R^T \nabla s - R_0^T \nabla s_0 = \tilde{\nu} + \tilde{\kappa} \times \tilde{t} + \tilde{\rho}_0 \times (\tilde{t} - \tilde{t}_0) + \nabla(\tilde{t} - \tilde{t}_0)\,.$$

where the previously defined strain and curvature of the reference plane have been considered. The conventional matrix notation for the strains, namely $\varepsilon = \{\varepsilon_{11}, \varepsilon_{22}, \varepsilon_{33}, \gamma_{23}, \gamma_{31}, \gamma_{12}\}$, results from multiplying the difference between the gradients by a set of collocation matrices, $\Xi = \{\mathcal{X}, \mathcal{Y}, \mathcal{Z}\}$, defined as

$$\mathcal{X} = \begin{bmatrix} 1 & 0 & 0 \\ 0 & 0 & 0 \\ 0 & 0 & 0 \\ 0 & 0 & 0 \\ 0 & 0 & 1 \\ 0 & 1 & 0 \end{bmatrix}, \qquad \mathcal{Y} = \begin{bmatrix} 0 & 0 & 0 \\ 0 & 1 & 0 \\ 0 & 0 & 0 \\ 0 & 0 & 1 \\ 0 & 0 & 0 \\ 1 & 0 & 0 \end{bmatrix}, \qquad \mathcal{X} = \begin{bmatrix} 0 & 0 & 0 \\ 0 & 0 & 0 \\ 0 & 0 & 1 \\ 0 & 1 & 0 \\ 1 & 0 & 0 \\ 0 & 0 & 0 \end{bmatrix},$$

[13] The domain is required to be regular, so it degenerates in one segment only. In case of some delamination analysis, multiple segments may be considered, i.e. a discontinuity in the domain is allowed, provided there is some configuration-dependent force that keeps the segments together.

yielding

$$\tilde{\varepsilon} = \Xi\left(\tilde{\nu} + \tilde{\kappa} \times \tilde{t} + \tilde{\rho}_0 \times (\tilde{t} - \tilde{t}_0) + \nabla(\tilde{t} - \tilde{t}_0)\right).$$

The linearisation of the strains yields

$$\Delta\tilde{\varepsilon} = \Xi\left(\Delta\tilde{\nu} - \tilde{t} \times \Delta\tilde{\kappa} + (\tilde{\rho} \times + \nabla(\cdot))\, \Delta\tilde{t}\right),$$

while their virtual variation results in

$$\delta\tilde{\varepsilon} = \Xi\left(\delta\tilde{\nu} - \tilde{t} \times \delta\tilde{\kappa} + (\tilde{\rho} \times + \nabla(\cdot))\, \delta\tilde{t}\right).$$

The virtual variation of the position s and of its gradient are required for the computation of the external work:

$$\delta s = \delta p + \delta\varphi \times t + R\delta\tilde{t},$$

and

$$\nabla\delta s = \nabla\delta p + \nabla\delta\varphi \times t + \delta\varphi \times \rho \times t + \delta\varphi \times R\nabla\tilde{t} + \rho \times R\delta\tilde{t} + R\nabla\delta\tilde{t},$$

which, by exchanging the order of application[14] of operators $\nabla(\cdot)$ and $\delta(\cdot)$, results in

$$\nabla\delta s = \delta l + \delta\rho \times t + \rho \times \delta\varphi \times t + \delta\varphi \times R\nabla\tilde{t} + \rho \times R\delta\tilde{t} + R\delta\nabla\tilde{t}.$$

By taking a virtual variation of the reference plane strain $\tilde{\nu}$, δl can be replaced with $R\delta\tilde{\nu} + \delta\varphi \times l$, while by considering a virtual variation of the elastic curvature $\tilde{\kappa}$, $\delta\rho$ is replaced by $R\delta\tilde{\kappa} + \delta\varphi \times \rho$, finally yielding

$$\nabla\delta s = R\delta\tilde{\nu} + (R\delta\tilde{\kappa}) \times t + \delta\varphi \times (l + \rho \times t + R\nabla\tilde{t}) + \rho \times R\delta\tilde{t} + R\delta\nabla\tilde{t}.$$

5.6.2 Internal work

The internal work per unit volume is $\delta\varepsilon^T\sigma$; its linearisation results in $\delta\Delta\varepsilon^T\sigma + \delta\varepsilon^T\partial\sigma/\partial\varepsilon\Delta\varepsilon$. By mutuating the symbols from the beam section analysis formulation, the internal work per unit volume can be written as

$$\delta\tilde{\varepsilon}^T\tilde{\sigma} = \left\{\begin{array}{c} \delta\tilde{t}_{/\xi} \\ \delta\tilde{t}_{/\eta} \\ \delta\tilde{t} \\ \delta\tilde{\psi}_\xi \\ \delta\tilde{\psi}_\eta \end{array}\right\}^T \left\{\begin{array}{c} \Sigma^*_{t_\xi} \\ \Sigma^*_{t_\eta} \\ \Sigma^*_{t} \\ \Sigma^*_{\psi_\xi} \\ \Sigma^*_{\psi_\eta} \end{array}\right\}$$

[14] It is permitted, provided the configuration of the plate is sufficiently regular.

and its linearisation results in

$$\Delta\left(\delta\tilde{\varepsilon}^T\tilde{\sigma}\right) = \left\{\begin{array}{c}\delta\tilde{t}_{/\xi}\\ \delta\tilde{t}_{/\eta}\\ \delta\tilde{t}\\ \delta\tilde{\psi}_\xi\\ \delta\tilde{\psi}_\eta\end{array}\right\}^T \left[\begin{array}{ccccc}\mathcal{M}^*_{\xi\xi} & \mathcal{M}^*_{\xi\eta} & \mathcal{C}^*_\xi & \mathcal{L}^*_{\xi\xi} & \mathcal{L}^*_{\xi\eta}\\ & \mathcal{M}^*_{\eta\eta} & \mathcal{C}^*_\eta & \mathcal{L}^*_{\eta\xi} & \mathcal{L}^*_{\eta\eta}\\ & & \mathcal{E}^* & \mathcal{R}^*_\xi & \mathcal{R}^*_\eta\\ & \text{sym.} & & \mathcal{A}^*_{\xi\xi} & \mathcal{A}^*_{\xi\eta}\\ & & & & \mathcal{A}^*_{\eta\eta}\end{array}\right] \left\{\begin{array}{c}\Delta\tilde{t}_{/\xi}\\ \Delta\tilde{t}_{/\eta}\\ \Delta\tilde{t}\\ \Delta\tilde{\psi}_\xi\\ \Delta\tilde{\psi}_\eta\end{array}\right\},$$

the star $(\cdot)^*$ indicating that the submatrices, defined in Appendix F, are per unit volume. The generalised deformations $\psi = \{\nu, \kappa\}$ have been used for ease of notation.

5.6.3 External work

The external work is made of two parts, as described for the plate section analysis: the internal forces transmission work and the dead loads work,

$$\begin{aligned}\frac{\partial^2}{\partial\xi\partial\eta}\delta L_e &= \frac{\partial}{\partial\xi}\int_S \delta s^T \sigma_{S\xi}\ \mathrm{d}S + \frac{\partial}{\partial\eta}\int_S \delta s^T \sigma_{S\eta}\ \mathrm{d}S\\ &+ \int_S \delta s^T w_V\ \mathrm{d}S + \int_c \delta s^T w_c \cdot n\ \mathrm{d}c\end{aligned}$$

Due to the dimensionality of the domain of the plate fibre, their expressions are very simple

Transmission work

The transmission work basically consists in the sum of the gradients in directions ξ and η of the work made by a virtual variation of displacement agains the stresses on the respective sides of the fibre, $\sigma_{S\xi} = \mathcal{X}^T\sigma$ and $\sigma_{S\eta} = \mathcal{Y}^T\sigma$, or, in other words, by their in-plane divergence. The integrands result in

$$\begin{aligned}\left(\delta s^T\sigma_{S\xi}\right)_{/\xi} &= \delta\tilde{p}^T\left(\tilde{\rho}_\xi\times\tilde{\sigma}_{S\xi} + \tilde{\sigma}_{S\xi/\xi}\right) + \delta\tilde{\nu}_\xi^T\tilde{\sigma}_{S\xi/\xi}\\ &+ \delta\tilde{\varphi}^T\left(\tilde{l}_\xi\times\tilde{\sigma}_{S\xi} + \tilde{t}_{/\xi}\times\tilde{\sigma}_{S\xi} + \tilde{\rho}_\xi\times\tilde{t}\times\tilde{\sigma}_{S\xi} + \tilde{t}\times\tilde{\sigma}_{S\xi/\xi}\right)\\ &+ \delta\tilde{\kappa}_\xi^T\tilde{t}\times\tilde{\sigma}_{S\xi}\\ &+ \delta\tilde{t}^T\tilde{\sigma}_{S\xi/\xi} + \delta\tilde{t}_{/\xi}^T\tilde{\sigma}_{S\xi},\end{aligned}$$

$$\begin{aligned}\left(\delta s^T\sigma_{S\eta}\right)_{/\eta} &= \delta\tilde{p}^T\left(\tilde{\rho}_\eta\times\tilde{\sigma}_{S\eta} + \tilde{\sigma}_{S\eta/\eta}\right) + \delta\tilde{\nu}_\eta^T\tilde{\sigma}_{S\eta/\eta}\\ &+ \delta\tilde{\varphi}^T\left(\tilde{l}_\eta\times\tilde{\sigma}_{S\eta} + \tilde{t}_{/\eta}\times\tilde{\sigma}_{S\eta} + \tilde{\rho}_\eta\times\tilde{t}\times\tilde{\sigma}_{S\eta} + \tilde{t}\times\tilde{\sigma}_{S\eta/\eta}\right)\\ &+ \delta\tilde{\kappa}_\eta^T\tilde{t}\times\tilde{\sigma}_{S\eta}\\ &+ \delta\tilde{t}^T\tilde{\sigma}_{S\eta/\eta} + \delta\tilde{t}_{/\eta}^T\tilde{\sigma}_{S\eta}.\end{aligned}$$

By noting that the $\tilde{p}$, $\tilde{\varphi}$, $\tilde{l}$, $\tilde{\rho}$, $\tilde{\nu}$, $\tilde{\kappa}$ do not depend on ζ, the integration variable, and by defining

$$\begin{aligned}
F_\xi &= \int_S \sigma_{S\xi} \, \mathrm{d}S, \\
F_\eta &= \int_S \sigma_{S\eta} \, \mathrm{d}S, \\
M_\xi &= \int_S t \times \sigma_{S\xi} \, \mathrm{d}S, \\
M_\eta &= \int_S t \times \sigma_{S\eta} \, \mathrm{d}S,
\end{aligned}$$

the transmission work becomes

$$\begin{aligned}
\int_S \left(\left(\delta s^T \sigma_{S\xi} \right)_{/\xi} + \left(\delta s^T \sigma_{S\eta} \right)_{/\eta} \right) \mathrm{d}S \; = \; & \delta p^T \left(F_{\xi/\xi} + F_{\eta/\eta} \right) \\
& + \delta \nu_\xi^T F_\xi + \delta \nu_\eta^T F_\eta \\
& + \delta \varphi^T \left(l_\xi \times F_\xi + M_{\xi/\xi} + l_\eta \times F_\eta + M_{\eta/\eta} \right) + \delta \kappa_\xi^T M_\xi + \delta \kappa_\eta^T M_\eta \\
& + \int_S \left(\delta \tilde{t}^T \tilde{\sigma}_{S\xi/\xi} + \delta \tilde{t}_{/\xi}^T \tilde{\sigma}_{S\xi} + \delta \tilde{t}^T \tilde{\sigma}_{S\eta/\eta} + \delta \tilde{t}_{/\eta}^T \tilde{\sigma}_{S\eta} \right) \mathrm{d}S.
\end{aligned}$$

Notice that, by independently perturbing δp, the differential force equilibrium equation $\nabla F = 0$ is obtained; at the same time, by independently perturbing $\delta\varphi$, the moment equilibrium equation $(l \times) \, F + \nabla M = 0$ is obtained.

Dead loads work

The dead loads work does not require any special treatment. It is important to notice that the work of the forces per unit volume is simply represented by a line integral along S, while the boundary of S, c, is simply constituted of the two points that represent the intersection of S with the upper and lower faces of the plate, and thus the integral degenerates in two collocated evaluations,

$$\int_c \delta s^T w_c \cdot n \, \mathrm{d}c \; = \; s^T w_c \big|_u + s^T w_c \big|_l$$

where n is the normal to the surface of the plate, subscripts $(\cdot)_u$ and $(\cdot)_l$ standing for upper and lower. Because the dead loads do not participate in the characterisation of the plate fibre, they are not discussed here. They can be formulated in analogy with those of the beam, described in Appendix E; however, they are not discussed here since there has been no plate application yet in the present research work.

5.6.4 Discretisation

The warping is discretised by interpolating the nodal values in a finite element sense. The nodal warping unknowns u are used in conjunction with isoparametric shape functions N to approximate the warping $t = N(\zeta)\, u(\xi,\eta)$. The discretised internal work can be written in integral form, since the integration is performed with respect to ζ, and the nodal unknowns are carried out of the integral operator, yielding

$$\frac{\partial^2}{\partial\xi\partial\eta}\delta\Delta L_i = \left\{\begin{array}{c} \delta\tilde{u}_{/\xi} \\ \delta\tilde{u}_{/\eta} \\ \delta\tilde{u} \\ \delta\tilde{\psi}_\xi \\ \delta\tilde{\psi}_\eta \end{array}\right\}^T \left[\begin{array}{ccccc} \mathcal{M}_{\xi\xi} & \mathcal{M}_{\xi\eta} & \mathcal{C}_\xi & \mathcal{L}_{\xi\xi} & \mathcal{L}_{\xi\eta} \\ & \mathcal{M}_{\eta\eta} & \mathcal{C}_\eta & \mathcal{L}_{\eta\xi} & \mathcal{L}_{\eta\eta} \\ & & \mathcal{E} & \mathcal{R}_\xi & \mathcal{R}_\eta \\ & \text{sym.} & & \mathcal{A}_{\xi\xi} & \mathcal{A}_{\xi\eta} \\ & & & & \mathcal{A}_{\eta\eta} \end{array}\right] \left\{\begin{array}{c} \Delta\tilde{u}_{/\xi} \\ \Delta\tilde{u}_{/\eta} \\ \Delta\tilde{u} \\ \Delta\tilde{\psi}_\xi \\ \Delta\tilde{\psi}_\eta \end{array}\right\}.$$

The external work integrals related to the warping can be carried out as well, yielding

$$\int_S \left(\left(\delta\tilde{t}^T\tilde{\sigma}_{S\xi}\right)_{/\xi} + \left(\delta\tilde{t}^T\tilde{\sigma}_{S\eta}\right)_{/\eta} \right) \mathrm{d}S = \left(\delta\tilde{u}^T\tilde{P}_\xi\right)_{/\xi} + \left(\delta\tilde{u}^T\tilde{P}_\eta\right)_{/\eta},$$

where P_ξ, P_η are the nodal forces corresponding to the shape functions used in the discretisation.

5.6.5 Solution

The problem results from equating a perturbation of internal and external work

$$\left[\begin{array}{ccccc} \mathcal{M}_{\xi\xi} & \mathcal{M}_{\xi\eta} & \mathcal{C}_\xi & \mathcal{L}_{\xi\xi} & \mathcal{L}_{\xi\eta} \\ & \mathcal{M}_{\eta\eta} & \mathcal{C}_\eta & \mathcal{L}_{\eta\xi} & \mathcal{L}_{\eta\eta} \\ & & \mathcal{E} & \mathcal{R}_\xi & \mathcal{R}_\eta \\ & \text{sym.} & & \mathcal{A}_{\xi\xi} & \mathcal{A}_{\xi\eta} \\ & & & & \mathcal{A}_{\eta\eta} \end{array}\right] \left\{\begin{array}{c} \Delta\tilde{u}_{/\xi} \\ \Delta\tilde{u}_{/\eta} \\ \Delta\tilde{u} \\ \Delta\tilde{\psi}_\xi \\ \Delta\tilde{\psi}_\eta \end{array}\right\} = \left\{\begin{array}{c} \Delta\tilde{P}_\xi \\ \Delta\tilde{P}_\eta \\ \Delta\tilde{P}_{\xi/\xi} + \Delta\tilde{P}_{\eta/\eta} \\ \Delta\tilde{\vartheta}_\xi \\ \Delta\tilde{\vartheta}_\eta \end{array}\right\}.$$

By assuming a linear approximation of $\tilde{p}$ in the form $\tilde{p} \cong \tilde{l}_\xi\xi + \tilde{l}_\eta\eta$, and by considering the following indicial fluxes of internal forces

$$\Delta\tilde{\vartheta}_\xi = \left[\begin{array}{cc} I & 0 \\ (\tilde{l}_\xi\xi)\times & I \end{array}\right] \left\{\begin{array}{c} R^T F_{\xi 0} \\ R^T M_{\xi 0} \end{array}\right\},$$

$$\Delta\tilde{\vartheta}_\eta = \left[\begin{array}{cc} I & 0 \\ (\tilde{l}_\eta\eta)\times & I \end{array}\right] \left\{\begin{array}{c} R^T F_{\eta 0} \\ R^T M_{\eta 0} \end{array}\right\},$$

a solution is sought of the form

$$\begin{aligned}
\Delta\tilde{u} &= \left(\tilde{U}_0 + (\tilde{l}_\xi \xi)\times\tilde{U}_1^\xi + (\tilde{l}_\eta \eta)\times\tilde{U}_1^\eta\right)\tilde{\vartheta}_0,\\
\Delta\tilde{P}_\xi &= \left(\tilde{P}_{\xi 0} + (\tilde{l}_\xi \xi)\times\tilde{P}_{\xi 1}^\xi + (\tilde{l}_\eta \eta)\times\tilde{P}_{\xi 1}^\eta\right)\tilde{\vartheta}_0,\\
\Delta\tilde{P}_\eta &= \left(\tilde{P}_{\eta 0} + (\tilde{l}_\xi \xi)\times\tilde{P}_{\eta 1}^\xi + (\tilde{l}_\eta \eta)\times\tilde{P}_{\eta 1}^\eta\right)\tilde{\vartheta}_0,\\
\Delta\tilde{\psi}_\xi &= \left(\tilde{\Psi}_{\xi 0} + (\tilde{l}_\xi \xi)\times\tilde{\Psi}_{\xi 1}^\xi + (\tilde{l}_\eta \eta)\times\tilde{\Psi}_{\xi 1}^\eta\right)\tilde{\vartheta}_0,\\
\Delta\tilde{\psi}_\eta &= \left(\tilde{\Psi}_{\eta 0} + (\tilde{l}_\xi \xi)\times\tilde{\Psi}_{\eta 1}^\xi + (\tilde{l}_\eta \eta)\times\tilde{\Psi}_{\eta 1}^\eta\right)\tilde{\vartheta}_0,
\end{aligned}$$

where $\tilde{\vartheta}_0 = \left\{\tilde{\vartheta}_{\xi 0}, \tilde{\vartheta}_{\eta 0}\right\}$, yielding

$$\begin{aligned}
\Delta\tilde{u}_{/\xi} &= \tilde{l}_\xi \times \tilde{U}_1^\xi \tilde{\vartheta}_0,\\
\Delta\tilde{u}_{/\eta} &= \tilde{l}_\eta \times \tilde{U}_1^\eta \tilde{\vartheta}_0,\\
\Delta\tilde{P}_{\xi/\xi} &= \tilde{l}_\xi \times \tilde{P}_{\xi 1}^\xi \tilde{\vartheta}_0,\\
\Delta\tilde{P}_{\xi/\eta} &= \tilde{l}_\eta \times \tilde{P}_{\xi 1}^\eta \tilde{\vartheta}_0,\\
\Delta\tilde{P}_{\eta/\xi} &= \tilde{l}_\xi \times \tilde{P}_{\eta 1}^\xi \tilde{\vartheta}_0,\\
\Delta\tilde{P}_{\eta/\eta} &= \tilde{l}_\eta \times \tilde{P}_{\eta 1}^\eta \tilde{\vartheta}_0.
\end{aligned}$$

Actually, while the drill degree of freedom is considered for completeness of the formulas, it is undetermined, being the drill problem singular; the matrix will be constrained prior to solution. The indicial fluxes of internal forces must be augmented by six self-balanced fluxes, three sets of forces and three sets of moments, that will be used to restore the compatibility of the deformations, as mentioned in Section 5.5.4. By enforcing the compatibility equations, Eqs. 5.19, 5.20, the indetermination related to the six self-balanced solutions that are allowed by the differential equilibrium equations, Eqs. 5.17, 5.18, and that must be added to the set of 12 trial indicial load modes, will be reduced, resulting in a set of twelve compatible as well as balanced solutions to indicial loads. This topic will be discussed in the next section; from the solution standpoint it does not add any further complexity, only the solution is made of 18 instead of 12 load modes.
The problem is solved first in the linear unknowns, yielding

$$\begin{bmatrix} \mathcal{E} & \mathcal{R}_\xi & \mathcal{R}_\eta \\ & \mathcal{A}_{\xi\xi} & \mathcal{A}_{\xi\eta} \\ \text{sym.} & & \mathcal{A}_{\eta\eta} \end{bmatrix} \left\{ \begin{array}{c} \tilde{l}_\xi \times \tilde{U}_1^\xi \\ \tilde{l}_\xi \times \tilde{\Psi}_{\xi 1}^\xi \\ \tilde{l}_\xi \times \tilde{\Psi}_{\eta 1}^\xi \end{array} \right\} = \left\{ \begin{array}{c} 0 \\ \tilde{\Theta}_{\xi 1}^\xi \\ \tilde{\Theta}_{\eta 1}^\xi \end{array} \right\}$$

and

$$\left[\begin{array}{ccc} \mathcal{E} & \mathcal{R}_{\xi} & \mathcal{R}_{\eta} \\ & \mathcal{A}_{\xi\xi} & \mathcal{A}_{\xi\eta} \\ \text{sym.} & & \mathcal{A}_{\eta\eta} \end{array}\right] \left\{\begin{array}{c} \tilde{l}_{\eta} \times \tilde{U}_1^{\eta} \\ \tilde{l}_{\eta} \times \tilde{\Psi}_{\xi 1}^{\eta} \\ \tilde{l}_{\eta} \times \tilde{\Psi}_{\eta 1}^{\eta} \end{array}\right\} = \left\{\begin{array}{c} 0 \\ \tilde{\Theta}_{\xi 1}^{\eta} \\ \tilde{\Theta}_{\eta 1}^{\eta} \end{array}\right\}.$$

The linear solutions are combined to yield the right-hand of the constant part of the problem

$$\left[\begin{array}{ccc} \mathcal{E} & \mathcal{R}_{\xi} & \mathcal{R}_{\eta} \\ & \mathcal{A}_{\xi\xi} & \mathcal{A}_{\xi\eta} \\ \text{sym.} & & \mathcal{A}_{\eta\eta} \end{array}\right] \left\{\begin{array}{c} \tilde{U}_0 \\ \tilde{\Psi}_{\xi 0} \\ \tilde{\Psi}_{\eta 0} \end{array}\right\} = \left\{\begin{array}{c} 0 \\ \tilde{\Theta}_{\xi 0} \\ \tilde{\Theta}_{\eta 0} \end{array}\right\}$$

$$+\left[\begin{array}{ccc} \mathcal{C}_{\xi} - \mathcal{C}_{\xi}^T & \mathcal{L}_{\xi\xi} & \mathcal{L}_{\xi\eta} \\ & 0 & 0 \\ \text{skw.} & & 0 \end{array}\right] \left\{\begin{array}{c} \tilde{l}_{\xi} \times \tilde{U}_1^{\xi} \\ \tilde{l}_{\xi} \times \tilde{\Psi}_{\xi 1}^{\xi} \\ \tilde{l}_{\xi} \times \tilde{\Psi}_{\eta 1}^{\xi} \end{array}\right\}$$

$$+\left[\begin{array}{ccc} \mathcal{C}_{\eta} - \mathcal{C}_{\eta}^T & \mathcal{L}_{\eta\xi} & \mathcal{L}_{\eta\eta} \\ & 0 & 0 \\ \text{skw.} & & 0 \end{array}\right] \left\{\begin{array}{c} \tilde{l}_{\xi} \times \tilde{U}_1^{\eta} \\ \tilde{l}_{\xi} \times \tilde{\Psi}_{\xi 1}^{\eta} \\ \tilde{l}_{\xi} \times \tilde{\Psi}_{\eta 1}^{\eta} \end{array}\right\}.$$

The solution requires the matrix to be statically determined by adding extra constraints, because the warping functions contain the rigid displacements already held by the generalised degrees of freedom of the fibre. The drill degree of freedom must be constrained even in the generalised unknowns because a one-dimensional model of the fibre does not have any drill striffness.

5.6.6 Compatibility enforcement

The compatibility constraints of Eqs. 5.19, 5.20 applied to a perturbation of generalised deformations states

$$\begin{aligned} \tilde{\rho}_{\eta} \times \Delta\tilde{v}_{\xi} + \tilde{l}_{\eta} \times \Delta\tilde{\kappa}_{\xi} - \tilde{\rho}_{\xi} \times \Delta\tilde{v}_{\eta} - \tilde{l}_{\xi} \times \Delta\tilde{\kappa}_{\eta} + \Delta\tilde{v}_{\xi/\eta} - \Delta\tilde{v}_{\eta/\xi} &= 0, \\ \Delta\tilde{\kappa}_{\xi/\eta} - \Delta\tilde{\kappa}_{\eta/\xi} &= 0. \end{aligned}$$

Applied to the previously determined set of solutions, the compatibility condition yields

$$\left[\begin{array}{cc} \tilde{\rho}_{\eta} \times & \tilde{l}_{\eta} \times \\ 0 & 0 \end{array}\right] \Psi_{\xi 0} - \left[\begin{array}{cc} \tilde{\rho}_{\xi} \times & \tilde{l}_{\xi} \times \\ 0 & 0 \end{array}\right] \Psi_{\eta 0} + \Psi_{\xi 1}^{\eta} - \Psi_{\eta 1}^{\xi} = 0.$$

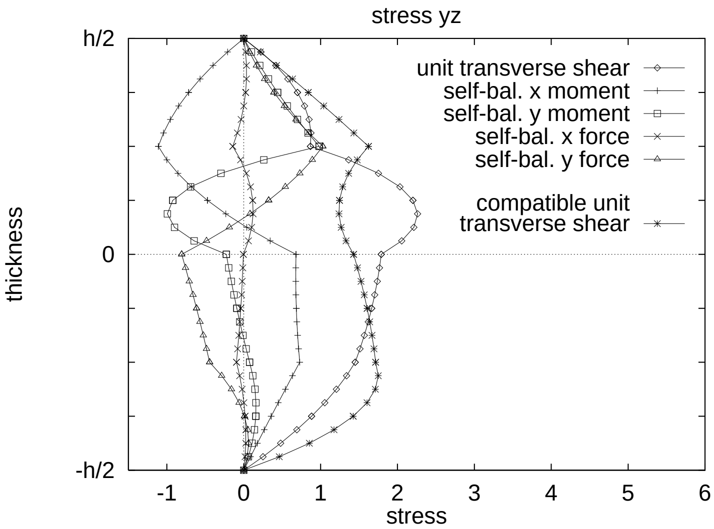

Figure 5.2: Transverse shear stress distribution — compatible vs. non-compatible and self-balanced solutions.

Matrices Ψ represent 18 balanced solutions, including 6 self-balanced solutions that can be linearly combined to the others to obtain 12 compatible solutions. Actually only four solutions are used, the remaining two referring to the drill degree of freedom and thus being constrained to avoid singularities. As an example, the transverse shear stress distribution through the thickness of a 0/90/0/90 laminate resulting from the compatibility enforcement procedure, compared to those due to the non-compatible solution and to the self-balanced solutions, is shown in Figure 5.2. The self-balanced modes and the compatibility enforcement procedure are described in detail in [33].

5.6.7 Characterisation of the fibre

After the solution is made compatibile, it can be used to compute the fibre properties. They result from substituting the indicial solutions into the definition of the discretised internal work, thus yielding the compliance matrix of the fibre

$$\frac{\partial^2}{\partial\xi\partial\eta}\Delta\delta L_i \;=\; \delta\tilde{\vartheta}_0^T C \Delta\tilde{\vartheta}_0.$$

The usual stiffness constitutive matrix D can be obtained from C by inverting it. The direct inversion is not possible since matrix C is singular because it shows null compliance for the drill degree of freedom; this solution is meaningless, because the drill degree of freedom was arbitrarily constrained to allow the solution of the problem. The compliance matrix can be pseudo-inverted, or the generalised deformations can be condensed to determine the minimum set of 8 independent deformations of the plate: the three membrane strains, the two transverse shears and the three curvatures[15].

5.7 Finite Volume Plate

The finite volume plate and shell formulation results from the direct writing of the equilibrium of a finite portion of plate. By dividing a plate in subportions, the equilibrium of each portion can be written by integrating the fluxes of internal forces along the boundary of the portion and by integrating the distributed loads on the surface and in the volume of the plate. By expressing the internal fluxes in terms of nodal displacements and rotations in a finite element way, the usual stiffness matrix results. The main advantages of the finite volume formulation are the reduced locking effect if compared to corresponding finite element formulations, and the reduced integration order, namely a line instead of a surface integration.

5.7.1 Finite Equilibrium

The weak equilibrium of the finite plate is written by integrating the differential equilibrium equations weighted by a piecewise constant weight function, as mentioned for the finite volume beam. A portion of a general plate, represented by domain B_c, supports a weight function w, that assumes unit value in B_c and is null outside B_c; as a result, its gradient is null everywhere except at the border of B_c, where it is represented by a *Dirac* δ that multiplies a vector normal to the boundary c and directed inside. The equilibrium equations of the plate, Eqs. 5.17, 5.18, multiplied by w and integrated over B_c yield

$$\int_{B_c} w\left(\nabla^T F + \phi\right) \mathrm{d}S = 0, \tag{5.21}$$

$$\int_{B_c} w\left(\nabla^T M + (l\times)^T F + \mu\right) \mathrm{d}S = 0, \tag{5.22}$$

where the distributed forces and couples ϕ, μ have been added. The product $w\nabla^T F$ can be transformed in

$$w\nabla^T F = \nabla^T (wF) - (\nabla w)^T F,$$

[15]Two are the bending curvatures, and one is the twist curvature; the latter is symmetric: it is the same in the two directions, as the membrane shear strain is.

where $\nabla w = -\delta(p-c)(\nabla c)\times$. The integration by parts of $w\nabla^T F$ yields

$$\int_{B_c} w\nabla^T F \, \mathrm{d}S = 1/2\int_c (\nabla c)\times F \, \mathrm{d}c - \int_{B_c} (\nabla w)^T F \, \mathrm{d}S,$$

where *Stokes* theorem has been applied to the divergence term. It is easy to prove that the two integrals at right-hand simply result in

$$\int_{B_c} w\nabla^T F \, \mathrm{d}S = \int_c (\nabla c)\times F \, \mathrm{d}c$$

The integration of the moment equilibrium equation is a bit more awkward because of the force moment term, but, by noting that

$$\begin{aligned} w\nabla^T M &= \nabla^T(wM) - (\nabla w)^T M, \\ w(l\times)^T F &= \nabla^T(wp\times F) - (\nabla w)^T p\times F - wp\times\nabla^T F, \end{aligned}$$

where $l = \nabla p$ has been used, and, by using $\nabla F + \phi = 0$, the integrand in Eq. 5.22 results in

$$\begin{aligned} w\left(\nabla^T M + (l\times)^T F + \mu\right) &= \nabla^T(wM + wp\times F) \\ &\quad - (\nabla w)^T(M + p\times F) + wp\times\phi. \end{aligned}$$

The same considerations made for the force equilibrium integration by part hold; in detail, the surface integration reduces to an integration on the boundary c of B_c. The two equilibrium equations, Eqs 5.21, 5.22 result in

$$\int_c (\nabla c)\times F \, \mathrm{d}c = -\int_{B_c} \phi \, \mathrm{d}S, \tag{5.23}$$

$$\int_c (\nabla c)\times(M + p\times F) \, \mathrm{d}c = -\int_{B_c} (\mu + p\times\phi) \, \mathrm{d}S. \tag{5.24}$$

The two equations can be condensed in one by extending to the plate the arms matrix $\mathcal{U}$ and the generalised internal force fluxes ϑ, resulting in

$$\int_c (\nabla c)\times\mathcal{U}(p-x_0)\,\vartheta \, \mathrm{d}c = -\int_{B_c} \mathcal{U}(p-x_0)\,\tau \, \mathrm{d}S,$$

where τ are the generalised distributed loads, and the pole x_0 has been introduced in the moment arm; it is arbitrary, because p results from the integration of l.

5.7.2 Compatibility

As mentioned earlier, the generalised strains, as defined in Section 5.5.2, do not describe a pure deformation, since they contain a rigid rotation. Their symmetry must be enforced, by adding the non-rotationality condition to the equilibrium equations. A penalty function approach is considered. Consider the non-rotationality condition of Eqs. 5.19, 5.20, weighted by the same function used for the equilibrium equations and integrated over B_c; in particular, consider, for the weighting function, the structure[16] $W = \{0, 0, Iw\}$. It yields

$$\begin{aligned} \int_{B_c} W^T \nabla \times \nu \, \mathrm{d}S &= 0, \\ \int_{B_c} W^T \nabla \times \kappa \, \mathrm{d}S &= 0. \end{aligned}$$

Consider $W^T \nabla \times \nu$ first; the same considerations hold for κ. By applying the product differentiation rule, it becomes

$$W^T \nabla \times \nu = -\nabla^T (W \times \nu) + (\nabla \times W)^T \nu.$$

By integrating by parts, and by applying *Stokes* theorem to the divergence term, it yields

$$\int_{B_c} W^T \nabla \times \nu \, \mathrm{d}S = -1/2 \int_c (\nabla c)^T \nu \, \mathrm{d}c + \int_{B_c} (\nabla \times W)^T \nu \, \mathrm{d}S.$$

It can be easily shown that the two integrals at right-hand are equal, thus yielding

$$\int_{B_c} W^T \nabla \times \nu \, \mathrm{d}S = -\int_c (\nabla c)^T \nu \, \mathrm{d}c.$$

Thus two compatibility equations result:

$$\begin{aligned} \int_c (\nabla c)^T \nu \, \mathrm{d}c &= 0, \\ \int_c (\nabla c)^T \kappa \, \mathrm{d}c &= 0; \end{aligned}$$

they can be added to the corresponding equilibrium equations by means of a penalty function γ that dimensionally is a stiffness (a force per unit length for ν and a moment for κ), or in form of algebraic constraints, in a *Lagrangian multipliers* sense.

[16] A more general structure would be $W = \{Iw, Iw, Iw\}$, but it can be easily shown that, since w, as well as ν and κ, does not depend on the abscissa in direction 3, only the third component of W is required to obtain the third component, the only non-null one, of the result of operations involving second order entities, like $\nabla \times \nu$.

5.7.3 Implementation notes

The finite volume plate or shell has not been implemented yet; for this reason, no discretisation nor linearisation is presented. The formulation has been developed and investigated, but at a first glance such a flexible element has not been retained significant for rotorcraft analysis, at least at the level of detail required by a conventional multibody analysis. It might be useful for the analysis of complicated, hingeless or bearingless rotor hubs, which sometimes use very flat components to implement stiff-in-plane, torsionally weak blade roots. Basically it resulted as a spin-off of the beam formulation, as it is apparent that most of the results can be obtained from the beam formulation by simply exchanging the support of the structural component and that of the section, and by appropriately redefining the integral and differential operators. Its development will be prosecuted in the future for more general applications.

5.8 Modal flexibility

A general way to introduce flexible behaviour in a multibody model is through the use of modes. Historically this has been the first approach followed in commercial codes [81]. Advantages of the modal approach are: 1) the ability to describe the behaviour of complex structural components, not reconductible to beams or plates, with a comparatively low number of degrees of freedom; 2) the ability to focus on the desired range of frequencies, thus allowing the use of explicit integration schemes with step size control to ensure the stability of the integration; 3) the ease in writing problems in relative coordinates, which makes the analysis of open-loop, or tree-like, mechanisms very compact and efficient.

The drawbacks mainly are: 1) the small flexible displacement implicit assumption, to allow the linear combination of modes; 2) the restriction to linear elastic structural components; 3) the poor description of the effect of concentrated loads/masses if dynamic modes are considered only, without enriching the modal base with appropriate static shapes.

In the outlined rotorcraft analysis the modal flexibility can be useful if the flexibility of the main body of the helicopter, or the wing-fuselage of a tiltrotor is to be considered, since a finite element-like discretisation is unreasonable when the dynamics of the rotor are the main focus of the analysis. As often addressed in the literature, the flexibility of the rotor support and of the fuselage are fundamental to correctly predict the vibratory level in the cockpit [26]. No modal flexibility has been used in the analyses presented in this work; however it is being implemented in the code that has been developed, and its use will be investigated in the near future. There is no practical interest in resorting to a modal model for rotor blades, because the finite element approach is expected to allow a more general modelling with the ability to account for geometric nonlinearities in a more realistic way than modes are. As a consequence, the modes are seen as a possible, reasonable choice when a trade-off between the level of detail and the efficiency of the computation must be reached. Anyway the question is still open, since may researchers and many research rotorcraft codes insist in using modal models for the blades, see for instance *Chopra*'s UMARC [57] and *Johnson*'s CAMRAD [61, 62], as opposed to the finite element approach of *Bauchau*'s DYMORE [7].

5.9 Aerodynamic forces

The task of modelling the aerodynamic forces that act on a rotorcraft, especially during unsteady advancing motion, is formidable. When attention needs be focused on very specific phenomena, like Blade-Vortex Interaction (BVI), noise generation, interaction of the main rotor wake with the fuselage or the tail rotor, a good model of the unsteady wake is mandatory. Unfortunately, the task of modelling the unsteady aerodynamics of an advancing rotorcraft is still immature, as shown for instance by the only partially satisfactory results obtained in Ref. [16], where some state-of-the-art rotorcraft analysis codes have been used to investigate the blade loads of a *Puma* helicopter with increasingly sophisticated aerodynamic models, including *Computational Fluid Dynamics* (CFD) determination of the pressure distribution on a swept blade tip, to match experimental measures.

5.9.1 Strip-theory, quasi-steady aerodynamic forces

A brief description of the aerodynamic model used in this work is presented[17]. The lifting devices, such as rotor blades and aircraft wings and control surfaces are modelled by the strip-theory, with steady or quasi-steady aerodynamic coefficients, as described in Ref. [54]. The coefficients account for *Mach* effect by means of *Glauert*'s correction, with further correction, i.e. reduced lift and increased drag, for very highly subsonic *Mach* numbers. They also account for static

[17]It might seem surprising that a couple pages only are spent about aerodynamics when an entire dissertation on the modelling of rotorcraft is presented. There are many reasons, which can be summarised in a few words: the dissertation presents what is novel, or has been developed during the current research activity, or at least is key to the comprehension of what is presented. Nothing new is being presented in the modelling of the aerodynamics of rotorcraft, so only a brief summary of the models that have been used is included.

post-stall correction and reverse flow, and for dynamic stall correction in an empirical manner; the drag resulting from radial flow is also considered. The boundary conditions for the aerodynamic forces, i.e. the configuration of the blade/wing stations at which the forces are computed, result from the combination of the motion of the reference point at the desired station, with the addition of a reference velocity that represents the asymptotic airstream speed and of the effects of spatially resolved gusts

$$\begin{aligned} v &= v_b + V_\infty + v_G, \\ \omega &= \omega_b, \end{aligned}$$

where subscripts b, ∞ and G respectively refer to *body*, *asymptotic* and *gust* quantities. A rigid-surface, lumped aerodynamic element, and a beam aerodynamic element have been formulated. They only differ in the manner the boundary conditions are computed and the loads are applied to the structure, so the simple case of lumped aerodynamic forces will be considered; the other case can be easily obtained by substituting the rigid-body velocities with those obtained by interpolating the velocities of a pool of nodes. The velocity of a point at a prescribed station is

$$v_b = \dot{x} + \omega \times f,$$

where $\dot{x}$ and ω are the velocity and the angular velocity of the node, and f is the offset from the node to the station. A reference frame on the airfoil is related to the node frame, identified by matrix R, by a rotation matrix R_a, that is used to bring the section velocities in the airfoil frame. The local velocities are thus

$$\begin{aligned} \overline{v}_b &= R_a^T R^T v_b \\ \overline{\omega} &= R_a^T R^T \omega \end{aligned}$$

An aerodynamic operator $\mathcal{A}(\overline{v}, \overline{\omega})$ is used to compute the forces and couples $\left\{\overline{F}, \overline{M}\right\}$ in the aerodynamic reference frame, which are transformed back to the global frame and applied to the node, yielding

$$\begin{aligned} F &= R R_a \overline{F} \\ M &= f \times R R_a \overline{F} + R R_a \overline{M} \end{aligned}$$

This aerodynamic model is not sophisticated, and should be considered only as a means to introduce the fundamental aerodynamic loads, irrespective of any memory effects, such as the wake, the BVI, and so on. Such a model is considered sufficient for instantaneous stability analysis, i.e. local linearisation and local stability assessment, while, for a global, or periodic stability analysis of the rotor, a more detailed and sophisticated model is mandatory. It is not the aim of this work to develop such a model, so the very first approximation given by the strip theory is accepted because it is considered sufficient for the analysis of the flight conditions we are interested in.

5.9.2 Induced velocity

A simple correction to the steady, collocated evaluation of the aerodynamic forces is given by the modelling of the inflow caused by the rotor. A dynamic inflow model has been considered, based on the work of *Peters* [76]. A dynamic system, made of three unknowns that represent the non-dimensional induced velocity and its first-order moments in pitch and roll directions, is written, with the rotor thrust and the pitch and roll moments as forcing terms. The induced velocity at each station thus depends on the radial and azimuthal position, and preserves some memory of the global forces acting on the rotor. Ideally it is added to the asymptotic steam velocity when forming the input for the aerodynamic operator, so the presence of an inflow model is transparent to the aerodynamic operator. The global thrust and moments are computed by adding the contribution of each aerodynamic element, referred to the frame of the mast. More sophisticated inflow models have been formulated, with higher order momenta and better spatial resolution of the induced velocity, but, due to the intrinsic approximation of such method, the increase in accuracy is not considered to be significant to the problem under investigation.

Part II

Control

Chapter 6

Rotorcraft control

The control of a rotorcraft may assume rather different meanings. There are many interesting aspects of the flight envelope of a rotorcraft some form of control can be applied to, ranging from the control of the flight path, usually accomplished by the pilot but with increasing automated assistance, to the reduction of vibrations in the cockpit and in critical components, e.g. avionics, to loads alleviation, noise reduction, flutter suppression, and more. All these goals have different requirements and possibly require different arrangements to be made. Different solutions have been proposed, and are being proposed at present; the requirement that represents a sort of common denominator is the need to be effective in a wide spectrum of flight conditions that result in a highly varying behaviour of the controlled system.

6.1 Introduction

This work is focused on load alleviation and vibration reduction. It is a fundamental task, since the helicopter is a restless source of vibrations, due to the way thrust is generated. The blade motion is periodic, so, when in forward flight, the combination of the blade rotation and of the helicopter advance speeds results in a periodic flow field on the blades. This on turn produces load unbalance, whose one per rev. harmonic is cancelled by the rotor flapping motion. However, higher-harmonics of the rotation speed are transmitted through the mast to the rest of the rotorcraft. In case of ideal blades, only the N_b/rev. and higher harmonics of the thrust are transmitted, being N_b the number of blades, while small unbalances in the inertial or aerodynamic properties of the blades can cause appreciable vibratory level even at 1/rev. The vibrations result in reduced life of critical components, significantly avionics, in reduced fatigue life of structural components, reduced operability of the crew and reduced comfort for the passengers and the payload in general. The cancellation of the vibrations is fundamental for a better exploitation of rotorcraft for civil and military use. The problem has gained attention in the '70s, when the first studies on active vibration reduction, significantly by means of *Higher-Harmonic Control* (HHC), began [78, 66, 93]. The currently accepted meaning of HHC is that of a simultaneous control of the blades by means of the conventional blade pitch control mechanism, the swashplate. Recently, attention moved towards more versatile and efficient control techniques, which can be generically identified as *Individual Blade Control* (IBC), see [53, 52, 26, 45] among the others, consisting in independently actuating each blade; nonetheless, HHC is still considered [72, 79, 74]. Perhaps some confusion exists in the terminology, because usually HHC is associated to periodic control, since the simultaneous actuation of the blades results in superimposing periodic pitching motions that can be different from blade to blade by properly choosing the frequency and the phase of each input, while IBC, usually associated to completely unrelated control for each blade, can be implemented to obtain a periodic, harmonic actuation of the blades. Moreover, while HHC is commonly related to the swashplate as actuator, there is no such clear identification of the actuation technique to be used best for IBC. Very different devices have been proposed and are currently investigated, and in some cases implemented. There are three basic solutions, shown in Figure 6.1, consisting in

1. deflecting a trailing edge trim tab in the outer portion of the blade that causes the flexible blade to twist, thus changing its angle of attack in a distributed manner;

2. applying a pitch change at the root of the blade, e.g. by varying the length of the pitch link;

3. directly twisting the blade by means of distributed induced strain actuators.

These actuation solutions can be obtained in different ways.

6.2 Trim tab

The trim tab solution is very attractive and is undergoing intensive investigation by many different research teams. Many wind tunnel rotor models exploiting the active trim tab have been built and tested in recent years [87, 70, 71]; a review of the state of the art can be found in [26, 45, 47]. Different means of controlling the tab have been explored; the most promising consisting in the use of smart materials to control a conventional trailing edge, hinged tab. While less than ± 2 degrees of pitch are enough to achieve a reasonable control authority when controlling the pitch of the whole blade, at least ± 15 degrees of excursion are needed to obtain

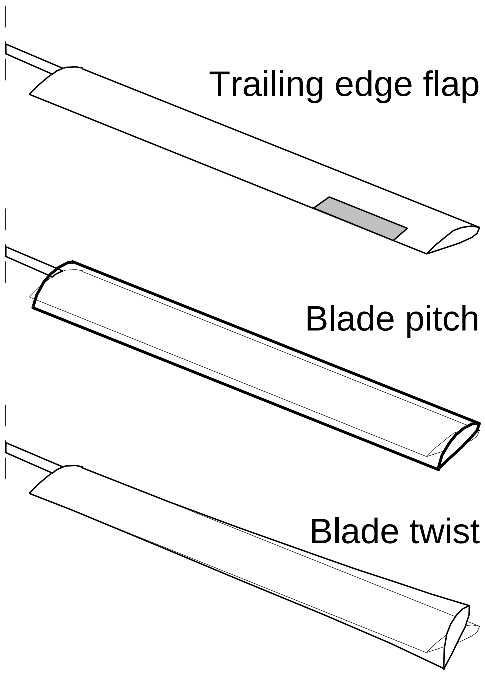

Figure 6.1: Rotor blade actuation techniques.

effective control by a trim-tab [45]. In this case only little power is required, but it must be applied to a really large stroke, so various stroke amplification mechanisms are being investigated, since smart materials such as piezoelectrics, and electro- and magneto-strictive materials, the best candidates for the actuation of the tab, show a very limited maximum stroke. While most of the stroke amplification schemes rely on mechanical devices, such as bimorph piezoelectrics, piezo-stack driven scissors, and so on, a very interesting idea is represented by the piezoelectric pump [46]. A piezoelectric device is used to pump hydraulic fluid in a large section cylinder by a small stroke piston, to drive a small section, large stroke actuator. A torsional actuator has been obtained by axially loading an open section cylinder with a piezo-stack at one end to obtain a rotation at the other end [47]. The idea of controlling the camber of the blade by strain-induced actuators is facing the arena, but since it proved to be a challenge even for the fixed-wing [92], it may be still too immature for rotorcraft application.

6.3 Blade pitch control

For the direct control of the blade pitch, both high-frequency hydraulic and induced strain actuators are investigated. The comparatively high frequencies required to control the higher-harmonic loads can be obtained by hydraulic actuators when only limited stroke is required [45]; hydraulic actuators can reach up to $50 \div 60$ Hz, which means $10 \div 12$/rev. in actual helicopters, for limited stroke. This is the case of the small pitch amplitudes that need be superimposed to the flight-control related pitch angles, i.e. the collective and the cyclic pitch. Piezoelectric stacks have been proposed as well, since they have a very broad band of operation and do not require any hydraulic power to be brought in the rotating system. There is no airborne IBC system yet; one form of IBC that is entering production is the *Total Vibration Reduction* (TVR) by *Kawasaki* [4], which relies on actuators at the rear mounts of the gear box for the reduction of higher-harmonic vibrations, while the length of the pitch links can be adjusted by means of a jackscrew, electrically actuated at very low speed, to cancel the 1/rev. vibrations caused by blade unbalance. The major unknown of an active pitch control device is the reliability; in fact a failure of the system could result in the complete loss of pitch control; the device should lock the blade pitch in case of failure, and should allow at least the pitch control related to flight control, i.e. collective and cyclic.

6.4 Induced twist actuation

The most challenging way of controlling the pitch of the blade is by directly twisting the whole blade by induced strain actuators. The strain-induced twisting of a slender body, like a rotor blade, requires the ability to induce shear strains in the beam section, that result in a global twist of the structure. A very promising material for distributed and embedded induced strain actuation has been found in the piezoelectrics. The piezoelectric effect is represented by the capability of a material to produce an electric field when loaded, and, on the contrary, to deform when subject to an electric field. In usual notation [3], the linearised piezoelectric constitutive law is:

$$\left\{ \begin{array}{c} S \\ D \end{array} \right\} = \left[\begin{array}{cc} s^{(E)} & d^T \\ d & \varepsilon^{(T)} \end{array} \right] \left\{ \begin{array}{c} T \\ E \end{array} \right\} \tag{6.1}$$

where $S_{6\times1}$ and $T_{6\times1}$ are the strain and stress arrays, and $E_{3\times1}$ and $D_{3\times1}$ are the electric field and the electric displacement arrays. Piezoeletric devices for distributed induced strain applications are manufactured in two-dimensional laminæ, to be applied on, or embedded into, the passive, or host, structure. The usual implementation consists in thin, thickness-wise (direction 3) polarised laminæ, that show an isotropic behaviour in their plane, thus being unable to induce the desired twisting. In fact, the shear strain in the plane of the piezoelectric lamina is:

$$\gamma_{xs} = 2\cos(\alpha)\sin(\alpha)(S_1 - S_2) \tag{6.2}$$

where direction s lies in the plane yz of the beam section, and x is the axis of the beam, while S_1 and S_2 are the principal strains in the plane of the piezoelectric in the material frame and α is the relative angle between the material and the beam reference frames, resulting in no shear when the two induced strains, S_1 and S_2, are equal, as happens for plane isotropic piezoelectric materials. An in-plane anisotropic piezoelectric material is required to obtain different electrically induced strains in directions 1 and 2. A material with such properties has been obtained by applying the fibre composite technology to the ceramic piezoelectric material, resulting in the *Active Fibre Composites* (AFC) [8]. Previous research resulted in the development of the *Inter-Digitated Electrodes* (IDE) principle [48] as a useful means to induce anisotropic in-plane actuation (Figure 6.2). The electrodes are aligned in pairs of conductive strips on both the upper and the lower surface of the piezoelectric. The pairs of strips are alternately charged planewise, so that an alternate, in-plane electric field normal to the strips (direction 1) is generated. The piezoeletric material is initially polarised by means of the strips themselves during the manufacturing process. The resulting device exploits the main piezoelectric coupling coefficient (d_{11}), which is usually larger than the secondary ones ($d_{12,13}$) and opposite in sign ($d_{12,13} = -kd_{11}$, with $k \simeq 0.2 \div 0.5$);

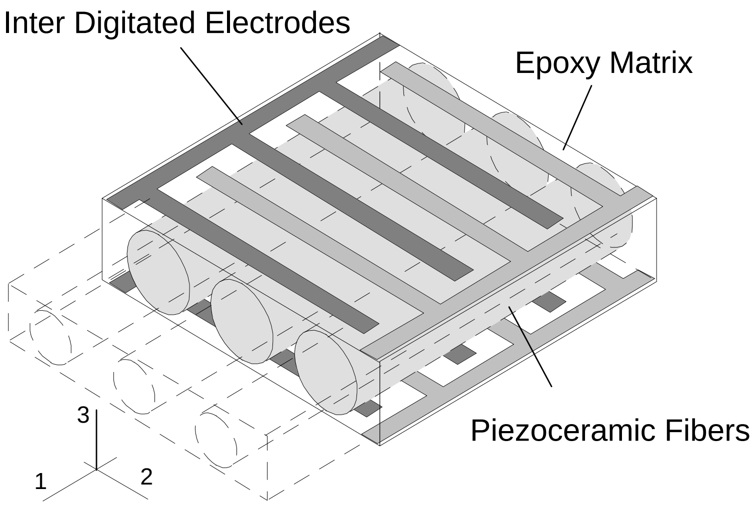

Figure 6.2: Active Fibre Composites with Inter-Digitated Electrodes.

both the fibres and the polarisation are in direction 1. When used in conjunction with AFC, the interdigitated electrodes can apply the control tension exactly in the direction of the fibre, thus completely decoupling the induced strain in the direction on the fibre from the strains in the other directions. The electrically induced strain is applied in the direction of the piezoelectric fibres only, resulting in a truly anisotropic actuation in the plane of the active ply. Equation 6.2 shows that when the fibres are oriented 45^{o} apart from the beam axis, and the two normal strains differ, the maximal coupled axial-shear actuation of the ply is obtained; the axial actuation loads can be cancelled by stacking the active plies oriented 90^{o} apart from each other.

The induced twist actuation is being investigated[1] and will be presented in Chapter 13. The characterisation of the material and of the beam section, following the beam section characterisation formulation described in Section 5.3, will be presented in Section 9.1. With currently available piezoelectric materials, the authority of a reasonable, embeddable induced strain actuation for a rotor blade is very limited. Compared to a minimal requirement of about ± 2 degrees of twist from root to tip [45, 80], about ± 0.35 degrees have been obtained by *Chopra* in 1993 with a minimum goal of ± 1 deg. [18][2], using a rather different material but

[1] Some preliminary results have been presented in [36]

[2] Reference [18] has not been directly consulted, information were obtained from Ref. [45].

exploiting the same principle of embedding an inplane anisotropic piezoelectric material oriented 45° apart from the beam axis to induce twist; *Rodgers* and *Hagood* obtained about ± 1.5 degrees with AFC and IDE [80] and about the same is expected by *Wilkie et al.* [89, 90, 91], but at the cost of dramatically reducing the torsional stiffness of the blade. This is necessary not only to allow moderately low authority actuators to statically twist the blade, but also to move the first torsional resonance frequency of the blade down to the frequency band at which the control is required. In this way the actuator operates close to resonance, exploiting large twist angles with limited control effort but with appreciable phase delay. This design goal requires a very careful investigation of the influence of a stiffness reduction on the aeroelastic stability of the rotor. The latter results have been substantially confirmed in [36] with a completely unrelated analysis.

Chapter 7

Discrete Control

This chapter describes the fundamental theory of discrete predictive control, which has been implemented for rotorcraft active control. Predictive control has been historically formulated in discrete time form due to its usual implementation in digital control systems; the theory has been formulated for continuous time as well [1]. The general, *Multi-Input Multi-Output* (MIMO) discrete time formulation proposed by *Juang* [63, 23, 64] will be used throughout the chapter; extensions will be made to coloured noise (moving average), measured disturbances (feedforward), and arbitrary weighting of both prediction error and control effort in the error function. The conventional discrete time formulation has been preserved in view of digital control applications [40].

$y(k)$	measure at time k
$u(k)$	input at time k (either imposed or from control)
$e(k)$	error at time k
$f(k)$	measured error at time k
a_i	i-th order measure regression coefficient
b_i	i-th order input regression coefficient
c_i	i-th order error regression coefficient
d_i	i-th order measured regression coefficient
m	number of measures (and of errors)
n	number of inputs
o	number of measurable errors
p	order of the model
q	advancing control horizon
r	receding prediction horizon
s	advancing prediction horizon
Θ	collection of model parameters
$\varphi(k)$	collection of measures at time k
$\hat{y}(k)$	predicted output at time k
μ	forgetting factor
λ	control input weight function

7.1 Discrete Time Equation

A discrete time, Auto-Regressive, Moving Average, with eXogenous input (ARMAX) equation has the form:

$$\begin{aligned} y(k) \quad = \quad & a_1 y(k-1) + \ldots + a_p y(k-p) \\ & + b_0 u(k) + \ldots + b_p u(k-p) \\ & + e(k) + c_1 e(k-1) + \ldots + c_p e(k-p) \\ & + d_0 f(k) + \ldots + d_p f(k-p)\,, \end{aligned} \tag{7.1}$$

where $y(t)$, $u(t)$ are the output and input arrays at time t, $e(t)$ is the error array at time t, $f(t)$ is a measurable but uncontrollable input at time t; a_j, $j = 1, \ldots, p$, b_j, $j = 0, \ldots, p$, c_j, $j = 1, \ldots, p$ and d_j, $j = 0, \ldots, p$ are the matrices of a p-order, time-independent, linear discrete system. The number of equations is represented by the number of outputs m; matrices a_i are $m \times m$, as matrices c_i are; matrices b_i are $m \times n$, being n the number of inputs; finally, matrices d_i are $m \times o$, being o the number of measurable errors. The difference between the inputs u and the measured errors f is purely formal, being the u reachable in principle, and thus usable to control the system, while the f are only observable and thus can be used only as measures for a feedforward control. Usually the matrices of the system are unknown, only measures of inputs and outputs being available; the error e is unmeasurable by definition, while f is assumed to be perfectly measurable. The order of the system, p, may differ for each signal; the case of a *Finite Impulse Response* (FIR)

$$y(k) \;=\; b_0 u(k) + \ldots + b_p u(k-p)$$

is the limit for a system with order 0 for y and very high order p for the u, as successfully implemented in [24]. It has been implemented and investigated, but the very complex dynamics of rotorcraft seem to require too long a time for the response to decay. In the following the same order p for all the signals is assumed throughout the chapter, the extension to different regression orders being straightforward.

7.2 System Identification (ID)

The yet unknown system matrices can be stacked in a matrix Θ, while the observations can be stacked in an array $\varphi(k)$, as follows:

$$\begin{aligned}
\Theta \;&=\; [a_1, \ldots, a_p, b_0, \ldots, b_p, c_1, \ldots, c_p, d_0, \ldots, d_p]\,, \\
\varphi \;&=\; \Big[\, y(k-1)^T, \ldots, y(k-p)^T, \\
&\quad\;\; u(k)^T, \ldots, u(k-p)^T, \\
&\quad\;\; e(k-1)^T, \ldots, e(k-p)^T, \\
&\quad\;\; f(k)^T, \ldots, f(k-p)^T \Big]^T .
\end{aligned}$$

The predicted output is

$$\hat{y}(k) \;=\; \Theta\varphi(k)\,, \tag{7.2}$$

and the difference between the current and the predicted output represents the error at the current time step, which is unknown by definition. Matrix Θ depends on k as far as it is estimated from a finite set of measures; it approaches the exact value provided the true system has the form of the assumed model. Equation 7.2 gives a means to estimate the error at every time step in a recursive manner. The error may be due to unmeasured disturbances, errors in measures, and errors in the parameters of the model (type, order, and so on):

$$e(k) \;=\; y(k) - \hat{y}(k)\,.$$

The observations at time steps ranging from i to j can be stacked by columns: $y = y(i:j)$, $\varphi = \varphi(i:j)$, $e = e(i:j)$, resulting in

$$e \;=\; y - \Theta\varphi, \tag{7.3}$$

where the expected output that results from the yet to be identified system, $y_e = \Theta\varphi$, is used. If the error is unbiased, Equation 7.3 does not depend on the error itself (the error does not participate in array φ) and thus Θ can be solved for a finite set of measures to determine the optimal value of the unknown parameters. In case of biased error, instead, it can be determined by recursively adding columns to Equation 7.3, and using each parameter estimate to compute the current estimate of the error. A global measure of the error is:

$$J = \frac{1}{2} e e^T .$$

The minimisation of J with respect to Θ gives a least squares fit of the system:

$$\Theta = y\varphi^T \left(\varphi\varphi^T\right)^{\dagger} ,$$

where the † denotes the pseudo-inversion, that is required in case the system is only semi-definite. In this case, the excitation is not persistent, or the system is not completely controllable.

7.2.1 Recursive Implementation

The recursive expressions of matrices $\varphi\varphi^T$ and $y\varphi^T$ are:

$$\left(\varphi\varphi^T\right)_{j+1} = \left(\varphi\varphi^T\right)_j + \varphi(k+j)\,\varphi(k+j)^T$$

and:

$$\left(y\varphi^T\right)_{j+1} = \left(y\varphi^T\right)_j + y(k+j)\,\varphi(k+j)^T .$$

The inverse of matrix $\varphi\varphi^T$ can be directly updated instead of factorising the updated matrix, by using the LDL^T factorisation, since the matrix is symmetric and positive definite or semidefinite in the worst case; the positive definiteness can be artificially enforced. In this way, the numerical loss of accuracy can be reduced while improving the efficiency of the computation. The recursive algorithm is:

$$\Phi(k)^{\dagger} = \mu\Phi(k-1)^{\dagger} + \varphi(k)\,\varphi(k)^T , \tag{7.4}$$

$$\psi(k) = \mu\psi(k-1) + y(k)\,\varphi(k)^T , \tag{7.5}$$

$$\Theta(k) = \psi(k)\,\Phi(k) , \tag{7.6}$$

$$e(k) = y(k) - \Theta(k)\,\varphi(k) , \tag{7.7}$$

Equations 7.4, 7.5 are used to update the matrices

$$\Phi(k) = \left(\sum_{j=1,k} \varphi(j)\,\varphi(j)^T\right)^{\dagger} ,$$

$$\psi(k) = \sum_{j=1,k} y(j)\,\varphi(j)^T ,$$

where a forgetting factor μ has been used to identify a comparatively slowly time-varying system. Equation 7.6 is used to update the estimate of the system parameters; finally, Equation 7.7 is used to estimate the error at the current step. As shown in the following section, artificial stabilisation of the moving average part of the system is required, since unstable error dynamics, that can occur during the identification, have no physical meaning [2].

7.2.2 Stabilisation of the Parameter Estimates

The matrices a_i can represent either a stable or an unstable system, depending on the nature of the system to be identified. Usually matrices b_i, as well as d_i, should describe a stable system unless a non-minimum phase system (a system with zeroes outside the unit circle) is considered. But matrices c_i, when a biased error system is considered, should describe a stable system, since the dynamics of the error cannot be unstable[1]. During the identification, and significantly during the initial phase of the recursion procedure, the system described by matrices c_i can temporarily become unstable, leading to a loss of physical meaning for the error model. A stabilisation algorithm is needed, that preserves the dynamic propeties of the error, namely the phase of the eigenvalues and the shape of the eigenvectors. A state space realisation of such system is

$$\left\{ \begin{array}{c} e(k) \\ e(k-1) \\ \vdots \\ e(k-p+1) \end{array} \right\} = \begin{bmatrix} -c_1 & \dots & -c_{p-1} & -c_p \\ I & \dots & 0 & 0 \\ \vdots & \ddots & \vdots & \vdots \\ 0 & \cdots & I & 0 \end{bmatrix} \left\{ \begin{array}{c} e(k-1) \\ e(k-2) \\ \vdots \\ e(k-p) \end{array} \right\},$$

or

$$E(k) = ME(k-1)\,.$$

If ρ_c are the eigenvalues of matrix M, and $\max(|\rho_c|) > 1$, the dynamics of the error becomes unstable. It can be easily stabilised by contracting the poles inside the unit circle, in other words by scaling the dynamics of the error by a coefficient w such that, being k a stability treshold, e.g. $k = 0.85 \div 0.90$, $\tilde{c}_i = wc_i$, with $w = k/\max(|\rho_c|)$, become the new error dynamics coefficients when $w > 1$. The errors at times $k-1, k-p$ on turn must be divided by w.

[1] The error is by definition the result of an ergodic process; the error regression coefficients simply represent the residualisation of the dynamic information that cannot fit in the system. If the dynamics of the error contain any significant information, such as some unstable dynamics, these must fit in the model.

7.2.3 Adaptive forgetting factor

The forgetting factor μ, introduced in Equations 7.4, 7.5, determines the memory of the identification. It is very important, basically for two reasons, one based on numerical considerations and the other on requirements for adaptive control. The first reason is related to the starting of the identification. When the extended, recursive least mean squares are implemented, the estimates of the parameters are required right from the very first steps, to allow to estimate the error; but the problem cannot be solved until the cross-covariance matrix is positive definite. To overcome the problem, the matrix is initialised as an identity matrix that is quickly cancelled by the addition of the covariance terms, and in the limit becomes negligible. The use of a forgetting factor allows to quickly cancel the initial, rough estimates of the parameters, which decay quadratically, since, being $|\mu| < 1$, the contribution to the covariance matrix related to a time step k steps behind is weighted in the parameter estimate by μ^k. The second reason is related to the fact that, when identifying a system that slowly varies with time, the identification must be able to follow as close as possible the new system. An alternative to the use of a forgetting factor is to resort to a moving window, as used by *Juang* [64] in a rather different way to compute the *Deadbeat*[2] control matrices directly from the raw data. This choice is considered interesting, but to allow an efficient implementation it requires to add the contribution that is entering the measure window to the covariance matrix and simultaneously to subtract the contribution that is falling out of the window; if the factorised matrix is directly updated, such operation can become numerically inconsistent and lead to a destabilising behaviour [2]. By forgetting what has been identified in the past, only the recent system behaviour affects the identification and appreciable changes in the system can be quickly reflected by the identification. On the other hand, if the system does not change much for long time, a short-memory identification requires a high persistent excitation to be able to continuously keep track of the system. This might be a drawback because it requires the system to be continuously excited, sometimes with detrimental effects on power consumption, fatigue life of components, comfort of the crew and of the payload. A good compromise has been found by implementing an adaptive forgetting factor, based on a global measure of the variance of the error. The forgetting factor is integrated by a difference equation, $\mu(k) = \rho\mu(k-1) + (1-\rho)\mu_{max}$, to reach an asymptotic value of $\mu_{max} \approx 1$, corresponding to nearly permanent memory; when the variance of the error overcomes a predefined treshold, implying that appreciable changes in the system took place, the forgetting factor is pulled back to a comparatively small value μ_{min}, thus allowing the identification to refresh the estimates of the parameters in a short time.

[2] Discussed in Section 7.3.1.

7.3 Predictive Control

As soon as an estimate of the system to be controlled is available, either by parametric modelling or by black box identification, the horizon of the prediction can be easily extended. By evaluating Eq. 7.1 at time $t = k+1$, the predicted value results in

$$\begin{aligned}
\hat{y}(k+1) \; = \; & a_1\hat{y}(k)+\ldots+a_p y(k-p+1) \\
& +b_0 u(k+1)+\ldots+b_p u(k-p+1) \\
& +c_2 e(k-1)+\ldots+c_p e(k-p+1) \\
& +d_2 f(k-1)+\ldots+d_p f(k-p+1)\,,
\end{aligned} \tag{7.8}$$

the difference between the predicted and the actual values being the error. Notice that the measured error at times $k+1$ and k, as well as the error at time k, are not considered because they are unknown, and by definition they are not predictable. By substituting the predicted value of the output at time $t = k$, Eq. 7.8 becomes

$$\begin{aligned}
\hat{y}(k+1) \; = \; & a_1^1 y(k-1)+\ldots+a_p^1 y(k-p) \\
& +b_0 u(k+1)+b_0^1 u(k)+\ldots+b_p^1 u(k-p) \\
& +c_1^1 e(k-1)+\ldots+c_p^1 e(k-p) \\
& +d_1^1 f(k-1)+\ldots+d_p^1 f(k-p)\,,
\end{aligned}$$

where the new system matrices are recursively defined as:

$$\begin{array}{rclcrclcrcl}
a_i^0 & = & a_i, & & a_i^j & = & a_1^{j-1}a_i^0+a_{i+1}^{j-1}, & & a_{p+1} & = & 0, \\
b_i^0 & = & b_i, & & b_i^j & = & a_1^{j-1}b_i^0+b_{i+1}^{j-1}, & & b_{p+1} & = & 0, \\
c_i^0 & = & c_i, & & c_i^j & = & a_1^{j-1}c_i^0+c_{i+1}^{j-1}, & & c_{p+1} & = & 0, \\
d_i^0 & = & d_i, & & d_i^j & = & a_1^{j-1}d_i^0+d_{i+1}^{j-1}, & & d_{p+1} & = & 0.
\end{array}$$

The predicted error at step k and beyond is assumed to be null since the error is assumed to be uncorrelated with the outputs, the inputs, the past errors and the past measured errors, while the estimates of the output are supposed to be exact. The predicted value at time $t = k+j$ becomes:

$$\begin{aligned}
\hat{y}(k+j) \; = \; & a_1^j y(k-1)+\ldots+a_p^j y(k-p) \\
& +b_1^j u(k-1)+\ldots+b_p^j u(k-p) \\
& +c_1^j e(k-1)+\ldots+c_p^j e(k-p) \\
& +d_1^j f(k-1)+\ldots+d_p^j f(k-p) \\
& +b_0^0 u(k+j)+\ldots+b_0^j u(k)\,.
\end{aligned}$$

Let s be the number of steps ahead of the prediction. The predicted outputs from time $t = k$ to time $t = k+s-1$ become:

$$\left\{\begin{array}{c} y(k+s-1) \\ \vdots \\ y(k) \end{array}\right\} = \begin{bmatrix} a_1^{s-1} & \dots & a_p^{s-1} \\ \vdots & \ddots & \vdots \\ a_1^0 & \dots & a_p^0 \end{bmatrix} \left\{\begin{array}{c} y(k-1) \\ \vdots \\ y(k-p) \end{array}\right\}$$

$$+ \begin{bmatrix} b_1^{s-1} & \dots & b_p^{s-1} \\ \vdots & \ddots & \vdots \\ b_1^0 & \dots & b_p^0 \end{bmatrix} \left\{\begin{array}{c} u(k-1) \\ \vdots \\ u(k-p) \end{array}\right\} + \begin{bmatrix} c_1^{s-1} & \dots & c_p^{s-1} \\ \vdots & \ddots & \vdots \\ c_1^0 & \dots & c_p^0 \end{bmatrix} \left\{\begin{array}{c} e(k-1) \\ \vdots \\ e(k-p) \end{array}\right\}$$

$$+ \begin{bmatrix} d_1^{s-1} & \dots & d_p^{s-1} \\ \vdots & \ddots & \vdots \\ d_1^0 & \dots & d_p^0 \end{bmatrix} \left\{\begin{array}{c} f(k-1) \\ \vdots \\ f(k-p) \end{array}\right\} + \begin{bmatrix} b_0^0 & \dots & b_0^{s-1} \\ \vdots & \ddots & \vdots \\ 0 & \dots & b_0^0 \end{bmatrix} \left\{\begin{array}{c} u(k+s-1) \\ \vdots \\ u(k) \end{array}\right\},$$

or:

$$Y_s = AY_p + BU_p + CE_p + DF_p + PU_s. \tag{7.9}$$

The arrays and the matrices in Equation 7.9 are obtained by stacking the equations of the output at the above mentioned time steps, i.e. Y_s contains the predicted output at s future time steps from the current one; Y_p, U_p, E_p and F_p contain the (measured) outputs, inputs, the unmeasurable and the measured errors at the previous p time steps, and thus are known; U_s contains the control inputs that must be determined to obtain the desired behaviour. The predicted output should be equal to a desired sequence of values, namely $Y_s = Y_d$, resulting in:

$$Y_d = AY_p + BU_p + CE_p + DF_p + PU_s. \tag{7.10}$$

7.3.1 Generalised Predictive Control

The so called *Minimum Variance Control* [1] descends from Equation 7.10 with $s = 1$, by directly imposing the desired output at step k and solving for the required control input. Under the assumption that the system have a full rank direct transmission term (namely, matrix b_0 be invertible), and provided that the system is minimum phase, a single-step prediction horizon is sufficient. Moreover, the response in one step follows the desired behaviour regardless of the required control effort, except for the (unpredictable, because uncorrelated by assumption) errors $e(k)$ and $f(k)$. As a consequence, the variance of the error is minimal. The *Generalised Predictive Control*, on the other hand, represents an extension and a generalisation of this behaviour. The control still tries to force the system to follow the desired output starting from the current step, but the desired behaviour is imposed over a higher number of steps ahead. A prediction horizon higher than the control one can be used; in this case the desired response is imposed in a least square sense. Moreover, the control effort is accounted for by weighting the control output against the prediction error, to avoid saturation of the actuators and too rough a behaviour. An interesting form of predictive control is called *Deadbeat Control*. It has not been considered in this work since it can be obtained as a special case of a more general formulation of the GPC (the same applies to the Minimum Variance), and because it resulted less efficient and less versatile than the GPC in the investigated cases. The control output results from the minimisation of the functional[3]

$$J = \frac{1}{2}\left((Y_d - Y_s)^T (Y_d - Y_s) + \lambda U_s^T U_s\right) \tag{7.11}$$

with respect to the control input U_s, yielding:

$$U_s = \left(P^T P + \lambda I\right)^{\dagger} P^T (Y_d - AY_p - BU_p - CE_p - DF_p),$$

where λ is the control weight function. The control input at time $t = k$ is given by:

$$u(k) = \alpha_c Y_p + \beta_c U_p + \gamma_c E_p + \delta_c F_p + \varepsilon_c Y_d,$$

where ε_c is the last block-row of matrix $Q = \left(P^T P + \lambda I\right)^{\dagger} P^T$, and the feedback matrices are $\alpha_c = -\varepsilon_c A$, $\beta_c = -\varepsilon_c B$, $\gamma_c = -\varepsilon_c C$ and $\delta_c = -\varepsilon_c D$.

7.3.2 Interpretation of the Predictive Control

The minimum variance control clearly represents a form of zero-pole cancellation. The control cancels the system poles and zeroes by inverting the system $A^{-1}B$. This operation is permitted only if the system is stable and minimum phase; the resulting close-loop system statically responds to the current, unpredictable input only. The GPC attenuates this abrupt behaviour by simply shifting the poles and zeroes of the system towards higher frequencies. This operation, as well as the minimum variance does, may lead to unstable behaviour when the control is applied to non-minimum phase systems. By appropriately choosing the weight function λ, both non-minimum phase and unstable systems can be controlled, with limited loss in performances. The choice of the model order and of the prediction and control horizons are key to the effectiveness of the control. The order p must be high enough to account for all the meaningful poles of the system (a rule of thumb says that $p \times m$ should be equal to or slightly higher than the number of physical poles). But too high an order could result in a poor, noisy and time consuming identification, that tries to follow a bunch of numerical, continuously

[3] By considering that the system identification and the control design require to minimise two functionals very similar in form and nature, *Juang* [64] integrated the two phases, obtaining the *Deadbeat* control matrices directly from the measures.

moving poles. The prediction horizon s should be as high as p to ensure that the complete dynamics of the system is accounted for, including any non-minimum phase behaviour of the system, at least up to the model order; higher prediction horizons do not add further information to the prediction, but, together with a smaller control horizon, result in an overcollocated enforcement of the desired behaviour, thus overconstraining, and implicitly reducing, the control effort.

7.3.3 Temporal weighting

The error measure of Equation 7.11 can be generalised by introducing two weighting matrices, W and R, that give different momentum to the prediction error and to the control effort depending on the distance from the current time step, namely

$$J = \frac{1}{2}\left((Y_d - Y_s)^T W (Y_d - Y_s) + \lambda U_s^T R U_s\right), \qquad (7.12)$$

yielding

$$U_s = \left(P^T W P + \lambda R\right)^{\dagger} P^T W \left(Y_d - A Y_p - B U_p - C E_p - D F_p\right).$$

The GPC results from setting[4] $W = R = I$ with appropriate λ, while the deadbeat control can be obtained by setting

$$W = Q = \begin{bmatrix} I & 0 \\ 0 & 0 \end{bmatrix}$$

regardless[5] of λ, with $s = 2p$, being submatrices I and 0 of order $(p \times m) \times (p \times m)$ for W and $(p \times n) \times (p \times n)$ for R respectively, yielding

$$\left(P^T W P + \lambda R\right)^{\dagger} P^T W = \begin{bmatrix} 0 & 0 \\ P_{db}^{\dagger} & 0 \end{bmatrix},$$

matrix $P_{db} = P(1 : p \times m, p \times n + 1 : 2p \times n)$ being the Q of the deadbeat control; in other words it results on one side in forcing the control effort to be null after p steps, while on the other side in weighting only the control effort after p steps. The pseudo-inversion is required since matrix P_{db} in general is rectangular and could be rank-deficient. Because the system is well-posed, the control is null after p steps, and there is no constraint on the response during the first p steps. Any intermediate combination of weighting matrices can be used to taylor the control behaviour, from scaling the way the response at different time steps is weighted

[4]Remember that matrices W, R in general have different dimensions unless the system has the same number of inputs and outputs.

[5]Provided $\lambda \neq 0$ to ensure the control effort is null after exactly p steps.

in J, to weighting the control effort also in the first steps to avoid control roughness. This formulation somehow unifies the different forms of predictive control here described, and extends the family of the generalised predictive controllers towards a complete tayloring of the error measure. Even more complicated, non-quadratic error functions, accounting for actuator saturation, output constraints, and virtually any other objective function, in the spirit of the suboptimal control, have been proposed [83, 51], with the major drawback of requiring a nonlinear solution to compute the control signals. In the mentioned works, the identification was performed by a neural network, so a Newton-Raphson procedure was already required for the identification. This aspect of the predictive control has not been thoroughly investigated in rotorcraft applications, but shows an interesting versatility, even if the addition of two new sets of control parameters, the weights W and R, makes it more complicate to tune the controller, in the absence of a simple, reliable design algorithm. An adaptive, self-adjusting algorithm is sought, based on some performance measure, that computes the weighting factors in matrix R, or at least the value of the weight λ.

Chapter 8

Multidisciplinary problems

This chapter looks like a todo list, indeed. A lot of work is still under development in the field of multidisciplinary modelling. In this dissertation only the part directly related to rotorcraft control is illustrated, but efforts towards the integrated solution of multidisciplinary problems involving aeroelastic, electric and hydraulic models are underway.

8.1 Control

The analysis of active control-related problems require the modelling of several components when a high detail level is desired. They can be grouped as follows:

1. Actuators
2. Sensors
3. Networking
4. General purpose

The physical actuation and sensing principles determine how the behaviour of the mechanical system interacts with the control and measure signals. Regardless of their nature, there is some relationship of the kind

$$\begin{aligned} s &= s(x), \\ f &= f(a), \end{aligned}$$

where x generally represents a kinematic unknown, regardless of the differentiation order that is actually exploited by the sensing principle; s and a respectively are the measure and the actuation signals, while f is the force generated by the actuator, regardless of its nature.

8.2 Actuators

As specialised actuators for rotorcraft control, the following has been implemented:

1. Swashplate
2. Piezoelectric beam
3. Other

8.2.1 Swashplate

The swashplate results from the assembly of basic joint elements, usually:

- two in-plane joints that force the non-rotating plate to slide along the mast;
- three variable-distance pin joints that enforce the distance and the attitude of the fixed plate with respect to the rotorcraft frame;
- one in-plane joint that prevents the axial rotation of the fixed plate with respect to the fuselage, emulating the scissors; as an alternative, the scissors can be entirely modelled by two plane hinges and one spherical hinge, requiring two additional nodes;
- one plane rotation joint that constrains the two plates;
- one in-plane joint that prevents the axial rotation of the rotating plate with respect to the hub, emulating the scissors.

An alternative solution consists in:

- one prismatic joint that forces a node to slide along the mast, allowing no rotation with respect to the rotorcraft frame;
- one universal joint that constrains the fixed plate on the sliding node, restraining the axial rotation only;
- three variable-distance pin joints that enforce the distance and the attitude of the fixed plate with respect to the rotorcraft frame;
- one plane rotation joint that constrains the two plates;
- one in-plane joint that prevents the axial rotation of the rotating plate with respect to the hub, emulating the scissors.

The swashplate transmits the pitch to the blade by means of a pitch link, usually modelled as a rigid or flexible distance pin joint. The elongation of the non-rotating links can be independently assigned as function of the time, or of some control signal. To obtain a smoother behaviour, the imposition of the elongation time rate represents a more viable choice, that is more respective of the principle that is used to apply the control, namely by means of control forces that result from a controller that follows some desired actuator position; in this case a change in elongation rate corresponds to an impulsive change in control force. To ease the application of the desired controls, a distributor element has been implemented, which determines the elongations of the links based on the desired collective and cyclic pitch.

8.2.2 Piezoelectric beam

The Active Twist Rotor requires the impelementation of a beam model for the blades that allows to exploit the piezoelectric effect at the constitutive level, to accout for any effects related to the geometric nonlinearity of the blade motion. The piezoelectric beam model, from a beam characterisation and a structural analysis standpoint, is described in Chapter 9; here its use is briefly anticipated from a control standpoint. The finite volume beam element, presented in Section 5.4, describes a three-node beam element whose constitutive properties are considered at two intermediate sections. The piezoelectric generalisation introduces electric field-dependent internal forces at these sections, that participate in the determination of the beam equilibrium. Due to the nature of the piezoelectric patches and to the negligible low frequency electrodynamics of the systems under analysis, it is reasonable to assume that the electric voltage is applied to the patches simultaneously at every point, both throughout the section and along the axis. So, even if a long blade, with refined mesh discretisation is considered, the number of electric unknowns is limited to the number of independent piezoelectric patches that are distributed along the blade; the control signal is applied directly to those unknowns.

8.2.3 Other actuation means

The generality of the implementation of exogenous forces allows a high degree of freedom in determining their amplification factor, as described in Appendix H.1.1. As a result, any exogenous force, mechanical as well as generalised, can depend on the value of an arbitrary combination of unknowns, thus exploiting a simple but effective form of indirect feedback. This dependence is not exploited in the computation of the Jacobian matrix, of course, thus introducing some explicit

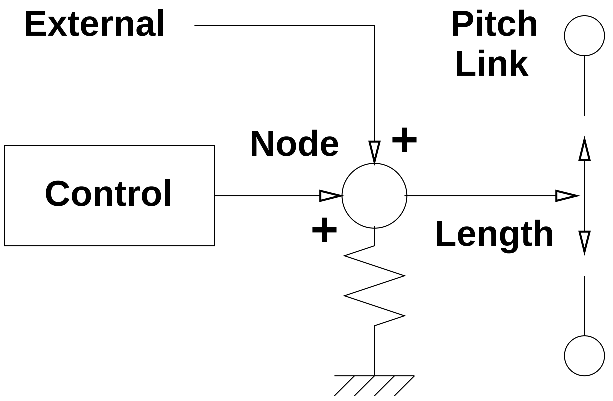

Figure 8.1: Pitch control scheme

behaviour in the solution algorithm, but this is usually acceptable in terms of convergence rate when such behaviour is confined in few degrees of freedom with comparatively small gains. As an example, a node can be grounded by a spring by introducing a force whose amplitude is function of the position of the node in one direction. This trick has been exploited, for example, to superimpose the control signal to some external pitch control signal. Consider for instance the collective pitch. Its amplitude is contained in a variable θ_{actual}, and the length of the pitch links is read from such variable at run-time by the imposed length joint. The value of θ_{actual} results from a simple equation of the form $\theta_{actual} = \theta_{external} + \theta_{control}$. The two inputs are applied by means of generalised force elements, the former, $\theta_{external}$, representing a truly exogenous contribution, e.g. the desired reference pitch, and the latter, $\theta_{control}$, resulting from the controller, as shown in Figure 8.1. Eventually, such equation will be extended by including the dynamics of the hydraulic actuators here described by the variable length distance joints, and the resulting desired elongation will be converted in some electrovalve control signal. The same approach can be used, for instance, to stabilise the rotation speed of the rotor, instead of directly prescribing it with a joint. A couple, proportional to the difference between the desired and the actual speed, and to the speed time rate, can be a good first approximation of a speed control scheme. The gains of the proportional and derivative parts must be designed with care to avoid any possible instability.

8.3 Sensors

The following sensors have been implemented:

1. Linear and rotational accelerometers

2. Strain gages attached to beam elements
3. Piezoelectric beam elements
4. Direct measure of any unknown, and of many derived entities.

8.3.1 Accelerometers

Accelerometers, attached to the nodes, have been implemented. They return the measure of the acceleration in a prescribed direction, which is fixed in the node reference frame. Such measure can be filtered through a transfer function, as described in Section 8.5, that accounts for the dynamics of the device, consisting in a band-pass filter with a zero at the origin followed by a pole, a flat response part terminating with a resonance peak, and with two coincident poles governing the high frequency decay. The built-in transfer function may be overridden by a user-defined one.

8.3.2 Strain gages

The beam elements allow to easily introduce some strain measure. The direct measure of the generalised strains is a very simple task, although it is important to remember that the strains resulting from the direct interpolation of the derivatives of the nodal displacements and rotations are highly inaccurate, a reasonable measure of the strains resulting only from an internal force and couple balance reconstruction *a posteriori*. To allow some more realistic measure, a strain gage element has been implemented, which computes the strains at some point of the beam section by combining the strains resulting from axial extension and flexural bending.

8.3.3 Piezoelectric beams

The sensing equation of the piezoelectric beam allows to introduce some interesting measure of the average strain over a portion of beam. Although very interesting in case a collocated control is addressed, this kind of measurement has not been investigated yet in active twist rotorcraft applications.

8.3.4 Direct unknown measure

The last type of measure, although very simple and at a first glance unrelated from any physical measure principle, can be viewed as the simplification and the idealisation of an arbitrary measure principle; as an example, one can consider the direct measure of a reative rotation angle in a plane rotation hinge: there is no need to detail how the measure is obtained, whether by a potentiometer or by some non-intrusive electromagnetic device or anything else, as far as the dynamics of the transfer function from the angle to the electric signal in the frequency range of interest can be neglected. Moreover, the measured signal can be filtered through an arbitrary transfer function element to emulate the dynamics of some actual measurement device, as described in Section 8.5.

8.4 Networking

The modelling of control systems up to some detail level may require the direct inclusion of some electric component behaviour. Basic network devices such as resistors, capacitors, inductors, diods, tension as well as current generators have been implemented. They act on scalar degrees of freedom that represent the electric tensions at the nodes of the electric network. To parallel the structural formulation, the electric tensions are the nodal displacements, and the nodal current balance equations mimic the force balance equations of the structural case. As an example, after defining the output y and the input u as the current and the tension affecting a node, and x as an internal degree of freedom when required, consider a linear resistor in the form:

$$\left\{ \begin{array}{c} y_1 \\ y_2 \end{array} \right\} = k \left[\begin{array}{rr} 1 & -1 \\ -1 & 1 \end{array} \right] \left\{ \begin{array}{c} u_1 \\ u_2 \end{array} \right\}$$

where $k = 1/R$ is the conductance, which parallels a spring; a linear capacitor in the form

$$\left\{ \begin{array}{c} y_1 \\ y_2 \end{array} \right\} = k \left[\begin{array}{rr} 1 & -1 \\ -1 & 1 \end{array} \right] \left\{ \begin{array}{c} \dot{u}_1 \\ \dot{u}_2 \end{array} \right\}$$

where $k = C$ is the capacitance, which parallels a damper; a linear inductor in the form

$$\begin{aligned} \left\{ \begin{array}{c} y_1 \\ y_2 \end{array} \right\} &= \left\{ \begin{array}{r} -1 \\ 1 \end{array} \right\} x, \\ \dot{x} &= k \left[\begin{array}{rr} -1 & 1 \end{array} \right] \left\{ \begin{array}{c} u_1 \\ u_2 \end{array} \right\} \end{aligned}$$

where $k = 1/L$ is the inverse of the inductance. Those elements are general, and can be used to describe ideal components common to many types of problems. An accurate programming allows to use them in conjunction with any degree of freedom in a safe and intuitive manner.

In some cases, "algebraic" constraint equations between tensions need be defined, for instance in case of voltage generators; in such cases, the resulting reaction unknowns are electric currents that participate in the node current balance, i.e.

$$\begin{aligned} y &= x \\ u &= u_0 \end{aligned}$$

To add generality to the formulation, most of such components have been implemented referring to arbitrary equations involving arbitrary unknowns. Such elements have been called "general purpose elements", or GENELs. For instance, a single degree of freedom voltage generator can be used to impose the tension of a node of the network, or to impose the displacement as well as the velocity of a degree of freedom of a structural node, or the pressure of some hydraulic network node, and so on. Strictly speaking, GENEL elements are those described in Section 8.5, the networking ones rather representing some "bulk" element type, but the difference is very subtle.

8.5 General purpose

The strict definition of "general purpose elements" (GENEL) refers to elements that are user-defined[1], and write some arbitrary relationship between unknowns that do not need to have any precise physical meaning. Examples of implemented GENELs are:

- State-space systems, of the form

  $$\begin{aligned} \dot{x} &= Ax + Bu, \\ y &= Cx + Du, \end{aligned}$$

  where the x are internal states and u, y are the inputs and the outputs respectively. This element allows to model an arbitrary transfer function between signals and thus is very useful in adding the dynamics of actual devices to bulk measure or control signals, or in implementing analog filters.

- Generalised Predictive Control elements, as detailed in Chapter 7; in such case, a discrete signal of the form

  $$u_c(t) = \sum_i a_{ci} y(t-i) + \sum_i b_{ci} u(t-i) + \ldots$$

[1]The implementation of general purpose and user-defined elements has been simplified and enhanced by allowing the use of run-time linked elements.

is computed from arbitrary measured signals to estimate the next control input. At the same time, the control matrices are redesigned, if required, to adapt the control according to the dynamic content of the measures.

- Dynamic Inflow element, exploiting the formulation proposed in Ref. [76], where the inflow velocity at some point on the rotor disk is written in terms of a trigonometric series expansion, whose coefficients result from the time integration of normalised velocity parameters that account for the dynamics of the aerodynamic system.

The difference between networking and general purpose elements is apparent now: networking elements are implemented in a general form because analogies between different disciplines have been exploited, while general purpose elements have the same function regardless of the discipline they are applied to, as in the case of control elements ans state space systems, where the nature of inputs and outputs are irrelevant, or are confined to one discipline only, because they perform a very specialised task. So networking elements are implemented as GENELs only to exploit code reusability and to add flexibility to the program, instead of duplicating the implementation of basic elements for every discipline.

8.6 Other problems

The most common elements related to the modelling of any network based discipline have been presented in Section 8.4; they provide a basis for defining simplified, essential scalar valued network problems. But any discipline, when practical problems must be addressed, may require specialised elements to consider specific problems; for instance, if an incompressible laminar fluid in a pipe is to be modelled, a general purpose resistor may suffice, but when a turbulent flow condition needs be analysed, an equivalent nonlinear resistor should be used; moreover, when transition from laminar to turbulent flow and viceversa is required, a dedicated element needs be implemented. Moreover, a fundamenteal care is required to interface different networks; prosecuting in the hydraulic parallel, the hydraulic actuator that interfaces the hydraulic plant with the mechanical system requires a dedicated modelling if any detail is desired, e.g. inertia and compressibility of the fluid, pressure losses at orifices, friction at interfaces between moving parts, and so on. For these reasons, the modelling of hydraulic plants is being pursued, and the modelling of electric networks is being improved, based on demands from the task of multidisciplinary analysis of controlled rotorcrafts.

Chapter 9

Piezoelectric beam analysis

The beam analysis formulated in Chapter 5 is extended to the analysis of beams including piezoelectric materials. The section is characterised by extracting electric degrees of freedom related to the conductors applied to the piezoelectric patches incorporated into the structural component, and the finite volume beam model [69, 37] is extended by including piezoelectric coupling terms [35] and the charge balance equation resulting from the electrostatic simplification of *Maxwell* laws.

9.1 Beam section characterisation

The beam section analysis procedure presented in Section 5.3 has been extended to the analysis of beam sections embedding piezoelectric devices, to allow the characterisation of embedded actuators [32, 34], and significantly of the active twist blade discussed in Section 6.4 [68, 36].

9.1.1 Electric field

A piezoelectric device embedded in a structural component, under the assumption that the frequencies it operates at are relatively small, behaves like a capacitor, namely its electromagnetic behaviour is negligible. As a consequence, only the electric field inside the device needs be modelled. The formulation presented herein allows the modelling of the electric field even anywhere outside the device, under the assumption it can be regarded as static. This feature can be useful in case the loss of electric field due to the electric permittivity of the surrounding environment needs be accounted for. In a more general sense, as described in [30], the piezoelectric effect may be regarded as a specialisation of a more general multi-field characterisation of materials that accounts for mechanical, electric, magnetic and thermal interactions. The linear piezoelectric constitutive law of Eq. 6.1 results from the linearisation of the stresses σ and of the electric displacement D_e under the assumption of small frequencies, resulting in negligible influence of magnetic and electromagnetic effects, and of very slow changes in temperature T, accounted for by evaluating the material properties at the actual reference temperature. Consider a section of the beam, in the material frame[1]. The electric potential scalar field V is defined anywhere in the *electric domain*, which can be limited to the piezoelectric device or extended to the rest of the structure and to the air or vacuum outside the beam. The opposite of its gradient represents the electric field $\tilde{E} = -\nabla V$, which is naturally expressed in the material frame. In analogy with the elastic formulation, it can be decomposed in the derivative along the axis of the beam, and in the gradinet in the plane of the section, namely

$$\tilde{E} = -\begin{bmatrix} 1 & 0 & 0 \end{bmatrix}^T V_{/\xi} - \mathcal{D}_e(V),$$

operator $\mathcal{D}_e(\cdot)$ being

$$\mathcal{D}_e(\cdot) = \begin{bmatrix} 0 \\ (\cdot)_{/\eta} \\ (\cdot)_{/\zeta} \end{bmatrix}.$$

Notice that, in analogy with the structural analysis, a generalised mean electric field oriented along the axis of the beam could have been defined, paralleling a sort of "rigid", or global, axial strain, i.e. uniform among the section; this possibility has not been exploited since the usual implementation of piezoelectric patches involves the transverse polarisation of the piezoelectric materials, and thus the mean electric field in axial direction is null. This is not the case when interdigitated electrodes are considered, because they can apply a strong axial electric field component, but in any case, since it usually is very closely spatially alternated, a different procedure has been considered to mimic the IDE behaviour, as described in Chapter 13.

9.1.2 Internal work

The internal work in the beam section can be extended from the elastic form introduced in the conventional beam section analysis to the piezoelectric case by considering the electric domain of the section. The virtual variation of dielectric energy per unit volume is $\delta {D_e}^T E$; to obtain the energy per unit length of the beam, it must be integrated over the electric domain. There is no need to explicitly define

[1] Because the electric potential is scalar, it is independent of the reference frame choice; the reference frame is significant when its gradient is considered. Anyway the material reference frame is used to allow an easy description of the integration domain and of the directions that are considered.

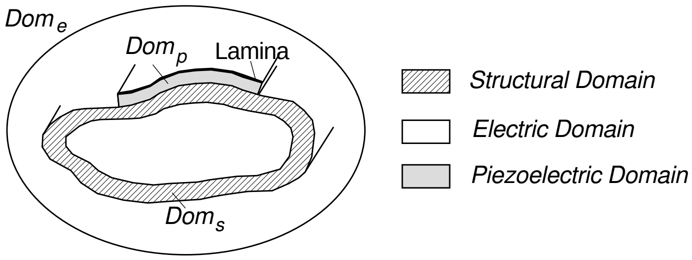

Figure 9.1: Piezoelectric beam section.

any piezoelectric domain; only, where in the intersection between the structural and the electric domains the material constitutive law is truly piezoelectric, the stresses σ and the electric displacement D_e depend on both the strains ε and on the electric field E. A sketch of a typical piezoelectric beam section is reported in Figure 9.1, where the different domains are highlighted.
The internal work per unit length is

$$\frac{\partial}{\partial \xi}\delta L_i = \int_{S_s} \delta\tilde{\varepsilon}^T \tilde{\sigma}\,\mathrm{d}S + \int_{S_e} \delta\tilde{E}^T \tilde{D}_e\,\mathrm{d}S;$$

its perturbation is

$$\begin{aligned}\frac{\partial}{\partial \xi}\Delta\delta L_i &= \int_{S_s}\left(\delta\tilde{\varepsilon}^T\left(\frac{\partial\tilde{\sigma}}{\partial\tilde{\varepsilon}}\Delta\tilde{\varepsilon}+\frac{\partial\tilde{\sigma}}{\partial\tilde{E}}\Delta\tilde{E}\right)+\left(\Delta\delta\tilde{\varepsilon}\right)^T\tilde{\sigma}\right)\mathrm{d}S\\ &+\int_{S_e}\left(\delta\tilde{E}^T\left(\frac{\partial\tilde{D}_e}{\partial\tilde{\varepsilon}}\Delta\tilde{\varepsilon}+\frac{\partial\tilde{D}_e}{\partial\tilde{E}}\Delta\tilde{E}\right)\right)\mathrm{d}S,\end{aligned}$$

where the partial derivatives of stresses and electric displacement are the coefficients of the linear piezoelectric constitutive law

$$\begin{aligned}\frac{\partial\tilde{\sigma}}{\partial\tilde{\varepsilon}} &= D^{(E)},\\ \frac{\partial\tilde{\sigma}}{\partial\tilde{E}} &= -e^T,\\ \frac{\partial\tilde{D}_e}{\partial\tilde{\varepsilon}} &= e,\\ \frac{\partial\tilde{D}_e}{\partial\tilde{E}} &= \varepsilon^{(\varepsilon)},\end{aligned}$$

while the perturbation of electric field is

$$\Delta\tilde{E} = \begin{bmatrix}1\\0\\0\end{bmatrix}\Delta V_{/\xi} + \mathcal{D}(\Delta V),$$

and its virtual variation is

$$\delta\tilde{E} = \begin{bmatrix} 1 \\ 0 \\ 0 \end{bmatrix} \delta V_{/\xi} + \mathcal{D}(\delta V)\,.$$

The matrix representation of the internal work is a trivial extension of the structural case, in which the dielectric and the electroelastic coupling terms appear; it is detailed in Appendix G. The internal work per unit volume $\delta L_i^* = \delta\tilde{\varepsilon}^T\tilde{\sigma} + \delta\tilde{E}^T\tilde{D}_e$ is

$$\delta L_i^* = \left\{ \begin{array}{c} \delta\tilde{t}_{/\xi} \\ \delta V_{/\xi} \\ \delta\tilde{t} \\ \delta V \\ \delta\tilde{\psi} \end{array} \right\}^T \left\{ \begin{array}{c} \Sigma^*_{t_\xi} \\ \Sigma^*_{V_\xi} \\ \Sigma^*_t \\ \Sigma^*_V \\ \Sigma^*_\psi \end{array} \right\},$$

while its perturbation results in

$$\Delta\delta L_i^* = \left\{ \begin{array}{c} \delta\tilde{t}_{/\xi} \\ \delta V_{/\xi} \\ \delta\tilde{t} \\ \delta V \\ \delta\tilde{\psi} \end{array} \right\}^T \begin{bmatrix} \mathcal{M}^*_{ss} & \mathcal{M}^*_{se} & \mathcal{C}^*_{ss} & \mathcal{C}^*_{se} & \mathcal{L}^*_s \\ & \mathcal{M}^*_{ee} & \mathcal{C}^*_{es} & \mathcal{C}^*_{ee} & \mathcal{L}^*_e \\ & & \mathcal{E}^*_{ss} & \mathcal{E}^*_{se} & \mathcal{R}^*_s \\ & \text{sym.} & & \mathcal{E}^*_{ee} & \mathcal{R}^*_e \\ & & & & \mathcal{A} \end{bmatrix} \left\{ \begin{array}{c} \Delta\tilde{t}_{/\xi} \\ \Delta V_{/\xi} \\ \Delta\tilde{t} \\ \Delta V \\ \Delta\tilde{\psi} \end{array} \right\},$$

the matrices being defined in Appendix G. Subscripts $(\cdot)_s$ and $(\cdot)_e$ respectively stand for structural and electric. Notice that the problem should not be symmetric, due to the different signs that matrix e takes in the "acuation" and in the "sensing" equations of the material; symmetry is restored by changing the sign of the "sensing" equations, at the price of losing the positive definiteness of the matrix. The change of sign is not merely a trick; it is allowed in view of the arbitrariness of the virtual variation of potential.

9.1.3 External work

In strict analogy with the structural case, the external dielectric work is made of a transmission work, the axial transmission of the electric displacement, plus an external work made by charging the conductors that bound the piezoelectric patches. In this case the charge work is fundamental since it represents the way piezoelectrics are controlled. The section is topologically divided in piezoelectric regions of influence, that represent portions of the plane the section lies in that are self-contained from an electric standpoint. This is a simplification, because the electric region should extend to the universe, but, since the electric field is usually concentrated into the piezos due to their high dielectric permittivity compared to that of the air or vacuum, and being the conducting parts substantially equipotential, it might be convenient not to model any electric field outside the piezelectric materials, thus logically dividing the section in as many regions as the patches are. In each active region one of the conductors, if any[2], needs be grounded to avoid the singularity of the problem. The electric load is applied by independently applying unit charge per unit length to each of the remaining conductors. The conductors are equipotential by definition, thus such constraint, in the discretised model, can be imposed by numbering each node on a conductor with the same label. Then the assembly procedure will automatically take care of imposing the constraint. The conductor nodes are preserved in the condensation of the warping unknowns, since they hold the tension applied through a piezo and thus represent global degrees of freedom of the smart section. The external electric work results in

$$\frac{\partial}{\partial \xi} \delta L_e = \frac{\partial}{\partial \xi} \int_{S_e} \delta V^T \tilde{D}_e \, \mathrm{d}S + \int_{c_e} \delta V^T q \, \mathrm{d}c.$$

The last work term is related to the free charge density required to charge the equivalent capacitor, where c_e represents the boundary of the piezoelectric regions, including the lines of discontinuity that ideally describe the internal conductors; since the potential V is constant on the conductors, such work contribution simply results in the sum of the products of the virtual variations of tension by the total charges per unit length on the conductors

$$\frac{\partial}{\partial \xi} \delta L_e = \int_{S_e} \left(\delta V^T \tilde{D}_e \right)_{/\xi} \mathrm{d}S + \sum_{c_e} \delta V_c q_c;$$

the section characterisation will require the solution of the problem for indicial charge densities.

9.1.4 Solution

The solution does not basically differ from that of the purely structural problem, so it is not detailed here. One important remark, first introduced in [34] to the authors' knowledge, concerns the equipotentiality constraint along the axis of the beam. A conductor is equipotential by definition; if the conventional procedure for the structural characterisation is followed, the electric tension degrees of freedom will have linear form along the axis of the beam, at least in case of transverse shear loads. While this is correct for internal electric nodes, it violates the equipotentiality constraint on the conductors, which on the contrary must obey to the

[2] One might be interested in analysing the passive behaviour of a structure embedding piezoelectric patches, with no electric work terms defined, and thus with no active electrodes.

non-holonomic constraint of null axial derivative of the tension, the tension itself being unknown. This requires an extra constraint on the potential of the conductors during the first, linear step of the solution, that must be removed for the last, constant solution step. As shown in [68], the reaction charges that result from this extra, overdetermined electrical constraint at first step, linearly depend on the axial position and do not affect the section characterisation.

9.1.5 Remarks

There are many possible extensions to the beam section characterisation presented in this work, ranging from the generalisation to the nonlinear electro-magneto-thermoelastic problem, considering aspects such as the modelling of the current into the conductors that are used to polarise the piezoelectrics, with the thermal effect it has on the surrounding material, to the propagation of the charge along the beam axis, at very high speed, to the modelling of porous beams including electro- and magneto-rheologic fluids, and more. One important aspect is the ability to model very complex composite laminate sections with high accuracy in details such as boundary and extremity effects [42], and to allow the analysis of critical conditions such as fracture mechanics [43], with possible extensions to delamination of composites, as will be investigated in forthcoming works. While the research interest on such topics is very high, its immediate application is beyond the current needs of practical engineering in smart materials applications, mainly due to intrinsic technological limitations of current materials and to the lack of information about material characterisation other than the basic, linear elastic properties of very common piezoelectric materials.

9.2 Finite volume piezoelectric beam

The piezoelectric formulation of the finite volume beam model is straightforward with regard to the beam equilibrium equations; in fact, the electric contribution only affects the constitutive law of the beam, introducing some dependence of the internal forces and couples on the voltage applied to the piezoelectric patches.

9.2.1 Equilibrium

The internal forces at the evaluation points of the finite volume beam element, in case of smart beam sections depend on the electric degrees of freedom as well as on the generalised strains. The actuating part of the linearised beam section constitutive law is

$$\tilde{\vartheta} = D\tilde{\psi} - \theta^T V,$$

the novel term, $\theta^T V$, represents the piezoelectric contribution to the internal forces, θ being the generalised piezoelectric matrix resulting from the beam section characterisation procedure, and V being the electric voltages applied to the conductors embedded in the section. The addition of such contribution to the finite volume beam formulation is straightforward.

9.2.2 Charge balance

The electric charge balance equation needs be formulated. It is obtained by considering the charge balance per unit length, contained in the piezoelectric beam section characterisation, i.e.

$$q = \theta\tilde{\psi} + \varepsilon V, \tag{9.1}$$

being θ and ε the piezoelectric coupling and the dielectric matrices of the section, and $\tilde{\psi}$ and V the generalised deformations of the beam in the local frame and the tensions applied to the piezoelectric patches. The weighted integral of Equation 9.1 yields the discrete form of the charge accumulated on the conductors in a finite portion of beam

$$Q|_a^b = \int_a^b w\left(\theta\tilde{\psi} + \varepsilon V\right) \,\mathrm{d}\xi, \tag{9.2}$$

where $Q|_a^b$ is the resulting polarisation charge and w is the finite volume weight function, i.e. a stepwise unit function. This equation can be written “as is”, and the charge can be transformed into a current by means of a derivator GENEL, or Eq. 9.2 can be written in differential form

$$I|_a^b = \int_a^b w\left(\theta\dot{\tilde{\psi}} + \varepsilon\dot{V}\right) \,\mathrm{d}\xi,$$

directly yielding a current contribution that can be added to an electric node.

9.2.3 Discrete form

It is interesting to notice that a very simple discrete form of the charge balance equation can be easily obtained. Consider the discretisation proposed in Section 5.4 for the three-node finite volume beam element. The discrete charge balance equation needs not be integrated over the subdomains used for the mechanical formulation; on the contrary the whole beam element can be considered at once, since the electric potential is constant all along the beam. In this case, by considering a numerical integration by *Gauss* point collocation, and recalling that the optimal evaluation points for the segmentation of the beam coincide with the two *Gauss* points that exactly integrate polynomials up to third degree, with unit weights, the discrete charge equation can be computed as

$$Q|_1^3 = (\|l_0\| \theta \tilde{\psi})|_I + (\|l_0\| \theta \tilde{\psi})|_{II} + ((\|l_0\| \varepsilon)|_I + (\|l_0\| \varepsilon)|_{II}) V$$

being 1 and 3 the two end-nodes of the beam element, and *I* and *II* the two evaluation points. The charge related to the beam element can be connected to a sensing network.

Part III

Applications

Chapter 10

Preliminary studies

The proposed methodologies for the analysis of multidisciplinary systems have been investigated and assesses first by considering simple examples and benchmarks, usually taken from the literature.

10.1 Rigid body mechanisms

10.1.1 Pendulum

A simple pendulum is considered, made of a concentrated unit mass constrained to be at unit distance from the origin of the global reference frame, under unit gravity acceleration in the negative direction of y axis. This plane problem has been taken from Ref. [17], Chapter 6, pp. 150–157. The problem is defined as

$$\begin{aligned}
\dot{x} - u &= 0 \\
\dot{y} - v &= 0 \\
\dot{u} + x/l\lambda &= 0 \\
\dot{v} + y/l\lambda &= -g \\
x^2 + y^2 &= l^2
\end{aligned}$$

In the mentioned reference, the problem has been stabilised by adding the derivative of the constraint equation; on the contrary, in the present implementation, the model has been built from simple entities in a multibody framework. One second of simulation is considered; the mentioned reference integrates the problem by two-step, second-order backward differences. A consistent set of initial conditions $x(0) = 1$, $y(0) = 0$, $\dot{x}(0) = 0$, $\dot{y}(0) = -1$, $\lambda(0) = 1$ is considered. On the contrary, in this work the initial values of the constraint reaction and of the derivatives of the momenta are inconsistent. Nonetheless, the desired second-order accuracy is obtained, and moreover, by using the second-order formula proposed in Section 4.2

Table 10.1: Pendulum accuracy ($\rho_\infty = 0.0$).

Variable	Solution	$h = .01$	$h = .005$	$h = .0025$
x	0.1349949261	3.1e-3	7.8e-4	2.0e-4
y	0.9908462897	5.7e-5	1.4e-5	3.6e-6
$\dot{x}$	-1.710951582	3.1e-4	7.6e-5	1.9e-5
$\dot{y}$	0.2331035448	3.0e-3	7.4e-4	1.9e-4
λ	3.972538869	2.4e-4	5.9e-5	1.4e-5

Table 10.2: Pendulum accuracy ($\rho_\infty = 0.6$).

Variable	Solution	$h = .01$	$h = .005$	$h = .0025$
x	0.1349949261	9.5e-4	2.4e-4	6.0e-5
y	0.9908462897	1.8e-5	4.4e-6	1.1e-6
$\dot{x}$	-1.710951582	9.2e-5	2.3e-5	5.6e-6
$\dot{y}$	0.2331035448	9.1e-4	2.2e-4	5.7e-5
λ	3.972538869	7.1e-5	1.8e-5	4.3e-6

with an asymptotic radius of 0.6, a higher accuracy has been obtained than that resulting from Ref. [17]. Tables 10.1, 10.2 report the error in the pendulum motion after one second for different time steps; the first is a pure two-step backward difference, while the second exploits the proposed second-order two-step integrator. They should be compared to Table 6.2.1 in Ref. [17]. In particular, Table 10.1 shows a constant increase of about 20% in the error with respect to the reference, which is ameanable to the nonconsistent initial conditions of the present method[1], while Table 10.2 shows a reduction of about 60÷80% in the error due to the higher accuracy of the proposed method when partial algorithmic dissipation is used.

10.1.2 Spinning top

A very simple spinning top is considered, made of a rigid body, whose properties are indicated in Table 10.3; three cases are analysed, following Ref. [25][2]. The three cases differ in the initial linear and angular velocity. The spin top has its x axis oriented in the direction of the global one, while its z axis is rotated away from the global one by 10 degrees about the x axis. The center of gravity is at distance $d = 0.20$ units from the pin point in the local z direction. All the properties are dimensionless. Gravity orientation is opposite to the global z axis.

[1]See Section 4.3 for a discussion on the start-up of the simulation.

[2]First reported in *F. Mello*'s Ph.D. dissertation in 1989 at *Georgia Tech.*, not directly consulted.

Table 10.3: Spin top properties (Ref. [25])

d	0.20
mass	1.00
J_x	0.75
J_y	0.75
J_z	0.40
grav.	-3.00

Table 10.4: Spin top initial conditions (Ref. [25])

	Case 1	Case 2	Case 3
	0.19776	0.04181	0.
v	0.	0.	0.
	0.	0.	0.
	0.	0.	0.
ω	0.9888	0.20905	0.
	7.5167	6.2964	6.3794

The initial conditions in the three cases are reported in Table 10.4; each of the three cases has been integrated with a time step of 0.001 s for a duration of 10 s, to obtain a baseline computation. The last case has been integrated with longer time steps to obtain information on the sensitivity of the method to the time step for a problem that, due to the presence of two overlapping motions at different speeds, one related to the basic spinning of the top and the other to the precession caused by the gravity, is somewhat stiff.

Figures 10.1, 10.2, 10.3 report the plot of the x and y positions of the spin top in the three cases considered. The plots perfectly match those of Ref. [25].

Figure 10.4 shows the differences in Case 3 when different time steps are considered. The differences are appreciable only for $\Delta t = 0.05$, to which a rotation increment of about 0.3 rad. for each step, about $1/10\,\pi$, corresponds.

10.1.3 Bipendulum

A rigid bipendulum is considered, again from Ref. [25]. The properties are reported in Table 10.5. The two rigid links are connected by a spherical hinge; the first link is grounded at the other extremity to the origin of the global reference system by a pin joint. The two links are aligned along the negative half of the y axis, and are rotating about the z axis at a speed $\omega = 4.0$ rad/s. Due to the grav-

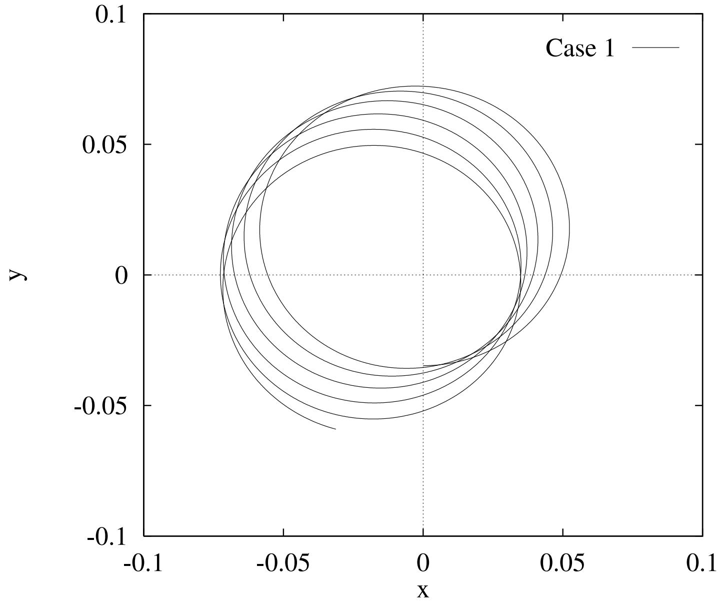

Figure 10.1: Spin top — case 1

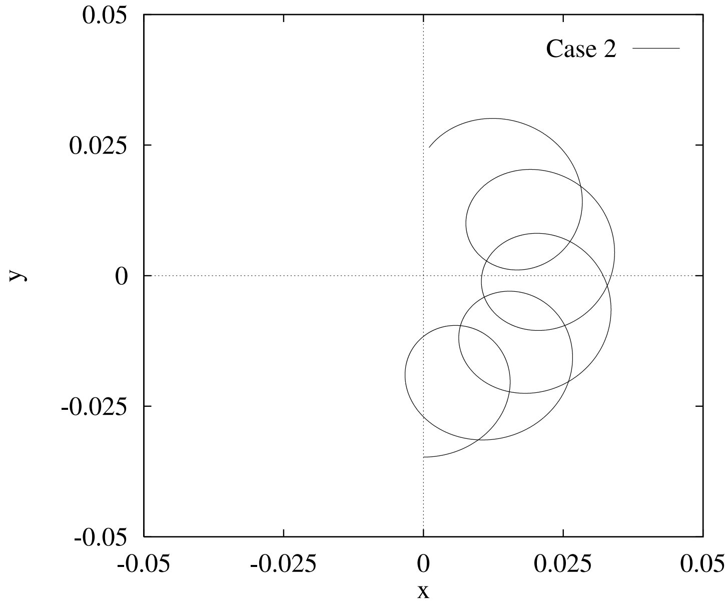

Figure 10.2: Spin top — case 2

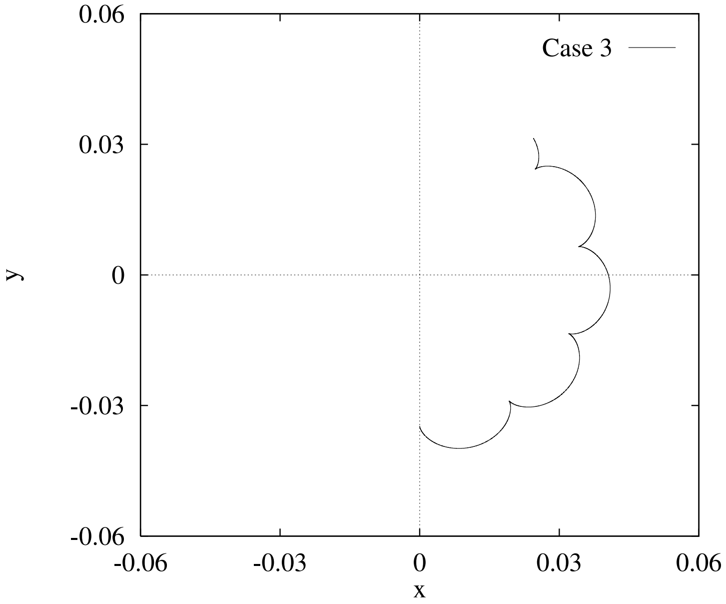

Figure 10.3: Spin top — case 3

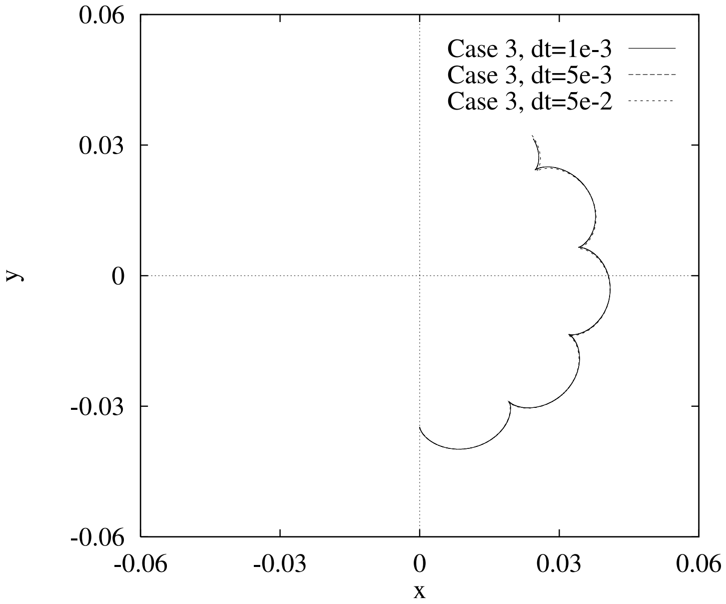

Figure 10.4: Spin top — convergence

Table 10.5: Bipendulum properties (Ref. [25])

L	1
mass	0.4565
$J_{trans.}$	0.0308
J_{axial}	0.0001
grav.	-32.175

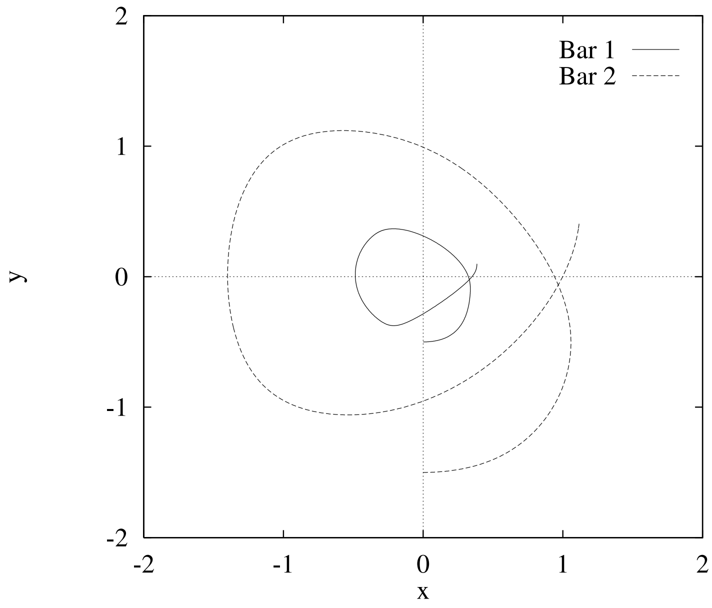

Figure 10.5: Bipendulum — x_{CG} vs. y_{CG}

ity, opposed to axis z, the motion becomes three-dimensional. Figures 10.5, 10.6, 10.7 show the path of the centers of gravity of the two links; Figure 10.8 shows the time history of the two reactions in direction z. The plots practically overlap those of Ref. [25]. An extra plot is shown in Figure 10.9, containing the time history of the total reaction between the two joints.

10.2 Flexible elements

10.2.1 Flexible pendulum

Two problems are considered. The first, the so-called *Bathe* pendulum [5], is a particularly ill-posed problem, consisting in a very stiff pendulum subject to large

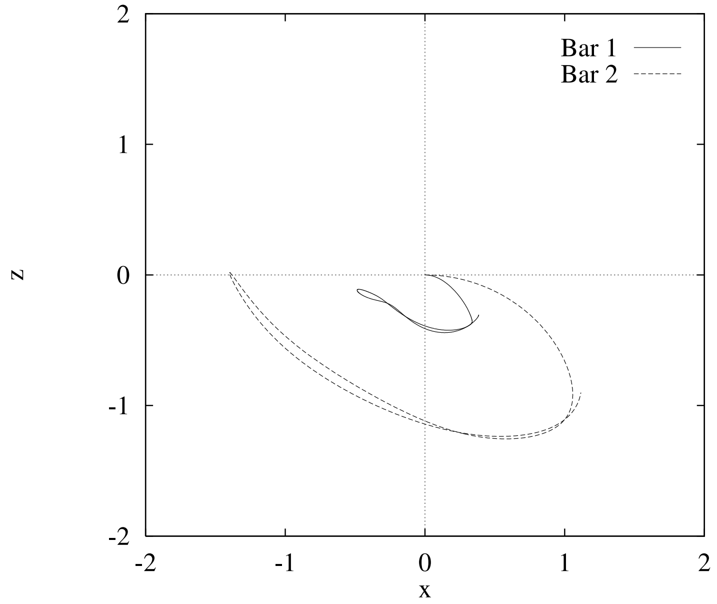

Figure 10.6: Bipendulum — x_{CG} vs. z_{CG}

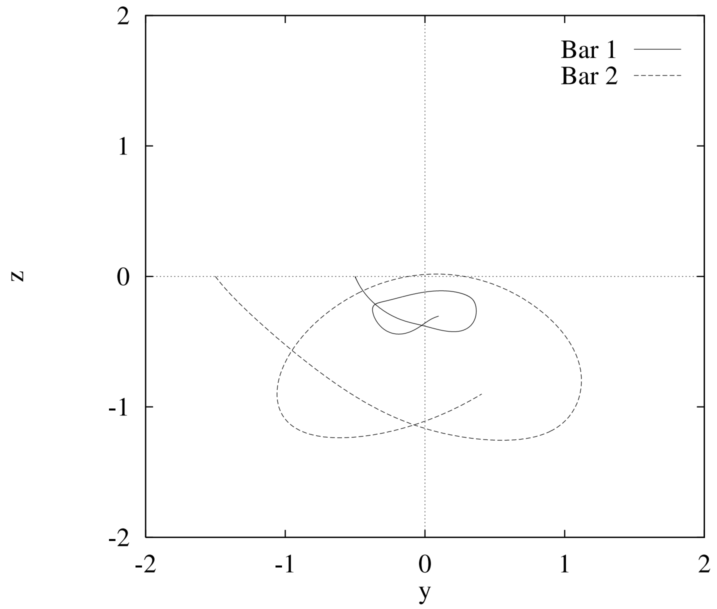

Figure 10.7: Bipendulum — y_{CG} vs. z_{CG}

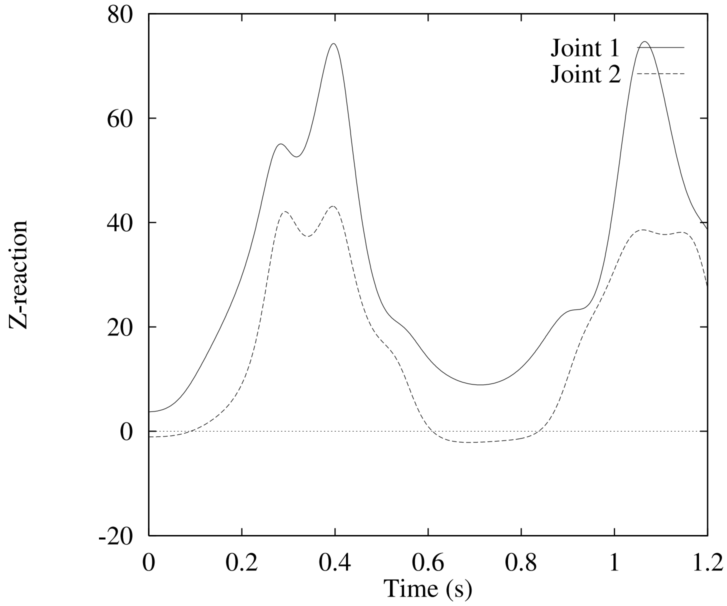

Figure 10.8: Bipendulum — z reaction

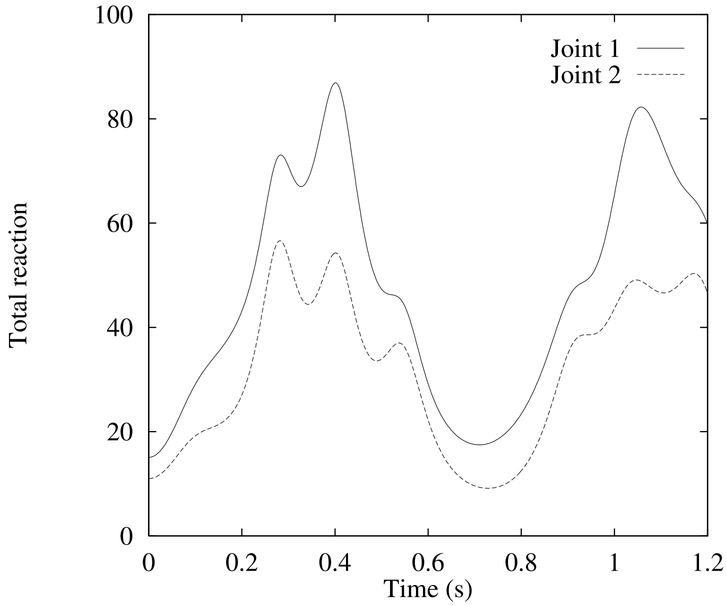

Figure 10.9: Bipendulum — total reaction

amplitude oscillations. The second is a more conventional problem, integrated as an ODE, showing how algorithmic dissipation may be used to obtain the desired behaviour in terms of convergence to a forced solution.

Bathe pendulum

The properties of *Bathe*'s pendulum are summarised in Table 10.6. The pendulum starts in horizontal position and is dropped with null initial velocity. The period of the ± 90 degrees oscillations is about 4 s, while that of the support is about 2.0e-4. *Newmark* integration is shown by some authors to fail when too long a time step is used (≈ 0.025), while energy preserving and enery dissipating algorithms can use larger time steps (of the order of 0.5, one order of magnitude larger) even if with a large phase error. The present algorithm, when the problem is implemented using the rotation as unknown, i.e.

$$\begin{aligned}
\dot{\vartheta} &= \varphi, \\
\dot{u} &= w, \\
\dot{\varphi} &= -\left(2\vartheta w + g\sin(\vartheta)\right)/l, \\
\dot{w} &= l\varphi^2 - (k/m)\,u + g\cos(\vartheta),
\end{aligned}$$

being ϑ the angular position of the pendulum and u the elongation of the rod, obtains very good results, while the global coordinate implementation, namely

$$\begin{aligned}
m\dot{x} - q_x &= 0, \\
m\dot{y} - q_y &= 0, \\
\dot{q}_x + k\,(x - l_0/l) &= 0, \\
\dot{q}_y + k\,(y - l_0/l) &= -g,
\end{aligned}$$

as well as the index 1 DAE implementation,

$$\begin{aligned}
m\dot{x} - q_x &= 0, \\
m\dot{y} - q_y &= 0, \\
\dot{q}_x + x/l\lambda &= 0, \\
\dot{q}_y + y/l\lambda &= -g, \\
\lambda/k - (l/l_0 - 1) &= 0,
\end{aligned}$$

where $l = \sqrt{x^2 + y^2}$, in the multibody framework[3] behaves more like the *Newmark* scheme, i.e. it requires a comparatively short time step ($\approx 0.04 \div 0.10$, depending on the algorithmic dissipation and on the type of joint at the clamped end of the

[3] Actually, there were algebraic constraints as well, because in the current implementation the rod element requires two connection nodes, so the pin point needs be grounded by a clamp joint.

Table 10.6: *Bathe* pendulum properties (Ref. [5]).

L	3.0443	m
mass	10.0	kg
grav.	9.80	m/s^2
EA	1.e10	N

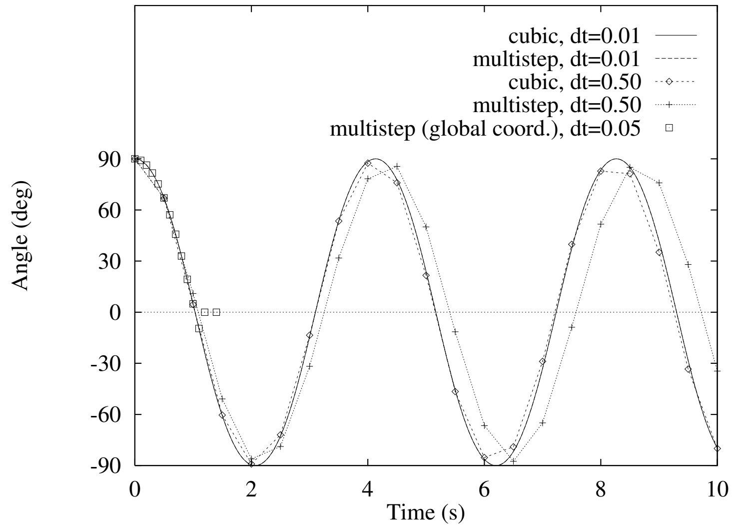

Figure 10.10: *Bathe* pendulum — angular position.

rod) not to fail, while still yielding accurate results, because of the extreme stiffness of the problem. Figure 10.10 shows how the angular position is integrated by some integrators of the proposed family. Notice that, in case the higher-order scheme is considered, a time step of 0.5 yields a solution that is still very close to the accurate one, with limited phase error; on the contrary, when the second order scheme is used, it yields an appreciable phase error but no divergence from the solution or excessive loss in total energy due to algorithmic dissipation. Both cases consider an asymptotic radius $\rho_\infty = 0.6$. This is a typical case of ill-posed problem; by using a rigid link instead of an extremely stiff rod, the stiffness can be eliminated without appreciable differences in the solution for slow dynamics simulations. In fact, if accuracy is the goal, very short time steps are required to exploit the flexibility of the rod; on the contrary, when a quick integration with long time steps is sought, the flexible rod is definitely not required.

Table 10.7: Deformable pendulum properties.

L	1	m
mass	1	kg
grav.	9.81	m/s^2
EA	9.81e4	N

Deformable pendulum

Consider a deformable pendulum, whose properties are summarised in Table 10.7. The link frequency is 100 times that of the pendulum for small oscillations. The pendulum starts at the stable rest position with initial speed $v = 6.3$ m/s, which is sufficient to reach the unstable rest position with some residual kinetic energy. The initial conditions are consistent and balanced, but having the rod null initial elongation, the inertia force due to the centrifugal acceleration strains it during the very first steps and causes oscillations that are problem-related, and not induced by the algorithm. The system is integrated with a time step of 0.02 s, corresponding to about a hundredth of the period of the pendulum, but very close to the period of the rod. As a result, the motion of the rod cannot be captured by the integration, but it leaves numerical oscillations in the solution. The problem is integrated with both the multistep and the cubic formulas with algorithmic damping $\rho_\infty = 0.6$, compared to a baseline solution that correctly integrates the oscillations of the rod, as shown in Figure 10.11. Figure 10.12 shows that the effect of the algorithmic damping is to drive the solution close to the one with no oscillations, where the initial elongation of the rod has been accounted for. In fact, in such case, there is no source of spurious oscillations.

10.2.2 Buckling of axially compressed beam

The buckling critical load due to a conservative axial force that compresses a bar is a classical benchmark for nonlinear beam formulations. From linear elasticity theory, the value of the critical load is:

$$P = \left(\frac{\pi}{2}\right)^2 \frac{EJ}{l^2}$$

for a clamped-free beam. This static stability result is correct when the axial dead load is conservative [9]. The finite volume linearised pre-stress matrix of a straight, untwisted beam follows from the linearisation of the moment arms matrix, Eq. 5.15, about a previously calculated pre-stress condition; by discretising the displacements at the evaluation points by means of the nodal displacements

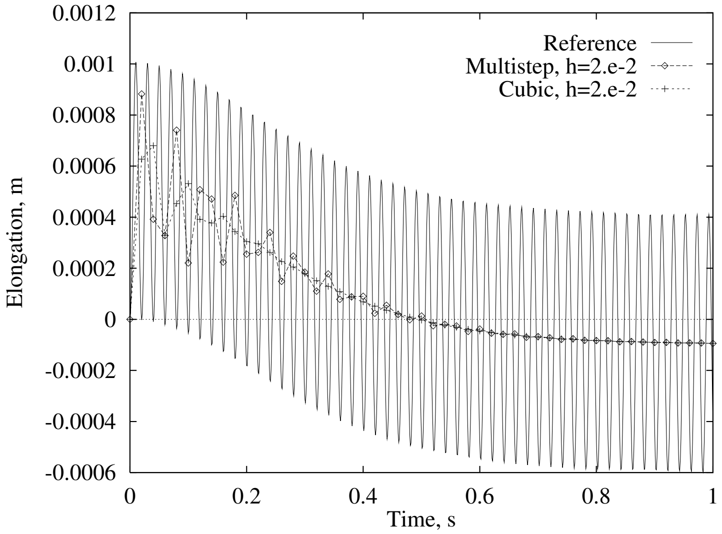

Figure 10.11: Deformable pendulum — elongation.

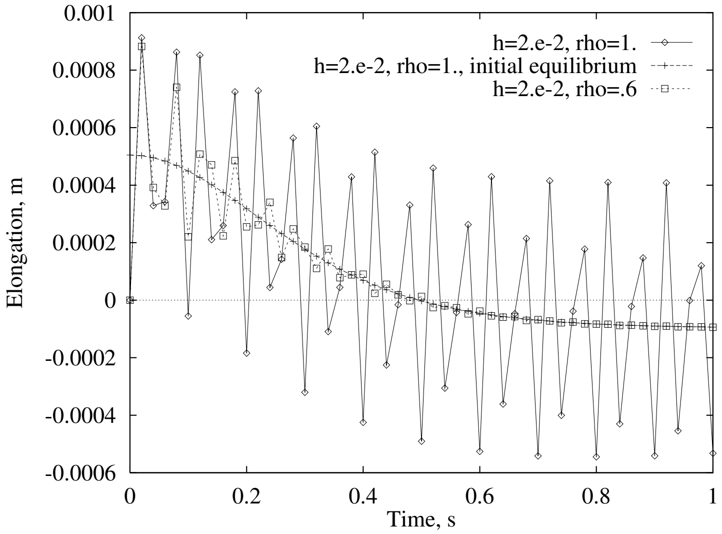

Figure 10.12: Deformable pendulum — correct initial elongation.

as detailed in Section 5.4.4, the following expression for the pre-stress stiffness matrix of the three-node beam element is obtained:

$$K_p = \begin{bmatrix} 0 & 0 \\ t_{I0} \times (N_{Ii} - \delta_{i1} I) & -t_{I0} \times N_{Ii} f_i \times \\ 0 & 0 \\ \begin{pmatrix} -t_{I0} \times (N_{Ii} - \delta_{i2} I) \\ +t_{II0} \times (N_{IIi} - \delta_{i2} I) \end{pmatrix} & \begin{pmatrix} t_{I0} \times N_{Ii} f_i \times \\ -t_{II0} \times N_{IIi} f_i \times \end{pmatrix} \\ 0 & 0 \\ t_{II0} \times (N_{IIi} - \delta_{i3} I) & -t_{II0} \times N_{IIi} f_i \times \end{bmatrix} \left\{ \begin{array}{c} x_i \\ \varphi_i \end{array} \right\}$$

The critical loads and the buckling shapes have been calculated for a straight, uniform beam modelled with a single element, with equally spaced nodes and loaded by an axial compression force. Two buckling modes have been found in each transverse direction, whose critical values are:

$$P_{fv} = 6 \left(5 \pm \sqrt{21} \right) \frac{EJ}{l^2} \tag{10.1}$$

The lower value gives an error of about 1.48%. Quasi-static simulations of the buckling condition have been performed using a slowly growing axial compression load and a small transverse load. An abrupt increase of the lateral deviation takes place when the axial load approaches the lowest critical value. Subsequently, the transverse load is removed, and if the critical value has been exceeded, the beam remains bent. The numerical simulations can only determine lower and upper bounds for the critical values, because when the exact value is approached, the Jacobian matrix of the system becomes singular. The lower and upper bounds obtained by means of a single element model exactly bound the analytic value given by Eq. (10.1). The bounds obtained using a 4 element model are correct to within ±0.04% with regard to the analytical value, showing the effectiveness of a relatively coarse model. The beam can resist a load that is larger than the critical load when the full nonlinear behaviour is taken into account, but a large curvature develops, as shown in Fig. 10.13. In this figure a four-element beam carries a load up to twice the buckling critical value. Figure 10.14 shows the internal forces at the evaluation points due to the 2 P_{cr} load.

10.2.3 Rotor blade modal analysis

The results of the modal analysis of a rotor blade are presented to assess the validity of the finite volume beam model. A linearised implementation of the finite volume beam, with both lumped and consistent inertia matrices, has been used to perform a standard eigenvalue analysis of a previously validated rotor blade model [27]. These results have been published in Ref. [37], where the multibody

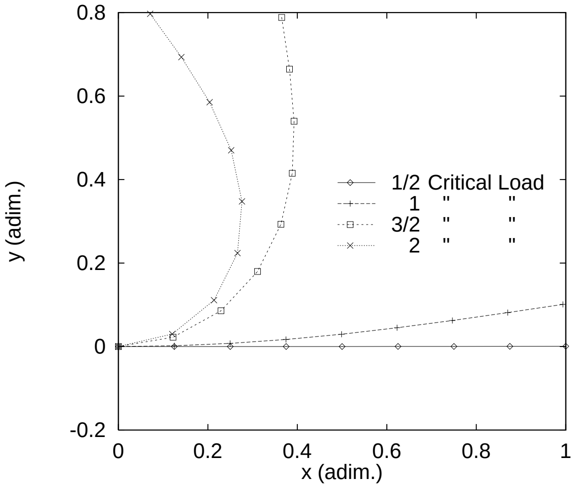

Figure 10.13: Deformed shapes of a 4 three-node element beam under 1/2, 1, 3/2 and 2 times the critical buckling load

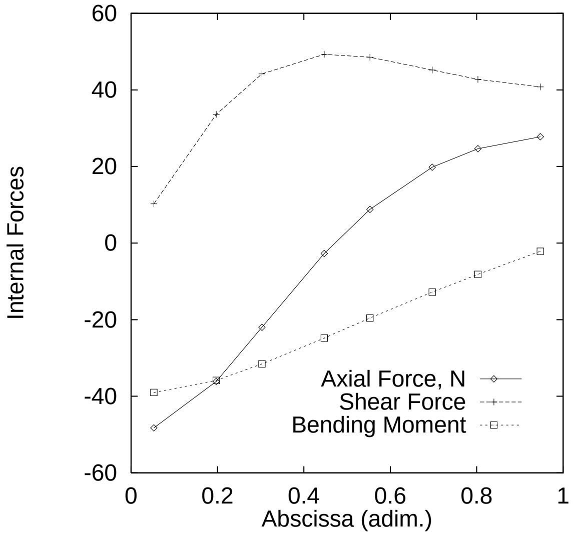

Figure 10.14: Internal forces due to twice the critical buckling load, at the evaluation points of the four beam element model

Table 10.8: Frequencies of a helicopter rotor blade

Mode	Mode Type	Exper.	Ref. [27]	Lumped	Consist.
1	1st Beam	7.42	7.49	7.49	7.49
2	2nd Beam	21.90	21.93	21.91	21.89
3	3rd Beam	42.55	43.17	42.72	42.88
4	1st Chord	43.36	44.45	44.51	44.47
5	1st Torsional	65.70	66.35	68.32	66.22
6	4th Beam	70.81	73.34	72.64	72.62
7	5th Beam	105.78	110.20	107.51	107.85
8	2nd Chord	121.97	125.34	125.69	125.57

implementation of the finite volume beam has been presented first. The model represents the rotor blade of a commercial helicopter. The blade is made of a ‘C’ shaped aluminum main spar, closed by a rear spar. The whole structure is covered by an aluminum sheet and represents about one third of the chord. The trailing part of the airfoil is honeycombed and covered by an aluminum skin. The trailing edge is made of a ‘V’ shaped aluminum rib. A steel antiabrasive strip is put on the leading edge. Non-structural masses have been taken into account, as well as glue and paint weight. Fourteen cross sections of the blade have been independently analysed by means of the beam section analysis presented in Section 5.3 [27]. The spars and the honeycomb have been modelled by means of brick elements, while two dimensional laminæ have been used for the skin and the antiabrasive strip. A three dimensional model was then generated, made of fifteen three-node beam elements (Figure 10.15). The Frequency Response Function (FRF) of the blade has been calculated by analysing the Power Spectral Density (PSD) of the blade excited with a random force at one end. The response has been computed by means of the multi-body code, using the same model of the linear analysis. The results of the spectral analyses are reported in Table 10.8. The modal frequencies obtained by means of the PSD of the response computed with the multi-body code are in a good agreement with the experiment and with previous analyses.

10.2.4 Flexible leverage

The analysis of a flexible leverage is presented. This example is taken from Ref. [84][4]. It consists in two rigid links grounded at one end, and connected to a beam to the other end, as shown in Figure 10.16. The beam carries a lumped mass

[4]The reference was not directly available; data has been accessed thanks to *Lorenzo Trainelli* [85].

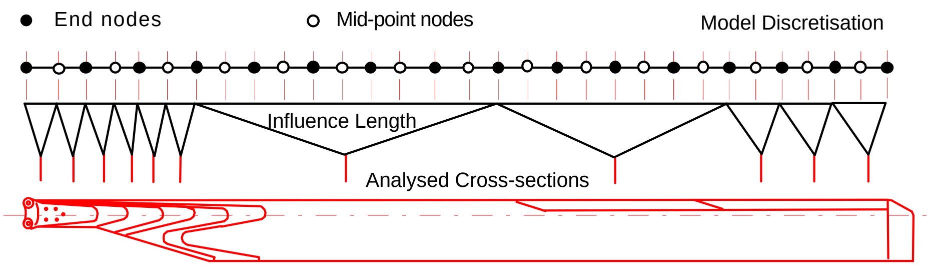

Figure 10.15: Sketch of the discretised helicopter blade

at midpoint; the mass is large compared to the inertia of the beam. An impulsive force is applied to the mass along the axis of the beam (x direction); the force has been actually modelled as a triangle impulse, with a total duration of 0.256 s and a maximum value of 2 N. The properties of the system are reported in Table 10.9. This problem is very significant because, due to the geometry of the leverage, after about 0.5 seconds the mechanism reaches a singular point, in which the beam and the first link are aligned; as a consequence, the opposite end of the beam stops abruptly and inverts its motion. This causes impulsive loads to propagate nearly axially along the beam, as shown in Figures 10.17 and 10.18, and an impulsive reaction force on the left hinge, see Figure 10.21. The movement of the flexible leverage, after the singular point, is dominated by bending oscillations due to the high-frequency, internal dynamics of the beam, as shown in Figures 10.22, 10.24, 10.25, while the mid node, attached to the big mass, behaves smoothly, see Figure 10.23. Figures 10.19 and 10.20 show the transverse shear and the bending moment at the left end of the beam. The oscillatory behaviour is apparent; but since the discretisation is very different, due to the impulsive nature of the load, the response has a very different spectral content. The beam has been discretised with 2 and 4 beam elements, corresponding to 5 and 9 nodes respectively. A rigid case has also been considered, as a baseline. Figure 10.26 shows a portion of the frequency content of the bending moment close to the leftmost end of the beam; it clearly shows that the two discretisations behave quite differently. Notice that none of the frequencies depicted is in the range of the axial frequencies of the beam, the lowest being of the order of 3.5 kHz. Actually, a time step of 1.5e-5 s is required to correctly capture the axial frequencies ($\approx$20 steps per cycle). The axial frequencies of the free beam are given by $\omega = \lambda\sqrt{EA/m}$, where λ is:

1. 0 for the rigid body mode;

2. for the symmetric modes, in which the mass stands still and the beam oscillates symmetrically, $\lambda = \pi/l + 2k\pi/l$, with the integer $k > 0$; the first mode has $\omega \approx 3.6$ kHz;

3. for the skew symmetric modes, where the lumped mass oscillates about the midpoint and the two parts of the beam oscillate in phase opposition, λ is the root of

$$\tan(\lambda l/2) - M/(ml)\,\lambda l/2 \;=\; 0;$$

the first mode has $\omega \approx 3.5$ kHz. Notice that when $M/(2m)$ is very large, the solution at the limit approaches that of the symmetric modes from below, as in the present case, because the lumped mass acts like a clamp; on the contrary, when $M/(2m)$ is very small, the system degenerates into a simple uniform beam, approaching $\lambda = 2k\pi/l$ from above.

The coarser model has the peaks related to the first modes at little higher frequencies, with no frequency content above 60 Hz, while the model with finer discretisation shows the same peaks of the previous one shifted towards lower frequencies, with the addition of higher modes up to 250 Hz. In this specific problem, the addition of degrees of freedom adds frequency content to the model and makes things worse because the excitation activates all the modes. So, not only to achieve accuracy, but also to be able to find a solution, the integration requires smaller and smaller time steps to capture the propagation of the effects of the singular point throughout the deformable part of the model. In fact, while the four-beam model has not been able to pass the singular point with a time step longer than 4.e-4 s, the two-beam model could use a time step up to 1.e-3 s, with very little differences between the two cases. When a variable step has been used with the four-beam model, the first part of the integration was carried out with a time step of 5.e-3 s; the time step dropped to 2.e-4 s during the transition through the singular point; gradually it was restored to about 8.e-4÷9.e-4 for the rest of the simulation. Compared to the maximum fixed time step feasible simulation, only about 40% of the steps were performed, with about 60% of the iterations.
The plots in Figures 10.22–10.25 are comparable to those found in the literature; no exact solution to this problem is available due to its intrinsic stiffness: the higher the mesh refinement, the higher the number of modes that are excited by the impulsive load, resulting in a chaotic, discretisation dependent response.

10.3 Generalised Predictive Control

10.3.1 Three masses system

A very simple system, shown in Figure 10.27, is studied. It is taken from Ref. [63]. The system is made of three masses in series with three springs and dampers, grounded at one end; an excitation force is applied at the free end, and the control

Table 10.9: Flexible leverage properties.

beam length	0.72	m
link 1 length	0.36	m
link 2 length	$0.36\sqrt{2}$	m
lumped mass	0.5	kg
beam mass	9.76e-3	kg
Axial stiffness	3.65e5	N
Bending stiffness	3.04e-2	Nm^2

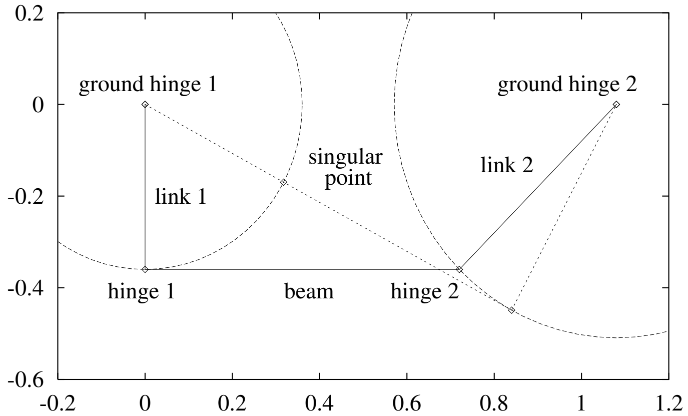

Figure 10.16: Flexible Leverage — scheme.

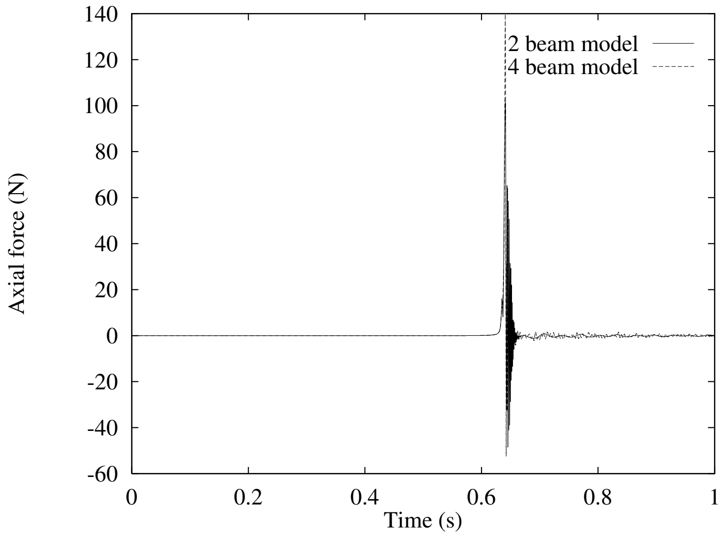

Figure 10.17: Flexible Leverage — axial force close to the left end of the beam.

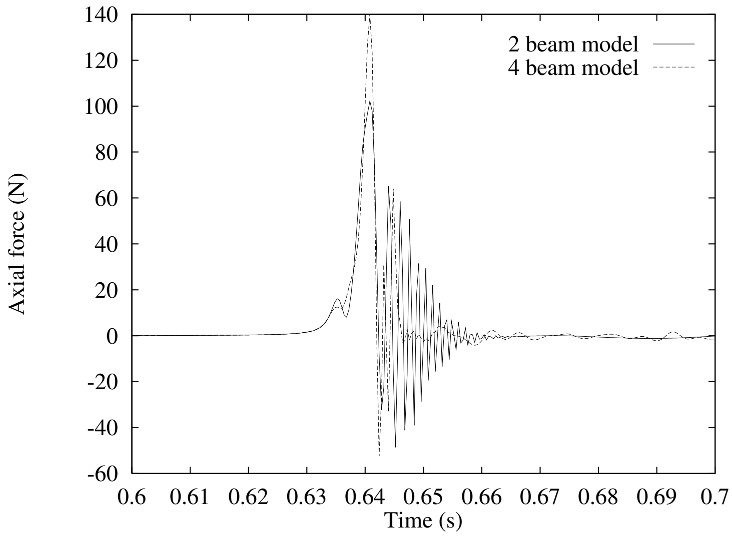

Figure 10.18: Flexible Leverage — zoom of Figure 10.17.

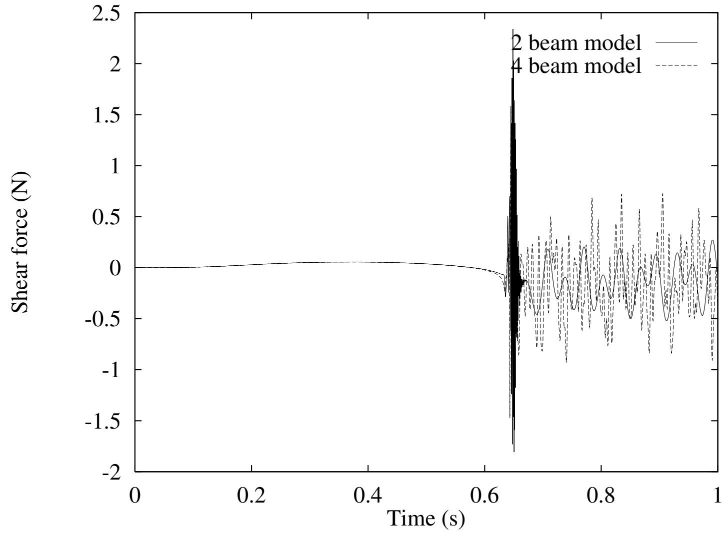

Figure 10.19: Flexible Leverage — transverse shear force close to the left end of the beam.

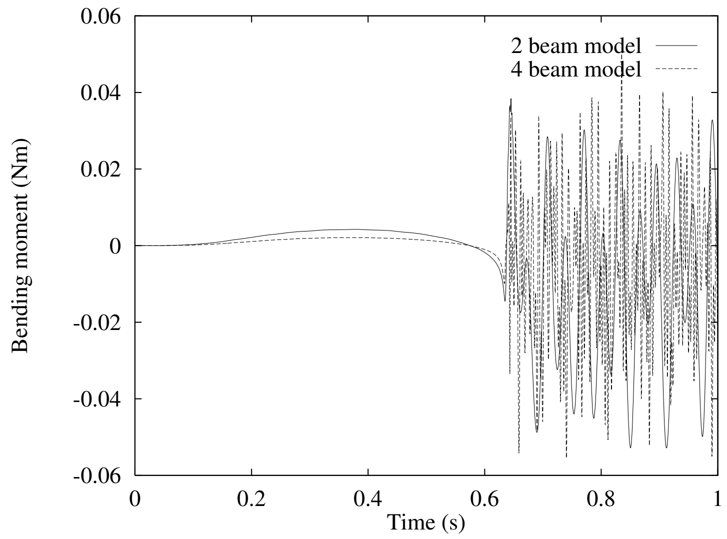

Figure 10.20: Flexible Leverage — bending moment close to the left end of the beam.

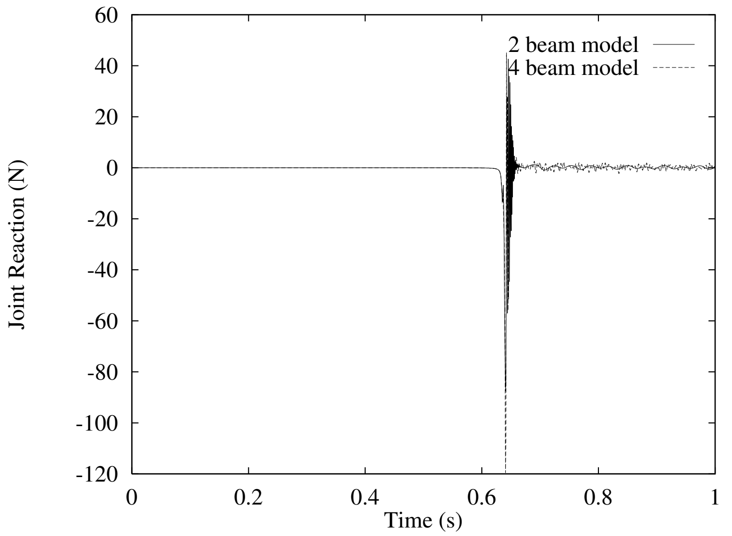

Figure 10.21: Flexible Leverage — left link x reaction.

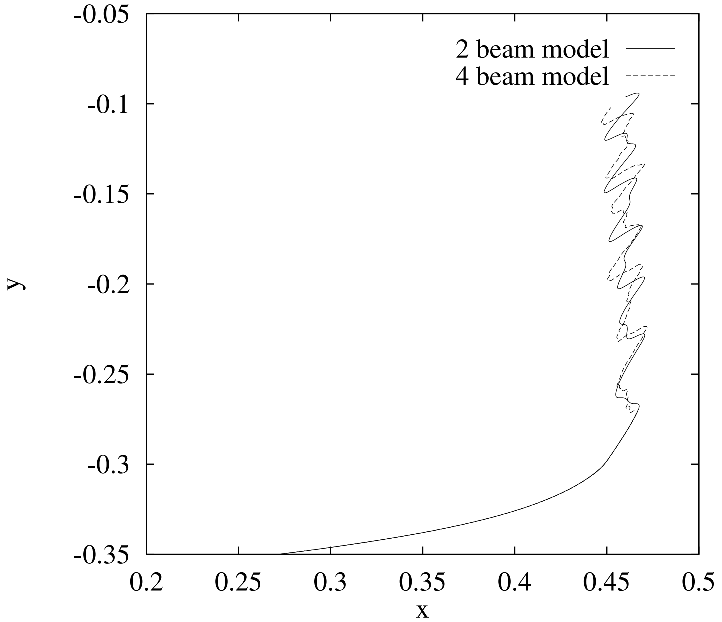

Figure 10.22: Flexible Leverage — intermediate node 1 path.

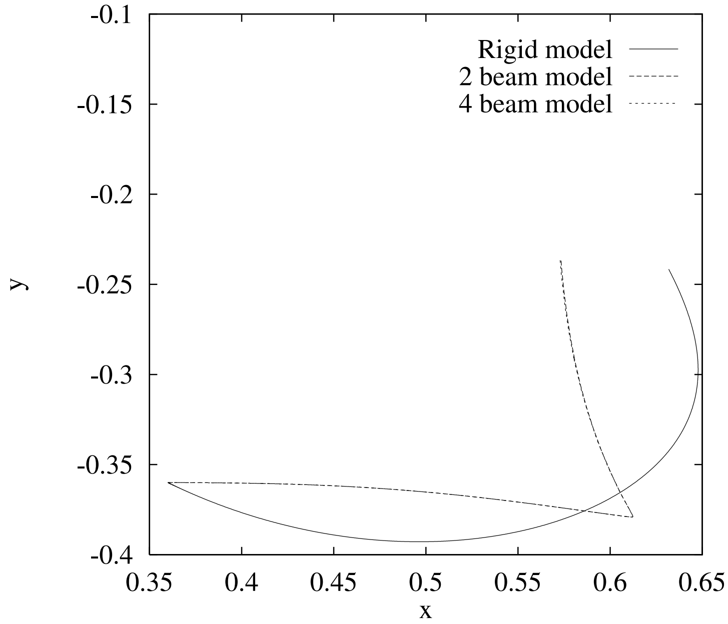

Figure 10.23: Flexible Leverage — mid-node path.

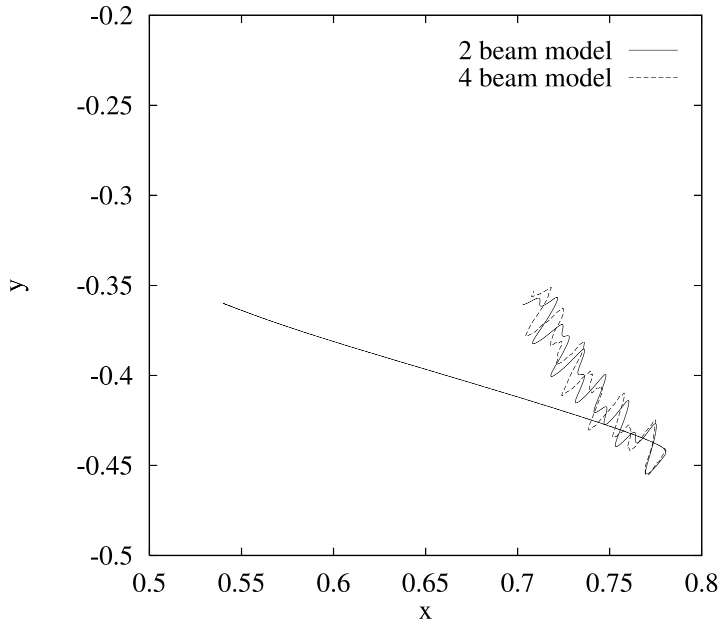

Figure 10.24: Flexible Leverage — intermediate node 2 path.

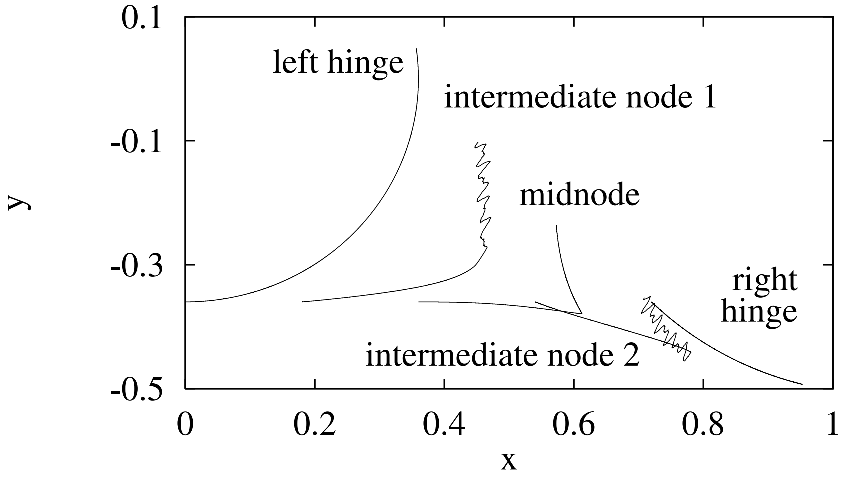

Figure 10.25: Flexible Leverage — node paths of the 4 beam model.

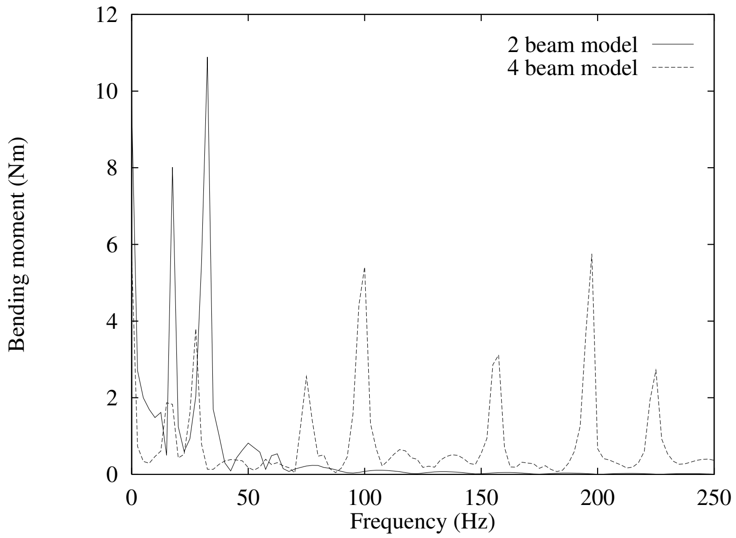

Figure 10.26: Flexible Leverage — frequency content of the bending moment close to the left end of the beam.

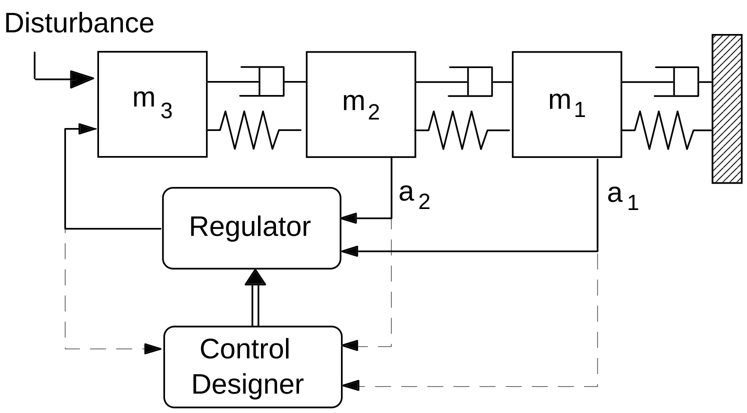

Figure 10.27: Three masses — scheme

measures are the accelerations at the other two points, thus implementing a system with no direct transmission term. The properties are: $m_1 = m_2 = m_3 = 1$, $k_1 = 1$, $k_2 = 2$, $k_3 = 3$; the damping is assumed[5] proportional to the square root of the stiffness, i.e. $c_i = 0.05\sqrt{k_i}$. The system has 6 poles.

Generalised Predictive Control

Different values for the order of the identified system p as well as for the control weight λ have been tested. The prediction and control advancing horizons have been chosen equal to p. The integration time step is 0.01 s; the sampling for the discrete controller is taken every 10 time steps. The system is excited by a unit amplitude harmonic force at 0.4 Hz; a white noise with 0.001 amplitude is applied and measured to identify the system. The control is activated after 40 s of simulation. An order $p = 6$ has been used, with $\lambda = 10^{-3}$. The control weight is gradually reduced to the nominal value in about ten seconds to avoid an abrupt intervention of the control. Figures 10.28, 10.29 show the two measured accelerations and the control force, and the displacements at the three nodes, respectively.

Stabilisation

When the first damping coefficient is set to a negative value $c_1 = -0.15\sqrt{k_1}$, the response, Figure 10.30, shows the effectiveness of this form of adaptive control for unstable systems. It is interesting to notice that the control is not collocated

[5] There seems to be an ambiguity in Ref. [63] in the definition of the damping.

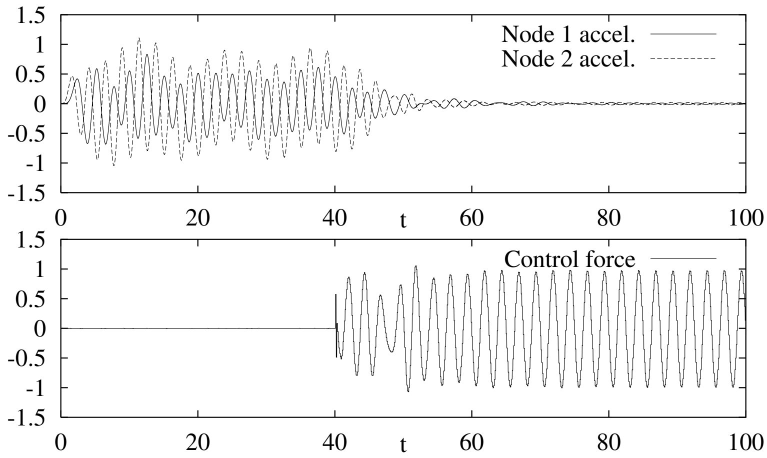

Figure 10.28: Three masses — control signals

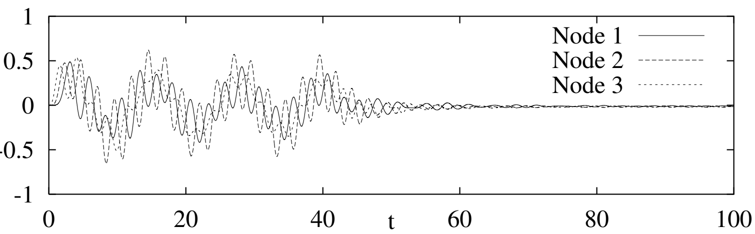

Figure 10.29: *Three masses — displacements*

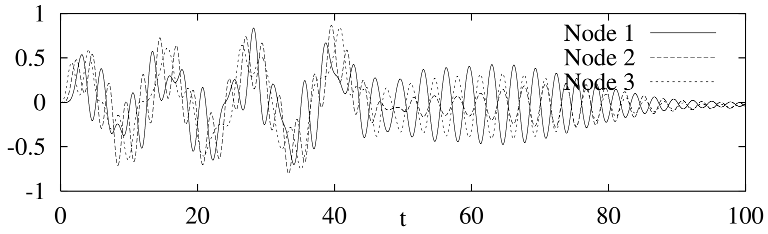

Figure 10.30: *Three masses — stabilised displacements*

and the unstable section of the system is close to one of the measures, but it is not directly controllable. The effect of the controller is to drive mass 3 in phase with mass 2, and then to move these two masses in phase opposition with mass 1, the unstable one, to cancel its oscillations. The control weight λ can be reduced even more, with performance improvements expecially in the unstable case, but with excessively rough behaviour of the control force.

Chapter 11

Tiltrotor model analysis

Introduction

The 1/5-scale aeroelastic model of the V-22 (Figure 11.1) was built and tested in the period from 1983 to 1988, to support the preliminary design and the full scale development of the tiltrotor aircraft later known as the JVX. The wind tunnel tests began at the *Transonic Dynamic Tunnel* (TDT) of the NASA *Langley Research Center* (LaRC) on a semispan model, and were globally performed in three different facilities, including the Boeing Helicopter VSTOL tunnel for both the semispan and the full span model configurations. The semispan model is currently referred to as the *Wing Rotor Aeroelastic Testing System* (WRATS), and is located at the LaRC.

A tiltrotor aircraft is a complex system that has the behaviour of both a conventional airplane and of a rotorcraft, with peculiar maneuvres, e.g. the conversion. Its aerodynamics are characterised by the high influence of the rotor on the airstream that affects the wing, in both helicopter and airplane configuration. In fact the WRATS project has been mainly focused on the reduction of the vibration level induced by these interactions in the airplane mode by means of an actively controlled swashplate with the Higher Harmonic Control (HHC) technique, coupled to an active flap [74]. The blades of the rotor represent a compromise between helicopter and propeller blades. Since they are optimised for the high axial airstream speed typical of the airplane mode, they are highly twisted, thus showing high elastic couplings between twist and in- and out-of-plane bending [73]. The conversion maneuvre, when performed at typical rates for aircraft control, introduces gyroscopic effects that are unusual in conventional helicopters. The flexibility of the wing can magnify the effects of ground and air resonances, the latter being typical of automatically controlled rotorcrafts. Many of these problems are well known, but have never been faced to this extent, while others are completely new.

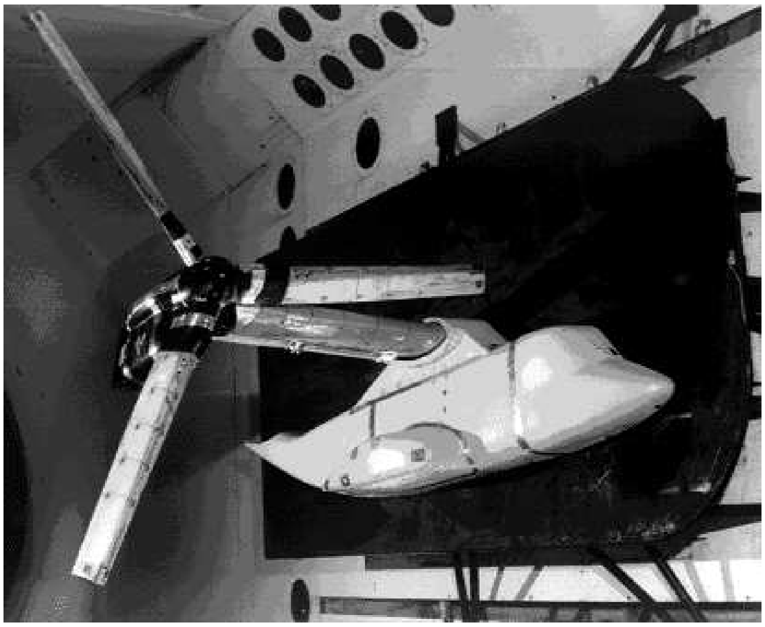

Figure 11.1: WRATS Model at Langley's Transonic Dynamics Tunnel

For this reason, a particularly intensive experimental campaign preceeded and accompanied the whole development of the JVX [65], supported by numerical analyses of the related subproblems. Eigenvalue analyses of the rotor dynamics, the determination of flutter margins of the rotor, of the wing and of the ensemble, by means of analytical models based on comprehensive rotorcraft analysis codes, and dynamic simulations of the rotor mechanisms by means of early multibody codes have been performed at each step of the wind tunnel investigations [77], [82]. A pictorial history of proprotor investigation at Langley is depicted in Figure 11.2, where in recent years the proposed multibody analisis formulation, implemented in a code called *MBDyn*, is mentioned. The figure is taken from the viewgraphs accompanying a talk that Dr. *Kvaternik* recently gave at Langley. Figure 11.3 refers to test campaign 529, performed in August '98. The results of the present work have been presented in [38], and subsequently published in [39] and presented in [41].

Most of the analyses of the WRATS model were performed by means of comprehensive rotorcraft codes, with properly simplified models. In this work the use of a single, state-of-the-art, multipurpose multibody code, capable of performing most of the required simulations starting from a single bulk model that can be specialised for each analysis, is considered as a possible means to accomplish most of the tasks previously undertaken by specialised analysis tools.

Each subpart of the tiltrotor is modelled and analysed in its basic kinematic and

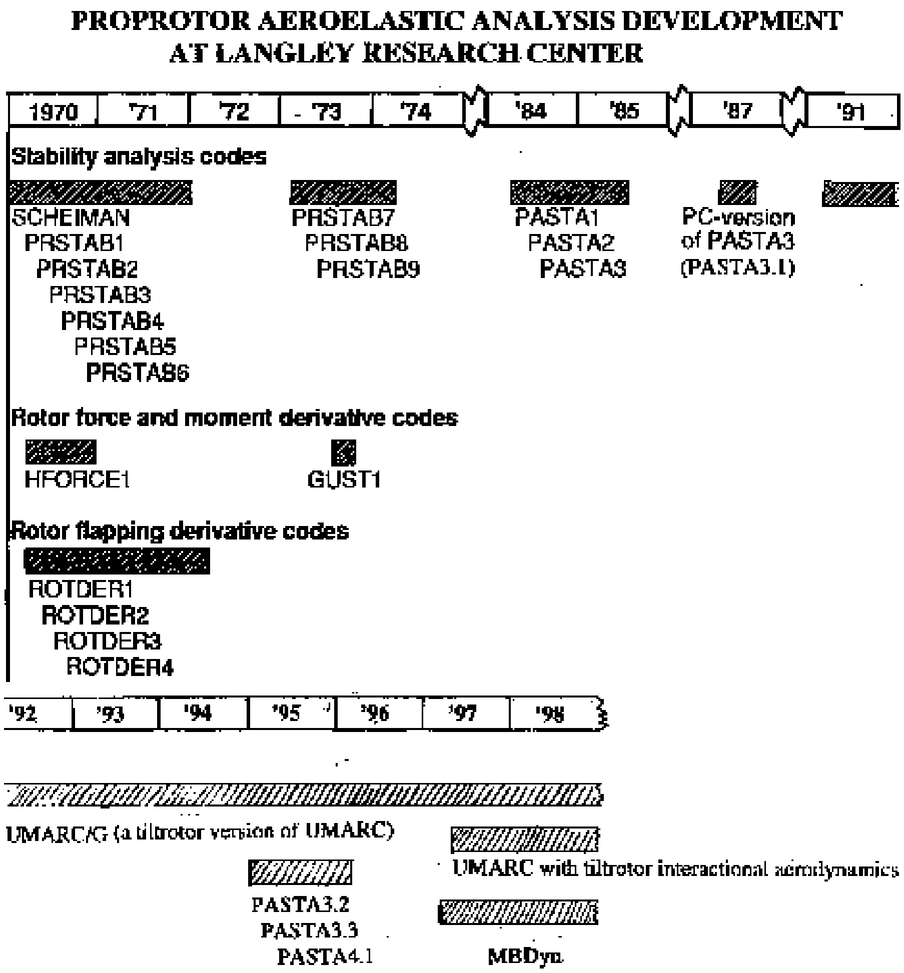

Figure 11.2: Pictorial history of proprotor/tiltrotor investigation at Langley.

Figure 11.3: From the left, *Pierangelo Masarati* and Dr. *Mark W. Nixon* in the TDT during August '98 test campaign 529.

dynamic features; subsequently the parts are assembled together, and the system is analysed as a whole. By using the same code and the same modelling for the single parts and the assembly, and by using a rather general approach in the kinematic and mechanical description of the single parts, any undue approximation is avoided.

11.1 Tiltrotor submodels

The tiltrotor has been split in the following subsystems:

1. The blade, made up of a flexbeam and a pitch hinge mechanism, connecting the blade to the hub, and a pitch link transmitting the pitch control from the swashplate. Either rigid or flexible blades have been considered.

2. The gimbal, a constant velocity joint made of all of its mechanical components in order to give an accurate kinematic description of the joint.

3. The swash plate, made of the two plates, the two scissors that constrain the axial rotation of the plates with respect to the pylon and to the hub, and the three non-rotating links that control the collective and the cyclic position of the plates.

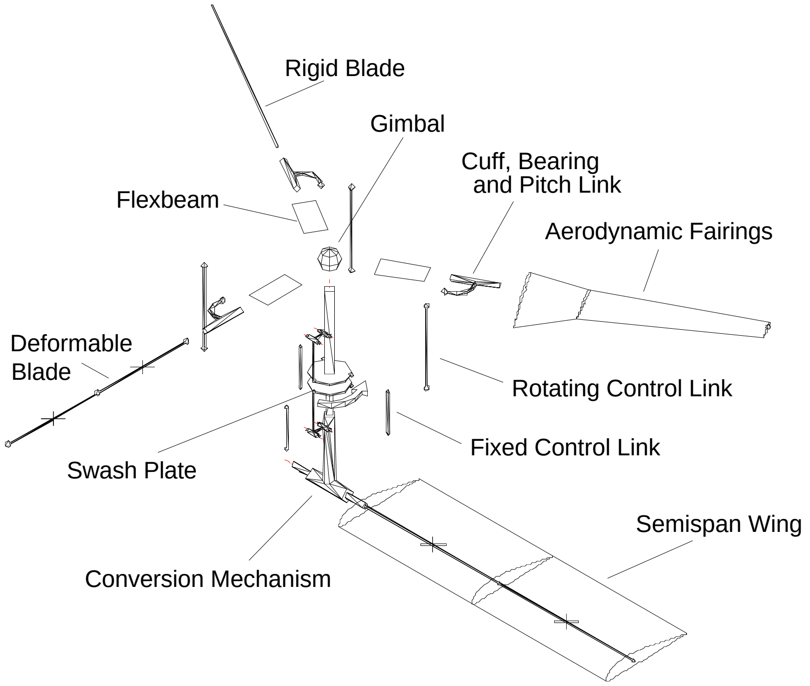

Figure 11.4: Analytical Model

4. The half-wing model, made of the deformable wing, the pylon, modelled as a rigid body, the conversion hinge, the downstop spring and the mast.

The complete model is sketched in Figure 11.4.

11.1.1 Blade

The single blade model has been used to analyse the dynamic properties of the isolated blade, such as frequencies and aerodynamic properties. Three different models have been considered, with increasing discretisation refinement. All the models share the description of the flexbeam, that uses a three-node beam element, and of the controls. The blade is joined to the flexbeam by a spherical hinge at the outer end, and by a spanwise oriented in-line joint, 2.2 in outwards of the rotor axis. The bending of the flexbeam accounts for flexible flap and lag motion, while the pitch rotation is allowed by the bearings. A distance joint between the rotating swashplate and an offset point aft of each blade cuff models the control link. It can be both rigid or flexible, to account for the flexibility of the control system. A rigid blade has been considered first, which proved to be poor because the yoke is very stiff, so even the very first in-plane bending mode implies appreciable deformation of the blade itself. On the other hand, the rigid blade may represent an acceptable

Table 11.1: Cantilevered blade frequencies, Hz

Mode	Exp	UMARC	NASTRAN	MBDyn	
				4 elem.	2 elem.
1 Beam	12.29	12.3	11.5	11.3	11.7
1 Chord	34.11	34.1	33.4	33.1	32.7
2 Beam	52.44	53.0	56.7	55.8	55.0
1 Tors.	113.35	111.4	127.0	119.0	122.0

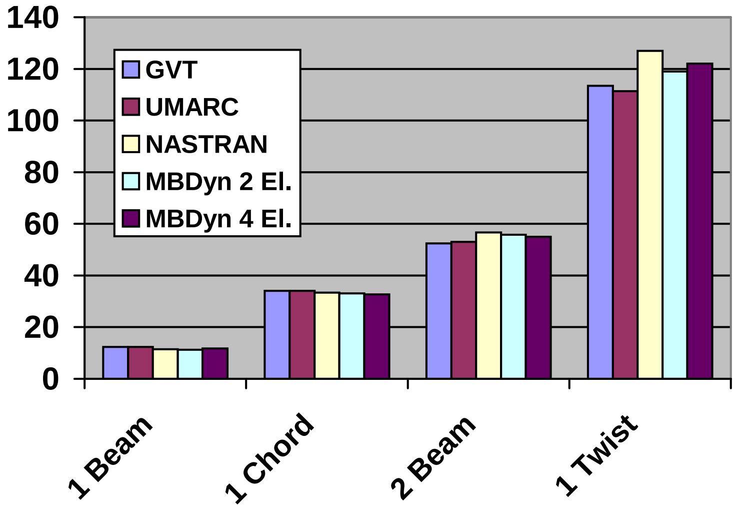

Figure 11.5: Cantilevered blade frequencies, Hz

tradeoff when only the performances of the rotor are addressed. A flexible blade has been subsequently modelled, with two and four beam elements respectively. The first frequencies of the cantilevered blade obtained by the present analysis are reported in Table 11.1 and in Figure 11.5, compared to Ground Vibration Tests (GVT), and to UMARC and NASTRAN Finite Element Analysis codes results.

11.1.2 Gimbal

The gimbal model has been used to determine the kinematic and gyroscopic properties of the rotor. It consists in a constant velocity joint, made by two universal joints, linked to the mast and to the hub respectively at one arm of each cross. The other arm of the crosses is connected to a linkage, that transmits the torque between the mast and the hub and keeps constant the distance between the two U-joints. The hub is also linked, by means of an in-line joint, to a spherical joint on the mast that allows the gimbal motion. The gimbal allows the rigid flapping of the whole rotor and, since the direction of the angular velocity tilts together with the hub, no Coriolis forces due to this motion result in the blades when the flapping is steady. At the same time, the 1 per rev. flapping motion has no stiffness due to centrifugal effects, but only that provided by a set of springs.

11.1.3 Swashplate

The swashplate model has been used to analyse the kinematics of the control system and, together with the gimbal and the rigid blade, to evaluate the pitch-flap-lag couplings for the whole collective pitch range. It has been used also to apply the desired controls to the rotor during realistic maneuvre simulations. It consists in the two plates, modelled as rigid bodies joined by a plane hinge. The fixed plate is linked to the pylon by means of an in-line joint that forces it to translate along the mast. A fixed and a rotating scissor constrain the rotation of the two plates about the rotor axis, with respect to the pylon and the mast. Three variable distance joints are used to control the translation along the mast (collective pitch) and attitude (cyclic pitch) of the non-rotating plate. The elongation of the fixed control links is imposed by means of a dedicated general purpose element that splits the three fundamental control inputs, namely collective, and fore/aft and lateral cyclic pitch angles, into the elongations of the links. Figures 11.6–11.7 respectively represent the kinematic pitch-flap coupling due to the gimbal and the flexible flapping, and the control stiffness as function of the collective pitch, compared to data obtained from Bell Helicopter and from model calibrations.

11.1.4 Wing-Pylon

The half wing model has been used for aeroelastic clearance of the isolated wing. Both dynamic and aeroelastic properties of the wing in forward flight have been analysed. It consists in two beam elements for the wing, and in the pylon, modelled with a rigid body. The pylon is connected to the wing by means of a flexible spindle, modelled with a beam element, and a downstop spring. The spindle models the conversion bearing. Its bending allows the pylon to rotate with respect to the wing about the roll and yaw axes; it mimics the flexibility of the transmission shaft at the conversion bearing. The conversion actuator constrains this rotation, and controls the conversion angle. In the wind tunnel model, springs with different properties are used to simulate the behavior of the conversion actuator in helicopter and airplane configuration, both on- and off-downstop. The

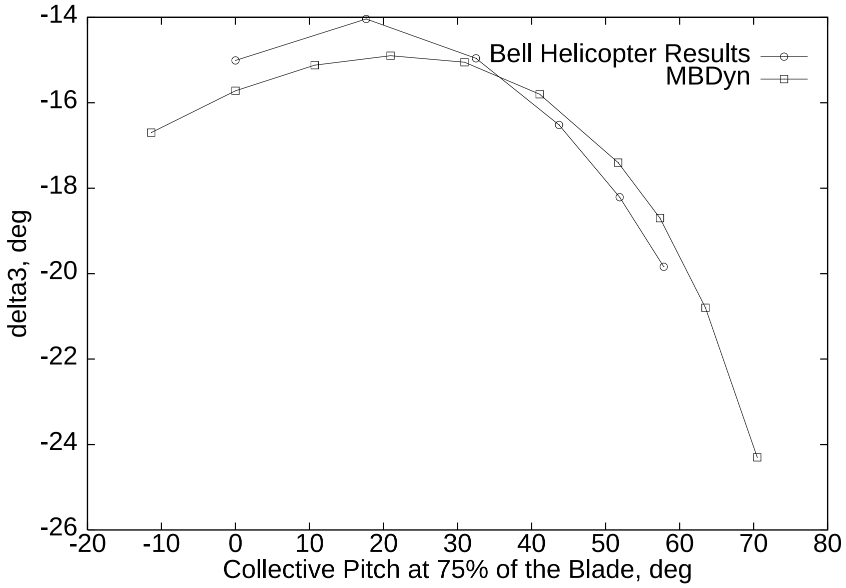

Figure 11.6: Pitch-flap coupling as function of the collective pitch $\theta_{75\%}$

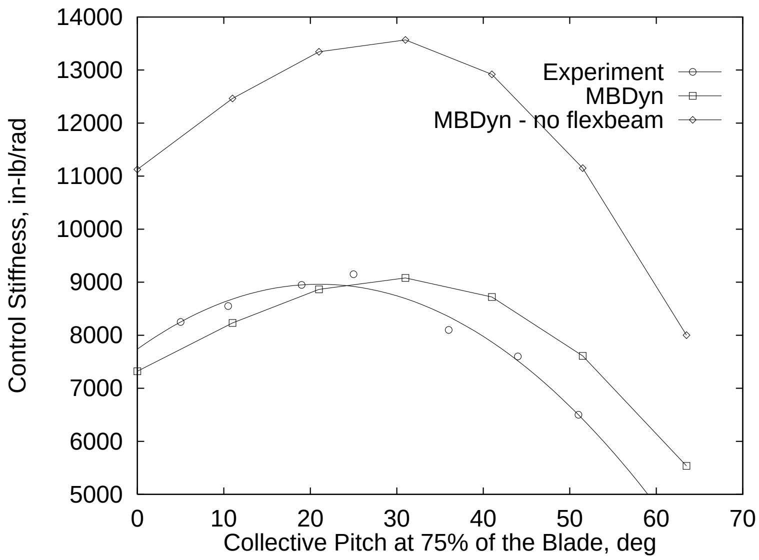

Figure 11.7: Control stiffness as function of the collective pitch $\theta_{75\%}$

Table 11.2: Wing frequencies, Hz

Mode	GVT	NASTRAN	MBDyn
	downstop on		
Beam	6.00	6.16	5.9
Chord	8.45	9.33	9.1
Twist	12.5	12.6	12.5
Pylon Yaw	16.5	18.9	17.2
	downstop off		
Beam	5.51	5.45	5.4
Chord	8.45	8.74	8.8
Twist	10.6	10.6	11.0
Pylon Yaw	16.7	16.7	16.6

main frequencies of the wing-pylon are reported in Table 11.2 and in Figure 11.8, compared to both GVT and NASTRAN results.

11.2 Preliminary considerations

Some preliminary considerations on the flapping motion: the rotation axis for the flapping due to the gimbal, namely 1 per rev. flapping, is located on the rotor rotation axis, 2 in above the rotor plane, while the one for the flapping due to the flexbeam deformation, namely the cone and >1 per rev. flapping, lies about 1.5 in outboard along the blade axis. The pitch control is linked to the blade 75^o aft of the blade itself and thus introduces a pitch-flap coupling $\delta_3 \cong -15^o$ that is negative (flap up causes pitch up) for the 1 per rev. motion, and slightly positive for the flexible flapping. It is known that, for a stiff-in-plane rotor, a positive δ_3 can give raise to a pitch-flap aeroelastic instability when the first out-of-plane and in-plane frequencies nearly meet [60]. The occurrence of this instability in the simulations required a deeper analysis of the flexibility of the yoke. In detail, the flexibility of the inner part of the yoke, from the hub to the inner pitch bearing, proved to be fundamental in describing the correct coupling between the blade pitch and the flexible, symmetric flapping motion. After this part was properly modelled, the slight, symmetric instability in the analytical model disappeared. Figure 11.9 shows the change in pitch-flap coupling for the cone flapping motion both for rigid and flexible root of the flexbeam. The experimental data seem to indicate that the correct flexible pitch-flap coupling be somwhat between the rigid and the deformable flexbeam case, biased towards the flexible case at lower collective angles, and towards the rigid case at higher collective. A three-dimensional modelling of the yoke is possibly required to determine the exact coupling effect.

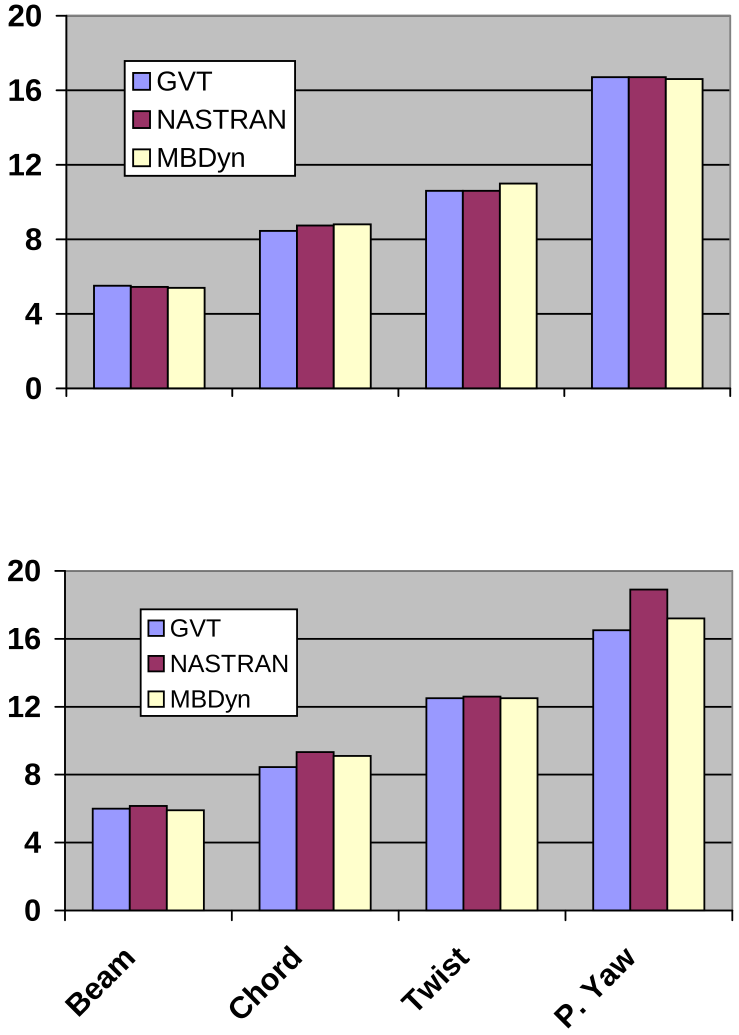

Figure 11.8: Wing frequencies, Hz — downstop off (top) and on (bottom).

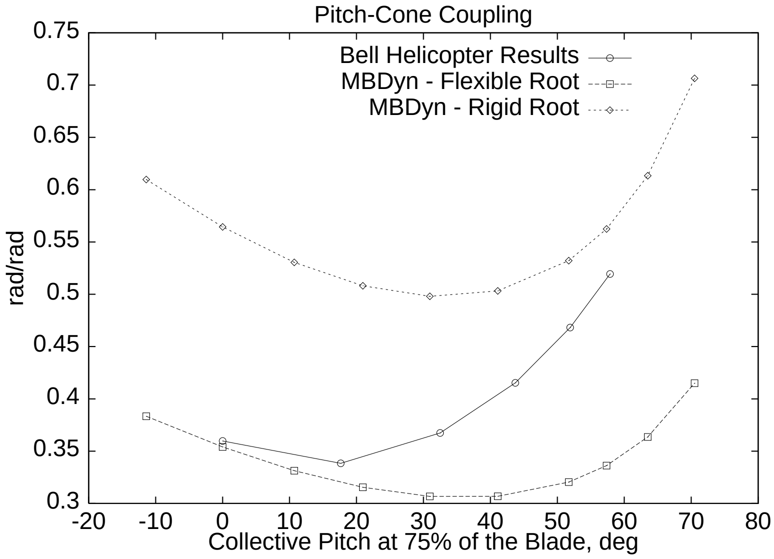

Figure 11.9: Pitch-cone coupling as function of the collective pitch $\theta_{75\%}$

11.3 Rotor models

The model, consisting in the rotor with rigid/deformable blades, the gimbal and the swashplate, has been used to investigate the stability of the rotor, with particular regard to the pitch-flap-lag coupling, and to evaluate the aerodynamic response to the controls. The rigid blade model matched the first out-of-plane frequency, but gave poor results even for the first in-plane frequency, so it was of little use in other than performance analyses. The flexible blade models agreed very well with available data for the low frequencies of the rotor, both in the rotating and non-rotating cases *in vacuo*. Both the single blade and the complete, three blade rotor models have been analysed. For this purpose, UMARC has been modified to allow the modelling of multiple blade rotors in the finite elements analysis module, with multiple load paths to account for the control links. Tables 11.3 and 11.4 show that the presence of the gimballed hub modifies the natural frequencies of the system by breaking the symmetry. In fact, non-symmetric modes are found, as shown both by the analysis and the experiment. Results from Bell Helicopters were available for the locked gimbal case, since they were obtained for a single blade model. They refer to an old configuration of the hub, with calibrated springs at the blade root to simulate the stiffness of the controls. These results are not completely representative of the current configuration. The GVT results with locked gimbal are also not completely significant, since the gimbal could not be perfectly locked. As an example, in Tables 11.5 and 11.6, the rotating frequencies

Table 11.3: Single blade with flexbeam (locked gimbal), non-rotating, Hz

Mode	BELL		GVT	UMARC	MBDyn	
	10 deg.	50 deg.	10 deg.	10 deg.	10 deg.	50 deg.
Cone	6.6	7.2	6.6	6.3	6.8	7.8
2nd Flap	26.6	35.1	25.2	30.8	28.5	39.0
3rd Flap	68.8	77.3	69.3	77.9	73.5	82.0
1st Lag	19.3	12.5	20.6	19.3	19.5	12.6
1st Twist	114.5	109.9	112.6	110.0	109.0	107.0

Table 11.4: Full rotor (free gimbal), non-rotating, Hz

Mode	GVT	MBDyn	
	10 deg.	10 deg.	50 deg.
Gimbal	2.0	1.8	1.5
Cone	6.8	7.0	7.8
2nd Flap	25.0	26.5	36.5
2nd Flap asym.	64.2	57.1	55.0
3rd Flap	76.2	78.0	82.5
1st Lag	19.7	19.0	12.7
2nd Lag	91.3	98.0	92.0
1st Twist	112.1	109.0	107.5

of the complete, three blade rotor are reported at two typical rotating speeds and collective pitches, related to hover and cruise flight conditions, respectively.

11.4 Wing model

The wing model shows good correlation for the lowest modes, as reported in Table 11.2. The results are compared to experimental measurements and to numerical results based on NASTRAN code [75]. The beam[1] and twist modes are strongly coupled and are influenced by the properties of the downstop, the spring that is used to lock the conversion actuator in airplane mode. At present there is no conversion actuator on the wind tunnel model, so it is simulated by a set of springs that model its stiffness in different configurations.

[1] As the flapwise, or out-of-plane bending modes are conventionally called.

Table 11.5: Rotating frequencies, 888 rpm, $\theta_{75\%} = -3$ deg., Hz

Mode	Myklestad	UMARC	MBDyn
Gimbal	-	14.8	14.8
Cone	17.2	17.3	17.5
1^{st} Lag	22.4	20.8	24.0
"Coll. Lag"	42.0	44.0	36.0
2^{nd} Flap	37.3	49.6	41.0
2^{nd} Flap asym.	-	70.2	65.0
3^{rd} Flap	75.3	90.3	73.0
Flap/Twist	89.3	92.7	90.0
Lag/Twist	-	113.4	104.0
Twist	-	116.0	110.0

Table 11.6: Rotating frequencies, 742 rpm, $\theta_{75\%} = 55$ deg., Hz

Mode	Myklestad	UMARC	MBDyn
Gimbal	-	12.4	12.6
Cone	14.7	14.9	15.1
1^{st} Lag	15.3	15.8	16.5
2^{nd} Flap asym.	-	42.3	44.2
"Coll. Lag"	32.7	45.9	46.9
2^{nd} Flap	45.3	45.6	49.1
3^{rd} Flap asym.	-	46.9	60.3
3^{rd} Flap	66.0	60.1	65.2
Flap/Twist	89.3	90.6	97.8
Lag/Twist	90.0	90.8	89.7
3^{rd} Lag	-	92.0	92.9
Twist	-	116.0	108.5

11.5 Wing-rotor models

The previously mentioned models have been merged by mounting the rotor models on the flexible wing. In the rigid blade version, the complete model has been used to evaluate the performances of the aircraft during maneuvres, an example of which is the conversion. The deformable blade model has been used to test the stability of the elastically mounted rotor and to assess the feasibility of the multi-body model for the simulation of the whole, detailed deformable system. Moreover, the effects of the flexibility of the blades on the dynamics of the system, in terms of transmission of the higher harmonics of the rotor system to the body of the aircraft, have been investigated. The first wing modes are not directly affected by the modelling of the flexibility of the rotor. The torsion mode of the wing is very close, and at some airstream speeds coincident, to the rotor speed; this gives raise to resonance that can be seen in the frequency analyses of the internal forces of the wing. Four wing modes are mainly considered: the beam, chord and torsion modes of the wing itself, and the so called "pylon yaw" mode, a low frequency yaw oscillation of the pylon due to the flexibility of the conversion actuator. When considered in the fixed frame, the retreating rotor modes interact with the wing modes. This can be clearly appreciated from a frequency analysis of the wing response when the rotor modes are excited. Most of these modes cannot be easily identified when the aerodynamics are modelled, since they are highly damped. For this reason, a comprehensive analysis of the structural properties of the model has been performed by simulating *in vacuo* operations, while the aeroelastic properties have been estimated in different ways. The damping of the wing modes in forward flight has been estimated by system identification of the (damped) response to a given input, as is usually done during actual wind tunnel tests, while the aeroelastic pitch-flap coupling has been estimated by measuring the phase shift between an harmonic control input and the flapping response.

11.6 Test cases

11.6.1 Response to controls

Figures 11.10, 11.11 refer to a collective pitch maneuvre. They show the internal moments at the wing root and the geometric pitch of blade #1 as the collective control is raised from 0 to 10 degrees in one second. The simulation is performed in helicopter mode; the nominal hover rotation speed of 888 rpm is reached in one second to obtain a trimmed condition (not shown). There is no airstream speed. The difference between the given control and the actual pitch of the blade is due to the deformation of the flexbeam and of the flexible link.

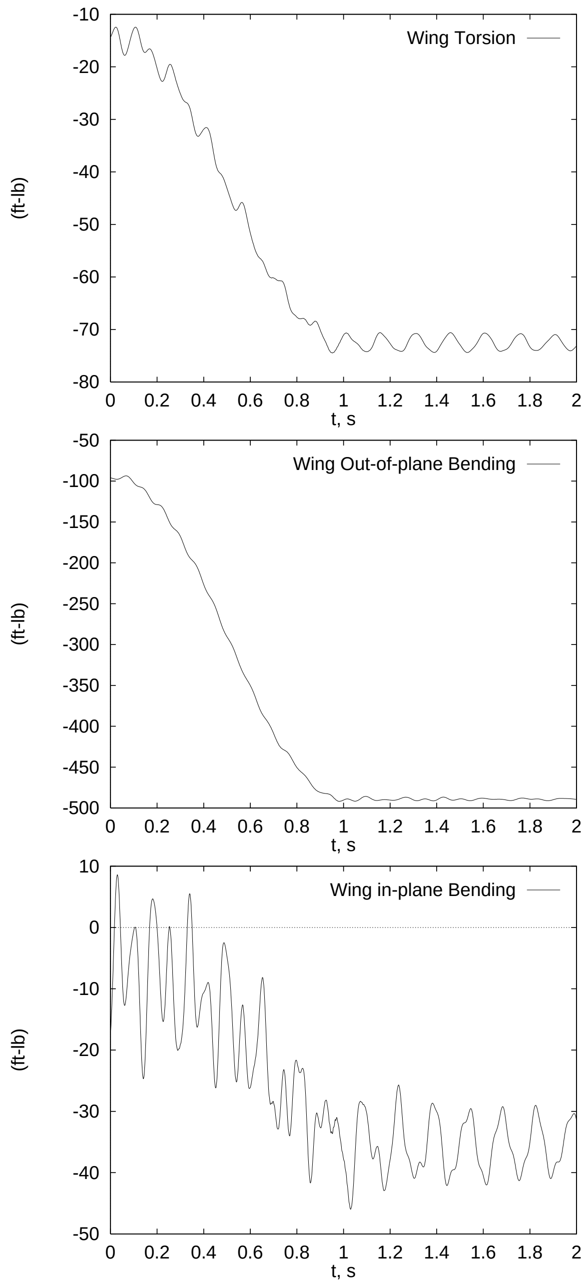

Figure 11.10: Internal moments at the wing root during a 10 deg. collective pitch maneuvre, flexible blade model

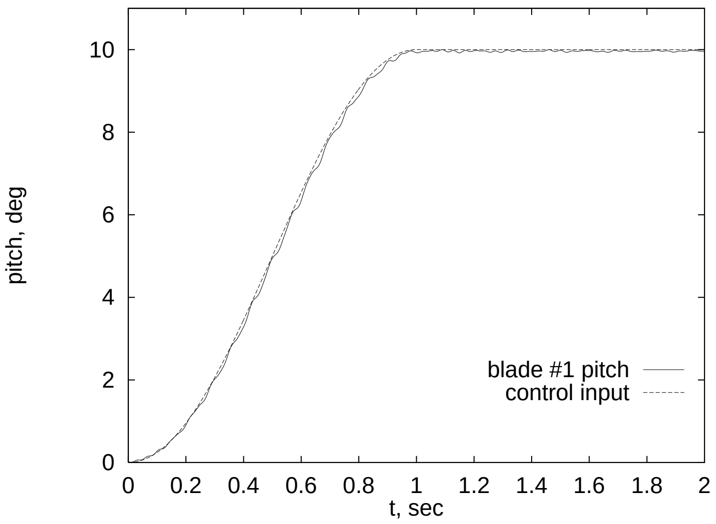

Figure 11.11: Blade #1 pitch during a 10 deg. collective pitch maneuvre, flexible blade model

Figures 11.12, 11.13 refer to a 5 degrees fore/aft cyclic pitch maneuvre. As the rotor tilts forwards, the high frequency in-plane modes of the wing are excited, as shown by the plot of the internal moments. The oscillations in the pitch link are 1/rev., partially due to 1/rev. flexbeam flapping that is superimposed to the gimbal flapping (which implies no appreciable pitch link loads), that is needed to counteract the gimbal springs. It should be noted that while the frequency content of the pitch link loads is acceptably correct, the amplitude of the loads has not been validated and it is likely to be even an order magnitude different from measurements, depending on the frequencies that are considered. In fact the loads in the links heavily depend on the aerodynamics of the blade, whose model is relatively poor, especially with regard to the dynamics of the aerodynamics; so only the constant and the 1/rev. loads may be considered reasonable.

11.6.2 Conversion maneuvre

Figure 11.14 refers to the conversion maneuvre performed by a deformable blade model. It shows the internal forces at the wing root. The conversion is performed at a 10 deg/s constant angular speed. Oscillations of the internal forces due to the untrimmed initial conditions are appreciably damped as the maneuvre proceeds to the end, at 9 s. The following abrupt raise of the internal forces is due to the transient caused by the end of the maneuvre.

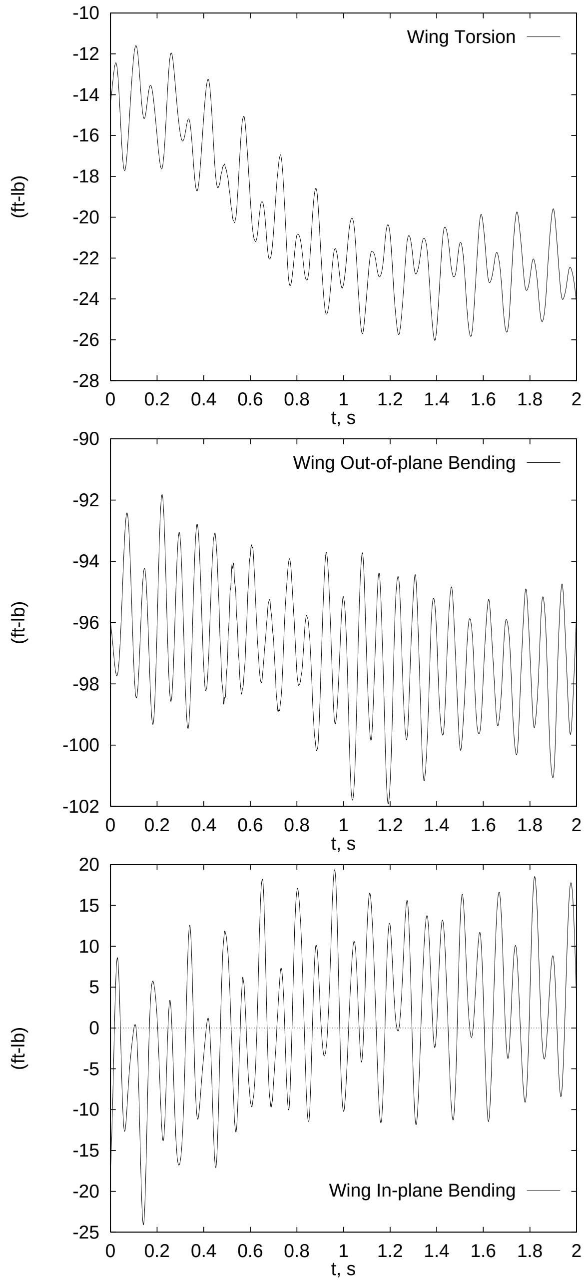

Figure 11.12: Internal moments at the wing root during a 5 deg. fore/aft cyclic pitch maneuvre, flexible blade model

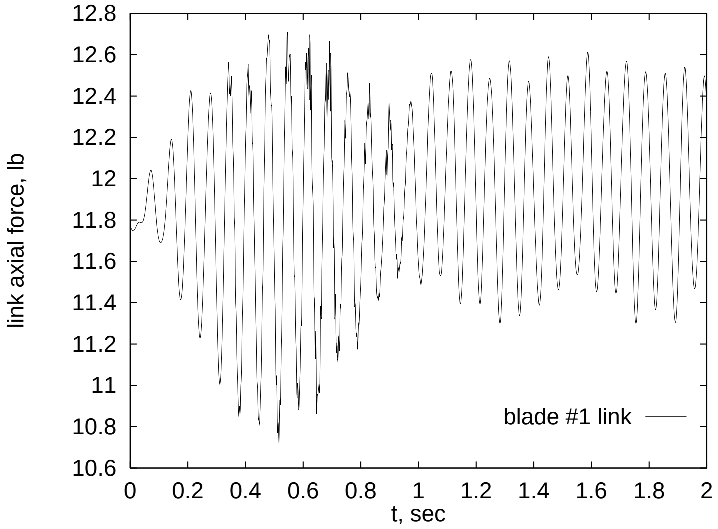

Figure 11.13: Blade #1 control link axial force during a 5 deg. fore/aft cyclic pitch maneuvre, flexible blade model

11.6.3 Gust response

The flexible blade model has been used to simulate the response to a cosinusoidal vertical gust in airplane mode, of 10 ft/s amplitude. Both the stability and the sensitivity of the tiltrotor have been addressed. Figures 11.15, 11.16 show the wing out-of-plane bending moment due to the gust at different airstream speeds, for both off- and on-downstop configurations. In figure 11.15 the off-downstop configuration is clearly less damped than the other one, in fact the stability boundary in air is about 137 Kts, compared to 173 Kts of the on-downstop configuration. When the rotating speed is increased, the stability boundary moves towards lower speeds, as shown by previous analyses and experiments [77].

11.7 Computational notes

The complete flexible model has nearly 600 degrees of freedom. The physical flexible elements have been used throughout the analyses, without any modal condensation. A typical model of the tiltrotor is made of 45 nodes, 39 rigid bodies, 35 joints of different kind, 18 beam elements, 14 aerodynamic elements, 6 control-related nodes and 4 control-related elements. Most of the simulations have been performed with off-the-shelf PCs. The time step initially required for the rigid blade model was $\Delta t = 0.0005$ s, while the deformable blade model re-

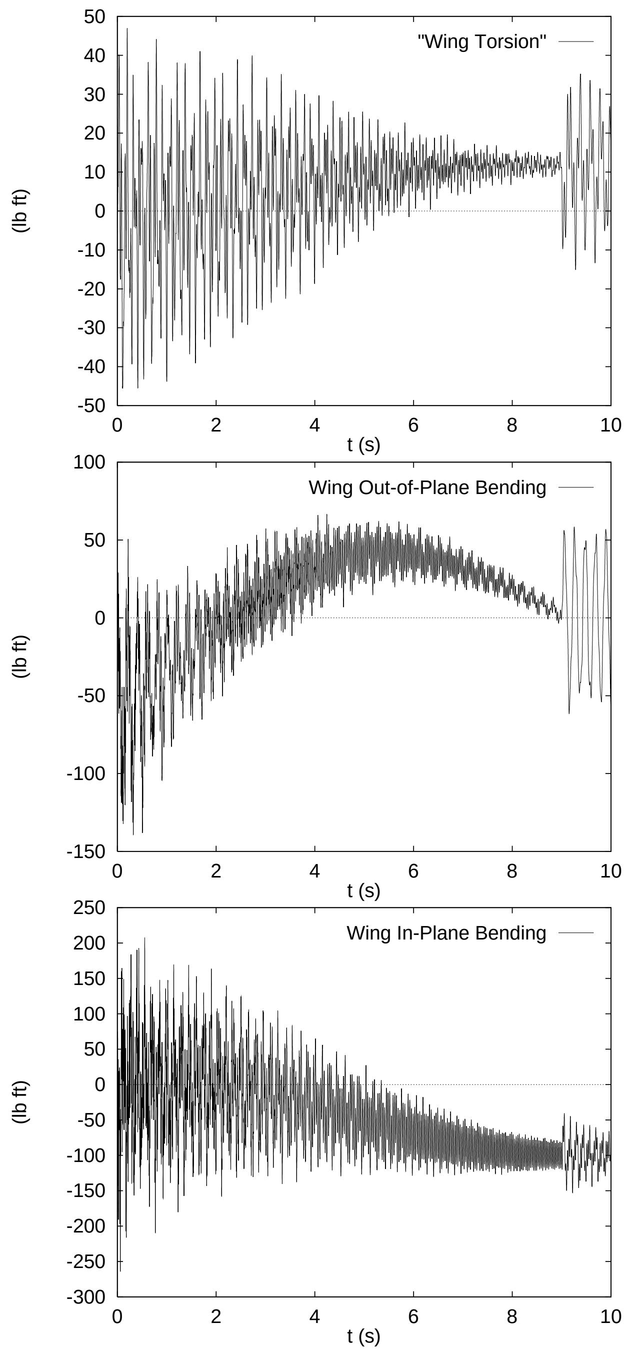

Figure 11.14: Internal moments at the wing root during the conversion maneuvre, flexible blade model

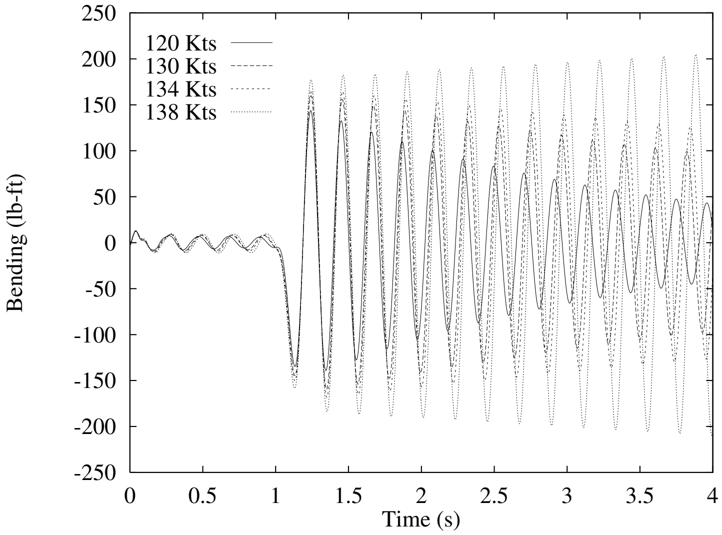

Figure 11.15: *Gust — off-downstop: wing bending*

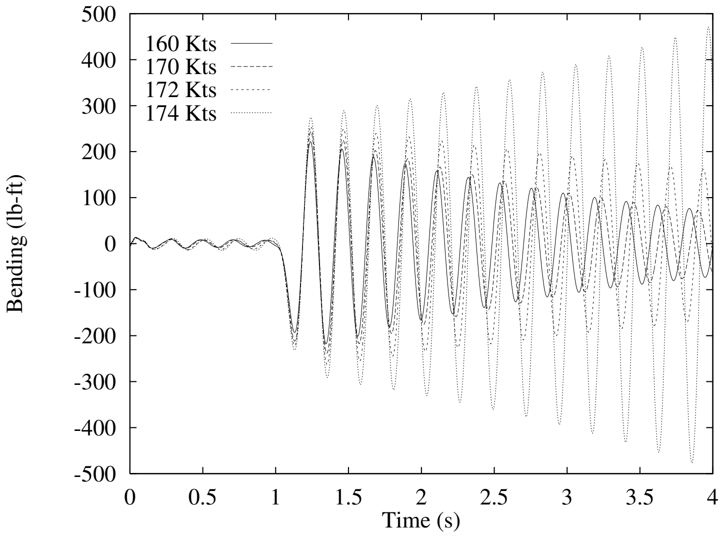

Figure 11.16: *Gust — on-downstop: wing bending*

quired $\Delta t = 0.00025$ s to start correctly. When a variable time step was used, the rigid blade model simulations quickly reached a value of $0.003 \div 0.0035$ s, while the deformable blade model ones reached about $0.001 \div 0.0012$ s. The conversion simulation required about 4.5 hours on a Pentium PRO 200 for a total of 40000 fixed size time steps (10 s at $\Delta t = 0.00025$ s). When performed with variable step size, it required about one hour. After model refinement, and with a soft start, the flexible blade model is able to start with $\Delta t = 0.001$ s, requiring about 1.7 hours, or 1.1 hours on a Pentium II 333 and 0.8 hours on a Pentium II 450, for the full conversion simulation. Tests are being performed on Digital workstations with Alpha processor. The speed has been increased of a factor 4.5 for typical simulations. These numbers make this kind of analysis interesting even for a large, time consuming parametric study for rotorcraft design.

Chapter 12

Tiltrotor vibration control

The predictive control described in Chapter 7 and assessed in Section 10.3 is applied to the tiltrotor model described and analysed in Chapter 11. This form of control may be regarded as HHC, since the swashplate is used to actuate the rotor; nevertheless, there is no exploitation of the knowledge of the rotating speed of the rotor, the controlled system being used as a black box.

12.1 Hover — harmonic excitation

The effectiveness of the GPC applied to a realistic system has been assessed by performing simple SISO control analyses of the WRATS model in hover. Analogous preliminary hover tests have been performed by Bell Helicopter and LaRC personnel with a prototype, proprietary implementation of the GPC that required off-line identification of the system. Wind tunnel tests are being scheduled. The rotor is rotating at 888 rpm, and it is externally excited by a shaker with a harmonic load at 5 Hz, close to the first wing out-of-plane bending frequency, at about 5.5 Hz. The time step is 0.001 s, and the control samples are taken every 8 steps, resulting in a frequency of 125 Hz, which is higher than the first torsional frequency of the blade, to avoid blade resonance.
The bending strain at the root of the wing is measured, filtered by a washout (band-pass) analog filter to cut out of the measure the static signal as well as the higher frequencies, and the rotor thrust is used as actuator by controlling the collective pitch. A band-pass filtered measure of the vertical acceleration at the pylon is alternatively used. A good compromise for the system order has been found in $p = 60$. The results in the two cases, compared to a baseline analysis with harmonic excitation but without control, are presented in Figures 12.1, 12.2, for two different values of λ. They show the bending out-of-plane moment at the wing root.

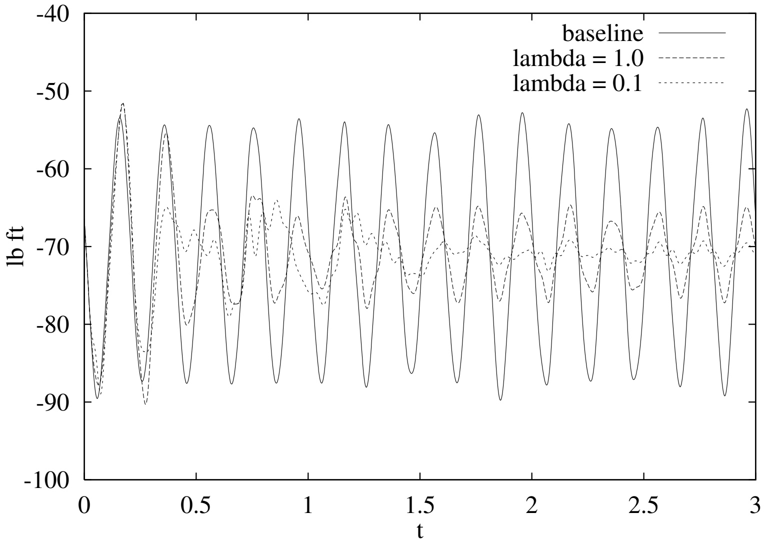

Figure 12.1: Hover bending moment, strain measure

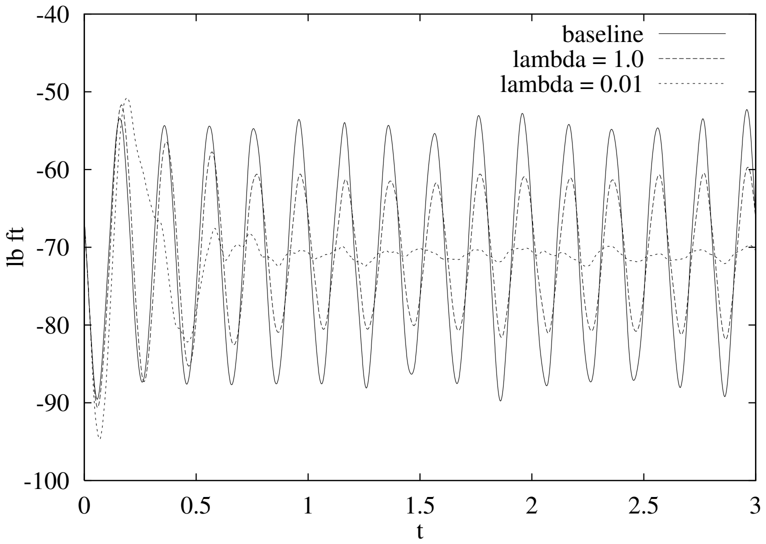

Figure 12.2: Hover bending moment, acceleration measure

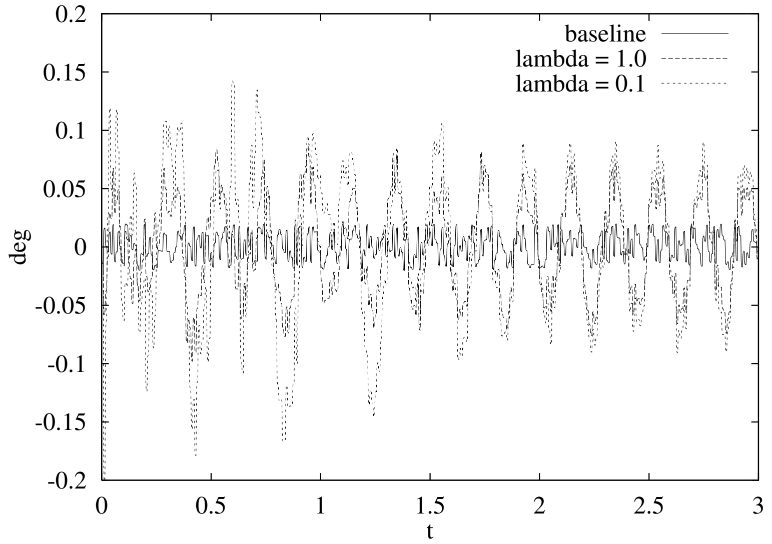

Figure 12.3: Hover collective, strain measure

The control signals are shown in Figures 12.3, 12.4, while the vertical acceleration at the pylon in the latter case is shown in Figure 12.5; the high frequency noise is the persistent excitation that is used to continuously identify the system, while the control of the harmonic motion determines the main, low frequency oscillation.

12.2 Forward flight — harmonic excitation

Forward flight analyses have been performed by controlling the collective and the cyclic pitch of the blades based on different measures of strain at the wing root. The model is in airplane configuration, at an airspeed of 100 ft/s, and the rotor is rotating at 742 rpm. In this case the order is $p = 20$, since the number of measures is higher (3 vs. 1). First the wing out-of-plane excitation force is offset aft of the wing to obtain also a twisting excitation. The rotor has little control authority in its plane in terms of force, the flapping of the disk being required to tilt the thrust. Since the flapping response has a delay of about 90^{o}, the accuracy of the prediction is key to the effectiveness of the control. In this case the actuation force, transverse to the wing, lies in the plane of the rotor, thus being not directly controllable by a simple change in thrust. Moreover, since the motion of the gimballed rotor is characterised by a wide spectrum dynamics, from the high frequency vibrations induced by the advancing blade modes, to the wing elastic modes, down to the very low frequency precession motion, a high number of physical and numerical poles are required for an adequate identification. The results of the simulations are reported in Figure 12.6, that shows the wing root

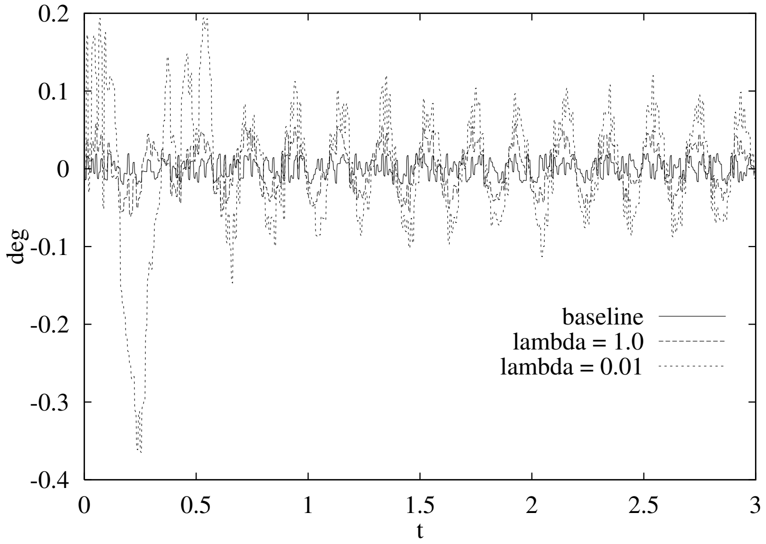

Figure 12.4: Hover collective, acceleration measure

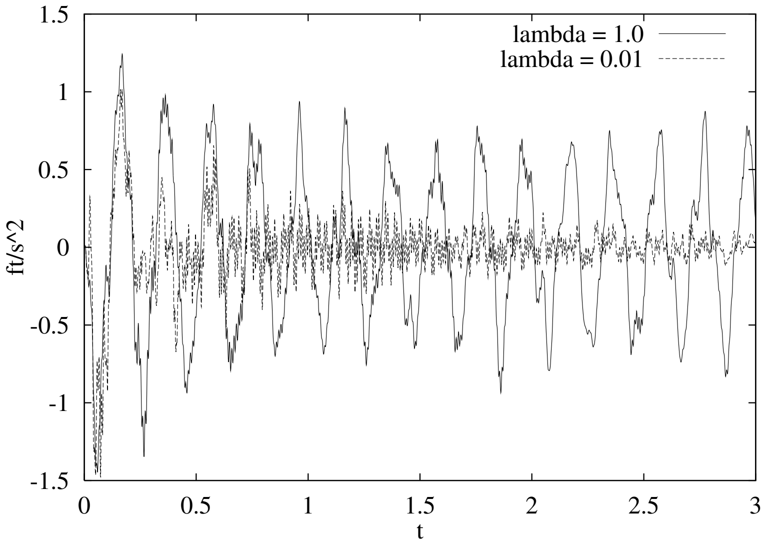

Figure 12.5: Hover accelerometer signal

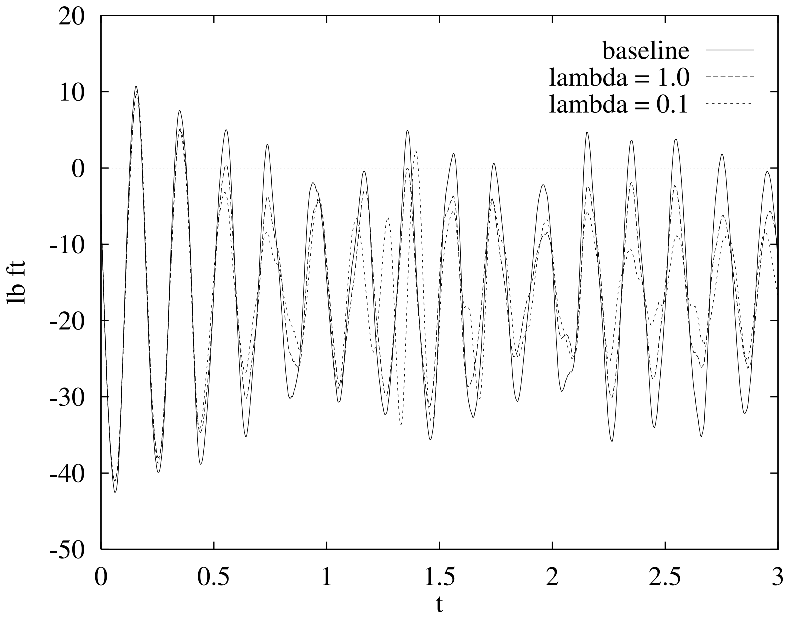

Figure 12.6: Forward flight bending

bending moment. Figure 12.7 shows the control signals. The initial low frequency oscillations in the control signals are due to the precession of the rotor during the transient following the application of the harmonic excitation. The uncertain initial behaviour of the controller is related to a poor initial identification of the low frequency poles of the system. In fact, with $\lambda = 1.0$ the control authority is low, but with $\lambda = 0.1$, after a few cycles the system goes slightly unstable (after about 1.5 s), returning under control as soon as the identification is improved. The following behavior is definitely better than the previous case, as can be appreciated in the last part of the plot.

12.3 Forward flight — gust response

A more realistic case is considered, by using the control parameters tuned with the former case. A cosinusoidal vertical gust, with an amplitude of 4 ft/s and a wavelenght of 20 ft, is encountered by the model while the control is working. The effect of the control on the wing bending is shown in Figure 12.8: the free oscillations resulting from the wind-up of the rotor are damped as the control starts; when the model encounters the gust, the peak of the moment is attenuated first, then the control overshoots due to the need to re-identify the system. The newly identified system brings the bending moment, as well as the other measured internal moments, to a neglibible value in a few cycles. The control signals, i.e.

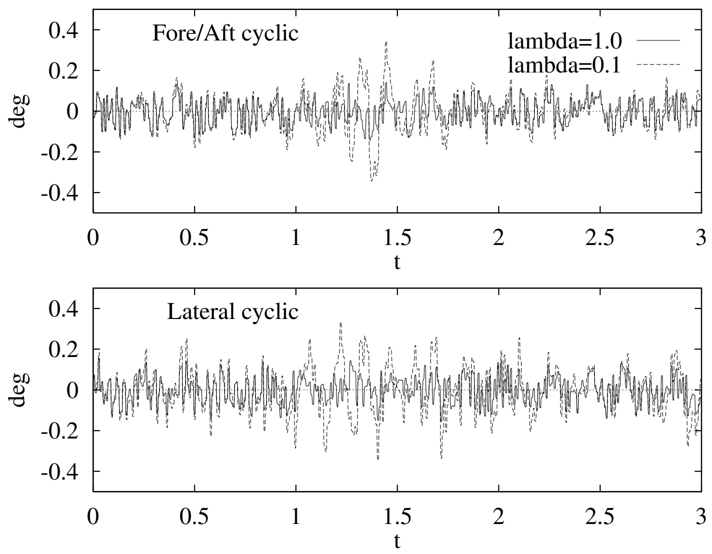

Figure 12.7: Forward flight control signals

the pitch controls determined by the controller, are particularly meaningful. The collective is negligible, since it mainly controls the in-plane bending of the wing, that is not directly excited by the vertical gust. The cyclic controls instead are heavily used by the controller to generate the rotor aerodynamic moment required to tilt the rotor disk. Since the disk tilts about a horizontal axis due to the wing bending and torsion excited by the gust, the rotor is mainly required to generate a pitch moment (in airplane sense) that counteracts this motion. In fact the higher cyclic control signal is the lateral pitch, about twice as large as the fore/aft pitch, which causes a fore/aft flapping of the rotor. Figure 12.9 shows a detail of the control signals across the gust input.

The gust problem has been investigated further, to address the effect of the choice of the measures on the quality of the performances of the controlled system. A longer learning time has been used, together with higher excitation signals. Four control configurations are considered, whose results are shown in figures Figures 12.10–12.13; the figures report the wing root out-of-plane bending and the transverse acceleration at the wing tip. All the figures compare to a reference measure addressed as baseline, that is a reference simulation with two consecutive gusts and total absence of disturbs and excitation signals. The three blade pitch controls are used as actuators. In the first three cases the measures of the two bending and of the twisting strains are used, thus resulting in a 3 input-3 output control system. In the fourth case, the fore-aft and two transverse accelerations at different chord stations, measured at the wing tip, have been added to the measure set, resulting in a 3 input-6 output control system.

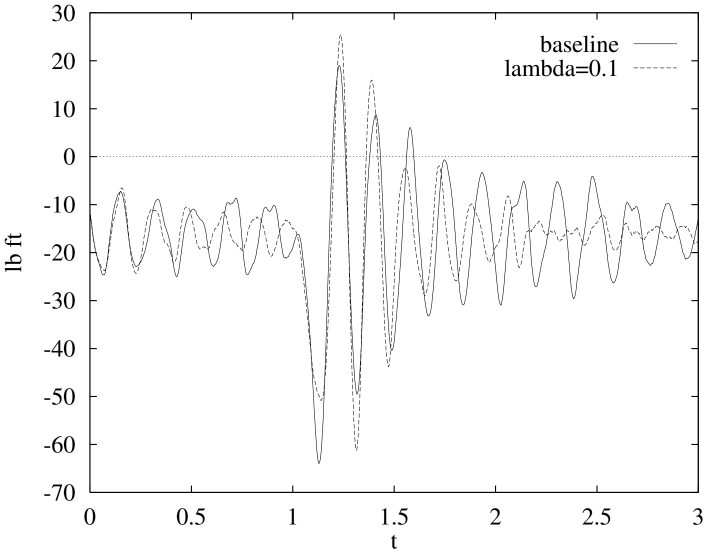

Figure 12.8: Gust bending

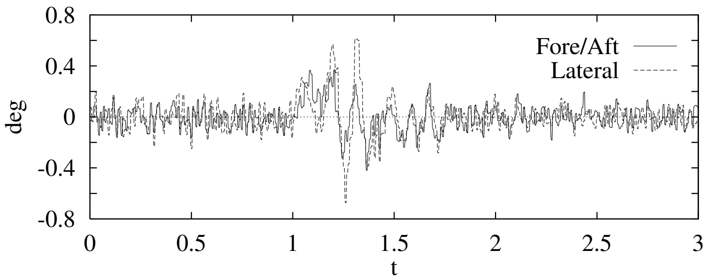

Figure 12.9: Gust control signals

The first case, shown in Figure 12.10, simply addresses the persistent excitation the four cases are subject to in order to allow the correct identification of the system.
The second case, considered in Figure 12.11, refers to non-adaptive control: the controller is designed once for all after the initial identification, and there is no further control design. The response to the gust is quite smooth, and the initial peak in the bending moment is cancelled very quickly with no oscillations, but the responses to the two consecutive gusts are nearly the same, with no attenuation of the initial peak in either case.
The third case, Figure 12.12, shows the reponse due to the adaptive control: the system is continuously identified on-line, and the controller is redesigned to learn from the response. The control is very effective, but the continuous learning results in high frequency disturbancies added to the response of the system. This is apparent from the plot of the accelerations in Figure 12.12. They are not measured, so there is no attenuation; on the contrary, the continuous attempt to counteract the excitation input magnifies them. The bending is damped very quickly, but there is no peak attenuation at the first gust. The adaptivity of the controller results in the system learning about the gust; as a consequence, the peak due to the second gust is neatly attenuated.
The fourth case, Figure 12.13, shows how the addition of the acceleration measures to the output pool of signals allows the system to prevent the peak due to the gust from the very first time. In fact, the system can detect the arrival of the gust from the very beginning, due to the initial acceleration, while in case of strain measure it was able to detect the adverse condition only after the bending of the wing. There is no appreciable change in the response to the second gust, the attenuation being satisfactory during both occurrences of the disturbance. In this case the accelerations at the tip are neatly attenuated, especially at low frequencies. As expected, there is some increment in the acceleration at higher frequencies, because the control moves the poles of the system towards higher frequencies.

12.4 Forward flight — flutter suppression

As a final test, a flutter suppression case has been investigated. The system, in the locked-downstop configuration, is flown slightly above the flutter limit speed, at 174 Kts, and the controller based on both strain and acceleration measures described in the fourth case of the previous section is applied at time $t = 1.0$ s, as a vertical gust arrives. Figure 12.14 show the twist and the beam and chord bending at the root of the wing, while Figure 12.15 shows the transverse acceleration at the pylon, and Figure 12.16 shows the pitch controls. This example should be intended as a demonstration of the possibilities of the proposed control technique

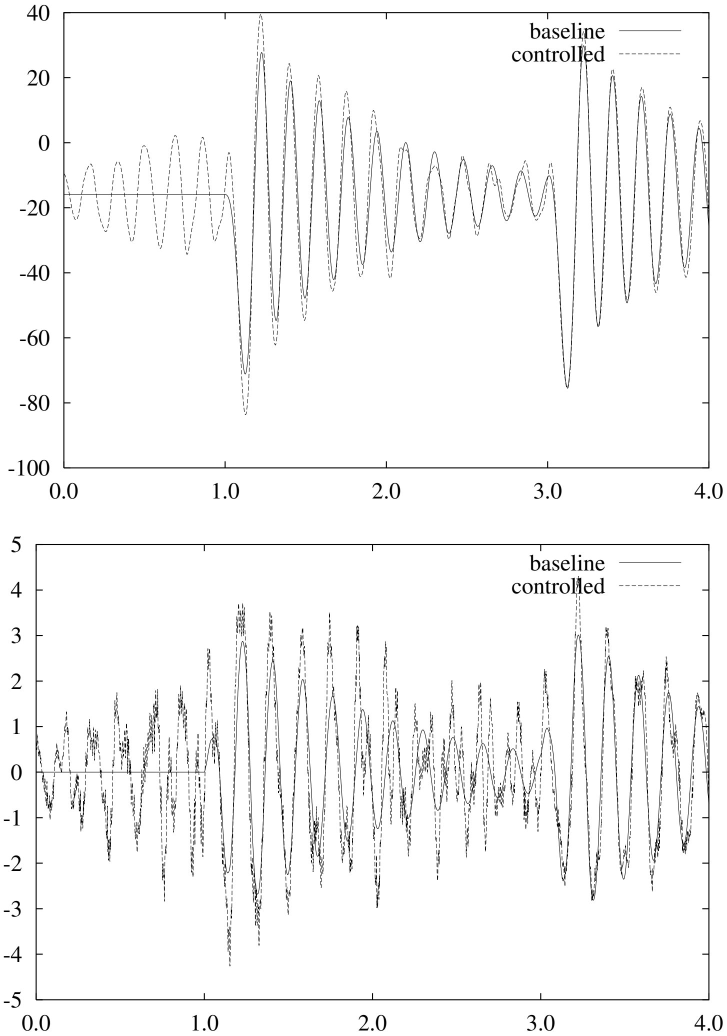

Figure 12.10: Baseline/persistent excitation; wing root bending, top (lb-ft); wing tip acceleration, bottom (ft/s^2).

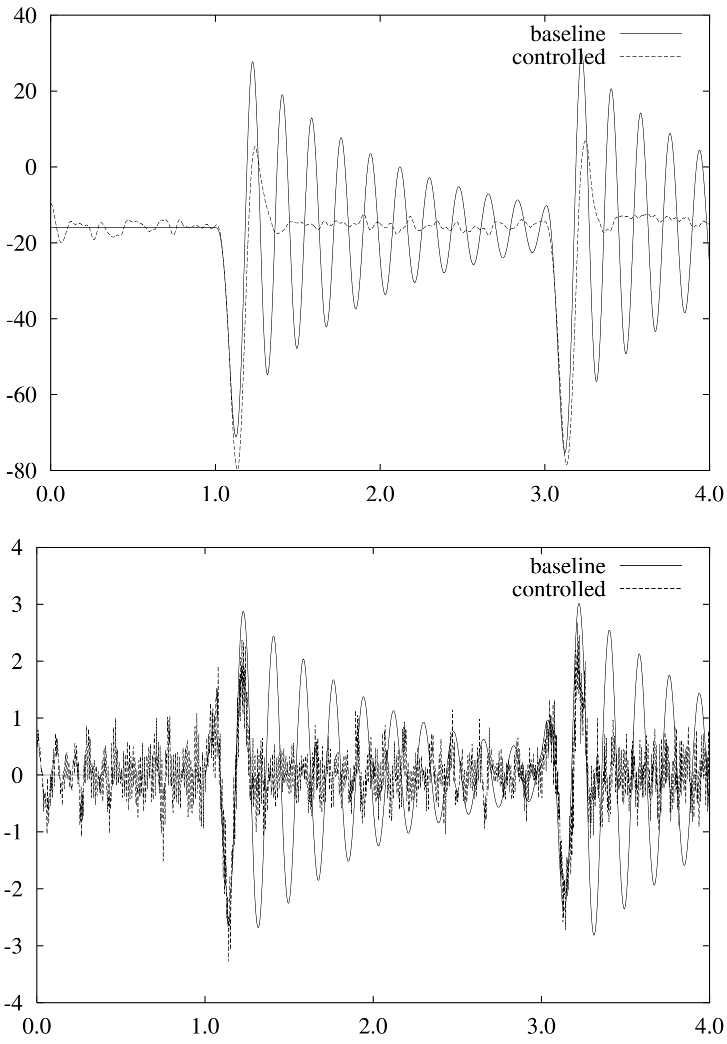

Figure 12.11: Baseline/non-adaptive control; wing root bending, top (lb-ft); wing tip acceleration, bottom (ft/s^2).

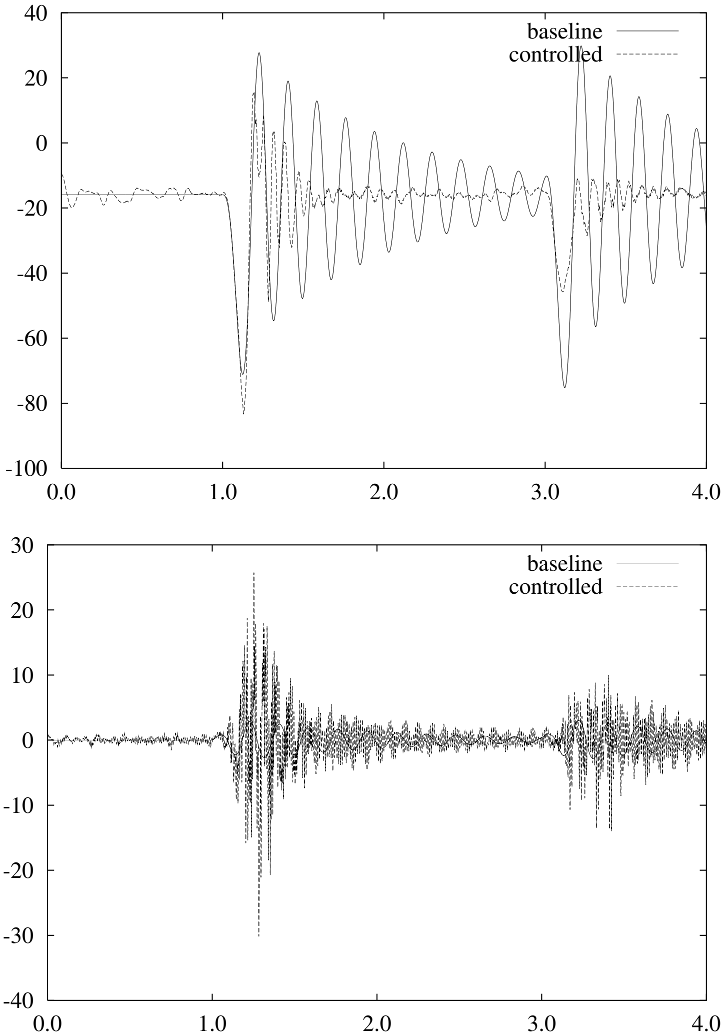

Figure 12.12: Baseline/adaptive control; wing root bending, top (lb-ft); wing tip acceleration, bottom (ft/s^2).

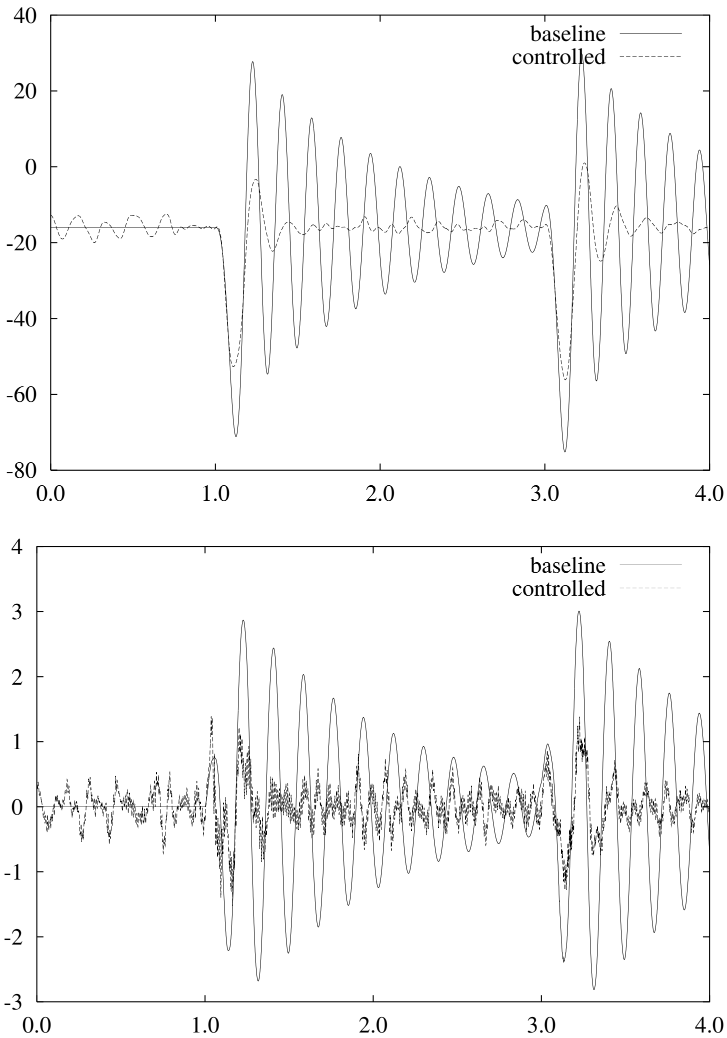

Figure 12.13: Baseline/mixed strain-acceleration control; wing root bending, top (lb-ft); wing tip acceleration, bottom (ft/s^2).

rather than a flutter suppression investigation; however, it is apparent how the control is effective both in cancelling the response to the gust and in stabilising the system. Flutter suppression represents a future aim of this research, and current results are encouraging.

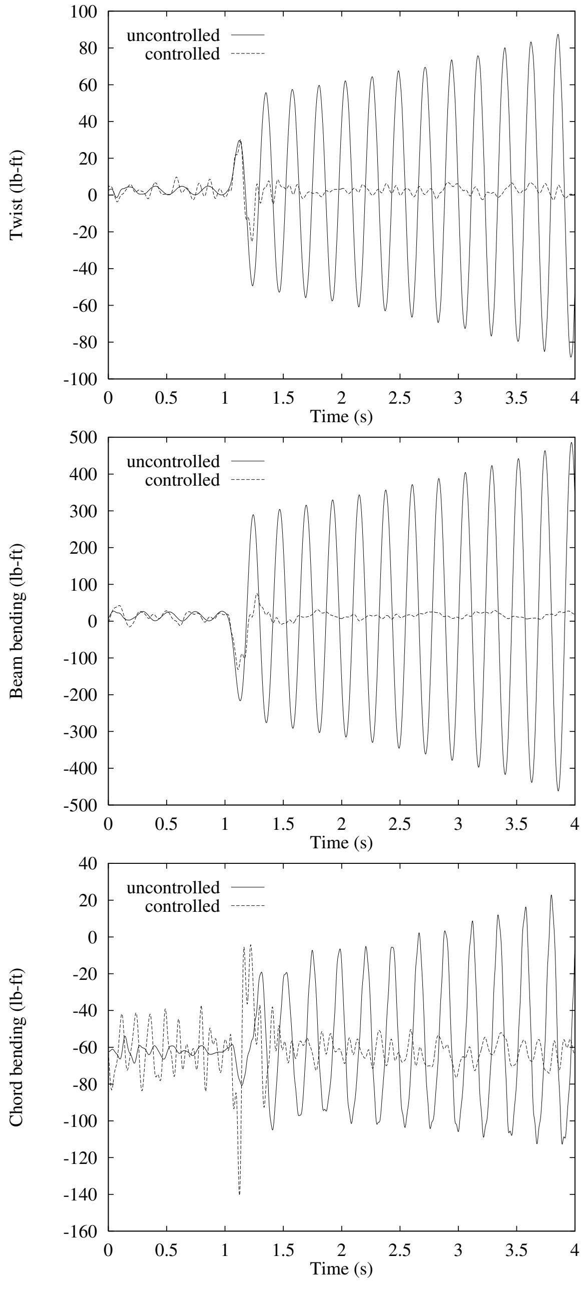

Figure 12.14: mixed strain-acceleration control: flutter suppression; internal couples at the wing root.

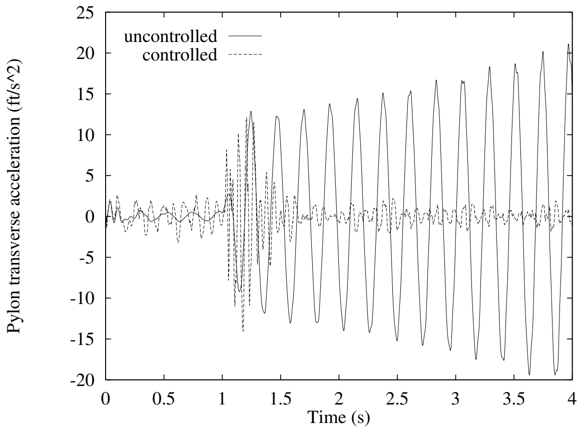

Figure 12.15: mixed strain-acceleration control: flutter suppression; pylon transverse acceleration.

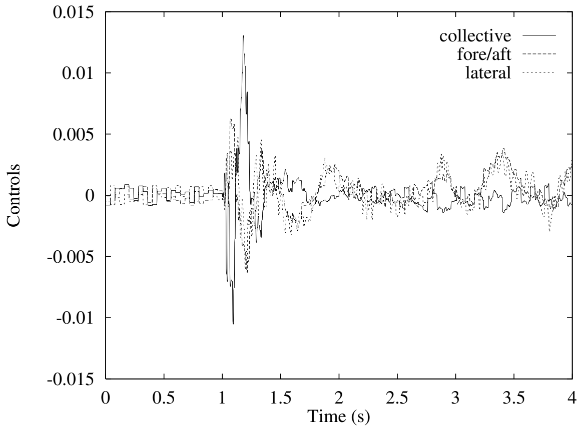

Figure 12.16: mixed strain-acceleration control: flutter suppression; pitch control signals.

Chapter 13

Active Twist Rotor analysis

The analysis of an active twist rotor is presented. The model proposed in Ref. [90] for the preliminary investigation on the feasibility of an induced twist control for helicopter rotors has been reproduced starting from the piezoelectric properties of the material. The equivalent homogeneous properties of the Active Fibre Composite material have been determined by three-dimensional finite element analysis of an active fibre specimen. The blade section properties have been subsequently computed based on the geometry and on the lamination characteristics proposed in [90], following the procedure outlined in Section 9.1. Finally, a multibody model of the active twist rotor has been investigated to assess the authority of the induced twist actuation in hover and in forward flight conditions. Preliminary results have been reported in [36].

13.1 Material characterisation

The characterisation of a composite material is a complex topic. Different techniques have been developed to predict the elastic properties of a fibrous composite material starting from the elastic properties of its components, namely the fibres and the matrix [19]. Extensions to the case of thermoelectroelastic materials have been proposed in the literature [22, 21]. Such analytical models rely on the symmetry and the simplicity of the analytical modelling of a single, indefinitely long fibrous inclusion. The case of the AFC with IDE is far more complicated due to the peculiar geometry of the electrodes, that add a higher degree of complexity to the behaviour of the material. A ply of AFC material is usually made of a single layer of piezoelectric fibres, bounded to two thin films that carry the electrode patterns. It represents a three-dimensional, discrete, repetitive structure both from the mechanical and the electric standpoint. As a consequence, the elastic and electric fields are fully three-dimensional and periodical, due to the repetitivity of the

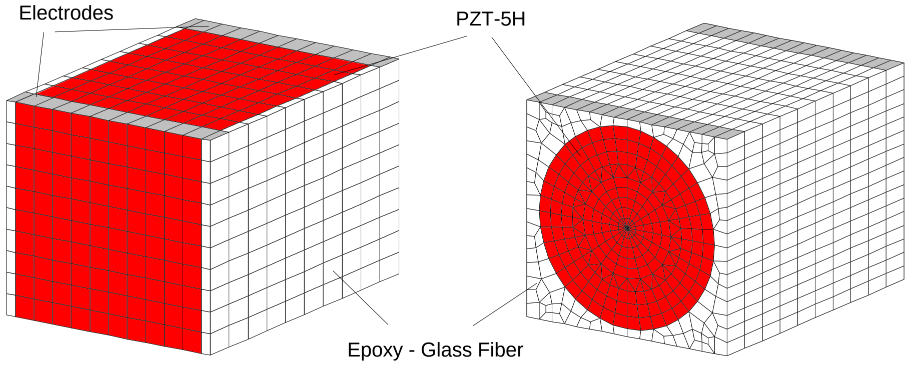

Figure 13.1: FE models of the two specimen

pattern of the fibres in direction 2 and of the electrodes in direction 1. The present technology allows the manufacturing of one-fibre thick plies of the order of 0.10 mm [8]. The granularity of the repetitive pattern is such that, from a macroscopic point of view, an equivalent, homogeneous orthotropic piezoelectric material is expected to exist, and to be able to capture the fundamental behaviour of the AFC material. Here an attempt is made to predict the properties of such corresponding continuum, by conventional electroelastic Finite Element Analysis (FEA). By exploiting the symmetry of the piezoelectric component, a finite portion of fibre, comprised between the centerlines of two rows of electrodes, is modelled by a commercial FEA code; the FE models are shown in Figure 13.1.

The figure refers to the circular section fibre presently investigated at MIT [8] and to the rectangular section fibre under investigation at NASA LaRC [90]. The latter geometry seems to be more promising in terms of ease of manufacturing, accuracy in bonding the IDEs to the fibres, and homogeneity of properties. The fibre is made of raw piezoelectric material (presently Morgan Matroc PZT-5H is being used at MIT's Active Materials and Structures Laboratory [80]). The circular fibre manufactured by CeraNova Corp. has a diameter of 0.13 mm, and dimensions smaller than 0.10 mm are expected soon; the rectangular fibre, obtained by cutting monolithic ceramic sheets, can be manufactured down to 0.13×0.07 mm sections [59]. The piezoelectric properties of the specimen are determined by imposing one by one the boundary conditions pertaining to each independent strain and electric field conditions (i.e. the three unit extensions, the three unit shear deformation conditions, and the condition of unit electric field between two electrode sets) and computing the stress resultants. All these boundary conditions are required because the beam section analysis presented in Section 9.1 is based on the full three-dimensional properties of the material. The resulting properties of

Table 13.1: Equivalent homogeneous piezoelectric material properties

Property	Circular	Rectangular	
C_{11}	10.43e6	12.11e6	[psi]
C_{12}	1.12e6	2.14e6	[psi]
C_{13}	1.25e6	2.93e6	[psi]
C_{22}	2.39e6	6.15e6	[psi]
C_{23}	0.91e6	2.26e6	[psi]
C_{33}	3.90e6	8.14e6	[psi]
C_{44}	1.16e6	2.36e6	[psi]
C_{55}	2.47e6	0.78e6	[psi]
C_{66}	2.47e6	0.29e6	[psi]
e_{11}	64.52e-6	104.48e-6	[psi in/V]
e_{12}	-5.71e-6	-17.13e-6	[psi in/V]
e_{13}	-6.85e-6	-25.69e-6	[psi in/V]

the equivalent material are reported in Table 13.1.
Figures 13.2 and 13.3 respectively show the Von Mises stress and the electric field due to unit axial strain applied to the clamped and close-circuit specimen and to unit tension applied to the pairs of electrodes of the completely clamped specimen.

13.2 Blade section characterisation

Figure 13.4 shows the FEM model of the NACA 0012 airfoil that has been used in this analysis, while Figure 13.5 refers to the warping due to different mechanical and electric load conditions of the blade section under analysis.
Table 13.2 presents the structural properties resulting from this analysis compared to those given in Reference [90]; three different meshes of increasing refinement have been considered. The properties in Table 13.2 converge very quickly to their final value; the most challenging term is the position of the shear center, that travels from negative to positive with respect to the reference point at 25% of the chord as the mesh is refined. Further analyses with finer meshes confirmed that the presented value has reasonably converged to the final value. The AFC with rectangular fibre described in Table 13.1 has been used. The other materials used, namely $\pm 45^{\circ}$ fiberglass (E-glass) for the outer skin and between the piezoelectric plies, and T300 unidirectional graphite-epoxy for the inner part of the spar, are described in Table 13.5. The laminate of the spar has been obtained by stacking, from the inner side, a ply of fiberglass, followed by 9 plies of T300 and by three sets of substacks made of fiberglass, $+45^{\circ}$ AFC, fiberglass and -45° AFC. A final ply of fiberglass has been used to wrap the whole section, including the trailing

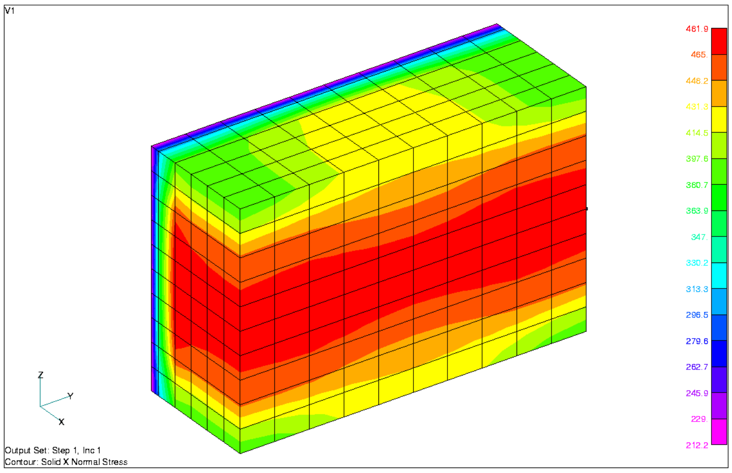

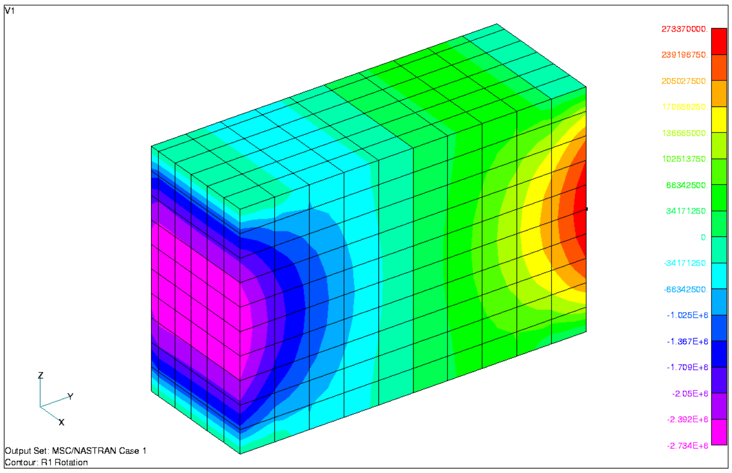

Figure 13.2: *Von Mises* stress (top) and electric field (bottom) due to axial strain in the square fibre.

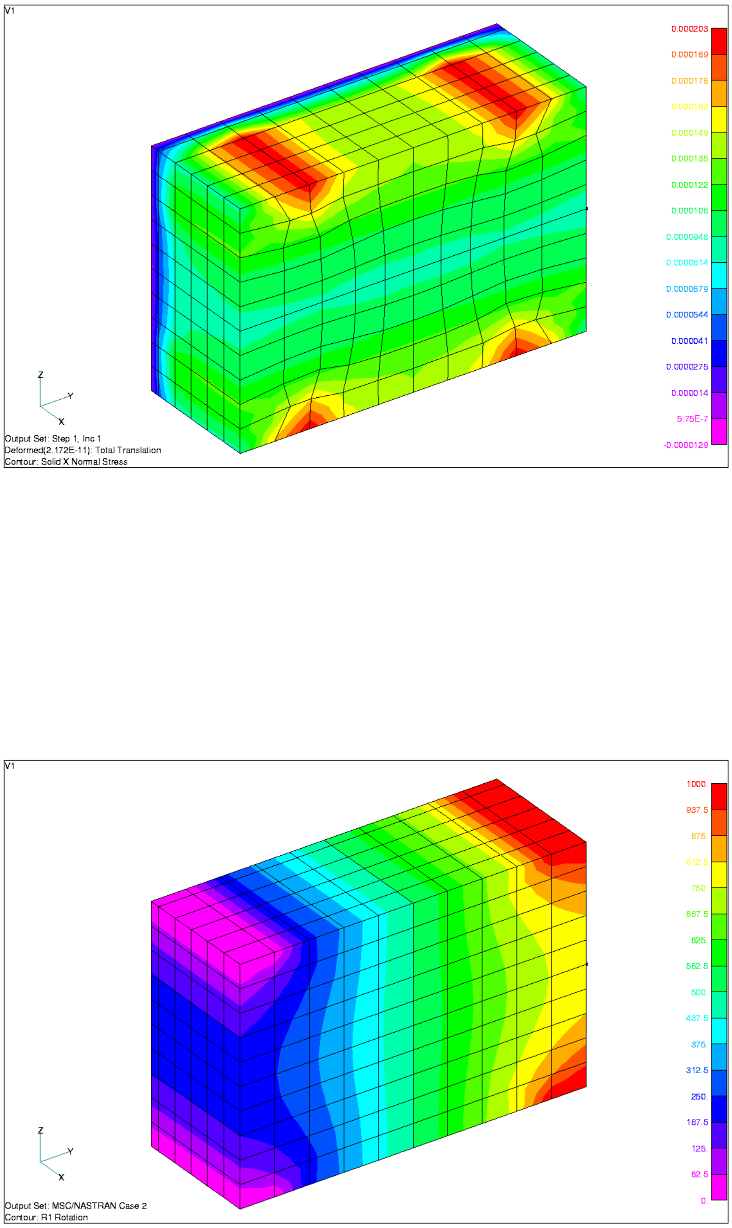

Figure 13.3: *Von Mises* stress (top) and electric field (bottom) due to electric voltage between the electrodes.

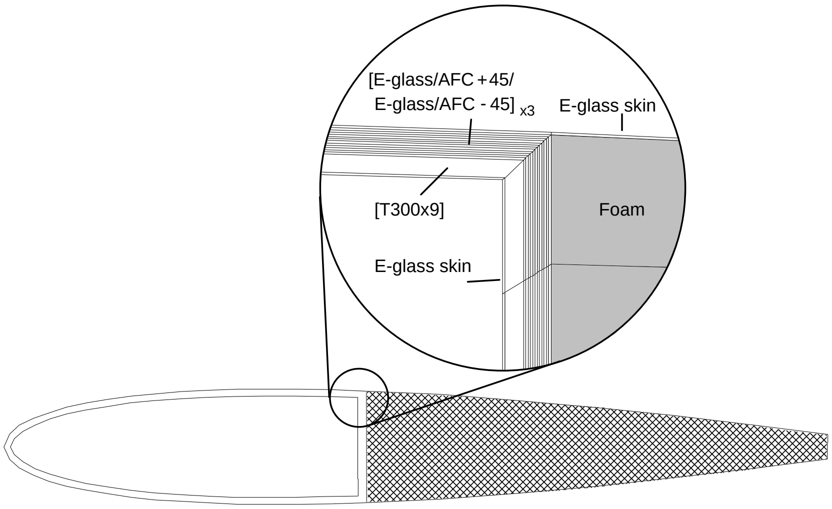

Figure 13.4: Sketch of the blade section, with detail of the plies in the spar

Table 13.2: Blade stiffness properties with rectangular fibre.

Stiffness		Mesh 1	Mesh 2	Mesh 3	Ref. [90]
Axial	[lb]	1.79e7	1.85e7	1.86e7	n.a.
Shear i.p.	[lb]	1.83e6	1.81e6	1.79e6	n.a.
Shear o.o.p.	[lb]	2.48e5	2.06e5	1.96e5	n.a.
Twist	[lb ft^2]	2.94e4	2.80e4	2.77e4	2.61e4
Bending o.o.p.	[lb ft^2]	6.89e4	7.07e4	7.11e4	9.16e4
Bending i.p.	[lb ft^2]	5.36e5	5.92e5	6.08e5	n.a.
Axial force center	[% chord]	2.28	2.79	2.96	0.00
Shear center	[% chord]	-1.68	1.26	2.18	0.00
Nodes		175	362	662	—
Elements		162	336	618	—

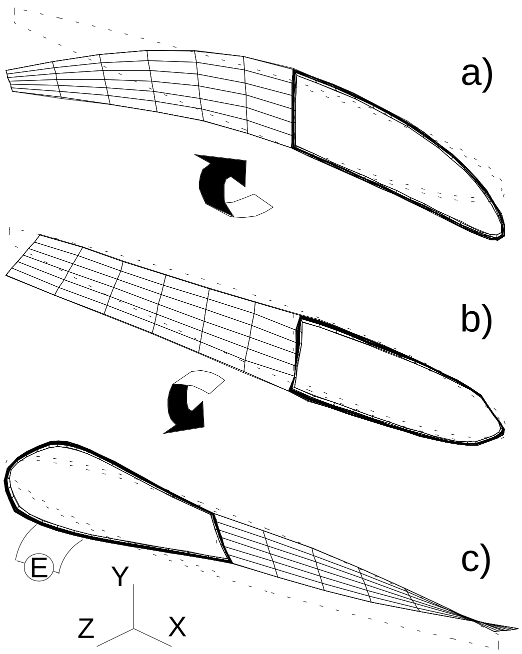

Figure 13.5: *Warpings due to (a) out-of-plane bending, (b) torsion, (c) electric tension that gives induced twist*

part, that has been filled with foam, without any structural function; a schematic is shown in the detail of Figure 13.4. The thicknesses of the single plies are reported in Table 13.5. The spar goes from the leading edge to 40% of the blade chord; the piezoelectric plies are applied on the top and bottom surfaces approximately from 5% to 40% of the chord; in the web and in the nose the fiberglass is used instead of the AFC. The full stiffness and piezoelectric matrices obtained with the most refined mesh are reported in Table 13.3. Notice that the coupling coefficients that are marked in italics cannot be captured by a conventional, geometry-based beam cross-section analysis method. In the present work, many of them are null due to geometric or material symmetry, but there are significant cases of non-null coupling coefficients, as the axial strain/twist coupling, the axial strain/out-of-plane shear coupling, the twist/out-of-plane bending coupling that are due to the anisotropy of the material, and the piezoelectric twist and out-of-plane shear couplings that are due to the anisotropy of the inverse piezoelectric effect of the material.

Table 13.3: Section stiffness and piezoelectric matrices, ref. 25% chord; units: lb, ft and V.

	Axial	Shear		Twist	Bending	
		i.p.	o.o.p.		i.p.	o.o.p.
Axial	1.86e+7	*0.00e+0*	*1.91e+2*	*4.29e+2*	0.00e+0	-7.53e+5
Sh. i.p.		1.79e+6	0.00e+0	0.00e+0	*-7.44e+1*	*0.00e+0*
Sh. o.o.p.			1.96e+5	5.85e+3	*0.00e+0*	*-3.16e+2*
Twist				2.77e+4	*0.00e+0*	*-8.47e+1*
B. o.o.p.		sym.			7.11e+4	0.00e+0
B. i.p.						6.08e+5
Piezo	0.00e+0	*0.00e+0*	*1.29e-1*	*1.86e-1*	0.00e+0	0.00e+0

13.3 Active Twist Rotor model description

The numerical analysis is based on an analytical model of the active twist rotor presented in Reference [90]. This is the analytical bench full-scale helicopter rotor the NASA Langley Research Center ATR wind tunnel model refers to [88, 91]. It is representative of a large class of medium weight helicopter rotors. The basic properties of the rotor are described in Table 13.4. Two analytical models have been studied in this paper, both based on the main properties of the mentioned rotor. The first one uses the same elastic and piezoelectric coefficients described in the mentioned paper, for direct comparison and model validation purposes. The second model is based on the proposed blade section characterisation method. The numerical results cannot be considered completely representative of the model they refer to, because the final active twist fitting of the ATR model is still under refinement. These results should be considered as a sample application of the proposed analysis procedure. A flexible model of the benchmark active twist rotor has been implemented. The model consists in the hub, a rigid body rotating at constant speed with respect to the ground, and carrying the hinges of the four blades. Coincident hinges for flap and lag have been considered, at 0.027 R from the rotation axis. A pitch bearing is placed right outwards of the hinges. The flexible blades are modelled by four three-node beam elements, with lumped inertia. The swashplate is modelled, with scissors to prevent the relative rotation about the rotor axis between the fixed plate and the ground, and between the rotating plate and the hub, with the three variable distance actuators from the ground to the fixed plate, and with fixed distance links from the rotating plate to each blade to impose the blade pitch.

Table 13.4: Active Twist Rotor geometric and dynamic properties (Ref. [90])

Symbol	Property	baseline	AFC blade
R	blade radius [in]	336	(same)
Ω	rotation speed [rad/s]	22.25	(same)
m	section mass, [lb-s^2/in/in]	1.11e-3	1.03e-3
c/R	nondimensional chord	0.0488	(same)
θ_1	linear pretwist [deg/R]	-8	(same)
γ	Lock number	9.77	(same)

Table 13.5: Blade section materials

Property	glass-epoxy	graphite-epoxy	
c_{11}	2.15e6	26.36e6	[psi]
c_{12}	0.19e6	0.42e6	[psi]
c_{22}	1.98e6	1.50e6	[psi]
c_{66}	0.28e6	1.04e6	[psi]
ρ	6.50e-2	5.78e-2	[lbs/in^3]
thickness[a] h	5.10e-3	4.92e-3	[in]

[a]The thickness of the AFC plies is 5.50e-3 in.

13.4 Model validation

The model has been first validated from a dynamic standpoint by comparing the *in vacuo* rotating frequencies to those obtained in Ref. [90]. The frequencies have been obtained by system identification from the time domain response of the rotor subject to random excitation. The results are presented in Table 13.6. No lead-lag frequencies are presented, because no reference data is available for comparison. The first, rigid lead-lag frequency, due to an hinge offset of 9 in (0.027 R), is 0.20 Ω. The results from the model with beam properties taken from Ref. [90] are presented first, followed by those obtained with the beam properties estimated by the proposed procedure. The agreement of the frequencies obtained with the given, diagonal stiffness matrix is excellent; the frequencies obtained by computing the stiffness of the section with the proposed procedure is good, especially on the lower flap frequencies because they are dominated by the centrifugal stiffness; the frequency of the fourth flapping mode, obtained from the model with calculated stiffness properties, is appreciably lower than in Ref. [90], due to the higher contribution of the structural stiffness to higher frequency flapping modes.
The simplified, diagonal stiffness matrix commonly used, as in Ref. [90], represents a first approximation of the true stiffness properties of such a complicated beam, that can be useful for preliminary performance evaluation, but may cause

Table 13.6: Comparison of in-vacuo rotating frequencies [1/rev]

Mode	AFC blade			reference blade	
	MBDyn	MBDyn[a]	[90]	MBDyn	[90]
1st flap	1.02	1.02	1.02	1.02	1.02
2nd flap	2.59	2.58	2.62	2.61	2.62
3rd flap	4.69	4.55	4.79	4.67	4.79
4th flap	7.31	6.89	7.85	7.20	7.85
1st twist	3.31	3.38	3.38	6.48	6.16
2nd twist	9.65	10.0	9.78	18.4	18.3

[a] Stiffness properties from beam section analysis

Table 13.7: Hover simulations with different stiffness properties

		Ref. [90]	diagonal	coupled
Tip vertical displacement	[ft]	1.1053	1.1057	1.0343
Flap at flap hinge	[deg]	2.275	2.276	2.129
Elastic twist from root to tip	[deg]	-0.006	-0.005	-0.120
Thrust	[lb]	5.119e+03	5.133e+03	4.906e+03

underestimation of cross-coupling effects due for instance to the anisotropy of the materials. The importance of the cross-coupling coefficients, with particular regard to the dynamics of composite rotor blades, has been highlighted in [29]. The stiffness matrix reported in Table 13.3 shows significant couplings; some of them can be accounted for, in a conventional beam analysis, by applying offsets to the shear center or to the normal strain center, namely the couplings between twist and out-of-plane shear, or the couplings between axial force and in-plane bending. Other couplings are strongly related to the anisotropy of the material, namely the coupling between axial and out-of-plane shear forces, and that between axial force and twist. A simple hover simulation, with 4^o of collective pitch, has been performed first with the properties form Ref. [90], then with properties from the proposed analysis, both complete and “diagonalised” by neglecting the coupling terms. A comparison of some significant results is reported in Table 13.7. It clearly shows how the stiffness coupling terms heavily affect the configuration of the system, while by using the diagonal coefficients only, nearly the same behaviour of the reference case is obtained.

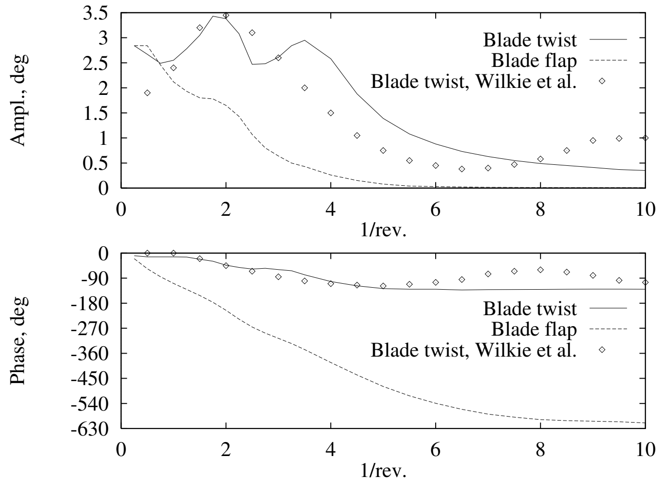

Figure 13.6: Frequency response of root-to-tip twist and root flap at maximum control voltage

13.5 Hover harmonic actuation

The effectiveness of the active twist of the rotor blade has been investigated by performing analyses of the rotor in air with harmonic actuation of the blade. The hover condition is considered first. Root to tip twist, and root flap angles due to harmonic actuation of the active twist blade are reported in Figure 13.6 in the frequency range from 0.25 to 10 Ω. 250 V are applied to the electrodes of the AFC, corresponding to an average electric field of 850 V/mm. The frequency response shows a peak at about 3.5/rev. corresponding to the first twist mode of the blade, that is slightly damped by the aerodynamics. Another peak at about 2/rev. results from the excitation of the first flexible flap mode of the blade, that resonates at a lower frequency due to the high aerodynamic damping of the flap modes. The blade twist from Ref. [90] does show the peak at 2/rev., but the first twist mode is missing, possibly due to the unsteady aerodynamics model used in the mentioned reference, that adds considerable aerodynamic damping to the pitch movement; in the present work, the pitch movement is mainly dampened by structural damping. As expected, the frequency response of the thrust (not shown) shows a peak at zero frequency, due to the steady change in pitch, and the two above mentioned peaks at 2/rev. and 3.5/rev.; it is nearly zero at 1.02/rev., because at the first, rigid flap frequency, all the work made by the aerodynamic forces is spent in rigidly flapping the blades at resonance. A primary goal for the active control of rotorcraft by controlling the pitch of the blades is to obtain an induced twist of the order of 2^o in the range of 0–5 Ω [45, 90]; Fig. 13.6 clearly shows that the goal is achievable.

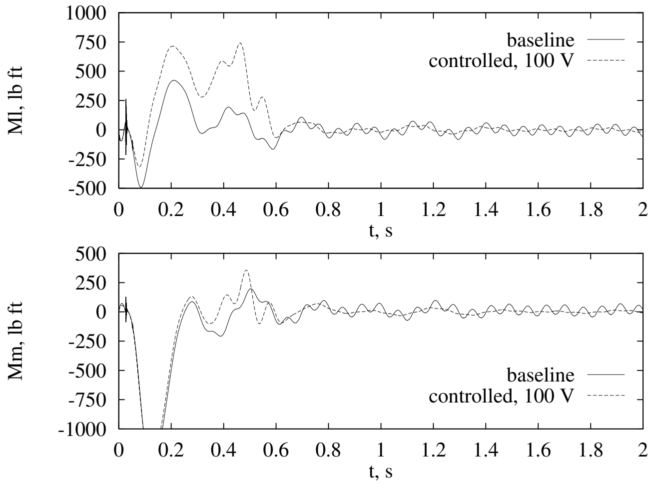

Figure 13.7: Bending moments about x and y axes at the mast; advancing ratio $\mu = 0.20$; actuating tension: 100 V (40% of allowable) at 2/rev.; 131^{o} phase shift

13.6 Forward flight open-loop control

Forward flight conditions at different advancing ratios have been subsequently considered; open-loop 2/rev. actuation has been performed with the objective of reducing the vibrations at the mast induced by the steady forward flight. These vibrations mainly are 4/rev. due to the periodic forces generated by the four blades of the rotor; they can be cancelled by using 2/rev. actuation since 2/rev. pitch change causes 2/rev. flapping of the rotor, which in turn results in Coriolis forces in the plane of the rotor at twice the frequency of the flapping motion. Open loop control results are reported in Figures 13.7, 13.8, 13.9 at different advancing ratios ranging from 0.20 to 0.30; convergence at higher advancing ratios is difficult.

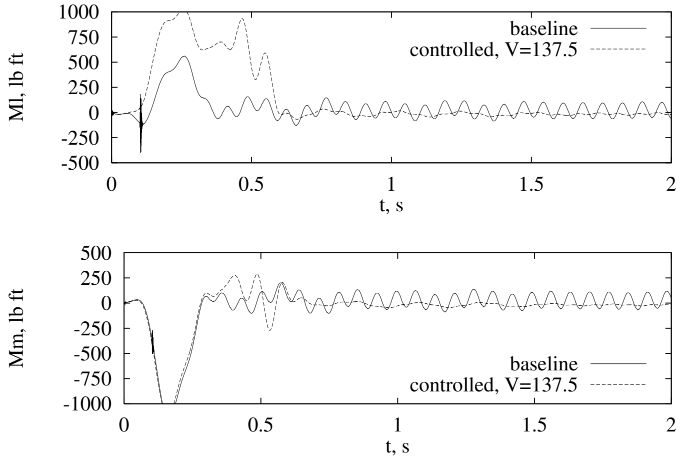

Figure 13.8: Bending moments about x and y axes at the mast; advancing ratio $\mu = 0.25$; actuating tension: 137.5 V (55% of allowable) at 2/rev.; 128^o phase shift

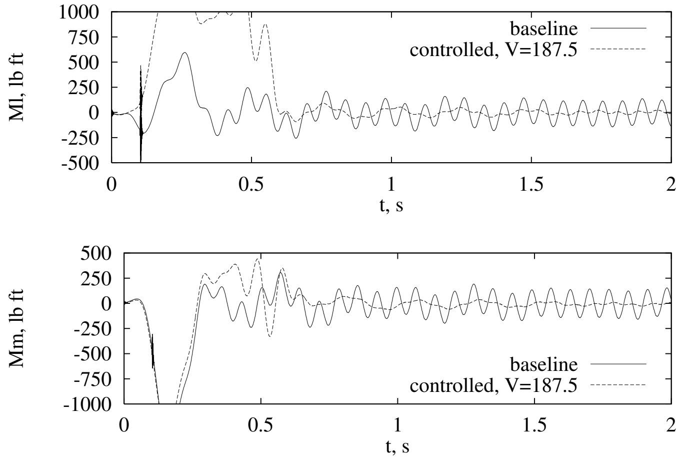

Figure 13.9: Bending moments about x and y axes at the mast; advancing ratio $\mu = 0.30$; actuating tension: 187.5 V (75% of allowable) at 2/rev.; 127^o phase shift

Chapter 14

Conclusions and future research

The analysis and the design of active controls for rotorcraft applications represent very complex and difficult tasks, involving many analytical and experimental aspects. In this work a multibody analytical framework for the dynamic analysis of rotorcraft (Chapters 1–4), including a self-contained formulation for the analysis and design of rotor blades (Chapter 5), and the implementation of a general, discrete, predictive control (Chapter 7), has been presented. The formulation is based on the direct writing of the equilibrium equations of discrete bodies, connected by holonomic constraints described by means of algebraic constraint equations and by flexible elements, mainly modelled as beams. The state-of-the-art for rotorcraft actuation means is discussed (Chapter 6), and the related extension of the formulation, including a detailed, comprehensive piezoelectric beam analysis scheme, is presented (Chapters 8–9). The foundations of the proposed approach have been validated (Chapter 10); its application to rotorcraft analysis has been validated by analysing the wind-tunnel model of the V–22 tiltrotor aircraft (Chapter 11). The Generalised Predictive Control has been considered to evaluate the feasibility of vibration reduction of the V–22 model (Chapter 12). An advanced actuation scheme, based on the concept of induced blade twist by means of piezoelectric embedded devices has been investigated, by comparing the results of open-loop control analyses to the state-of-the-art in such research field (Chapter 13). Although direct comparison of results is often difficult or even impossible because of restrictions on the availability of dependable and comprehensive data, the work shows the feasibility of the proposed approach for the analysis and the design of rotorcraft as well as the feasibility of the proposed control schemes, and clearly outlines the opportunity of prosecuting the research in this direction.

Very different interesting fields still have to be explored. Different actuation schemes and control strategies must be implemented to allow an extensive evaluation of the feasibility and of the efficiency of controlling a rotorcraft in a wide spectrum of operational conditions. One of the conditions we expect to investigate is the dynamics of the free helicopter, with an adaptive controller working as an autopilot that flies the rotorcraft following some desired path. A completely different, but really interesting field is that of the simulation of ground and air resonance phenomena related to the tiltrotor, that may occur when a soft-in-plane hub is mounted. Plans in this direction have been made at NASA Langley, funded by Bell Helicopter, in order to obtain useful information on a possible soft-in-plane rotor design for the civil tiltrotor Bell-Agusta 609. From a formulation standpoint, near future plans involve the integration into the multibody code of modal flexibility to allow the modelling of the flexibility of the body of the rotorcraft, hydraulic and electrohydraulic circuitry for aeroservoelasticity analysis, modelling of landing related devices for helicopter landing and taxiing analyses and for a better modelling of the contact with the ground for ground resonance analyses. The coupling with an uncompressible, unsteady wake analysis code is being implemented. From a computational standpoint, a simple but effective parallelisation scheme based on distributed computing and message passing, with local matrix-free solution of subsystems, is being investigated. A significant reduction in time for typical runs is expected. Some of the mentioned improvements have already been separately implemented; their integration in one analysis tool will allow to meet the fundamental goal that inspired the research project this work contributed to: the integrated analysis of the entire rotorcraft in free flight.

Appendix A

Rigid body momenta

The rigid body momenta result from the integration of the momentum of a continuous body whose motion can be described by means of a rigid rototranslation. The position of an arbitrary point p in the global frame, is made of a reference position x and a relative position f that can be expressed as a local vector $\tilde{f}$ rotated in the global frame by an orthonormal rotation matrix R, defined in Chapter 3, resulting in $p = x + f$. The momentum and momentum moment densities of a material point, referred to the reference pole of the global frame, O, are

$$\left\{ \begin{array}{lcl} \beta^* & = & \rho \dot{p}, \\ \gamma_O^* & = & \rho p \times \dot{p}, \end{array} \right.$$

where ρ represents the density at point p. The linear and angular momenta of the rigid body result from the integration of the momentum densities over the volume of the body, as follows:

$$\left\{ \begin{array}{lcl} \beta & = & \int_V \rho \dot{p} \,\mathrm{d}V, \\ \gamma_O & = & \int_V \rho p \times \dot{p} \,\mathrm{d}V. \end{array} \right.$$

By noting that $\dot{p} = \dot{x} + \omega \times f$, and considering that the reference point position and velocity can be carried out of the integral, the momenta become

$$\left\{ \begin{array}{lcl} \beta & = & \left(\int_V \rho \,\mathrm{d}V\right) \dot{x} + \omega \times \left(\int_V \rho f \,\mathrm{d}V\right), \\ \gamma_O & = & x \times \beta + \left(\int_V \rho f \,\mathrm{d}V\right) \times \dot{x} - \left(\int_V \rho f \times f \times \mathrm{d}V\right) \omega, \end{array} \right.$$

and the integrals involve only the density of the body and the relative position vector f; notice that the angular momentum is made of a contribution related to the velocity and the angular velocity of the reference point, plus a contribution due to the transport of the momentum β; the momentum moment referred to point x is simply $\gamma = \gamma_O - x \times \beta$, as directly determined in the second of Eqs. 1.1. When expressed in the local frame, the inertial invariants result in

$$
\begin{aligned}
m &= \int_V \rho \,\mathrm{d}V, \\
S &= \int_V \rho f \,\mathrm{d}V \\
&= R \int_V \rho \tilde{f} \,\mathrm{d}V \\
&= R\tilde{S}, \\
J &= -\int_V \rho f \times f \times \,\mathrm{d}V \\
&= -R \int_V \rho \tilde{f} \times \tilde{f} \times \,\mathrm{d}V R^T \\
&= R\tilde{J}R^T,
\end{aligned}
$$

where the tilde $\tilde{(\cdot)}$ refers to the local frame of the body.

Appendix B

Integration formulas

The proposed integration scheme is described in detail, by formulating some interesting higher-order formulas.

B.1 Definitions

Consider an Ordinary Differential Equation (ODE) in explicit form, and an Initial Value (IV) problem:

$$\dot{y} = f(y,t), \qquad y(t_0) = y_0 \tag{B.1}$$

The unknown y is approximated by a polynomial interpolation ranging from time step $k-r$ to the current one k, being r the number of steps of the formula and y_k the unknown solution:

$$y = \sum_{i=0}^{r} \left(m_i(\xi)\, y_{k-i} + h n_i(\xi)\, \dot{y}_{k-i} \right), \tag{B.2}$$

where h is the time step, ξ is the non-dimensional time; the origin for the ξ is at the current time step, i.e. $\xi = (t - t_k)/h$; m_i, n_i are the polynomial shape functions related to y_i, $\dot{y}_i$.

B.2 Numerical integration

The integration is carried on by weighting the value of the derivative at appropriate points:

$$y_k = y_{k-r} + \int_{t_{k-r}}^{t_k} f(y,t)\, dt \tag{B.3}$$

$$\cong y_{k-r} + h \sum_i w_i f(y(t_i), t_i), \tag{B.4}$$

where the problem $f(y,t)$, Eq. B.1, has been used *in lieu* of $\dot{y}$. In the following, a one-step formula is considered without any loss in generality.

B.3 Solution

The perturbation of the numerical solution, Eq. B.4,

$$y_k + \Delta y_k = y_{k-1} + h \sum_i w_i \left(f(y(t_i), t_i) + \frac{\partial f(y(t_i), t_i)}{\partial y} \frac{\partial y(t_i)}{\partial y_k} \Delta y_k \right),$$

where

$$\frac{\partial y(t_i)}{\partial y_k} = m_0(\xi_i) + h n_0(\xi_i) \frac{\partial f(y_k, t_k)}{\partial y}$$

descends from the interpolation formula of Eq. B.2, after substitution becomes:

$$\left(I - h \sum_i w_i \frac{\partial f(y(t_i), t_i)}{\partial y} \left(m_0(\xi_i) I + h n_0(\xi_i) \frac{\partial f(y_k, t_k)}{\partial y} \right) \right) \Delta y_k$$

$$= -(y_k - y_{k-1}) + h \sum_i w_i f(y(t_i), t_i).$$

The key idea is that given the order of the interpolation for the y, the $\dot{y}$ is one order less, thus determining the minimum required order for the numerical integration. However, the higher the order of the numerical integration, the higher the order of accuracy, as will be shown in the following section. This interpretation is only euristic; one should be aware of the fact that the goal is not to achieve the exact integration of the approximated form of the solution, but rather to determine the coefficients that make the numerical method stable as well as accurate.

B.3.1 Cubic interpolation

Shape functions:

$$\begin{aligned} m_0 &= 1 - \xi^2(3 + 2\xi), & m_1 &= \xi^2(3 + 2\xi), \\ n_0 &= \xi(1+\xi)^2, & n_1 &= \xi^2(1+\xi). \end{aligned}$$

Gauss Quadrature

Two points are required, but three Jacobians must be computed, respectively at the two integration points and at the end of the step. Two Jacobian multiplications must be performed, making this choice inefficient with respect to the following one. Points and weights are:

point, ξ_i	weight, w_i
$\left(-1-1/\sqrt{3}\right)/2$	1/2
$\left(-1+1/\sqrt{3}\right)/2$	1/2

Trapezoid rule

Three points are used, but only two Jacobians must be computed, at mid- and end-point; only one Jacobian multiplication is required. Points and weights are:

point, ξ_i	weight, w_i
-1	1/6
-1/2	2/3
0	1/6

The integration becomes:

$$y_k = y_{k-1} + h\left(\frac{1}{6}\,f|_{\xi=-1} + \frac{2}{3}\,f|_{\xi=-1/2} + \frac{1}{6}\,f|_{\xi=0}\right),$$

and the solution is:

$$\begin{aligned}
&\left(I - h\left(\frac{2}{3}\left.\frac{\partial f}{\partial y}\right|_{\xi=-1/2}\left(\frac{1}{2}I - \frac{h}{8}\left.\frac{\partial f}{\partial y}\right|_{\xi=0}\right) + \frac{1}{6}\left.\frac{\partial f}{\partial y}\right|_{\xi=0}\right)\right)\Delta y_k \\
&= -\left(y_k - y_{k-1}\right) + h\left(\frac{1}{6}\,f|_{\xi=-1} + \frac{2}{3}\,f|_{\xi=-1/2} + \frac{1}{6}\,f|_{\xi=0}\right).
\end{aligned}$$

B.3.2 Parabolic interpolation

Shape functions:

$$\begin{aligned}
m_0 &= 1-\xi^2 & m_1 &= \xi^2 \\
n_0 &= \xi(1+\xi) & n_1 &= 0
\end{aligned}$$

Gauss Quadrature

One point is required, at $\xi = -1/2$, with unit weight, but two Jacobians ought to be computed, and one Jacobian multiplication is required.

Points and weights are:

point, ξ_i	weight, w_i
-1/2	1

The integration becomes:

$$y_k = y_{k-1} + h\, f|_{\xi=-1/2}$$

and the solution is:

$$\begin{aligned}
&\left(I - h \left.\frac{\partial f}{\partial y}\right|_{\xi=-1/2} \left(\frac{3}{4} I - \frac{h}{4} \left.\frac{\partial f}{\partial y}\right|_{\xi=0} \right) \right) \Delta y_k \\
&\quad = -(y_k - y_{k-1}) + h\, f|_{\xi=-1/2}
\end{aligned}$$

Trapezoid rule

Two points are required, the start- and the end-point. One Jacobian must be computed and no Jacobian multiplication is required. This integration is degenerate, and a higher-order numerical integration scheme is required to achieve higher accuracy. Points and weights are:

point, ξ_i	weight, w_i
-1	1/2
0	1/2

The integration becomes:

$$y_k = y_{k-1} + h \left(f|_{\xi=-1} + f|_{\xi=0} \right)$$

and the solution is:

$$\begin{aligned}
&\left(I - h \left.\frac{\partial f}{\partial y}\right|_{\xi=0} \right) \Delta y_k \\
&\quad = -(y_k - y_{k-1}) + h \left(f|_{\xi=-1} + f|_{\xi=0} \right)
\end{aligned}$$

Ad hoc integration

Two points are used, one inside the time step, the other at the end; two Jacobians and only one Jacobian multiplication are required. Points and weights are:

point, ξ_i	weight, w_i
ζ	$-1/(2\zeta)$
0	$(2\zeta+1)/(2\zeta)$

They allow to exactly integrate a linear function, regardless of the value of ζ; however, notice that for $\zeta = -2/3$ the exact integration of a second-order polynomial is achieved. The integration becomes:

$$y_k \;=\; y_{k-1} + h\left(-\frac{1}{2\zeta}\,f|_{\xi=\zeta} + \frac{2\zeta+1}{2\zeta}\,f|_{\xi=0}\right)$$

and the solution is:

$$\begin{aligned}
&\left(I - h\left(-\frac{1}{2\zeta}\left.\frac{\partial f}{\partial y}\right|_{\xi=\zeta}\left(\left(1-\zeta^2\right)I + \zeta\left(1+\zeta\right)h\left.\frac{\partial f}{\partial y}\right|_{\xi=0}\right)\right.\right.\\
&\left.\left.+\frac{2\zeta+1}{2\zeta}\left.\frac{\partial f}{\partial y}\right|_{\xi=0}\right)\right)\Delta y_k \;=\; -\left(y_k - y_{k-1}\right)\\
&+h\left(-\frac{1}{2\zeta}\,f|_{\xi=\zeta} + \frac{2\zeta+1}{2\zeta}\,f|_{\xi=0}\right)
\end{aligned}$$

B.3.3 Linear interpolation

Shape functions:

$$\begin{aligned}
m_0 &= 1+\xi & \qquad m_1 &= -\xi\\
n_0 &= 0 & \qquad n_1 &= 0
\end{aligned}$$

Gauss Quadrature

One point is required, $\xi = -1/2$, with unit weight, along with one Jacobian evaluation at midpoint. No Jacobian multiplication is needed since n_0, the shape function of $\dot{y}_k$, is identically zero. The integration becomes:

$$y_k \;=\; y_{k-1} + h\,f|_{\xi=-1/2}$$

and the solution is:

$$\left(I - h\frac{1}{2}\left.\frac{\partial f}{\partial y}\right|_{\xi=-1/2}\right)\Delta y_k \;=\; -\left(y_k - y_{k-1}\right) + h\,f|_{\xi=-1/2}$$

Trapezoid rule

Two points are used, at the beginning and at the end of the time step, weighted by $1/2$. Only one Jacobian is required, at the end of the time step. Points and weights are:

point, ξ_i	weight, w_i
-1	1/2
0	1/2

The integration becomes:

$$y_k = y_{k-1} + h\left(\frac{1}{2}\,f|_{\xi=-1} + \frac{1}{2}\,f|_{\xi=0}\right)$$

and the solution is:

$$\left(I - h\frac{1}{2}\left.\frac{\partial f}{\partial y}\right|_{\xi=0}\right)\Delta y_k = -\left(y_k - y_{k-1}\right) + h\left(\frac{1}{2}\,f|_{\xi=-1} + \frac{1}{2}\,f|_{\xi=0}\right)$$

Backward Differences

The function is evaluated only at the end of the time step, with unit weight. The integration becomes:

$$y_k = y_{k-1} + h\,f|_{\xi=0}$$

and the solution is:

$$\left(I - h\left.\frac{\partial f}{\partial y}\right|_{\xi=0}\right)\Delta y_k = -\left(y_k - y_{k-1}\right) + h\,f|_{\xi=0}$$

B.4 Stability

Consider a linear differential equation $\dot{y} = \lambda y$, with λ complex.

B.4.1 Cubic interpolation

Trapezoid rule

With the three-point trapezoid rule the integral is:

$$y_k = y_{k-1} + \frac{1}{2}\lambda h y_k + \frac{1}{2}\lambda h y_{k-1} - \frac{1}{12}(\lambda h)^2 y_k + \frac{1}{12}(\lambda h)^2 y_{k-1}$$

$$y_k = \frac{\left(1+\frac{1}{2}\lambda h+\frac{1}{12}(\lambda h)^2\right)}{\left(1-\frac{1}{2}\lambda h+\frac{1}{12}(\lambda h)^2\right)} y_{k-1}$$

The integrator is A-stable; it has unit spectral radius norm regardless of the time step ratio h/T. Figure B.1 shows the error in phase for undamped systems (λ imaginary). The solution is exact (fourth-order) in the damping, since no numerical damping is added. Accuracy is fourth-order for the phase error regardless of the physical damping of the problem (real part of λ), see Figures B.1, 4.3. It decreases as the time step increases.

Gauss integration

The same expression for the asymptotic radius is found with the previously mentioned two-point Gauss quadrature.

B.4.2 Parabolic interpolation

Gauss integration

In case of single-point Gauss integration, the integral is:

$$y_k = y_{k-1}+\frac{3}{4}\lambda h y_k+\frac{1}{4}\lambda h y_{k-1}-\frac{1}{4}(\lambda h)^2 y_k$$

$$y_k = \frac{\left(1+\frac{1}{4}\lambda h\right)}{\left(1-\frac{3}{4}\lambda h+\frac{1}{4}(\lambda h)^2\right)} y_{k-1}$$

This integrator is L-stable.

Trapezoid rule

In case of end-points trapezoid rule integration, the integral is:

$$y_k = y_{k-1}+\frac{1}{2}\lambda h y_k+\frac{1}{2}\lambda h y_{k-1}$$

$$y_k = \frac{\left(1+\frac{1}{2}\lambda h\right)}{\left(1-\frac{1}{2}\lambda h\right)} y_{k-1}$$

This integrator is A-stable and loses higher-order accuracy, resulting in the Crank-Nicholson rule.

Ad hoc integration

In case of the *ad hoc* integration formula, with moving mid-point, the integral is:

$$y_k = y_{k-1} + \frac{\zeta+2}{2}\lambda h y_k - \frac{\zeta}{2}\lambda h y_{k-1} - \frac{\zeta+1}{2}(\lambda h)^2 y_k$$

$$y_k = \frac{\left(1 - \frac{\zeta}{2}\lambda h\right)}{\left(1 - \frac{\zeta+2}{2}\lambda h + \frac{\zeta+1}{2}(\lambda h)^2\right)} y_{k-1}$$

The integrator is L-stable (Figure 4.1), except for $\zeta = -1$, where it yields once more the Crank-Nickolson rule. Figure 4.2 shows the error in damping for undamped systems (λ imaginary). The accuracy is cubic for the numerical damping, (Figure B.7), and quartic for the phase error (Figure B.1) when the system is undamped, otherwise it is cubic for both errors (Figure 4.3). It decreases as the time step increases, (Figure B.8), and with the value of the real part of λ. This is true when the "optimal" point $\zeta = -2/3$, which allows the exact integration of a second-order polynomial, is used. The same spectral radius can be obtained by using the symmetric combination of collocation points, namely the starting point of the time step, $\xi = -1$, and the point at $\xi = -1-\zeta$; the latter form is not as much appealing as the former one because in this case the conditions for *stiffly accurate* integration are violated. When a value of ζ other than $-2/3$ is used. the accuracy is quadratic, and the formula loses its appealing higher-order properties.

B.4.3 Linear interpolation

Trapezoid and Gauss integration

In case of both Gauss and trapezoid rule integration, the integral is:

$$y_k = y_{k-1} + \frac{1}{2}\lambda h y_k + \frac{1}{2}\lambda h y_{k-1}$$

$$y_k = \frac{\left(1 + \frac{1}{2}\lambda h\right)}{\left(1 - \frac{1}{2}\lambda h\right)} y_{k-1}$$

The two integration techniques are equivalent from the linear stability standpoint. The integrator is A-stable, with unit spectral radius. Indeed, it represents the well-known Crank-Nicholson second-order integration technique.

Backward differences

In case of Backward Differences the integral is:

$$y_k = y_{k-1} + \lambda h y_k$$

$$y_k = \frac{1}{(1-\lambda h)} y_{k-1}$$

which represents the well-known Implicit Euler formula, the single-step case of the Backward Differentiation Formulas [17]:

$$\sum_{i=1}^{n} \frac{1}{i} \nabla^i y_k = f(y_k)$$

B.5 Tunable Algorithmic Damping

Consider a cubic interpolation, and an integration by means of the three points trapezoid rule that is required to exactly integrate the second-order polynomial only. Points and weights are:

point, ξ_i	weight, w_i
-1	$\frac{(2+3\zeta)}{6(1+\zeta)}$
ζ	$\frac{-1}{6\zeta(1+\zeta)}$
0	$\frac{(1+3\zeta)}{6\zeta}$

where ζ is the position of the mid-point, which becomes a parameter. The integration becomes:

$$y_k = y_{k-1} + h\left(\frac{(2+3\zeta)}{6(1+\zeta)} f|_{\xi=-1} + \frac{-1}{6\zeta(1+\zeta)} f|_{\xi=\zeta} + \frac{(1+3\zeta)}{6\zeta} f|_{\xi=0}\right)$$

and the solution is:

$$\begin{aligned}
&\left(I - h\left(\frac{-1}{6\zeta(1+\zeta)} \left.\frac{\partial f}{\partial y}\right|_{\xi=\zeta} \left(\left(1-\zeta^2(3+2\zeta)\right) I + h\left(\zeta(1+\zeta)^2\right) \left.\frac{\partial f}{\partial y}\right|_{\xi=0}\right)\right.\right. \\
&\left.\left. + \frac{(1+3\zeta)}{6\zeta} \left.\frac{\partial f}{\partial y}\right|_{\xi=0}\right)\right) \Delta y_k = -(y_k - y_{k-1}) \\
&+ h\left(\frac{(2+3\zeta)}{6(1+\zeta)} f|_{\xi=-1} + \frac{-1}{6\zeta(1+\zeta)} f|_{\xi=\zeta} + \frac{(1+3\zeta)}{6\zeta} f|_{\xi=0}\right)
\end{aligned}$$

When applied to the linear differential problem $\dot{y} = \lambda y$, this formula gives:

$$\begin{aligned} y_k &= y_{k-1} + \frac{(2+\zeta)}{3}\lambda h y_k + \frac{(1-\zeta)}{3}\lambda h y_{k-1} \\ &\quad - \frac{(1+\zeta)}{6}(\lambda h)^2 y_k - \frac{\zeta}{6}(\lambda h)^2 y_{k-1}, \end{aligned}$$

which, by collecting y_k and y_{k-1}, yields

$$y_k = \frac{\left(1 + \frac{(1-\zeta)}{3}\lambda h - \frac{\zeta}{6}(\lambda h)^2\right)}{\left(1 - \frac{(2+\zeta)}{3}\lambda h + \frac{(1+\zeta)}{6}(\lambda h)^2\right)} y_{k-1}.$$

The asymptotic radius is $\rho_\infty = -\zeta/(1+\zeta)$, where ρ_∞ is the absolute value of the asymptotic radius. It vanishes for $\zeta = 0$, which means that the mid-point moved to the end of the time step. Notice that for $\zeta < -1/2$ the formula is no longer unconditionally stable. It should be noted that the last two weights become singular, but since they weigh the function $f(y,t)$ evaluated at the same point, their sum must be considered, whose limit is $2/3$; the Jacobian product does not vanish, reducing to the square of the Jacobian evaluated at the end of the time step. The asymptotic radius at $\zeta = 0$ is exactly the same that is obtained with the parabolic interpolation. For $\zeta = -1/2$ the previously described fourth-order *A*-stable integrator is obtained. So as the mid-point moves towards the end point, the asymptotic radius of the method goes from 1 to 0, thus allowing the tuning of the algorithmic dissipation. The position of the mid point can be written as function of the desired radius:

$$\zeta = -\rho_\infty/(1+\rho_\infty)$$

Figures B.1 and 4.3 show the comparison of the phase error for an undamped and a damped system when the midpoint is moved from $\xi = -1/2$, corresponding to unit asymptotic radius, to $\xi = -3/8$, corresponding to an asymptotic radius $\rho_\infty = 0.6$. In case of $\zeta = 0$ the integrator becomes *L*-stable, requiring the evaluation of only one Jacobian, and of its square. The integration in this case is:

$$y_k = y_{k-1} + h\left(\frac{1}{3} f|_{\xi=-1} + \frac{2}{3} f|_{\xi=0}\right)$$

and the solution is:

$$\begin{aligned} &\left(I - h \left.\frac{\partial f}{\partial y}\right|_{\xi=0}\left(\frac{2}{3}I + h\frac{1}{6}\left.\frac{\partial f}{\partial y}\right|_{\xi=0}\right)\right)\Delta y_k \\ &= -(y_k - y_{k-1}) + h\left(\frac{1}{3} f|_{\xi=-1} + \frac{2}{3} f|_{\xi=0}\right) \end{aligned}$$

which is obtained as the limit for $\zeta \to 0$ of the general expression. It is worth recalling that the three points integration rule used herein allows one to exactly integrate polynomials up to the third degree when the mid-point is in the middle of the step, otherwise only second-degree polynomials are exactly integrated. This explains the change in order of accuracy when the mid-point is moved.

B.6 Concluding remarks

Accuracy and stability results are summarised in Table B.1. The higher-order formulas are illustrated first, followed by second- and first-order formulas that result from the degeneration of the general scheme. At the bottom of the table, the two degenerate methods that are second-order but require the overhead of a mid-step Jacobian computation are illustrated for completeness. Figures 4.1–4.3 and B.1–B.9 show some of the properties of the proposed formulas. Figure 4.1 shows the spectral radii of the formulas. Notice the very steep descent of the higher order formulas, with a large initial plateau at $|\rho| \cong 1$; as a comparison, the BDF algorithm descends very smoothly, while the Implicit Euler does not really show any plateau, thus explaining the first order accuracy. The proposed two-step algorithm descends smoothly, but it shows an appreciably wide plateau. Figure B.9 shows the complex plane plot of the spectral radii; notice that the asymptotic phase angle of the formulas is almost always proportional to the accuracy, e.g. the Implicit Euler has a -90 deg. phase, while the Crank-Nicholson rule, the BDF and the proposed two-step formula all have a -180 deg. asymptotic phase; the higher order algorithms with no dissipation or with tunable dissipation have a phase angle of -360 deg. and the fully dissipative one shows an angle of -270 deg. Figure B.8 shows some irregular behaviour of the accuracy order for the damping of the two-step formulas, but the limit value for $h/T \to 0$ is clearly 2. The errors in damping (Figures 4.2 and B.5) and phase (Figures B.2 and B.3) offer a very good insight into the properties of the different algorithms. While the Crank-Nicholson and the fourth-order formulas do not introduce any error in damping, the proposed two-step formula is comparable to the third-order one with the same asymptotic radius in terms of damping error, and both are far better than the respective *L*-stable counterparts, the BDF and the third-order *Radau IIA* schemes. This is no longer true for higher algorithmic dissipation levels, where the higher-order formula shows a remarkably smaller error, thus confirming the optimality of $\rho_\infty = 0.6$ for the two-step formula. Where the higher-order formulas really show their advantage is in the phase error: while the Implicit Euler and the BDF have comparable, very poor accuracy (remember that the Implicit Euler is nothing but a BDF of order 1), the proposed two-step formula does not perform too bad when compared to the Crank-Nicholson rule, but their error is at least one order of magnitude higher

Table B.1: Summary of properties of some integration formulas

Integrator	Stability	Phase	Damp.	IRK
Cubic	A-stable	4	4	Lobatto IIIA
Cubic *ad hoc* ($-1/2 \leq \zeta \leq 0$)	A/L-stable	3	3	
Parabolic *ad hoc* ($\zeta = -2/3$)	L-stable	3	3	Radau IIA
Crank-Nicholson	A-stable	2	2	Lobatto IIIA
Implicit Euler	L-stable	1	1	
Multistep ($\rho_\infty \leq 1$)	A/L-stable	2	2	
Two-Step BDF	L-stable	2	2	
Parabolic (Gauss)	L-stable	2	2	
Parabolic *ad hoc* ($\zeta \neq -2/3$)	L-stable	2	2	

than that of the third- and fourth-order schemes. Figures B.6, B.4 show the effect of the asymptotic spectral radius on the damping and phase errors for the proposed two-step formula and for the third-order formula at $h/T = 0.01$. Figure B.6 clearly shows that for the damping, the two-step formula introduces an error that is about quadratic with the algorithmic dissipation, while the third-order one is about linear; the two lines cross for $\rho_\infty \cong 0.6$, yielding for higher dissipations a dramatically more accurate behaviour of the third-order formula. Figure B.4, on the contrary, clearly shows that the phase error of the higher-order formula is orders of magnitude smaller than that of the second-order one, regardless of the value of the asymptotic radius.

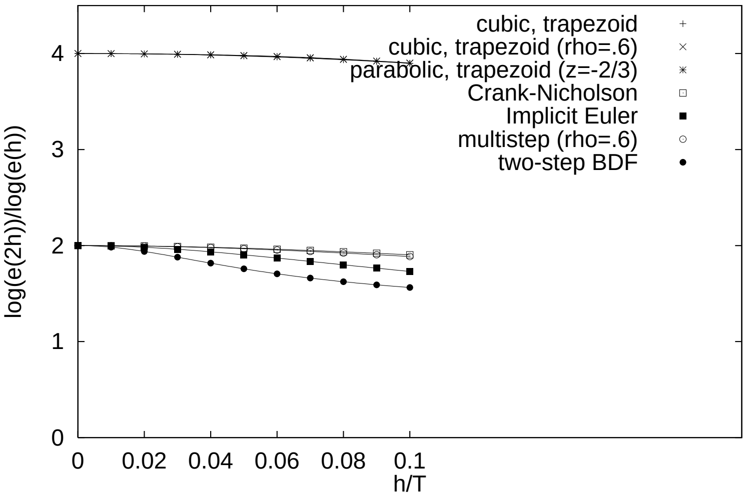

Figure B.1: Phase error order, $\log_2\left(\varepsilon_\varphi(2h)/\varepsilon_\varphi(h)\right)$ (undamped system)

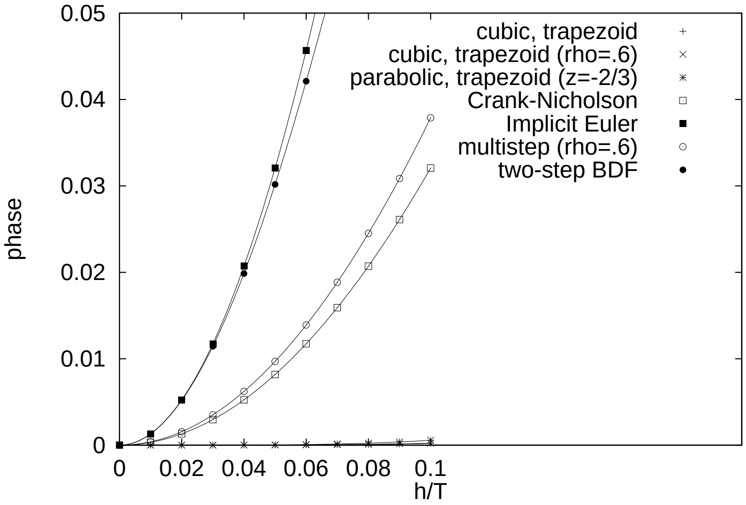

Figure B.2: Phase error, ε_φ (undamped system)

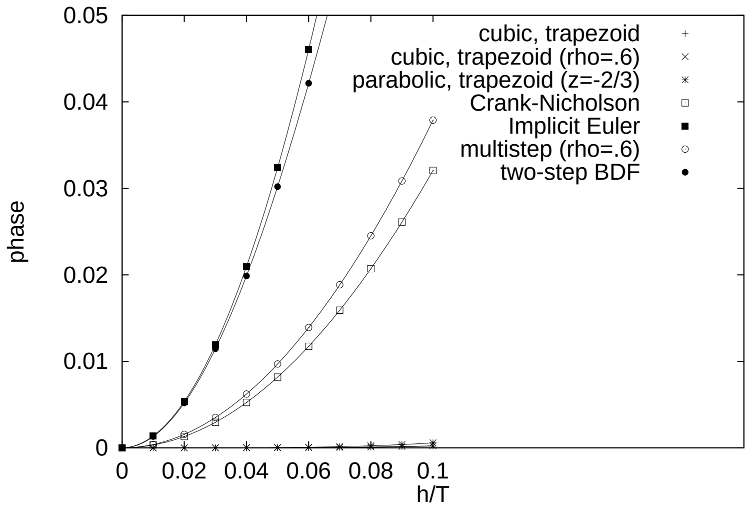

Figure B.3: Phase error, ε_φ (slightly damped system)

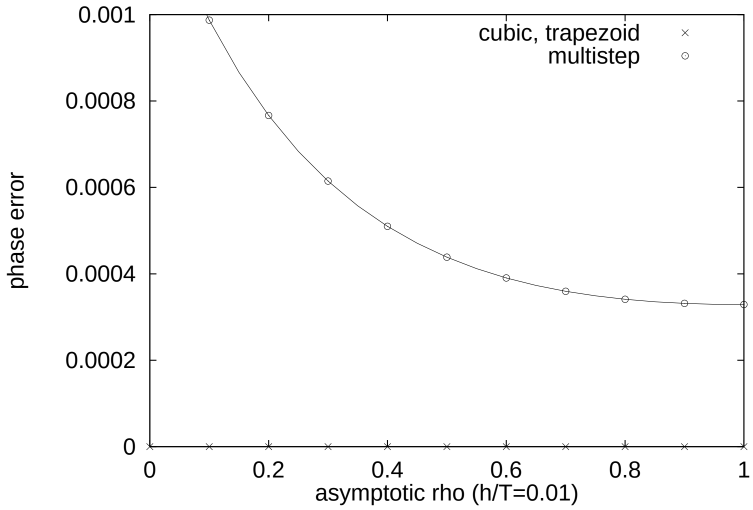

Figure B.4: Phase error, ε_φ, at $h/T = 0.01$ (undamped system)

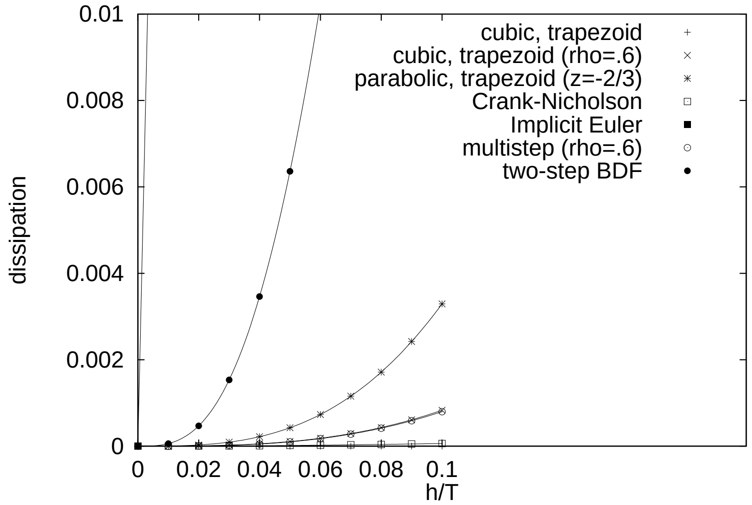

Figure B.5: Damping error, ε_ξ (damped system)

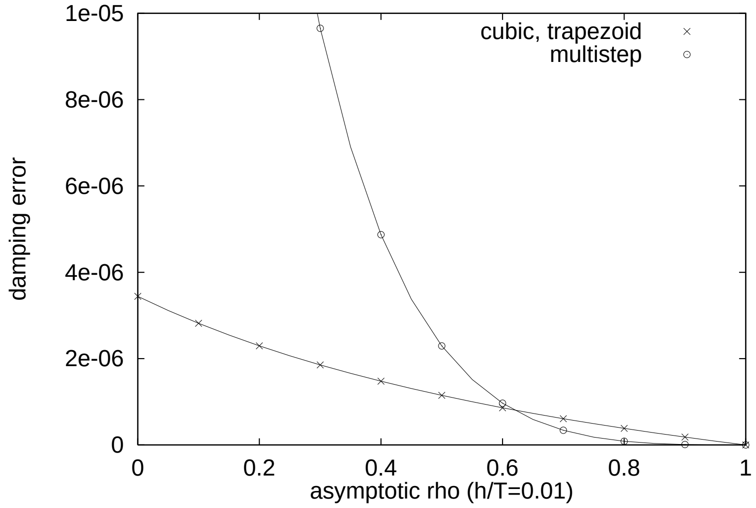

Figure B.6: Damping error, ε_ξ, at $h/T = 0.01$ (undamped system)

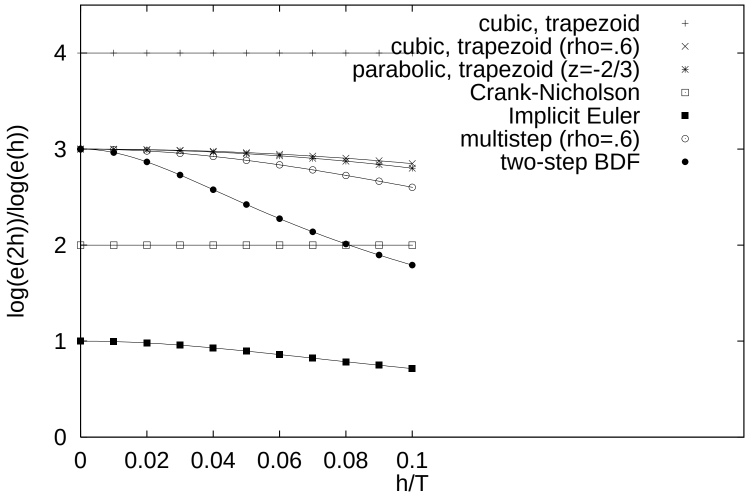

Figure B.7: Damping error order, $\log_2\left(\varepsilon_\xi(2h)/\varepsilon_\xi(h)\right)$ (undamped system)

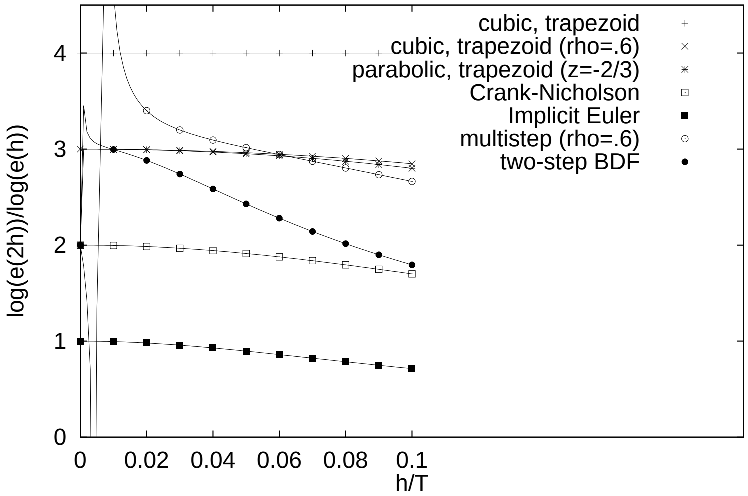

Figure B.8: Damping error order, $\log_2\left(\varepsilon_\xi(2h)/\varepsilon_\xi(h)\right)$ (damped system)

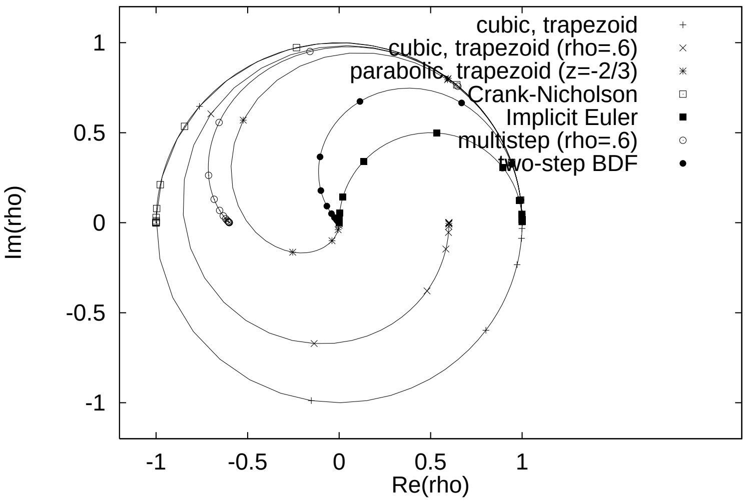

Figure B.9: Spectral radii, ρ, polar plot (undamped system)

Appendix C

Self-starting algorithm: convergence

The convergence of the *Backwards Differentiation Formulas* (BDF) and analogous integration algorithms applied to Differential-Algebraic problems is key to the *implementability* of a numerical solution. A *numerically consistent* to order $k+1$ set of starting values, introduced in [17], p. 56, is needed, where k is the number of steps of the method. It is defined as a set of values at steps $j = 0, \ldots, k-1$, whose differential unknowns must be known to $O\left(h^{k+1}\right)$, ans must solve the algebraic equations to $O\left(h^{k+2}\right)$. The basic concept is that when the solution starts with an error, there is a *boundary layer* between the exact and the numerical solution, in which the errors propagate. According to [17], theorem 3.2.3, p. 57, the algebraic equations need be solved to $O\left(h^4\right)$ regardless of $k = 1, 2$ to obtain a solution that converges with k-th order accuracy after $k+1$ steps. So the first, self-starting *Crank-Nicholson* step is used to provide a numerical solution that forms a numerically consistent set of starting points for the following *stiffly stable* integration. The *Crank-Nicholson* step ensures the differential unknowns are $k+1$ accurate for $k = 2$, but the accuracy on the satisfaction of the algebraic constrains can be achieved only by a *Newton-Raphson* correction. Consider the simple constrained dynamics problem

$$\begin{aligned} \dot{y} - v &= 0, \\ \dot{v} + \lambda &= 0, \\ y &= \cos(t), \end{aligned}$$

which is completely determined by the algebraic equation $y = \cos(t)$, and suppose to solve it as a DAE. A set of starting values that are *numerically consistent* to order 3 requires the knowledge of the values at time $t = 0$, supposedly given, and at time $t = h$. The latter can be determined by a *Crank-Nicholson* step followed by a *Newton-Raphson* correction, which allows to solve the algebraic equation to the required level of accuracy, while the differential unknowns are assumed to satisfy the required accuracy criteria because the *Crank-Nicholson* formula is second-order accurate. The solution propagation is

$$
\begin{aligned}
\Delta y &= \cos(t) - P(y) \\
\Delta \dot{y} &= \Delta y / c \\
\Delta v &= \Delta \dot{y} + P(\dot{y}) - P(v) \\
\Delta \dot{v} &= \Delta v / c \\
\Delta \lambda &= -\Delta \dot{v} - P(\dot{v}) - P(\lambda) \\
\Delta I(\lambda) &= c \Delta \lambda
\end{aligned}
$$

where the prediction operator $P(\cdot)$ has been used; $I(\lambda)$ is the integral of the reaction λ, while $c = h/2$ is the coefficient of the *Crank-Nicholson* formula. The solution is obtained by adding the perturbations to the predicted values. The second-order BDF is applied to the previously defined *numerically consistent* starting values for 3 steps, to reach a solution that converges with second-order accuracy to the exact solution. Notice that the correction with the BDF requires $c = 2h/3$. The results, for exact initial conditions, are reported in Table C.1 on the left. The initial conditions are $y(0) = 1$, $\dot{v}(0) = -1$, $\lambda(0) = 1$, all the other unknowns being zero. The differential unknowns are always second-order accurate, while the reactions are first-order accurate. Consider now the modified starting values that result from violating the second derivative of the constraints, namely $\dot{v}(0) = \lambda(0) = 0$. The results, reported in Table C.1 on the right, differ from those on the left only for the first step, after which the solution exactly matches the previous one. In this case, during the first step the error in the reaction unknown is $O\left(h^0\right)$.

Table C.1: Crank-Nicholson/Backward Difference solution of constrained problem.

Initial conditions satisfying the second derivative of the constraint

step	time	y	v	λ
0	0	1	0	1
1	h	$\cos(h)$	$2/h\,(\cos(h)-1)$	$-4/h^2\,(\cos(h)-1)-1$
2	$2h$	$\cos(2h)$	$1/(2h)\,(3\cos(2h)-4\cos(h)+1)$	$-1/(2h)^2\,(9\cos(2h)-28\cos(h)+19)$
3	$3h$	$\cos(3h)$	$1/(2h)\,(3\cos(3h)-4\cos(2h)+\cos(h))$	$-1/(2h)^2\,(9\cos(3h)-24\cos(2h)+23\cos(h)-8)$
4	$4h$	$\cos(4h)$	$1/(2h)\,(3\cos(4h)-4\cos(3h)+\cos(2h))$	$-1/(2h)^2\,(9\cos(4h)-24\cos(3h)+22\cos(2h)-8\cos(h)+1)$
5	$5h$	$\cos(5h)$	$1/(2h)\,(3\cos(5h)-4\cos(4h)+\cos(3h))$	$-1/(2h)^2\,(9\cos(5h)-24\cos(4h)+22\cos(3h)-8\cos(2h)+\cos(h))$

Initial conditions not satisfying the second derivative of the constraint

step	time	y	v	λ
0	0	1	0	0
1	h	$\cos(h)$	$2/h\,(\cos(h)-1)$	$-4/h^2\,(\cos(h)-1)$
2	$2h$	$\cos(2h)$	$1/(2h)\,(3\cos(2h)-4\cos(h)+1)$	$-1/(2h)^2\,(9\cos(2h)-28\cos(h)+19)$
3	$3h$	$\cos(3h)$	$1/(2h)\,(3\cos(3h)-4\cos(2h)+\cos(h))$	$-1/(2h)^2\,(9\cos(3h)-24\cos(2h)+23\cos(h)-8)$
4	$4h$	$\cos(4h)$	$1/(2h)\,(3\cos(4h)-4\cos(3h)+\cos(2h))$	$-1/(2h)^2\,(9\cos(4h)-24\cos(3h)+22\cos(2h)-8\cos(h)+1)$
5	$5h$	$\cos(5h)$	$1/(2h)\,(3\cos(5h)-4\cos(4h)+\cos(3h))$	$-1/(2h)^2\,(9\cos(5h)-24\cos(4h)+22\cos(3h)-8\cos(2h)+\cos(h))$

Appendix D

Constraints

Two classes of constraints can be clearly identified: those that express a kinematic relationship between nodes, and those that express a dynamic relationship between the kinematics of the nodes and the forces that act on the nodes themselves. In the first case the index three differential-algebraic system of equations described earlier in the dissertation results. The second case, which refers to elastic constraints, may result in index one differential-algebraic equations if the constraint relationship is explicitly written, or the system can be cast in the normal ordinary differential form if the constraint forces are explicitated as functions of the coordinates of the nodes. The latter approach has been basically followed in this work, the former one giving a higher accuracy and a better behaviour only when the constraint degenerates in a very stiff, rigid kinematic relationship [49].

D.1 Kinematic constraints

Kinematic constraints, as described in Chapter 2, consist in writing an algebraic relationship among some kinematic unknowns, namely position and velocity of nodes, resulting in holonomic or non-holonomic constraint equations. As an example, two basic constraints are outlined. Most of the algebraic constraints can be obtained as a combination of the coincidence and orthogonality conditions here presented.

D.1.1 Coincidence

Let x_i and f_i, $i = 1, 2$, represent the position of two independent nodes $1, 2$ and the offsets from the nodes to the position of the joint, both in the global frame. For sake of simplicity, the offsets f_i are assumed to be constant in the local frame. The constraint equation is:

$$(x_2 + f_2) - (x_1 + f_1) = 0.$$

This constraint generates a reacting force r at the coincidence point, which, transported to the nodes, results in a force and a couple applied to each node, due to the offsets:

$$\begin{aligned} F &= \pm r, \\ C &= \pm f_i \times r. \end{aligned}$$

The differentiation of the constraint gives

$$(\Delta x_2 - f_2 \times \theta_{\Delta 2}) - (\Delta x_1 - f_1 \times \theta_{\Delta 1}) = -(x_2 + f_2) + (x_1 + f_1)$$

and that of the forces and couples at the nodes yields

$$\begin{aligned} \pm \Delta r &= \mp r, \\ \pm (f_i \times \Delta r - r \times f_i \times \theta_{\Delta i}) &= \mp f_i \times r, \end{aligned}$$

where θ_Δ refers to the perturbation of rotation, namely $G \Delta g$.

D.1.2 Orthogonality

Let e_i, $i = 1, 2$, represent the unit vectors of some coordinate direction referred to two independent nodes $1, 2$ and expressed in the global frame. The orthogonality constraint equation is

$$e_2^T e_1 = 0.$$

This constraint generates a reacting couple r that is scalar, and acts in direction $e_2 \times e_1$:

$$C = \pm (e_2 \times e_1)\, r.$$

The differentiation of the constraint equation gives

$$(e_2 \times e_1)^T \theta_{\Delta 2} - (e_2 \times e_1)^T \theta_{\Delta 1} = -e_2^T e_1$$

and that of the couple at the nodes yields

$$\pm r (e_1 \times e_2 \times \theta_{\Delta 2} - e_2 \times e_1 \times \theta_{\Delta 1}) \pm (e_2 \times e_1)\, \Delta r = \mp (e_2 \times e_1)\, r.$$

By combining 1, 2 and 3 constraints of this kind, universal, plane and prismatic hinges can be respectively obtained.

D.2 Dynamic Constraints

Dynamic constraints, as described in Chapter 5, can be written both in terms of ordinary differential and of algebraic-differential equations, the latter form usually yielding only a better conditioning of the problem and the possibility of accounting for ill-posed configurations, i.e. extremely varying stiffness of flexible components. An arbitrary relationship between force and configuration is assumed, in the form

$$s(\sigma, \varepsilon) = 0,$$

where σ and ε respectly refer to some stress and strain measure, regardless to their dimension. If the relationship can be directly written, the usual form

$$\sigma = \sigma(\varepsilon)$$

can be directly used to add the contribution of the constraint to the equilibrium equations of the nodes it is applied to. Otherwise, the stresses σ become the constraint reaction unknowns, and their definition in terms of constitutive relationship is added to the system. In a general sense, the σ may depend on the relative configuration of the system, thus involving the strain time rate as well to account for some viscous effects, i.e.

$$\sigma = \sigma(\varepsilon, \dot{\varepsilon})$$

The linearisation of the direct constitutive law yields

$$\Delta\sigma = \frac{\partial\sigma}{\partial\varepsilon}\Delta\varepsilon + \frac{\partial\sigma}{\partial\dot{\varepsilon}}\Delta\dot{\varepsilon};$$

this is true regardless of the dimensions and of the nature of stresses and strains. This fact has been exploited by introducing the concept of *template*[1] constitutive law, namely a formal separation of the constitutive law properties from its use in writing the equilibrium equations. In the following, three simple elastic/viscoelastic constraints are described. It is interesting to notice that the finite volume beam formulation presented in Section 5.4 may be regarded as a generalisation of the dynamic constraints here presented.

D.2.1 Rods

A rod is defined as an elastic/viscoelastic element that generates an internal force between two points, oriented as the line that connects the points themselves, and

[1]See Section H.1.2 for some details on the implemenetation of the constitutive laws.

whose amplitude depends on the distance/relative velocity of the points themselves. Consider two points, 1 and 2, whose positions $p_i = x_i + f_I$ are rigidly offset from the corresponding node positions x_i by f_i. The relative distance is $d = p_2 - p_1$. The strain is defined as

$$\varepsilon = \frac{l}{l_0} - 1,$$

being $l = |d|$ and l_0 the current and the reference length of the rod, respectively. The strain time rate is

$$\dot{\varepsilon} = \frac{1}{l_0} \frac{d^T}{l} \dot{d}$$

which corresponds to the normalised (i.e. divided by l_0) projection of the relative velocity (i.e. $\dot{d}$) along the direction of the rod (i.e. d/l). In this case the strain, the strain rate and the stress are scalars. Their linearisation yields

$$\begin{aligned} \Delta\varepsilon &= \frac{1}{l_0} \frac{d^T}{l} \Delta d, \\ \Delta\dot{\varepsilon} &= \frac{1}{l_0} \left(\frac{d^T}{l} \Delta\dot{d} - \frac{\dot{d}^T}{l} \frac{d}{l} \times \frac{d}{l} \times \Delta d \right), \end{aligned}$$

where

$$\begin{aligned} \Delta d &= (\Delta x_2 - f_2 \times \Delta\theta_2) - (\Delta x_1 - f_1 \times \Delta\theta_1), \\ \Delta\dot{d} &= (\Delta\dot{x}_2 - f_2 \times \Delta\omega_2 - \omega_2 \times f_2 \times \Delta\theta_2) \\ &\quad - (\Delta\dot{x}_1 - f_1 \times \Delta\omega_1 - \omega_1 \times f_1 \times \Delta\theta_1). \end{aligned}$$

The forces and the couples the rod applies to the nodes are

$$\begin{aligned} F_i &= \pm \frac{d}{l} \sigma, \\ M_i &= \pm f_i \times \frac{d}{l} \sigma. \end{aligned}$$

Their linearisation yields

$$\begin{aligned} \Delta F_i &= \pm \left(-\frac{\sigma}{l} \frac{d}{l} \times \frac{d}{l} \times \Delta d + \frac{\partial\sigma}{\partial\varepsilon} \Delta\varepsilon + \frac{\partial\sigma}{\partial\dot{\varepsilon}} \Delta\dot{\varepsilon} \right), \\ \Delta M_i &= F_i \times f_i \times \Delta\theta_i + f_i \times \Delta F_i. \end{aligned}$$

Notice that the formulas do not rely on any specific constitutive law, provided the value of the force and the tangent stiffness and damping matrices are available.

D.2.2 Springs

Three-dimensional springs can be formulated as well; indeed their formula is even simpler. Consider a flexible element that generates a force related to the relative position and velocity of two points in some reference frame, which can be attached to point 1 without any loss in generality. The internal force is $\tilde{\sigma} = \tilde{\sigma}(\tilde{d}, \dot{\tilde{d}})$, where $\tilde{d}$ and $\dot{\tilde{d}}$ have the meaning defined for the rods, but are rotated back in the material frame by matrix R_1. In this case the "strains", "strain rates" and the "stresses" are three-dimensional vectors. Their linearisation yields

$$\begin{aligned}
\Delta\tilde{d} &= R_1^T \left((x_2 + f_2 - x_1) \times \Delta\theta_1 + \Delta x_2 - f_2 \times \Delta\theta_2 - \Delta x_1 \right), \\
\Delta\dot{\tilde{d}} &= R_1^T \left((\dot{x}_2 + \omega_2 \times f_2 - \dot{x}_1 - \omega_1 \times f_1) \times \Delta\theta_1 \right. \\
&\qquad + (\Delta\dot{x}_2 - f_2 \times \Delta\omega_2 - \omega_2 \times f_2 \times \Delta\theta_2) \\
&\qquad \left. - (\Delta\dot{x}_1 - f_1 \times \Delta\omega_1 - \omega_1 \times f_1 \times \Delta\theta_1) \right).
\end{aligned}$$

The forces and the couples acting at the nodes are

$$\begin{aligned}
F_i &= \pm R_1 \tilde{\sigma}, \\
M_i &= \pm f_i \times R_1 \tilde{\sigma}.
\end{aligned}$$

The linearisation of the internal force yields

$$\Delta\tilde{\sigma} = \frac{\partial\tilde{\sigma}}{\partial\tilde{d}} \Delta\tilde{d} + \frac{\partial\tilde{\sigma}}{\partial\dot{\tilde{d}}} \Delta\dot{\tilde{d}},$$

where the partial derivatives of the stresses, expressing the tangent stiffness and damping matrices, can represent any arbitrary anisotropic costitutive law; the linearisation of nodal forces and couples yields

$$\begin{aligned}
\Delta F_i &= \Delta\theta_1 \times F_i + R_1 \Delta\tilde{\sigma}, \\
\Delta M_i &= M_i \times f_i \times \Delta\theta_1 + f_i \times \Delta F_i.
\end{aligned}$$

D.2.3 Rotational springs

The rotational element corresponding to the spring applies an internal couple between two nodes depending on the relative rotation and rotation speed. The constitutive law is $\tilde{\sigma} = \tilde{\sigma}(\tilde{\psi}, \dot{\tilde{\psi}})$, where the angle θ is related to the relative rotation of the two nodes, i.e. $\tilde{\psi} = \mathrm{ax}\left(R_1^T R_2\right)$. Its linearisation is

$$\begin{aligned}
\Delta\tilde{\psi} &= \mathrm{ax}\left(\Delta\left(R_1^T R_2\right) \left(R_1^T R_2\right)^T \right) \\
&= \mathrm{ax}\left(\left(R_1^T \Delta\theta_1 \times {}^T R_2 + R_1^T \Delta\theta_2 \times R_2\right) \left(R_1^T R_2\right)^T \right) \\
&= \mathrm{ax}\left(R_1^T \left(\Delta\theta_2 - \Delta\theta_1\right) \times R_1 \right) \\
&= R_1^T \left(\Delta\theta_2 - \Delta\theta_1\right).
\end{aligned}$$

In analogous manner, the derivative of the angle is $\dot{\psi} = R_1^T\left(\omega_2 - \omega_1\right)$; its linearisation yields

$$\Delta\dot{\psi} \;=\; R_1^T\left(\left(\omega_2 - \omega_1\right) \times \Delta\theta_1 + \Delta\omega_2 - \Delta\omega_1\right).$$

The couples applied to the nodes are

$$M_i \;=\; \pm R_1 \tilde{\sigma}$$

and their linearisation yields

$$\Delta M_i \;=\; \Delta\theta_1 \times M_i + R_1 \Delta\tilde{\sigma}.$$

D.2.4 Remarks

The above described dynamic constraints should be used carefully. Apart from the relatively simple rod element, the spring and the rotational spring represent an idealisation of more complex elastic and viscous elements. The possibility to use anisotropic, viscoelastic, viscoplastic constitutive laws in a large strain, large rotation environment requires the user to have a deep knowledge of the system under investigation. In fact the idealised models here described are based on some underlying assumption, i.e. in case of the rotational spring that the rotations are spherical and independent on the path that is followed. This might not hold true for some cases, e.g. for elastomeric bearings used in some advanced articulated rotors. In some cases one might want to combine kinematic and dynamic constraints to obtain the desired behaviour; for instance, a rotational spring can be superimposed to a plane hinge joint to add some root stiffness and viscous damping to a lead-lag hinge; this solution is definitely preferable to using a rotational spring with very high stiffnesses about flap and pitch directions.

Appendix E

Beam section analysis

This chapter describes in detail some aspects of the beam section analysis.

E.1 Internal work per unit volume

The internal work submatrices, from Section 5.3.2, describe the contribution of each independent coordinate to the internal work of the beam section. The linear, or linearised constitutive matrix of the material is partitioned in two blocks, that separate the coefficients affecting the strains and the stresses on the section from the others, as described for the strains. It is

$$D = \begin{bmatrix} D_{II} & D_{IS} \\ D_{SI} & D_{SS} \end{bmatrix}$$

The submatrices are

$$\begin{aligned}
\mathcal{M}^* &= D_{SS}, \\
\mathcal{C}^* &= \begin{bmatrix} D_{SI} & D_{SS} \end{bmatrix} \left(\begin{bmatrix} 0 \\ \tilde{\rho}\times \end{bmatrix} + \mathcal{D}(\cdot) \right), \\
\mathcal{L}^* &= D_{SS} \begin{bmatrix} I & -\tilde{t}\times \end{bmatrix}, \\
\mathcal{E}^* &= \left(\begin{bmatrix} 0 \\ \tilde{\rho}\times \end{bmatrix} + \mathcal{D}(\cdot) \right)^T \begin{bmatrix} D_{II} & D_{IS} \\ D_{SI} & D_{SS} \end{bmatrix} \left(\begin{bmatrix} 0 \\ \tilde{\rho}\times \end{bmatrix} + \mathcal{D}(\cdot) \right), \\
\mathcal{R}^* &= \left(\begin{bmatrix} 0 \\ \tilde{\rho}\times \end{bmatrix} + \mathcal{D}(\cdot) \right)^T \begin{bmatrix} D_{IS} \\ D_{SS} \end{bmatrix} \begin{bmatrix} I & -\tilde{t}\times \end{bmatrix} + \begin{bmatrix} 0 & \tilde{\sigma}_S\times \end{bmatrix}, \\
\mathcal{A}^* &= \begin{bmatrix} I & -\tilde{t}\times \end{bmatrix}^T D_{SS} \begin{bmatrix} I & -\tilde{t}\times \end{bmatrix}.
\end{aligned}$$

Recalling that $\sigma_S = [0, I]\,\sigma$, the generalised stresses that work against the different parts of the strains are

$$
\begin{aligned}
\Sigma^*_{t_\xi} &= \tilde{\sigma}_S, \\
\Sigma^*_t &= \left(\begin{bmatrix} 0 \\ \tilde{\rho}\times \end{bmatrix} + \mathcal{D}(\cdot) \right)^T \tilde{\sigma}, \\
\Sigma^*_\psi &= \begin{bmatrix} I & -\tilde{t}\times \end{bmatrix} \tilde{\sigma}_S.
\end{aligned}
$$

E.2 Discretisation

Regardless of the nature of the shape functions that are used to discretise the nodal warping, they are written as $\tilde{t} = N(\eta,\zeta)\,\tilde{u}(\xi)$. Their gradient results in $\nabla\tilde{t} = B\tilde{u} + N\tilde{u}_{/\xi}$, where $B(\eta,\zeta) = \mathcal{D}(N)$ is the derivative of the shape functions. The internal work submatrices that result after discretistion and integration over the beam section are

$$
\begin{aligned}
\mathcal{M} &= \int_S N^T D_{SS} N \, J\mathrm{d}S, \\
\mathcal{C} &= \int_S N^T \begin{bmatrix} D_{SI} & D_{SS} \end{bmatrix} \left(\begin{bmatrix} 0 \\ \tilde{\rho}\times \end{bmatrix} N + B \right) J\mathrm{d}S, \\
\mathcal{L} &= \int_S N^T D_{SS} \begin{bmatrix} I & -\tilde{t}\times \end{bmatrix} J\mathrm{d}S, \\
\mathcal{E} &= \int_S \left(\begin{bmatrix} 0 \\ \tilde{\rho}\times \end{bmatrix} N + B \right)^T \begin{bmatrix} D_{II} & D_{IS} \\ D_{SI} & D_{SS} \end{bmatrix} \left(\begin{bmatrix} 0 \\ \tilde{\rho}\times \end{bmatrix} N + B \right) J\mathrm{d}S, \\
\mathcal{R} &= \int_S \left(\begin{bmatrix} 0 \\ \tilde{\rho}\times \end{bmatrix} N + B \right)^T \begin{bmatrix} D_{IS} \\ D_{SS} \end{bmatrix} \begin{bmatrix} I & -\tilde{t}\times \end{bmatrix} + \begin{bmatrix} 0 & \tilde{\sigma}_S\times \end{bmatrix} J\mathrm{d}S, \\
\mathcal{A} &= \int_S \begin{bmatrix} I & -\tilde{t}\times \end{bmatrix}^T D_{SS} \begin{bmatrix} I & -\tilde{t}\times \end{bmatrix} J\mathrm{d}S.
\end{aligned}
$$

The right-hand arrays are

$$
\begin{aligned}
\Sigma_{t_\xi} &= \int_S N^T \tilde{\sigma}_S \, J\mathrm{d}S, \\
\Sigma_t &= \int_S \left(\begin{bmatrix} 0 \\ \tilde{\rho}\times \end{bmatrix} N + B \right)^T \tilde{\sigma} \, J\mathrm{d}S, \\
\Sigma_\psi &= \int_S \begin{bmatrix} I & -\tilde{t}\times \end{bmatrix} \tilde{\sigma}_S \, J\mathrm{d}S.
\end{aligned}
$$

E.3 Beam properties from finite elements

It is interesting to notice that the matrices for the curved and twisted beam can be obtained from those of the straight beam (i.e. the previously defined matrices with $\tilde{\rho} = 0$) by considering the transformation

$$
\begin{aligned}
\mathcal{M} &= \hat{\mathcal{M}}, \\
\mathcal{C} &= \hat{\mathcal{C}} + \hat{\mathcal{M}} \tilde{\rho} \times^T, \\
\mathcal{L} &= \hat{\mathcal{L}}, \\
\mathcal{E} &= \hat{\mathcal{E}} + \hat{\mathcal{C}}^T \tilde{\rho} \times^T + \tilde{\rho} \times \hat{\mathcal{C}} + \tilde{\rho} \times \hat{\mathcal{M}} \tilde{\rho} \times^T, \\
\mathcal{R} &= \hat{\mathcal{R}} + \tilde{\rho} \times \hat{\mathcal{L}}, \\
\mathcal{A} &= \hat{\mathcal{A}},
\end{aligned}
$$

where the hat symbol $(\hat{\cdot})$ refers to the straight/untwisted beam matrices. This is true under the assumption that the discretisation and the multiplication by $\tilde{\rho} \times$ are commutable, i.e. $N\tilde{\rho} \times = \tilde{\rho} \times N$. Thus the technique, proposed in Ref. [31] by *Ghiringhelli* and *Mantegazza*, to compute the beam section properties by conventional finite-element codes, in principle can be extended to curved and twisted beams. The cited approach is based on using a conventional finite-element model of a slice of beam to determine matrices $\mathcal{M}$, $\mathcal{C}$ and $\mathcal{E}$ by condensing the nodes on one face of the slice. The other matrices result from reducing the first three by rigid rototraslation displacements. The curvature/twist correction can be added by modelling a slice with linearly varying thickness, to account for the change in volume related to J, and then correcting the matrices related to the axial derivative of the warping with the curvature/twist term, as shown above.

E.4 Distributed external loads

The form of the distributed external loads has been introduced in Section 5.3.3. It is presented here for the case of a straight, untwisted beam. The unknown nodal stresses can be discarded by differentiating the first block row of the problem and by substituting it in the second block row, thus yielding the following second-order differential problem

$$
-\begin{bmatrix} \mathcal{M} & 0 \\ \text{sym.} & 0 \end{bmatrix} \begin{Bmatrix} u \\ \psi \end{Bmatrix}_{/\xi\xi} - \begin{bmatrix} \mathcal{C} - \mathcal{C}^T & \mathcal{L} \\ \text{skw.} & 0 \end{bmatrix} \begin{Bmatrix} u \\ \psi \end{Bmatrix}_{/\xi}
$$

$$
+ \begin{bmatrix} \mathcal{E} & \mathcal{R} \\ \text{sym.} & \mathcal{A} \end{bmatrix} \begin{Bmatrix} u \\ \psi \end{Bmatrix} = \begin{Bmatrix} Q_u q \\ \vartheta \end{Bmatrix},
$$

where $Q_u q$ are the nodal forces resulting from the distributed external surface and volume loads, and ϑ are the internal forces, respectful of the differential equilibrium equations of the beam; $q = q(\xi)$ is a scalar function that describes the axial distribution of the load. Being H the matrix of the nodal displacements that correspond to the six rigid displacement and rotation motions, the force and the couple that result from the distributed loads are $Q_r = H^T Q_u$. The differential equilibrium equation of the beam is $\vartheta_{/\xi} - T^T \vartheta + Q_r q = 0$, matrix T being the derivative of the arms matrix $\mathcal{U}$ defined in Section 5.4. A function g is sought, whose second derivative is function q, i.e. $g_{/\xi\xi} = q$. Consider for the internal forces the form $\vartheta = \vartheta_0 g + \vartheta_1 g_{/\xi}$; the equilibrium equation yields $\vartheta_1 = -Q_r$, $\vartheta_0 = -T^T Q_r$. By defining the matrices

$$\mathcal{K}_2 = \begin{bmatrix} \mathcal{M} & 0 \\ \text{sym.} & 0 \end{bmatrix}, \quad \mathcal{K}_1 = \begin{bmatrix} \mathcal{C} - \mathcal{C}^T & \mathcal{L} \\ \text{skw.} & 0 \end{bmatrix}, \quad \mathcal{K}_0 = \begin{bmatrix} \mathcal{E} & \mathcal{R} \\ \text{sym.} & \mathcal{A} \end{bmatrix},$$

$$\mathcal{B}_2 = \begin{Bmatrix} Q_u \\ 0 \end{Bmatrix}, \qquad \mathcal{B}_1 = \begin{Bmatrix} 0 \\ -Q_r \end{Bmatrix}, \qquad \mathcal{B}_0 = \begin{Bmatrix} 0 \\ -T^T Q_r \end{Bmatrix},$$

and by collecting the nodal displacements and the generalised deformation unknowns in

$$\mathcal{U} = \begin{Bmatrix} u \\ \psi \end{Bmatrix},$$

the problem can be written as

$$-\mathcal{K}_2 \mathcal{U}_{/\xi\xi} - \mathcal{K}_1 \mathcal{U}_{/\xi} + \mathcal{K}_0 \mathcal{U} = \mathcal{B}_2 g_{/\xi\xi} + \mathcal{B}_1 g_{/\xi} + \mathcal{B}_0 g.$$

By seeking a solution of the form

$$\mathcal{U} = \sum_{i=0}^{\infty} \mathcal{U}_i g_{/\xi^i},$$

the coefficients $\mathcal{U}_i$ assume the recursive form

$$\mathcal{U}_i = \mathcal{K}_0^{-1} \left(\sum_{j=0}^{2} \mathcal{B}_j \delta_{ji} + \mathcal{K}_1 \mathcal{U}_{i-1} + \mathcal{K}_2 \mathcal{U}_{i-2} \right),$$

where negative index entities are assumed to be null, and δ_{ij} is the *Kronecker* operator. Notice the load function g is required to be indefinitely differentiable, and thus regular. This is consistent with the assumption of smooth variation of quantities along the beam axis that is implicit in the beam model. Impulsive, concentrated loads cannot be handled by this approach, and require the evaluation of an extremity problem, as mentioned in [44] and in subsequent works. The regularity properties that are required for the load function are exemplified by analysing the convergence of the recursion for an exponential load distribution. After the solutions related to arrays $\mathcal{B}_i$ are computed, the higher-order terms of the solution involve the propagation of the local effects. The recursive form results in

$$\lambda \left\{ \begin{array}{c} \mathcal{U}_{i-1} \\ \mathcal{U}_i \end{array} \right\} = \left[\begin{array}{cc} 0 & I \\ \mathcal{K}_0^{-1}\mathcal{K}_2 & \mathcal{K}_0^{-1}\mathcal{K}_1 \end{array} \right] \left\{ \begin{array}{c} \mathcal{U}_{i-1} \\ \mathcal{U}_i \end{array} \right\};$$

as a consequence, the solution at $\xi = 0$ takes the form

$$\mathcal{U}(0) \cong \mathcal{U}_0 \sum_{i=0}^{\infty} \lambda^i g_{/\xi^i}(0)\,.$$

The exponential load distribution $g \approx \mathrm{e}^{\xi/\sigma}$ gives

$$\mathcal{U}(0) \cong \mathcal{U}_0 \sum_{i=0}^{\infty} \lambda^i/\sigma^i,$$

which is finite for $\|\lambda/\sigma\| < 1$. The eigenvalue λ represents the largest propagation length of the beam section, which, in a heuristic sense, measures the distance from the extremities where the beam model correctly represents the behaviour of a beam-like structural component. The model here considered is a finite-element discretisation of the beam section, so the eigenvalues might be related to the numerical discretisation of the section; however, for practical models, the largest propagation lengths should be properly captured even by very coarse meshes, if a reasonably accurate characterisation is required; eventual mesh refinement should not significantly alter such eigenvalues. For practical purposes, polynomial load distributions best fit with the presented model, because their derivatives naturally vanish at some order.

Appendix F

Plate fibre analysis

The entities defined in Section 5.6 are detailed below.

F.1 Internal work per unit volume

Being $\Xi = \{\mathcal{X}, \mathcal{Y}, \mathcal{Z}\}$, and ranging both i and j from 1 to 2, the matrices that define the internal work per unit volume are

$$
\begin{aligned}
\mathcal{M}^*_{ij} &= \Xi_i^T D \Xi_j, \\
\mathcal{C}^*_i &= \Xi_i^T D \left(\mathcal{X} \tilde{\rho}_\xi \times + \mathcal{Y} \tilde{\rho}_\eta \times + \mathcal{Z} (\cdot)_{/\zeta} \right), \\
\mathcal{L}^*_{ij} &= \Xi_i^T D \Xi_j \left[\begin{array}{cc} I & -\tilde{t} \times \end{array} \right], \\
\mathcal{E}^* &= \left(\mathcal{X} \tilde{\rho}_\xi \times + \mathcal{Y} \tilde{\rho}_\eta \times + \mathcal{Z} (\cdot)_{/\zeta} \right)^T D \left(\mathcal{X} \tilde{\rho}_\xi \times + \mathcal{Y} \tilde{\rho}_\eta \times + \mathcal{Z} (\cdot)_{/\zeta} \right), \\
\mathcal{R}^*_i &= \left(\mathcal{X} \tilde{\rho}_\xi \times + \mathcal{Y} \tilde{\rho}_\eta \times + \mathcal{Z} (\cdot)_{/\zeta} \right)^T D \Xi_i \left[\begin{array}{cc} I & -\tilde{t} \times \end{array} \right], \\
\mathcal{A}^*_{ij} &= \left(\Xi_i \left[\begin{array}{cc} I & -\tilde{t} \times \end{array} \right] \right)^T D \Xi_j \left[\begin{array}{cc} I & -\tilde{t} \times \end{array} \right].
\end{aligned}
$$

F.2 Discretisation

The discretised warping unknowns are defined as $\tilde{t} = N(\zeta)\, \tilde{u}(\xi, \eta)$; their gradient thus results in $\nabla \tilde{t} = N u_{/\xi} + N u_{/\eta} + B u$, where $B = N_{/\zeta}$. The matrices that describe the discretised internal work per unit surface are

$$
\begin{aligned}
\mathcal{M}_{ij} &= \int_S N^T \Xi_i^T D \Xi_j N \, J \mathrm{d}S, \\
\mathcal{C}_i &= \int_S N^T \Xi_i^T D \left(\mathcal{X} \tilde{\rho}_\xi \times N + \mathcal{Y} \tilde{\rho}_\eta \times N + \mathcal{Z} B \right) J \mathrm{d}S,
\end{aligned}
$$

$$\begin{aligned}
\mathcal{L}_{ij} &= \int_S N^T \Xi_i^T D \Xi_j \left[\begin{array}{cc} I & -\tilde{t}\times \end{array} \right] J \mathrm{d}S, \\
\mathcal{E} &= \int_S \begin{array}{c} \left(\mathcal{X}\tilde{\rho}_\xi \times N + \mathcal{Y}\tilde{\rho}_\eta \times N + \mathcal{Z}B\right)^T \\ D\left(\mathcal{X}\tilde{\rho}_\xi \times N + \mathcal{Y}\tilde{\rho}_\eta \times N + \mathcal{Z}B\right) \end{array} J \mathrm{d}S, \\
\mathcal{R}_i &= \int_S \left(\mathcal{X}\tilde{\rho}_\xi \times N + \mathcal{Y}\tilde{\rho}_\eta \times N + \mathcal{Z}B\right)^T D \Xi_i \left[\begin{array}{cc} I & -\tilde{t}\times \end{array} \right] J \mathrm{d}S, \\
\mathcal{A}_{ij} &= \int_S \left(\Xi_i \left[\begin{array}{cc} I & -\tilde{t}\times \end{array} \right]\right)^T D \Xi_j \left[\begin{array}{cc} I & -\tilde{t}\times \end{array} \right] J \mathrm{d}S,
\end{aligned}$$

being $J = \det(\nabla s_0)$ the measure of the integration volume.

Appendix G

Piezoelectric beam section characterisation

The piezoelectric matrices used in the characterisation of a piezoelectric beam are detailed.

G.1 Internal work per unit volume

The piezoelectric linear constitutive matrices are partitioned in internal and section-facing coefficients as

$$\begin{aligned} D^{(E)} &= \begin{bmatrix} D_{II} & D_{IS} \\ D_{SI} & D_{SS} \end{bmatrix}, \\ e &= \begin{bmatrix} e_{SI} & e_{SS} \\ e_{II} & e_{IS} \end{bmatrix}, \\ \varepsilon^{(\varepsilon)} &= \begin{bmatrix} \varepsilon_{SS} & \varepsilon_{SI} \\ \varepsilon_{IS} & \varepsilon_{II} \end{bmatrix}. \end{aligned}$$

The internal work matrices, apart from the already defined structural ones[1], are

$$\begin{aligned} \mathcal{M}^*_{se} &= e^T_{SS}, \\ \mathcal{M}^*_{ee} &= -\varepsilon_{SS}, \\ \mathcal{C}^*_{se} &= \begin{bmatrix} e^T_{SS} & e^T_{IS} \end{bmatrix} \mathcal{D}_e(\cdot), \\ \mathcal{C}^*_{es} &= \begin{bmatrix} e_{SI} & e_{SS} \end{bmatrix} \left(\begin{bmatrix} 0 \\ \tilde{\rho} \times \end{bmatrix} + \mathcal{D}(\cdot) \right), \\ \mathcal{C}^*_{ee} &= -\begin{bmatrix} \varepsilon_{SS} & \varepsilon_{SI} \end{bmatrix} \mathcal{D}_e(\cdot), \end{aligned}$$

[1]See Appendix E

$$
\begin{aligned}
\mathcal{L}_e^* &= e_{SS}\left[\begin{array}{cc} I & -\tilde{t}\times \end{array}\right], \\
\mathcal{E}_{se}^* &= \left(\left[\begin{array}{c} 0 \\ \tilde{\rho}\times \end{array}\right] + \mathcal{D}(\cdot)\right)^T \left[\begin{array}{cc} e_{SI}^T & e_{II}^T \\ e_{SS}^T & e_{IS}^T \end{array}\right] \mathcal{D}_e(\cdot), \\
\mathcal{E}_{ee}^* &= -\mathcal{D}_e(\cdot)^T \left[\begin{array}{cc} \varepsilon_{SS} & \varepsilon_{SI} \\ \varepsilon_{IS} & \varepsilon_{II} \end{array}\right] \mathcal{D}_e(\cdot), \\
\mathcal{R}_e^* &= \mathcal{D}_e(\cdot)^T \left[\begin{array}{c} e_{SS} \\ e_{IS} \end{array}\right] \left[\begin{array}{cc} I & -\tilde{t}\times \end{array}\right].
\end{aligned}
$$

The electric displacement terms that work for the electric field terms are

$$
\begin{aligned}
\Sigma_{V\xi}^* &= \left[\begin{array}{c} 1 \\ 0 \\ 0 \end{array}\right]^T D_e, \\
\Sigma_V^* &= \mathcal{D}_e(\cdot)^T D_e.
\end{aligned}
$$

G.2 Discretisation

The discretisation of the electric unknowns is straightforward. The electric potential is discretised as $V = N(\eta, \zeta)\, u_e(\xi)$, where electric potential nodal values depending on the axial position only are used to interpolate by conventional shape functions the value of the potential in the section. Notice the shape functions are the same as used for the structural discretisation without any loss in generality. The electric field results in $\tilde{E} = -N u_{e/\xi} - B_e u_e$, with $B_e = \mathcal{D}_e N$. The discrete, integral matrices that describe the internal work per unit length are:

$$
\begin{aligned}
\mathcal{M}_{se} &= \int_{S_e} N^T e_{SS}^T N \, J \mathrm{d}S, \\
\mathcal{M}_{ee} &= -\int_{S_e} N^T \varepsilon_{SS} N \, J \mathrm{d}S, \\
\mathcal{C}_{se} &= \int_{S_e} N^T \left[\begin{array}{cc} e_{SS}^T & e_{IS}^T \end{array}\right] B_e \, J \mathrm{d}S, \\
\mathcal{C}_{es} &= \int_{S_e} N^T \left[\begin{array}{cc} e_{SI} & e_{SS} \end{array}\right] \left(\left[\begin{array}{c} 0 \\ \tilde{\rho}\times \end{array}\right] N + B\right) J \mathrm{d}S, \\
\mathcal{C}_{ee} &= -\int_{S_e} N^T \left[\begin{array}{cc} \varepsilon_{SS} & \varepsilon_{SI} \end{array}\right] B_e \, J \mathrm{d}S, \\
\mathcal{L}_e &= -\int_{S_e} N^T e_{SS} \left[\begin{array}{cc} I & -\tilde{t}\times \end{array}\right] J \mathrm{d}S, \\
\mathcal{E}_{se} &= \int_{S_e} \left(\left[\begin{array}{c} 0 \\ \tilde{\rho}\times \end{array}\right] N + B\right)^T \left[\begin{array}{cc} e_{SI}^T & e_{II}^T \\ e_{SS}^T & e_{IS}^T \end{array}\right] B_e \, J \mathrm{d}S,
\end{aligned}
$$

$$
\begin{aligned}
\mathcal{E}_{ee} &= \int_{S_e} B_e^T \begin{bmatrix} \varepsilon_{SS} & \varepsilon_{SI} \\ \varepsilon_{IS} & \varepsilon_{II} \end{bmatrix} B_e \, J\mathrm{d}S, \\
\mathcal{R}_e &= -\int_{S_e} B_e^T \begin{bmatrix} e_{SS} \\ e_{IS} \end{bmatrix} \begin{bmatrix} I & -\tilde{t}\times \end{bmatrix} J\mathrm{d}S.
\end{aligned}
$$

The right-hand arrays are

$$
\begin{aligned}
\Sigma_{V\xi} &= \int_{S_e} N^T \begin{bmatrix} 1 \\ 0 \\ 0 \end{bmatrix}^T D_e \, J\mathrm{d}S, \\
\Sigma_V &= \int_{S_e} B_e^T D_e \, J\mathrm{d}S.
\end{aligned}
$$

Appendix H

Implementation notes

A few implementation notes are presented. Their motivation is related to the large amount of coding that has been performed during this research project. The multi-body analysis program played an important role, and allowed to acquire a deep knowledge of some programming techniques that led to the realisation of an interesting research tool even from an implementation standpoint. These notes want to be a reminder for subsequent implementors, and offer suggestions for developing a policy for the implementation of medium/large projects, involving several persons with serious portability, maintenability and reusability issues. The phylosophy followed in writing such code was to privilege safe programming style even at the cost of sacrificing performance issues. As a result, lots of code are dedicated to debugging purposes. Optimisation and performance enhancements might be obtained by tuning some parts of the code once it is stabilised; however, since it is a research code particularly intended to investigating new problems, it is likely to never stabilise to a definitive form!

H.1 Object Oriented programming

H.1.1 Drives

Many items may require sophisticated parameter-dependent values to be easily assigned, and a common interface at input-file level. A basic issue is the assignment of the time history of a forcing term; in very simple cases constant, step or ramp functions may suffice, but in rather sophisticated situations one requires a wide flexibility in defining such history. Moreover, from the programmer's standpoint, reusability of the code is a key issue, as well as a common input interface is fundamental to allow the user to quickly gain confidence in the analysis code. A solution to such requirements has been found by introducing a family of `Drive-`

`Callers`, classes that basically provide a numeric value based on some input parameter. They can be used as normal real constants, and do not actually add any overhead when the constant value drive type is used. More sophisticated drives allow the user to exploit various basic math functions, interpolation of data from external files, linear combination of basic drives, run-time parsing and evaluation of symbolic math and logical expressions, evaluation of the current value of degrees of freedom. In normal use, the input is represented by the current time; in case of degree of freedom evaluation, it can be filtered through a drive, so the actual resulting value is the result of evaluating the drive with the dof value as input instead of the time. This allows to easily implement a simple direct feedback for basic control issues, e.g. stabilising the rotational speed of a rotorcraft.

H.1.2 Template constitutive laws

The C++ `template` programming technique has been exploited to implement a general constitutive law family independent of the use and of the dimensionality. It has been used to characterise elements ranging from rods and abstract general purpose elements (one-dimensional) to springs and rotational springs (three-dimensional) to viscoelastic finite-volume beam elements (six-dimensional). Being N the dimensionality of the problem, the idea is to provide the $N \times 1$ dimensional value of the force, the $N \times N$ dimensional tangent stiffness matrix and optionally the $N \times N$ dimensional tangent damping matrix as functions of the $N \times 1$ dimensional value of the strains and optionally of the strain rates. The `template` mechanism requires all the entitites it is generated for to have a common set of functions or methods they can work with. Without excessive detail, input methods, overloaded math operators and general purpose functions have been implemented to meet this requirement. As a result, basic constitutiv laws like linear elastic isotropic and anisotropic, linear viscous isotropic and anisotropic, and linear viscoelastic isotropic and anisotropic required to be implemented only once, with code and implementation time savings but with no computational overhead, since the template is resolved at compile time.

H.2 Generic programming

In many parts of the code, the generic programming paradigm has been used as much as possible to ease the abstraction from the details of the implementation of specific parts. As a result, a simple interface between the routines specific to the code, e.g. computation of elements' contribution to *Jacobian* matrix and residual computation, global Jacobian and residual assembly, *Jacobian* matrix factorisation and backwards substitution, has been established. This allowed to introduce different data organisation schemes and linear algebra routines with very limited effort, with particular regard to the debugging.

H.3 Reuse of code

A set of basic C++ libraries has been implemented to support the writing of the code, MBDyn, used for this research project. Most of them are related to linear algebra with the aim of simplifying the writing of problems, freeing the implementor from low-level details and allowing to focus on high-level, problem related issues.

H.3.1 Matrix Handling

A common interface to data handling has been implemented, based on an Application Programming Interface that standardizes the procedures to instantiate, resize and delete vectors and matrices. Basic operations, such as single coefficient input and output, higher-level structures input, addition, scalar multiplication and more, are provided for every member in form of general programming routines. Specialised routines, whenever convenient, are provided as well in case compile-time type detection is possible. Substructures (i.e. subvectors and submatrices) have been added, to ease the assembly process without allowing the elements to directly deal with the global data storage structures.

H.3.2 Linear Algebra

The operations related to matrix factorisation and back substitution in solving linear problems are hidden in the type definition. There is no explicit factorisation of matrices, but only back substitution which causes the system to be factored if the matrix has been changed since the last substitution. In such case, for instance, a *Newton-Raphson* solution scheme requires to call an *assembly* and a *solve* routine, i.e. Assume the matrix is owned by a `SolutionManager`, who knowns how to solve it, and lends it to a `DataManager` that knows how to fill it (and the residual, as well); then:

```
SolutionManager sm;
DataManager dm;
// ...
dm.AssJac(sm);
sm.Solve();
```

A modified *Newton-Raphson* can be simply obtained by calling the *assembly* routine only when required, e.g. after a certain number of iterations, i.e.

```
SolutionManager sm;
DataManager dm;
// ...
if ( iter++ > maxiter ) {
    dm.AssJac(sm);
    iter = 0;
}
sm.Solve();
```

Most of the linear algebra data structures and routines have been obtained by wrapping exisiting C, and in some cases Fortran77, code into C++ *classes* thus obtaining a simple, practical and "safe" interface at the cost of limited overhead. Moreover, the use of a safe interface frees the implementor from taking care of basic issues like memory allocation and handling during the factorisation and solution phase, data initialisation and related issues, resulting in a better, and less error prone, coding style.

H.3.3 Three-dimensional data structures

A set of data structures and methods for the handling of three (and six) dimensional entities has been developed. It allows the writing of most of the common operations involving three-dimensional vectors and matrices in a formal way that directly resembles normal hand-writing of formulas, which has been obtained by properly overloading most of the mathematical operators. As a result, operations arithmetic operations are straightforward, i.e.

```
Vec3 v, w;
Mat3x3 m;
Vec3 x = m * v + w;
```

To avoid excessive sophistication, no particular care has been put in handling temporaries; a careful programming style can take advantage of the ease of notation without incurring in excessive overhead related to temporaries. Operations such as creating a vector product matrix, or executing a vector product can be performed as follows:

```
Vec3 v;
Mat3x3 m(v); // overload of constructor accepting a vector
             // to yield m = v x
Vec3 w, z;
z = w.Cross(v); // cross product between vectors
```

Many other operations are available. Further details can be obtained by self-generating the code documentation:

```
$ make doc
```

H.3.4 Input handling

Particular care has been dedicated to implementing a safe, reliable, flexible input handling, which resulted in an input library independent of the multibody program. It is dedicated to the acquisition of card-like input lines, so it is not flexible in a general sense. In the future it might be modified to include some general features of general parsing routines and some syntax interpretation features. It is based on a low-level parsing tool that interprets the input, generating tokens. The higher-level interpreter extracts the meaningful tokens taking care of separators, punctuation, file inclusion, input-related crds and so on. When a specific token type is expected (i.e. required by the user), the related input routines are invoked, otherwise some token type recognition is attempted. Basic tokens are keywords, which can be built-in and user-defined, numeric values, and strings. Numeric values are parsed by a simple mathematical interpreter, that parses a sequence of mathematical expressions and returns the value of the last one. There is support for types (`integer` and `real`), variable declaration, and for a number of built-in mathematical functions. This makes parametric input very simple and reliable. Extensions allow MBDyn to consider also environment variable definition. A special `drive` (see Section H.1.1) returns a value based on evaluating, by means of the same parser, a string containing a mathematical expression which may contain variables defined furing the input, and the current time in built-in variable `Time`. For a detailed description of the input format, type

```
$ make man
```

or see `html://diamppl.aero.polimi.it/mbdyn/mbdyn-index.html`.

H.4 Debug/release approach

A fundamental task of implementing a complicated project is represented by debugging. For this purpose a debug/release approach has been followed, by introducing a lot of redundant debugging code that can be activated at compile-time by appropriate compiler flags. The phylosophy is that of building a self-debugging program, based on performing automatic consistence checks before and after many crucial operations, without excessivel reducing performances once the code is released. It is fundamental to follow some guidelines to make this strategy useful and reliable. The fundamental issue is to make the release code "smaller" than the debug code, but not different. In other words, the debug version of the code can add lines of code, but it must interfere as little as possible with the release part of the code, i.e. it must not alter variables, streams other than the standard output/error, it must resort as little as possible to routine calls that might alter the status of the stack, it must not create different logical paths, i.e. add conditional statements, or alter the logical path by altering conditional code execution. For this reason the best thing is to use macros that directly add code instead of function calls. After some code growth, the debug output became really huge, so the approach has been changed by adding some command-line tunable output selection to the debug version, to allow a selective debugging output.

H.5 Safe-pointer programming

Pointers can be a nightmare in C programming. C++ suggests a programming style that allows a safer use of pointers, but a lot of care must be taken anyway. To free the implementor from excessive attention to memory allocation and handling, and to ease dynamic allocation related debugging, a collection of memory allocation macros and routines has been implemented. Some of them have been recently obsoleted by the final ANSI C++ draft, and thus have been recoded and simplified. The idea is to provide macros that take care of allocating and freeing memory, which do only little more than standard memory management routines when compiled in debug version, but perform redundant and tedious consistency checks when compiled in debug version. For instance, during allocation a good idea is to test whether the target pointer is `NULL` or not, in the former case tracing a possible memory leak due to the cancellation of a possible reference to dynamically allocated memory. This test requires the implementor always to reset a pointer before allocating memory, reulting in a good programming style, at least in our humble opinion. Analogous operation shuld be done when freeing memory, i.e. a pointer should be reset to `NULL` after deletion, to ensure nobody can reference deleted memory. If it is done, it will result in a *segment violation* signal to be raised at run-time, which will suggest the implementor that there is some memory leakage. When the memory debug flag is activated, a parallel memory manager is maintained, which stores dynamically allocated memory information, and allows the implementor to add consistency checks on pointers when required. A set of checks are available, ranging from the strict validity of a memory chunk, i.e. a pointer is the base of a chunk of a prescribed size, to a weak validity of a pointer pointing to a sub-chunk entirely comprised in the allocated chunk. The following example, involving a simple allocation routine, that can be used for types with a default constructor, e.g. the fundamental C and C++ types, illustrates both the debug/release programming paradigm and the safe allocation concept. Consider the `SAFENEW` macro:

```
#ifdef DEBUG
#  ifdef DEBUG_MEMMAN
#    define SAFENEW( pnt, item, memman ) \
       do { \
         assert( !( pnt ) ); \
         assert( sizeof( item ) ); \
         ( pnt ) = new item; \
         if( !( pnt ) ) { \
           _Safenew( __FILE__, __LINE__ ); \
         } \
         ( memman ).add( (void *)( pnt ), sizeof( item ) ); \
       } while( 0 )
#  else // !DEBUG_MEMMAN
#    define SAFENEW( pnt, item, memman ) \
       do { \
         assert( !( pnt ) ); \
         assert( sizeof( item ) ); \
         ( pnt ) = new item; \
         if( !( pnt ) ) { \
           _Safenew( __FILE__, __LINE__ ); \
         } \
       } while( 0 )
#  endif // !DEBUG_MEMMAN
#else // !DEBUG
#  define SAFENEW( pnt, item, memman ) \
     ( pnt ) = new item
#endif // !DEBUG
```

It is important to remark that:

- the macro takes three arguments: the target pointer, `pnt`, the type of the object to create, `item`, and a memory manager, `memman`;

- the body of the macro is encapsulated in a `do { } while ()` loop, so that it can be used as a function, i.e. ended by a semicolon: `SAFENEW( p, int, m );`. However, since it expands to a portion of code, it cannot be used inside a conditional statement, i.e. an `if` clause, or as the argument of a function call;

- the user-defined memory manager is used only if the appropriate compiler flag, `DEBUG_MEMMAN`, is set, which on turn requires the flag `DEBUG` to be set;

- a function, `_Safenew()`, is invoked in case of failure; this is done to send a standard error message with limited code size overhead. In fact, if the error message were written directly inside the macro definition, it would expand to a constant string every time the macro is used, and only few compilers are able to recognise when a constant string is repeated to store it only once. The C preprocessor-defined macros `__FILE__` and `__LINE__` are used to customize the error message and make it a little more helpful. They are expanded to the file name and the line number they were used;

- the standard C function `assert` is used to assess whether the pointer is null or the size of the type is legal. So there are some function calls in the debug version of the code, but they are known not to alter any data; they simply write to the standard error stream. It is a good practice to force a flush of the stream before and after using it, to ensure the messages are printed in the correct sequence;

- finally, this macro is particularly dangerous because both `pnt` and `item` are evaluated more than once, so if non-appropriate values are used, a different (and erroneous) behaviour results when using the debug instead of the release version of the code.

A complete set of macros is provided, to account also for the allocation of objects requiring a constructor, for the allocation of arrays, and for their destruction.

H.6 Conclusion

This digression on implementation issues does not pretend to be exaustive, not to introduce novel ideas in programming techniques. Its aim is to focus the reader's attention on some programming topics that deserve a lot of attention even when writing very simple toy-codes, especially when other people will have to deal with those codes both as users and as maintainers. Big projects require thinking ahead, to save implementation time, cost, and to preserve from unpleasant surprises. During my short career as Graduate Student, Ph.D. Student and Staff Researcher I had to maintain and modify many codes, mainly written in Fortran, starting from the early Eighties and subsequently maintained, improved, modified, rewritten (not very often!), resulting in something really looking like unreadble sequences of random chars! Of course there was a logic in all those lines of code, but it was perfectly clear only to the implementor. Maybe at the moment I'm writing this sentence someone is thinking the same of my code, but my aim was being safe, redundant and hopefully readable. I hope someone will consider the importance of these issues when continuing this work.

Bibliography

[1] Karl Johan Åström and Björn Wittenmark, *Adaptive control*, Addison-Wesley, USA, 1989.

[2] M. Andrighettoni and Paolo Mantegazza, *Multi-input/multi-output adaptive active flutter suppression for a wing model*, Journal of Aircraft **35** (1998), no. 35, 462–469.

[3] ANSI/IEEE, *IEEE standard on piezoelectricity*, Tech. Report 176-1987, IEEE, 1987.

[4] Mitsuhiro Aso and Shun ichi Bandoh, *The development of the total vibration reduction (TVR) system*, American Helicopter Society 55$^{\text{th}}$ Forum (Montreal, Canada), May 25–27 1999, pp. 202–208.

[5] Klaus Jürgen Bathe, *Finite element procedures in engineering analysis*, Prentice-Hall, Englewood Cliffs, 1982.

[6] Olivier A. Bauchau, *Computational schemes for flexible, non-linear multi-body systems*, Multibody Systems Dynamics **2** (1998), no. 2, 169–225.

[7] Olivier A. Bauchau and N. K. Kang, *A multibody formulation for helicopter structural dynamic analysis*, Journal of the American Helicopter Society **38** (1993), no. 2, 3–14.

[8] Aaron A. Bent, Nesbitt W. Hagood, and John P. Rodgers, *Anisotropic actuation with piezoelectric fiber composites*, J. of Intell. Mat. Systems & Structures **6** (1995), 338–349.

[9] Vladimir Vasil'evich Bolotin, *Nonconservative problems of the theory of elastic stability*, Pergamon Press, Oxford, 1963.

[10] Marco Borri and Carlo L. Bottasso, *An intrinsic beam model based on a helicoidal approximation — part I: Formulation*, Intl. J. for Num. Methods in Engineering **37** (1994), 2267–2289.

[11] ______, *An intrinsic beam model based on a helicoidal approximation — part II: Linearization and finite element implementation*, Intl. J. for Num. Methods in Engineering **37** (1994), 2291–2309.

[12] Marco Borri, Gian Luca Ghiringhelli, and Teodoro Merlini, *Linear analysis of naturally curved and twisted anisotropic beams*, Composites Engineering **2** (1992), no. 5–7, 433–456.

[13] Marco Borri and Paolo Mantegazza, *Some contributions on structural and dynamic modeling of rotor blades*, l'Aerotecnica Missili e Spazio (1985), 143–154.

[14] Marco Borri and Teodoro Merlini, *A large displacement formulation for anisotropic beam analysis*, Meccanica **21** (1986), 30–37.

[15] Marco Borri, Lorenzo Trainelli, and Carlo L. Bottasso, *On representations and parametrizations of motion*, to be published on Multibody Dynamics.

[16] William G. Bousman, Colin Young, François Toulmay, Neil E. Gilbert, Roger C. Strawn, Judith V. Miller, Thomas H. Maier, Michel Costes, and Philippe Beaumier, *A comparison of lifting-line and CFD methods with flight test data from a research Puma helicopter*, TM 110421, NASA, October 1996.

[17] Kathryn Eleda Brenan, Stephen La Vern Campbell, and Linda R. Petzold, *Numerical solution of initial-value problems in differential-algebraic equations*, North-Holland, New York, 1989.

[18] P. C. Chen and Inderjit Chopra, *Induced-strain actuation of composite beams and rotor blades with embedded piezoceramic elements*, 1st Workshop on Smart Structures (University of Texas, Arlington, TX), September, 22–24 1993.

[19] T. Chen, *Micromechanical estimates of the overall thermoelectroelastic moduli of multiphase fibrous composites*, Intl. J. Solids Structures **31** (1994), no. 22.

[20] Javier Garcia de Jalon and Eduardo Bayo, *Kinematic and dynamic simulation of multibody systems : the real time challenge*, Springer-Verlag, New York, 1994.

[21] M. L. Dunn, *A theoretical framework for the analysis of thermoelectroelastic heterogeneous media with applications*, J. of Intell. Mat. Systems & Structures **6** (1995).

[22] M. L. Dunn and M. Taya, *Micromechanics predictions of the effective electroelastic moduli of piezoelectric composites*, Intl. J. Solids Structures **30** (1993), no. 2.

[23] K. W. Eure and Jer-nan Juang, *Broadband noise control using predictive techniques*, TM 110320, NASA, 1997.

[24] Walter Eversman and Indranil Danda Roy, *Active flutter suppression using multi-input/multi-output adaptive least mean square control*, J. Aircraft **34** (1997), no. 2, 244–250.

[25] C. G. Franchi, *A highly redundant coordinate formulation for constrained rigid bodies*, Meccanica **30** (1995), 17–35.

[26] Peretz P. Friedmann and T. A. Millot, *Vibration reduction in rotorcraft using active control: a comparison of various approaches*, J. of Guidance, Control, & Dynamics **18** (1995), no. 4, 664–673.

[27] Gian Luca Ghiringhelli, *On the linear three dimensional behaviour of composite beams*, Composites Part B (1997), no. 28B, 613–626.

[28] ———, *On the thermal problem for composite beams using a finite element semi-discretisation*, Composites Part B **6** (1997), 483–495.

[29] Gian Luca Ghiringhelli and Massimiliano Lanz, *Dynamic optimisation of bearingless helicopter rotors*, CEAS Intl. Forum on Aeroelasticity and Structural Dynamics (Rome, Italy), vol. III, June 17–20 1997, pp. 75–84.

[30] Gian Luca Ghiringhelli, Massimiliano Lanz, and Paolo Mantegazza, *Numerical modelling and experimental testing of distributed piezoelectric actuators*, Intl. Forum on Aeroelasticity and Structural Dynamics (Strasbourg, France), 1993.

[31] Gian Luca Ghiringhelli and Paolo Mantegazza, *Linear, straight and untwisted anisotropic beam section properties from solid finite elements*, Composites Engineering **4** (1994), no. 12, 1225–1239.

[32] Gian Luca Ghiringhelli, Paolo Mantegazza, and Pierangelo Masarati, *Numerical modelling of anisotropic non homogeneous beams with embedded piezoelectric sensors and actuators*, 7th International Conference on Adaptive Structures and Technologies (Rome, Italy), September 23–25 1996.

[33] Gian Luca Ghiringhelli and Pierangelo Masarati, *Semi-analytical characterisation of anisotropic, non-homogeneous plates*, Tech. Report SR 00–19, Dipartimento di Ingegneria Aerospaziale, Politecnico di Milano, Milano, Italy, 2000.

[34] Gian Luca Ghiringhelli, Pierangelo Masarati, and Paolo Mantegazza, *Characterisation of anisotropic, non-homogeneous beam sections with embedded piezo-electric materials*, J. of Intell. Mat. Systems & Structures **8** (1997), no. 10, 842–858.

[35] ______, *Multi-body aeroelastic analysis of smart rotor blades, actuated by means of piezo-electric devices*, CEAS Intl. Forum on Aeroelasticity and Structural Dynamics (Rome, Italy), vol. II, June 17–20 1997, pp. 115–122.

[36] ______, *Analysis of an actively twisted rotor by multi-body global modelling*, 1999 ASME Mechanics and Materials Conference (Blacksburg, VA), June 27–30 1999, Also published by *Composites & Structures*.

[37] ______, *A multi-body implementation of finite volume beams*, AIAA Journal **38** (2000), no. 1, 131–138.

[38] Gian Luca Ghiringhelli, Pierangelo Masarati, Paolo Mantegazza, and Mark W. Nixon, *Multi-body analysis of a tiltrotor configuration*, 7th Conference On Nonlinear Vibrations, Stability, and Dynamics of Structures (Blacksburg, VA), July 26–30 1998, also published as [39].

[39] ______, *Multi-body analysis of a tiltrotor configuration*, Nonlinear Dynamics **19** (1999), no. 4, 333–357.

[40] ______, *Multi-body analysis of an active control for a tiltrotor*, CEAS Intl. Forum on Aeroelasticity and Structural Dynamics 1999 (Williamsburg, VA), June 22–25 1999, pp. 149–158.

[41] ______, *Multi-body analysis of the 1/5 scale wind tunnel model of the V–22 tiltrotor*, American Helicopter Society 55th Forum (Montreal, Canada), vol. 2, May 25–27 1999, pp. 1087–1096.

[42] Gian Luca Ghiringhelli and Giuseppe Sala, *Interlaminar edge stress analysis of composite cross-ply flat specimens*, Meccanica **21** (1986), 151–158.

[43] ______, *Some aspects of damage mechanics for composite materials*, IX Congresso Nazionale della Associazione di Aeronautica ed Astronautica (Palermo, Italy), 26–28 October 1987, in Italian.

[44] Vittorio Giavotto, Marco Borri, Paolo Mantegazza, Gian Luca Ghiringhelli, V. Caramaschi, G. C. Maffioli, and F. Mussi, *Anisotropic beam theory and applications*, Computers & Structures **16** (1983), no. 1–4, 403–413.

[45] Victor Giurgiutiu, Zaffir Chaudry, and Craig A. Rogers, *Engineering feasibility of induced strain actuators for rotor blade active vibration control*, J. of Intell. Mat. Systems & Structures **6** (1995), 583–597.

[46] Victor Giurgiutiu, Sandip Dutta, and Craig A. Rogers, *Compact high-frequency solid-state modular pump for hydraulic actuation*, ICAST '98, Ninth International Conference on Adaptive Structures and Technologies (Cambridge, Mass.), October 14–16 1998.

[47] Victor Giurgiutiu and Craig A. Rogers, *Review of smart-materials actuation solutions for aeroelastic and vibration control*, CEAS Intl. Forum on Aeroelasticity and Structural Dynamics 1999 (Williamsburg, VA), June 22–25 1999.

[48] Nesbitt W. Hagood, R. Kindel, K. Ghandi, and Paolo Gaudenzi, *Improving transverse actuation of piezoceramics using interdigitated surface electrodes*, SPIE Smart Structures and Materials Conference, vol. 1917(1), February 1–4 1993, pp. 341–352.

[49] Ernst Hairer, Christian Lubich, and Michel Roche, *The numerical solution of differential-algebraic systems by runge-kutta methods*, Lecture Notes in Mathematics, Springer-Verlag, Berlin Heidelberg, Germany, 1989.

[50] Ernst Hairer and Gerhard Wanner, *Solving ordinary differential equations*, vol. II, Springer-Verlag, Berlin Heidelberg, Germany, 1996, 2$^{\text{nd}}$ rev. ed.

[51] Pamela J. Haley, Donald Soloway, and Brian Gold, *Real-time adaptive control using neural generalized predictive control*, 1999 American Control Conference (San Diego, California), June 2–4 1999.

[52] N. D. Ham, *Helicopter individual-blade-control research at MIT 1977–1985*, Vertica **11** (1987), no. 1/2, 109–122.

[53] Norman D. Ham, Brigitte L. Behal, and McKillip Robert M., Jr, *Helicopter rotor lag damping augmentation through individual-blade-control*, Vertica **7** (1983), no. 4, 361–371.

[54] F. D. Harris, F. J. Jr, Tarzanin, and R. K. Jr, Fisher, *Rotor high speed performance, theory vs. test*, Journal of the American Helicopter Society **15** (1970), no. 3, 35–41.

[55] Howard E. Hinnant, *Derivation of a tapered p-version beam finite element*, TP 2931, NASA, 1989.

[56] Dewey H. Hodges, *Review of composite rotor blade modeling*, AIAA Journal **28** (1990), no. 3, 561–565.

[57] C. H. Hong and Inderjit Chopra, *Aeroelastic stability analysis of a composite rotor blade*, Journal of the American Helicopter Society **30** (1985), no. 2, 57–67.

[58] Thomas J. R. Hughes and F. Brezzi, *On drilling degrees of freedom*, Computer Methods in Applied Mechanics and Engineering **72** (1989), 105–121.

[59] B. Z. Janos and Nesbitt W. Hagood, *Overview of active fiber composites technologies*, 6$^{\text{th}}$ International Conference on new Actuators - ACTUATOR98 (Bremen, Germany), June '98 1998.

[60] Wayne Johnson, *Helicopter theory*, Princeton University Press, Princeton, New Jersey, 1980.

[61] ———, *Development of a comprehensive analysis for rotorcraft — I. rotor model and wake analysis*, Vertica **5** (1981), 99–129.

[62] ———, *Development of a comprehensive analysis for rotorcraft — II. aircraft model, solution procedure and applications*, Vertica **5** (1981), 185–216.

[63] Jer-nan Juang, *State-space system realization with input- and output-data correlation*, TP 3622, NASA, 1997.

[64] Jer-nan Juang and M. Q. Phan, *Deadbeat predictive control*, Journal of the Chinese Society of Mechanical Engineers **19** (1997), no. 1, 25–37.

[65] Raymond G. Kvaternik, *A review of some tilt-rotor aeroelastic research at nasa-langley*, J. of Aircraft **13** (1976), no. 5, 357–363.

[66] R. G. Loewy, *Helicopter vibrations: A technological perspective*, Journal of the American Helicopter Society (1984), 4–30.

[67] Paolo Mantegazza, *Analysis of semimonocoque beam sections by the displacement method*, l'Aerotecnica Missili e Spazio (1977), 179–182.

[68] Pierangelo Masarati, *Travi piezoelettriche: Modellazione ed analisi (Piezoelectric beams: Modelling and analysis)*, Master's thesis, Politecnico di Milano, Milano, Italy, 1994–95, in Italian.

[69] Pierangelo Masarati and Paolo Mantegazza, *On the C^0 discretisation of beams by finite elements and finite volumes*, l'Aerotecnica Missili e Spazio **75** (1997), 77–86.

[70] T. Millott and Peretz P. Friedmann, *Vibration reduction in helicopter rotors using an active control surface located on the blade*, AIAA/ASME/AHS/ASC 33$^{\text{rd}}$ Structures, Structural Dynamics, and Materials Conference (Washington, DC), 1992, AIAA-92-2451, pp. 1975–1988.

[71] ______, *The practical implementation of an actively controlled flap to reduce vibrations in helicopter rotors*, 49$^{\text{th}}$ Forum of the American Helicopter Society (St. Louis, MO), 1993, pp. 1079–1092.

[72] Khanh Nguyen and Inderjit Chopra, *Application of higher harmonic control to hingeless rotor systems*, Vertica **14** (1990), no. 4, 545–556.

[73] Mark W. Nixon, *Aeroelastic response and stability of tiltrotors with elastically-coupled composite rotor blades*, Ph.D. thesis, University of Maryland, 1993.

[74] Mark W. Nixon, Raymond G. Kvaternik, and Thomas B. Settle, *Higher harmonic control tiltrotor vibration reduction*, CEAS Intl. Forum on Aeroelasticity and Structural Dynamics (Rome, Italy), vol. II, June 17–20 1997, pp. 327–334.

[75] T. Parham, Jr., *A3B semispan model stress report*, Internal Report 599-099-197, Bell Helicopter Textron Inc., 1994.

[76] Dale M. Pitt and David A. Peters, *Theoretical prediction of dynamic-inflow derivatives*, Vertica **5** (1981), 21–34.

[77] David Popelka, Mark Sheffler, and Jim Bilger, *Correlation of test and analysis for the 1/5-scale V–22 aeroelastic model*, Journal of the American Helicopter Society **32** (1987), no. 2, 21–33.

[78] G. Reichert, *Helicopter vibration control — a survey*, Vertica **5** (1981), no. 1, 1–20.

[79] Lawson H. Robinson and Peretz P. Friedmann, *A study of fundamental issues in higher harmonic control using aeroelastic simulation*, Journal of the American Helicopter Society (1991), 32–43.

[80] John P. Rodgers and Nesbitt W. Hagood, *Preliminary mach-scale hover testing of an integral twist-actuated rotor blade*, SPIE Conference (San Diego, California), March 1–5 1998.

[81] Werner Schiehlen, *Multibody systems handbook*, Springer-Verlag, Berlin, 1990.

[82] Thomas B. Settle and David L. Kidd, *Evolution and test history of the V–22 0.2-scale aeroelastic model*, Journal of the American Helicopter Society **37** (1992), no. 1, 31–45.

[83] Donald Soloway and Pamela J. Haley, *Neural generalized predictive control: A newton-raphson implementation*, TM 110244, NASA, February 1997.

[84] Nicolaas J. Theron, *Multi-body dynamic analysis of helicopter rotors*, Ph.D. thesis, Rensselaer Polytechnic Institute, Troy, NY, 1994, SCOREC Report 28-1994.

[85] Lorenzo Trainelli, *Studio della dinamica dei rotori di elicottero mediante algoritmi multicorpo conservativi/dissipativi (a study of the dynamics of helicopter rotors by multibody preservative/dissipative algorithms)*, Ph.D. thesis, Dipartimento di Ingegneria Aerospaziale, Politecnico di Milano, Milano, Italy, 1998.

[86] Vitali V. Volovoi, Dewey H. Hodges, Carlos E. S. Cesnik, and Bogdan Popescu, *Assessment of beam modeling methods for rotor blade applications*, American Helicopter Society 55th Forum (Montreal, Canada), May 25–27 1999, pp. 1209–1218.

[87] C. Walz and Inderjit Chopra, *Design, fabrication, and testing of a helicopter rotor model with smart trailing edge flaps*, AIAA/ASME/ASCE/AHS/ASC 35th Structures, Structural Dynamics, and Materials Conference — Adaptive Structures Forum (Hilton Head, SC), April 21–22 1994, AIAA-94-1767-CP, pp. 298–319.

[88] William K. Wilkie, Paul H. Mirick, and Chester W. Langston, *Rotating shake test and modal analysis of a model helicopter rotor blade*, TM 4760, NASA, 1997.

[89] William K. Wilkie, K. C. Park, and W. K. Belvin, *Aeroelastic analysis of helicopter rotor blades incorporating anisotropic piezoelectric twist actuation*, in ASME 1996 World Congress and Exposition, Adaptive Structures Symposium, Proceedings, Aerospace Division, November 1996.

[90] ______, *Helicopter dynamic stall suppression using piezoelectric active fiber composite rotor blades*, AIAA/ASME/AHS Structures, Structural Dynamics and Materials Conference (Long Beach, CA), April 20–23 1998, AIAA-98-2002.

[91] William Keats Wilkie, Matthew L. Wilbur, Paul H. Mirick, Carlos E. S. Cesnik, and SangJoon Shin, *Aeroelastic analysis of the NASA/Army/MIT active twist rotor*, American Helicopter Society 55$^{\text{th}}$ Forum (Montreal, Canada), May 25–27 1999.

[92] R. W. Wlezien, G. C. Horner, A. R. McGowan, S. L. Padula, M. A. Scott, R. J. Silcox, and J. O. Simpson, *The aircraft morphing program*, 39$^{\text{th}}$ AIAA/ASME/ASCE/AHS/ASC Structures, Structural Dynamics, and Materials Conference (Long Beach, California), April 20–23 1998, AIAA 98-1927.

[93] E. Roberts Wood, Righard W. Powers, John H. Cline, and C. Eugene Hammond, *On developing and flight testing a higher harmonic control system*, Journal of the American Helicopter Society (1985), 3–20.